Slow wave activity in the medial prefrontal cortex of the anaesthetised rat: sub-regional characterisation and dopaminergic modulation

Sabine Gretenkord

Thesis submitted in partial fulfilment of the requirements for the degree of:
Doctor of Philosophy

Institute of Neuroscience
Newcastle University

Advisors:
Dr. Fiona E. N. LeBeau
Dr. Sarah E. Gartside
Prof. Adrian Rees

September 2014

Newcastle University

Abstract

During non-rapid eye movement (NREM) sleep, information may be transferred from hippocampus to cortex for long-term storage through synchronised reactivation of these areas. Electrical brain activity during deep NREM sleep consists mainly of a slow (< 1 Hz) alternation between 'Up' and 'Down' states (UDS). UDS enable the coordination of fast oscillations (> 6 Hz) at different frequencies between different brain regions, which is thought to aid memory consolidation. Coordinated reactivation is though to be guided by the medial prefrontal cortex (mPFC) with its strong connections to many other cortical and subcortical regions. Dopamine strongly modulates mPFC function during wakefulness. However, UDS are not well characterized in the mPFC and little is know about how dopamine modulates mPFC activity during sleep.

We recorded UDS in the mPFC of urethane-anaesthetised rats and found significant variation in UDS characteristics both between mPFC sub-regions and between cortical laminae. Activation of the intrinsic dopamine system using tonic, high-frequency electrical stimulation of the ventral tegmental area abolished UDS in the mPFC, shifting activity to a low amplitude fast rhythm, as occurs during rapid eye movement (REM) sleep. This effect was blocked by a dopamine D_1 receptor (D_1R) antagonist, but not a D_2R antagonist. An increase of extracellular dopamine by systemic amphetamine application significantly decreased the power of spindle (6-15 Hz) and gamma (30-80 Hz) oscillations during the Up state. D_4R and D_1R agonists also affected high-frequency oscillations associated with Up states.

These results suggest that D_1 receptors might play a role in the change in mPFC activity associated with the transition from NREM sleep to REM sleep. In addition, dopaminergic modulation shows the ability to finely tune Up state-associated fast oscillations, which may potentially be relevant for the coordination between different brain regions, as is necessary for memory consolidation.

Acknowledgements

First of all I would like to thank my three supervisors Fiona LeBeau, Sarah Gartside and Adrian Rees, who have been incredibly supportive throughout my whole PhD. Patiently, they have taught me the fun of experimental neuroscience and seemed to have a sixth-sense for appearing at the right time, i.e. when I was in trouble. I am incredibly thankful to Fiona for the very fast turnaround during the final stages of thesis writing. Thanks also to my inspiring fourth supervisor, Miles Whittington, who moved to York during my PhD.

In addition, I am grateful for very helpful yearly advice from Andy Jackson and Marcus Kaiser, who formed my progress review panel.

During the three years of my PhD I have worked in three different labs and two offices, and many people have provided me with helpful advice, from best histology and ordering ☺ practice (Felix Chan), via rat taming (Claire Gillougley), to tips and tricks in Illustrator (Tom Hall) and the art of fixating coverslips to microscope slides with nail polish (Anna Simon). I would also like to thank Llwyd Orton who always had a smile on his face, even though working so incredibly hard. Thank you for letting me use your precious tungsten electrodes and for showing me how to cut brains and stain and mount sections. I have also especially enjoyed discussing statistical issues with Katherine Newling, as well as analysis/MATLAB stuff with Tom Hall, Vasileios Glykos, and Natalie Adams.

My special thanks also go to Karen Parkin, for 'subbing' my microscope slides, and cleaning the masses of glassware I used for my histology. I would also like to thank Trevor Booth who proved incredibly patient in showing me how to use the fluorescence microscope and the imaging software and worked with me again-and-again on ways to improve the quality of the tiling.

I have met many lovely people during my time in Newcastle, who have provided a friendly environment to work in. First, the people in HWB where I had an amazing office space during my MRes year: Jonas Zimmerman, Kari Schroeder and Bonne Habekost. Second, the equally amazing people in the 'Dark side-oscillations' office: Katherine Newling, Felix Chan, Yingdi Chen, Vasileios Glykos and Henrik Kjeldsen.

And third, the people in my current office: Reem Basoudan, Bas Olthof and Caroline McCardle, who had to cope with me during the very stressful write-up time.

I feel very lucky to have friends such as Annike, Christina, Nicole and Caro who made it all the way from Germany to the grim north of England to visit me.

I am also thankful for the support of my parents, who spared neither trouble nor expense to move their daughter 1025 kilometers from Berlin to Newcastle. I very much enjoyed our meetings in different (sunny!) parts of the UK, and all the food parcels have helped me a lot during my time here.

Finally, I am most grateful to Tom, who went through all the ups and downs of the last three years with me and never got tired of cheering me up. Although I might have reached the threshold with my constant complaints about the lack of bread. I am enjoying every minute I spend with you, even if it is falling asleep together on the last metro home from Newcastle to Tynemouth after a long day at work.

Publications

Gretenkord S, Gartside SE, Rees A, Whittington MA, LeBeau FEN (2013) The effect of ventral tegmental area stimulation on slow wave sleep Up-down states in the prefrontal cortex of anaesthetized rats. Published abstract, Annual meeting of the Society for Neuroscience.

Table of contents

List of figures

List of tables

List of abbreviations

ADHD	attention deficit-hyperactivity disorder
AMPA	α-amino-3-hydroxy-5-methyl-4-isoxazolepropionic acid
ANOVA	analysis of variance
AP	antero-posterior (anatomical axis)
AP5	(*2R*)-amino-5-phosphonovaleric acid
ART	aligned rank transform (statistical tool)
ATP	adenosine triphosphate
Ca^{2+}	calcium ion
cAMP	cyclic adenosine monophosphate
CAP	cyclic alternating pattern
Cg	cingulate cortex (mPFC sub-region)
ChAT	choline acetyl-transferase
CMN	central medial nucleus (of the thalamus)
D_1R to D_5R	dopamine receptor type 1 to type 5
DAPI	4',6-diamidino-2-phenylindole (a fluorescent stain)
DAT	dopamine active transporter
dCg	dorsal cingulate cortex
dDP	dorsal dorsal peducular cortex
df	degrees of freedom (statistics)
DiI	$DiIC_{18}(3)$; a fluorescent stain
DMSO	dimethyl sulfoxide
DP	dorsal peduncular cortex (mPFC sub-region)
dPrL	dorsal prelimbic cortex
DREADD	designer receptors exclusively activated by designer drugs
dTT	dorsal tenia tecta
DV	dorso-ventral (anatomical axis)
ECoG	electrocorticography
EEG	electroencephalography
EPSC	excitatory post-synpatic current
EPSP	excitatory post-synpatic potential
FFT	fast Fourier transform
FIR	finite impulse response (filter)
FITC	fluorescein isothiocyanate (filter)

GABA	gamma-aminobutyric acid
Gα	G-protein alpha subunit
HCN	hyperpolarization-activated cation-selective (channel)
HRP	horseradish peroxidase
I	current, in particular a membrane current e.g. I_{Leak}
i.p.	intraperitoneal (injection); route of drug administration
IBI	interburst interval
IL	infralimbic cortex (mPFC sub-region)
IPSC	inhibitory post-synpatic current
IPSP	inhibitory post-synpatic potential
IQR	inter-quartile range
K^+	potassium ion
LAF	low-amplitude fast (rhythm)
LC	locus coeruleus
LdeeperR	dataset in Chapter 3 in which data from the left hemisphere were recorded in a deeper layer than those from the right hemisphere
LDTN	laterodorsal tegmental (nuclei)
LFP	local field potential
LPAG	lateral periaqueductal grey matter
LPT	lateral pontine tegmentum
LS	light sleep
M1	primary motor cortex
MDN	mediodorsal nucleus (of the thalamus)
mGlu	metabotropic glutamate (receptor)
ML	medio-lateral (anatomical axis)
mPFC	medial prefrontal cortex
MPON	medial preoptic nucleus
MPTP	1-methyl-4-phenyl-1,2,3,6-tetrahydropyridin
MUA	multi-unit activity
Na^+	sodium ion
NMDA	*N*-methyl-*D*-aspartate
NREM	non-rapid eye movement (sleep)
PB	parabrachial (nucleus)
PBS	phosphate buffer solution
PC	precoeruleus

PD	Parkinson's disease
PFA	paraformaldehyde
PFC	prefrontal cortex
PKA	protein kinase A
PPN	pedunculopontine nucleus
PrL	prelimbic cortex (mPFC sub-region)
PV^+	parvalbumin-immuno positive (cell)
RBP	REM sleep behaviour disorder
RdeeperL	dataset in Chapter 3 in which data from the right hemisphere were recorded in a deeper layer than those from the left hemisphere
REM	rapid eye movement (sleep)
RM ANOVA	repeated measures analysis of variance
S1 to S4	sleep stages 1 to 4
SCN	suprachiasmatic nucleus
SCZ	schizophrenia
SLD	sublaterodorsal (nucleus)
SN	substantia nigra
SNc	substantia nigra pars compacta
SNr	substantia nigra pars reticulata
SO	slow oscillation
SWA	Slow wave activity
SWS	Slow wave sleep
TC	thalamo-cortical (cell/projection)
tDCS	transcranial direct current stimulation
TH	tyrosine hydroxylase
TRN	Thalamic reticular nucleus
UDS	Up-Down states
VAN	ventral anterior nucleus (of the thalamus)
vCg	ventral cingulate cortex
vDP	ventral dorsal peduncular cortex
vIL	ventral infralimbic cortex
vlPAG	ventro-lateral periaqueductal grey matter
VLPO	ventrolateral preoptic area/nucleus
VMN	ventral medial nucleus (of the thalamus)
vPAG	ventral periaqueductal grey matter

VSMP	very slow modulation of broadband LFP power
VTA	ventral tegmental area
αMT	alpha-methyl-para-tyrosine

Chapter 1. General introduction

The prefrontal cortex (PFC) plays an important role in sleep-dependent memory consolidation, which is thought to rely mainly on slow wave activity (SWA) during slow wave sleep (SWS). SWA consists of a slow oscillation (SO, <1 Hz) and nested faster (≥1 Hz) oscillations. Fast rhythms (>15 Hz) are involved in many cognitive functions during wakefulness, and during sleep, might be related to information processing for memory consolidation. Dopamine, as well as modulating fast rhythms in the PFC during wakefulness, is implicated in sleep regulation. However, how dopamine might affect the slow and fast rhythms during SWA is unknown. The main aims of this thesis were to characterise SWA, and particularly the nested fast network oscillations, in the rat PFC under urethane anaesthesia, and to investigate the effects of dopamine on SWA.

1.1 The mammalian prefrontal cortex

An abundance of different species are used in neuroscience research. In order to be able to compare scientific results obtained from different species, it is desirable to identify structural and functional similarities between brain regions in different species. Attempts have especially been made to compare brain regions in primates and rodents.

The PFC is a region of the mammalian neocortex that was originally defined using a single anatomical criterium, which was that it received afferent connections from the mediodorsal thalamic nucleus (Rose and Woolsey, 1948). According to this definition, the PFC consists of a medial, orbital and lateral part in primates, as well as in rodents (Uylings et al., 2003). However, the existence of a rat equivalent of the dorsolateral primate PFC has been questioned (Preuss, 1995). In response, Uylings and colleagues (2003) compared anatomy and function of non-human primate and rat PFC, coming to the conclusion that rats have a prefrontal cortex that is functionally sub-divided and contains areas that show anatomical and functional similarities with the dorsolateral PFC in non-human primates. These regions were mainly located in the rat medial prefrontal cortex (mPFC).

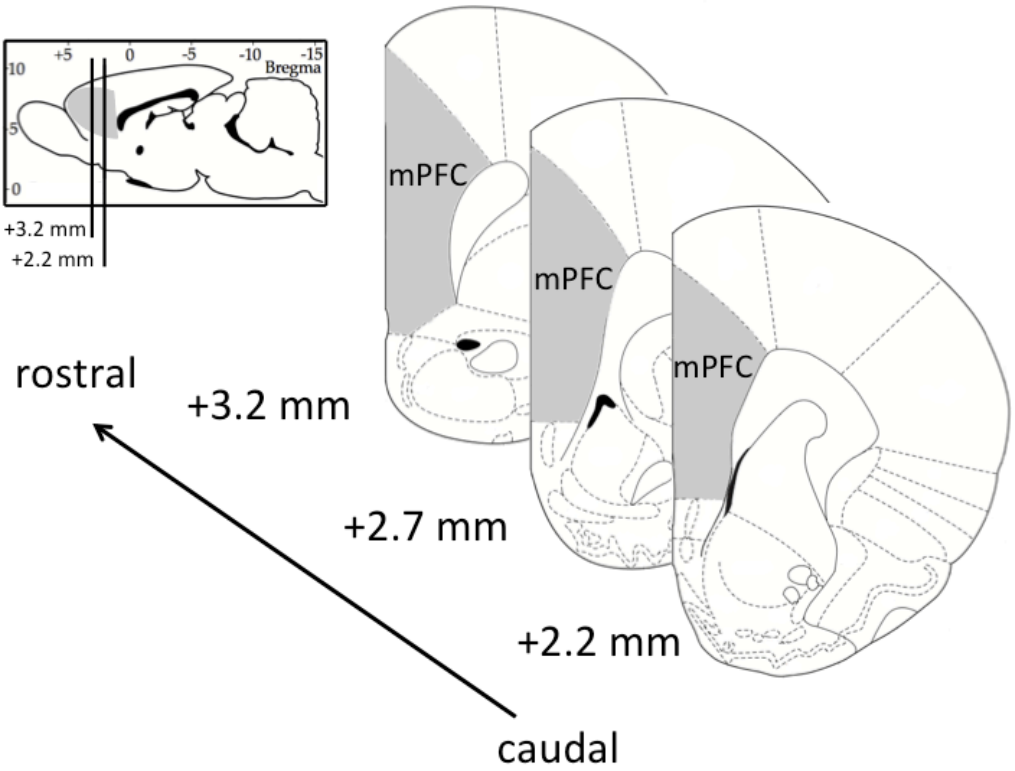

Figure 1.1. Location of the mPFC in the rat brain. The inset panel shows the mPFC location in one hemisphere of a sagittal section of the rat brain. The main figure shows schematic representations of the coronal mPFC sections in which the electrophysiological recordings documented in this thesis were recorded, with the mPFC shaded in grey (sagittal and coronal sections modified from Paxinos and Watson, 1998, 4th edition, Academic Press).

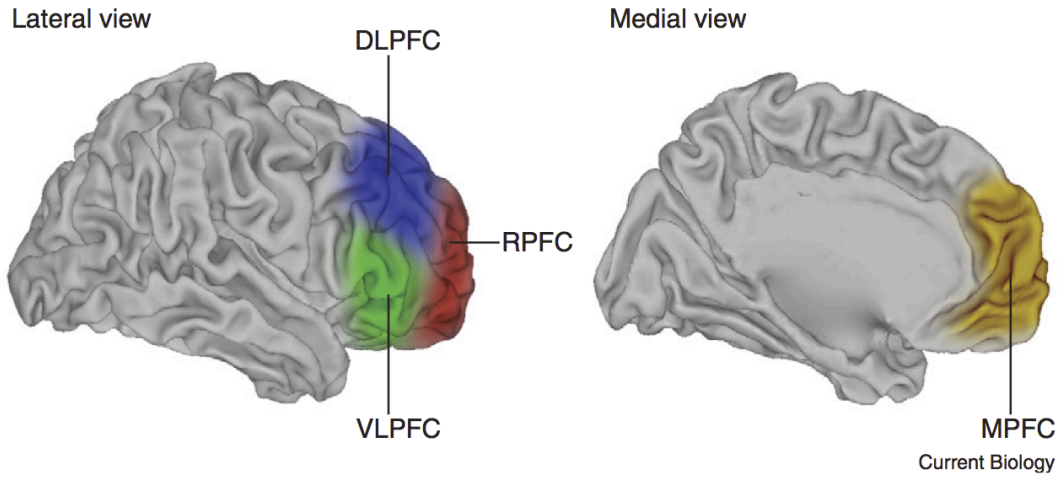

Figure 1.2. Human prefrontal cortex subdivisions. The lateral surface contains a ventrolateral region (VLPFC), dorsolateral region (DLPFC) and rostral region (RPFC). A portion of the human PFC is also located on the medial surface of the brain: the medial prefrontal cortex (MPFC). Figure adapted from Gilbert and Burgess (2008).

1.2 The rat medial prefrontal cortex

As this thesis is entirely based on experiments performed in rats, the anatomy and function of the rat mPFC will be discussed in more detail.

1.2.1 *Location and functional homology with the human brain*

The rat mPFC lies in the most frontal part of the cerebrum and extends along the medial wall of each cerebral hemisphere (Figure 1.1 shows the location of the mPFC in the rat brain). The rat mPFC is important for executive function, memory and decision making (Euston et al., 2012) and thus shares functions with the human dorsolateral PFC as well as the human medial PFC (Bechara et al., 1998). The location of the human dorsolateral PFC and medial PFC is shown in Figure 1.2 (adapted from Gilbert and Burgess (2008)).

1.2.2 *Laminar structure defines mPFC sub-regions*

The rat mPFC consists of four sub-regions: cingulate cortex (Cg), prelimbic cortex (PrL), infralimbic cortex (IL), and dorsal peduncular cortex (DP). The mPFC sub-regions are defined primarily on the basis of differences in laminar structure (Figure 1.3), as will be described in more detail below. This sub-division corresponds best to the one presented in the '*Chemoarchitectonic Atlas of the Rat Forebrain*', (Paxinos et al., 1999). However, the nomenclature used to distinguish the mPFC sub-regions is not consistent in the literature (Uylings et al., 2003); an issue which will be discussed in more detail in section 1.2.5.

The rat mPFC comprises the layers I, II, III, V, VIa and VIb, (Figure 1.3). In comparison with the primate prefrontal cortex, the rodent mPFC lacks a granular layer IV (Krettek and Price, 1977). The laminar separation is clearer in the dorsal mPFC compared to the ventral mPFC (Figure 1.3). The most ventral region, the dorsal peduncular cortex (DP), lies above the dorsal tenia tecta (dTT), which is characterised by a dense cell cluster in layer II (Akhter et al., 2014). The DP is characterized by a thick layer I and the border from DP to IL is defined by layer II becoming more dense (Akhter et al., 2014). In IL, however, the layer I to layer II transition is still not sharp, as layer II cells extend into layer I to varying degrees (Krettek and Price, 1977). The transition from IL to PrL is defined by the sudden transition to a clear border between layer I and layer II (Krettek and Price, 1977). The transition from PrL to Cg is defined by a broadening of layer V (Krettek and Price, 1977), and Cg is characterised by

vertical (i.e. parallel to the medial wall) clustering of cells and an enlargement of layer VIb (Gabbott et al., 1997).

1.2.3 *Connectivity of mPFC sub-regions*

The mPFC is heterogeneous in its connectivity with other parts of the brain, as reviewed by Heidbreder and Groenewegen (2003). The mPFC makes extensive cortico-cortical connections. The dorsal part of the mPFC (Cg and PrL) has connections with sensory and motor cortices, whereas the ventral part (IL and DP) has stronger connections with higher association areas and limbic cortices (Heidbreder and Groenewegen, 2003). Core limbic structures like the hippocampus and the amygdala are predominantly connected to the ventral mPFC, which receives input from the hippocampus and is reciprocally connected with the amygdala. There are also dorsal-to-ventral differences in the connectivity with the striatum, with the Cg projecting to the core of the nucleus accumbens, the PrL mainly to the caudate and putamen, and the ventral mPFC (IL and DP) projecting to the shell of the nucleus accumbens (Heidbreder and Groenewegen, 2003).

Dorsal and ventral mPFC also differ in their connectivity with the thalamus, with the dorsal mPFC reciprocally linked to the lateral thalamus (intralaminar nucleus and lateral segment of mediodorsal nucleus (MDN)) and the ventral mPFC reciprocally linked to the medial thalamus (midline nucleus and medial segment of the MDN) (Heidbreder and Groenewegen, 2003). Thalamic efferents arrive in layer III of the mPFC, whereas outputs to the thalamus leave the mPFC from layers V and VI (Heidbreder and Groenewegen, 2003).

1.2.4 *Functions of mPFC sub-regions*

The mPFC sub-regions differ in their function (reviewed in Gisquet-Verrier and colleagues (2000); Kesner (2000). In essence, the Cg is involved in generating rules associated with temporal ordering and motor sequencing of behaviour. The PrL is important for attentional and response-selection functions, visual working memory and goal-directed behaviour. The ventral mPFC regions (IL and DP) are associated with autonomic control, modulation of fear-related behaviour and habit formation.

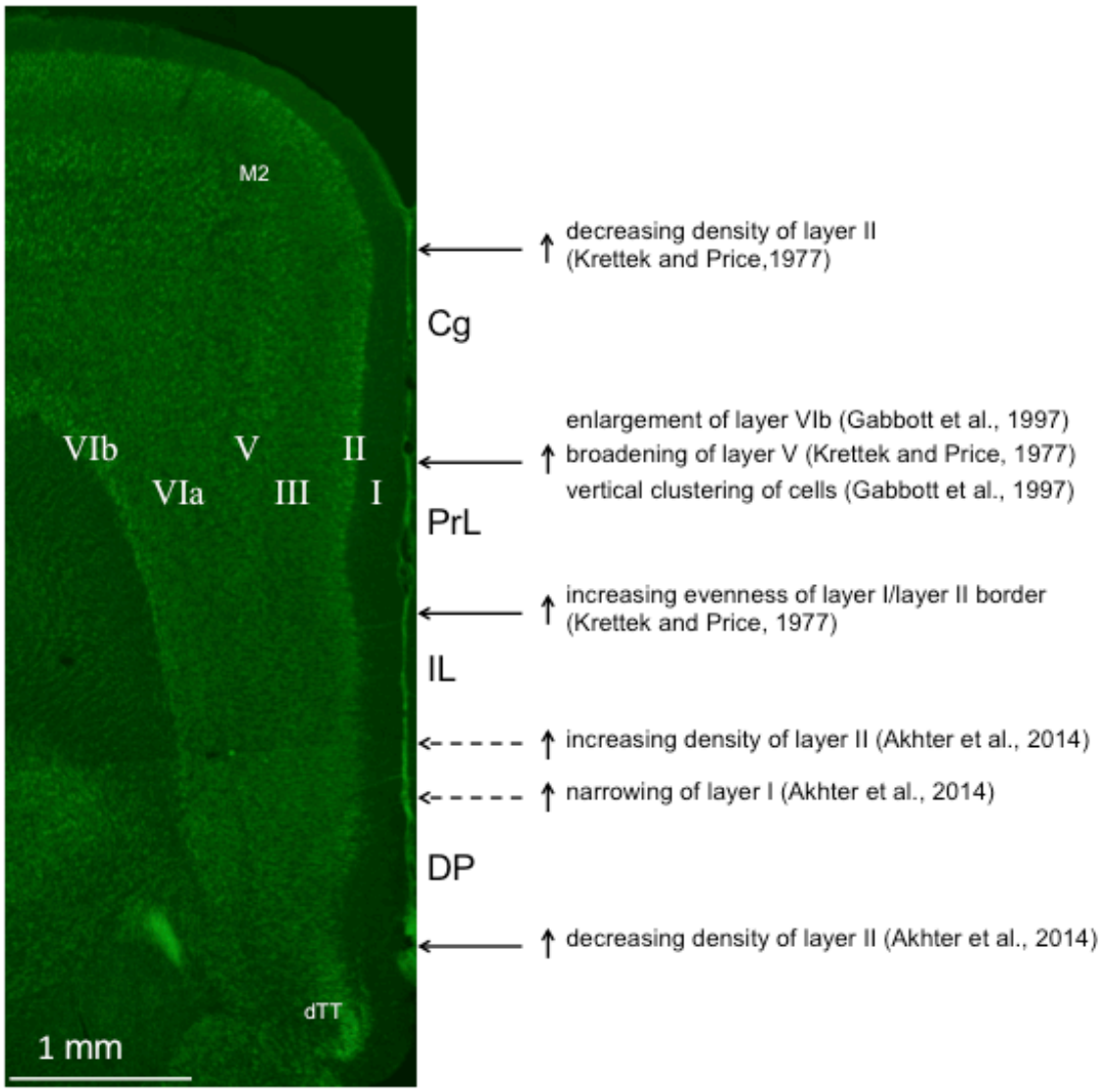

Figure 1.3. Laminar structure of the rat mPFC and sub-regional division. Coronal section through the rat mPFC, stained with green fluorescent Nissl stain to visualise the cytoarchitecture (produced by the author, as described in Chapter 2). The layers are indicated by white roman numerals. The definition of the mPFC subregions is indicated on the right, along with a description of the feature(s) that define the border to the next area above. The mPFC is limited ventrally by the dorsal tenia tecta (dTT), which is part of the olfactory cortex and dorsally by the secondary motor cortex (M2).

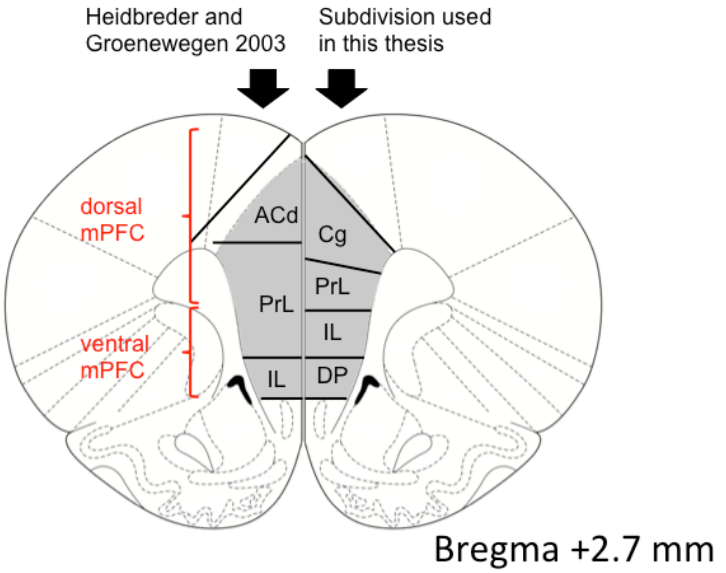

Figure 1.4. Comparison of nomenclatures for mPFC sub-regions. Dorsal-to-ventral distinction of the mPFC as suggested by Heidbreder and Groenewegen (2003), with the mPFC subdivision used in their paper (left hemisphere of brain section schema), and correspondence to the subareas used in this thesis (right hemisphere of brain section schema). Coronal section modified from Paxinos and Watson, 1998, 4th edition, Academic Press.

1.2.5 *A dorsal-to-ventral division of the mPFC*

Heidbreder and Groenewegen (2003) have extensively reviewed evidence for functional and connectivity differences within the mPFC and draw the conclusion that that the main differences are found between the dorsal and the ventral mPFC. They suggest a dorsal–ventral (D-V) distinction as indicated in Figure 1.4. However, they use a different nomenclature for the mPFC subareas. Hence, the sub-regional division used by Heidbreder and Groenewegen (2003) is plotted next to the sub-regional division used in this thesis (Figure 1.4), which is based on the '*Chemoarchitectonic Atlas of the Rat Forebrain'* (Paxinos et al., 1999). The suggested D-V border runs through the middle of the area that Heidbreder and Groenewegen (2003) define as PrL. However, using the nomenclature of Paxinos and colleagues (1999), used in this thesis, the border between dorsal and ventral mPFC is equivalent to the border between PrL and IL; and in this scheme the dorsal mPFC can be defined as Cg and PrL and the ventral mPFC as IL and DP (Figure 1.4). It is this nomenclature I shall refer to throughout this thesis.

1.2.6 *Evidence for a differential role of the DP and the underlying dorsal tenia tecta*

Recent results investigating the mouse connectome have shown differential innervation of the DP region and the dTT (Zingg et al., 2014), which is located just below the DP. The posterior part of the insular cortex sub-network heavily targets all layers of the DP, whereas the temporal association areas only target the dTT, and no part of the mPFC. The dTT is part of the olfactory cortex and the posterior insular cortex is mainly connected with the gustatory thalamic nucleus (Shi and Cassell, 1998). Hence, the temporal association cortex (which itself is connected with visual and auditory cortices), together with the DP and dTT, might form a sensory integration hub. Temporal association areas as well as DP and dTT are also heavily reciprocally connected with the lateral entorhinal cortex (Zingg et al., 2014), which in turn has reciprocal connections with the hippocampus and hence might be involved in memory consolidation.

1.3 Brain rhythms during wakefulness in the prefrontal cortex

Rhythmic electrical activity at a wide range of different frequencies can be observed in the cortex (Roopun et al., 2008) and other brain regions and these 'oscillations' are thought to support communication with other brain regions (Fries, 2005). Brain

oscillations can be recorded from the scalp (electroencephalography [EEG]), from the surface of the brain (electrocorticography [ECoG]), or within the brain, in the extracellular space (local field potential [LFP]). For this thesis, LFP recordings were used to record oscillations. The LFP signal is generated mainly by 'transmembrane current flow in ensembles of neurons' (Kajikawa and Schroeder, 2011). It is thought to represent mainly post-synaptic inhibitory and excitatory currents, as well as intrinsic membrane oscillations and synchronous afterhyperpolarisation (AHP), but also synchronous spiking activity (Buzsáki et al., 2012). The local origin of the LFP is debated: it was originally thought to be several hundred μm, some studies indicate a spread over 2-5 mm, but there is now an indication that the LFP might spread passively by more than a centimetre from the site of origin (Kajikawa and Schroeder, 2011).

Oscillations are commonly divided into particular frequency 'bands', and a large body of work has lead to the association of particular frequency bands with particular cortical functions. It is not possible within this introduction to provide an exhaustive list of all proposed associations between different cortical oscillations and functions, but I will here address some key examples relevant to the body of work reported in this thesis.

So-called 'gamma' (30-80 Hz) and 'beta' (10-30 Hz) oscillations are observed in the visual-prefrontal network, which is involved in the regulation of attention (Benchenane et al., 2011). Communication between mPFC and hippocampus is important for spatial working memory and memory consolidation and is associated with 'theta' (6-10 Hz) oscillations (Benchenane et al., 2011). Oscillatory activity in the 'delta' (0.5-4 Hz) range has been described in the mPFC of behaving rats (Fujisawa and Buzsáki, 2011), where a 4 Hz rhythm in mPFC and VTA was phase coupled to hippocampal theta during a working memory task.

Of particular relevance to this thesis, is the low-frequency (< 1 Hz) synchronous activity seen in the brains of animals during deep sleep when slow, large amplitude fluctuations can be observed in many parts of the brain. This so-called 'slow oscillation' seems to coordinate several faster rhythms during sleep (Steriade et al., 1993c) and is thought to be important for memory consolidation (Ackermann and Rasch, 2014). In the following section, I give a background to sleep stages, followed by a detailed

explanation of the slow oscillation and its involvement in memory consolidation during sleep.

1.4 Sleep and associated brain rhythms

1.4.1 *Sleep stages*

In mammals, sleep can be divided into two main stages, which alternate during a full night of sleep. The first stage is called rapid eye movement (REM) sleep, and is characterised by low-amplitude activity in the neocortex, composed of multiple frequencies similar to waking activity, and large-amplitude theta (4-8 Hz) activity in the hippocampus. This brain state is accompanied by a loss in muscle-tone. The second main sleep stage is simply called non-rapid eye movement (NREM) sleep, and is characterised by the large-amplitude 'slow oscillations' described above. During sleep, both humans and rodents alternate between REM sleep and NREM sleep, but with some key differences. Humans typically sleep during the dark period, and each NREM-REM sleep cycle is about 90 minutes long; hence ~ 4-5 cycles are traversed per night (Figure 1.5 A). Rodents, however, are typically nocturnal animals, sleeping during the light period. Another difference is that rodents have poly-phasic sleep with many very short cycles which are interrupted by phases of wakefulness (Genzel et al., 2014), (Figure 1.5 B). In humans, NREM sleep is further subdivided into four stages, S1-S4; S1 and S2 are classified as light sleep (LS), whereas S3 and S4 are classified as slow wave sleep (SWS) (Genzel et al., 2014). In rodents, however, all NREM sleep is called slow wave sleep (SWS). In rodents it is common to call all NREM sleep slow wave sleep (SWS). However, two sub-stages of SWS have been identified in the literature, called low-amplitude sleep and high-amplitude sleep (Bergmann et al., 1987). Gottesmann (1992) also distinguishes two SWS stages, as well as an intermediate stage between SWS and REM sleep, characterised by high amplitude spindles in the cortex and a low-frequency theta rhythm in hippocampus and occipital cortex.

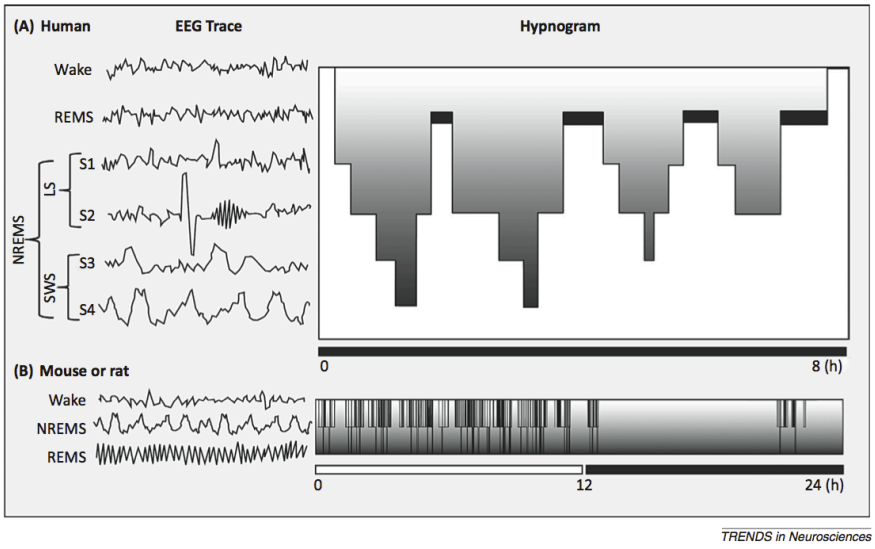

Figure 1.5 Sleep stages in humans and rats. *(A)* Electroencephalogram (EEG) traces recorded during human sleep and a hypnogram showing cycling between the sleep stages during a night of sleep. *(B)* EEG traces as they can be recorded in mouse or rat, and a hypnogram showing polyphasic sleep pattern with many short NREM-REM cycles, interrupted by episodes of wakefulness. Figure from (Genzel et al., 2004).

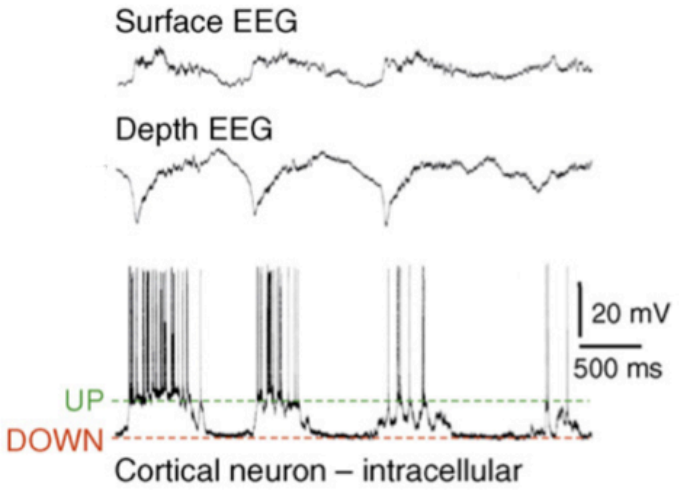

Figure 1.6 Up Down states as seen from an intracellular recording (bottom), from an extracellular electrode at depth (middle), and from a surface EEG recording (top). When recorded within a cell, the Up state is seen as a depolarization (positive deflection), and the Down state as a hyperpolarization (negative deflection). The Up state is accompanied by firing of the cell. In the extracellular depth recording, the polarity is inverted, with the Up state occurring as a negative deflection. In the surface EEG, the Up state is a positive deflection. Figure adapted from (Destexhe et al., 2007).

Both REM sleep-like and SWS-like states can be observed under urethane anaesthesia in rats (Clement et al., 2008) and mice (Pagliardini et al., 2013). In this thesis I report results obtained during the SWS-like state in rats anaesthetized with urethane. Hence, in the following section I give a detailed description of the history, mechanisms and function of slow wave activity (SWA), which is the electrophysiological pattern characterising both SWS and the SWS-like activity observed under anaesthesia.

1.4.2 *Discovery of cortical slow wave activity (SWA)*

Cortical SWA as a *cellular* phenomenon was first reported in 1993 (Steriade et al., 1993d). Steriade and colleagues (1993) recorded intracellular activity from sensory, motor and association cortices of anaesthetised cats and observed an activity pattern characterised by spontaneous fluctuations of the membrane potential between depolarisation (lasting for about a second) – with superimposed action potentials – and hyperpolarisation (lasting up to several seconds) – without action potential firing. The frequency of the observed fluctuations was below 1 Hz, which is slower than previously described brain rhythms, hence this activity was termed the 'slow oscillation (SO)' or 'slow wave activity (SWA)'. In this thesis, 'SWA' is used to denote an LFP recording exhibiting a slow (<1 Hz) oscillation, and 'SO' is used to denote the filtered (< 1Hz) LFP. Nowadays the membrane fluctuations characterising this activity pattern are often referred to as Up (depolarised) and Down (hyperpolarised) states (or 'Up-Down states', UDS) using terminology introduced by Wilson and Kawaguchi (1996).

The Up state is characterised by strong activity of excitatory pyramidal cells as well as inhibitory interneurons, and thus similar to activity in the awake brain (Destexhe et al., 2007). In stark contrast to the awake brain, however, this 'active' Up state is interrupted after about one second by the Down state, with complete cessation of action potential firing in most cortical neurons, lasting for several milliseconds during sleep and several seconds during anaesthesia. This feature of profound activity followed by almost complete neuronal silence is unique to SWA, and is not seen in alert behaviour or during REM sleep. An example of UDS recorded with different electrophysiological techniques is shown in Figure 1.6.

It is worth noting that UDS in human frontal cortex were already evident in the literature (although not identified as such) as early as 1952, in a paper recording

subdural activity from frontal cortex in patients with schizophrenia undergoing frontal lobotomy (Henry and Scoville, 1952). The 'supression-burst activity' (as the authors call UDS) occurred after they surgically disconnected the frontal cortex from deeper structures and persisted in the corticogram for a year after surgery. The persistence of this rhythm over many months (and the comparable results of similar surgeries performed under local anaesthetia) suggested that these phenomena were not just due to the general anaesthetic. Unfortunately, the authors do not elaborate on the state of the patients after this surgery. They do, however, acknowledge the possibility that their disconnection surgery might have induced a sleep-like state in the disconnected part of the brain as they speculate "whether undercut cortex should be regarded as 'asleep'".

1.4.3 *Occurrence of SWA/UDS*

Up-Down states have now been observed *in vivo* in many cortical (Steriade et al., 1993d) and subcortical areas (Wilson and Kawaguchi, 1996; Wolansky, 2006), under different kinds of anaesthesia (Steriade et al., 1993d), during natural sleep (Chauvette et al., 2011) and quiet wakefulness (Petersen et al., 2003). Modelling UDS *in vitro* (Sanchez-Vives and McCormick, 2000; Hughes et al., 2002) and recording from isolated cortical slabs (i.e. pieces of brain tissue that are still in place, but connections to surrounding areas have been severed), Timofeev et al. (2000) have given further insight into the underlying mechanisms.

As UDS are highly synchronous over the whole cortex, they have been documented for many years in surface EEG as K-complexes (Amzica and Steriade, 1997). More recently it has also been possible to observe SWA intra-cranially from humans (Csercsa et al., 2010; Valderrama et al., 2012).

1.4.4 *UDS – cortical or thalamic origin?*

Most studies on UDS have been performed in cortex or the thalamus, in isolation or in combined preparations. It is generally accepted that, in the intact brain, SWA activity involves recruitment of extensively connected cortical and thalamic networks. But there has been a long debate in the literature as to whether the thalamus or the cortex is the 'primary generator' of UDS. An extensive review on thalamo-cortical (TC) oscillations is given in Timofeev and Bazhenov (2005). Here I will describe the key findings fuelling the debate.

Cortical UDS are retained after lesioning of the thalamus (Steriade et al., 1993b), but thalamic UDS are abolished after decortication (Timofeev and Steriade, 1996). Therefore, it was assumed that TC UDS are of cortical origin. This is supported by the studies in which UDS are generated in isolated cortex *in vitro* (Sanchez-Vives and McCormick, 2000; Hughes et al., 2002). However, it has also been possible to generate UDS *in vitro* in thalamic neurons by tonic activation of metabotropic glutamate receptors (Hughes et al., 2002; Blethyn et al., 2006). *In vivo*, thalamic reticular neurons fire a burst, and TC neurons a single spike, at the beginning of the cortical Up state (Contreras and Steriade, 1995). In line with that, UDS in cortical slabs are characterized by longer Down states (Timofeev et al., 2000), perhaps due to the lack of thalamic excitation. Further evidence for a driving role of the thalamus comes from a study showing that thalamic cells fire more selectively at a given Up state phase than cortico-thalamic cells (Ushimaru et al., 2012) Hence, it is most likely that both cortical and thalamic contributions are important for UDS in the intact brain (Crunelli and Hughes, 2010). Indeed, both thalamic and cortical electrical stimulation can give rise to an evoked response sequence in cortical neurons consisting of an excitatory post-synaptic potential (EPSP), a Down state and an Up state (Contreras and Steriade, 1995).

Very recently, contradictory results to (Steriade et al., 1993b) have been published, showing that removal of thalamic input strongly decreases UDS occurrence in the cortex of cats (Lemieux et al., 2014). UDS were fully recovered in the cortex after 30 hours, which explains why Steriade and colleagues (1993b), who recorded two days after lesioning, did not find an effect of thalamic lesioning on UDS (David and Schmiedt, 2014). Hence, the thalamus is crucially involved in cortical UDS in the intact brain. As increased membrane potential fluctuations were observed several hours after thalamic inactivation, it is suggested that plastic processes lead to a recovery of cortical UDS (Lemieux et al., 2014).

1.4.5 *The three-oscillator model of UDS*

Crunelli and Hughes (2010) have unified these findings into a single theory of cortico-thalamic UDS generation, in which UDS in the intact brain emerge from an interplay between three ‘oscillators’ in thalamus and cortex (Crunelli and Hughes, 2010). According to this model, the cortical oscillator is primarily synaptic based (i.e.

relies on synaptic input) and is reciprocally connected with the thalamus (Crunelli and Hughes, 2010). The two thalamic oscillators – the reticular nucleus of the thalamus (TRN), and the TC neurons in different nuclei – are conditional thalamic oscillators, which means they have got the intrinsic ability to oscillate at slow wave frequency (<1 Hz), but only do so when some excitation from cortico-thalamic fibres is provided (Crunelli and Hughes, 2010). Strong interactions between these three oscillators lead to the emergence of UDS (Crunelli and Hughes, 2010); a more detailed description of how this might occur will be given later. First, the two kinds of oscillators (synaptic cortical and intrinsic thalamic) and their mechanism will be described.

UDS consists of regular transitions between two stable states, and these state transitions occur almost synchronously in the cortex of cats (at least as far as 12 mm apart, as shown by Volgushev et al. (2006)). Which cellular mechanisms initiate a transition from one state to another? And how can this remarkable synchrony be explained? Mechanisms of how the switching between Up- and Down state might be brought about, have been investigated *in vitro*, in cortical and thalamic slices.

Cellular mechanisms of cortical UDS in vitro

UDS can be observed *in vitro* in cortical cells when the calcium ion (Ca^{2+}) content in the artificial cerebrospinal fluid is reduced (Sanchez-Vives and McCormick, 2000; Shu et al., 2003; Cunningham et al., 2006; Haider, 2006; Rigas and Castro-Alamancos, 2007). Several mechanisms have been proposed to be involved in UDS generation *in vitro*.

In vitro, the Up state is characterised by strong synaptic activity, both excitatory and inhibitory in nature (Sanchez-Vives and McCormick, 2000; Haider, 2006). Excitation and inhibition is balanced during the middle of the Up state, whereas excitation dominates initiation and cessation of the Up state (Haider, 2006). Both pyramidal cells and interneurons respond more strongly to synaptic inputs when they arrive during an Up state (Shu et al., 2003) and this strong responsiveness might facilitate positive feedback, hence maintaining firing of both cell types during the Up state. Deep layers seem to be better for the generation of UDS, as slices containing layers V and VI reliably generate UDS, whereas slices containing only superficial layers generate weaker or no UDS (Sanchez-Vives and McCormick, 2000).

The Up state is terminated due to the inability of the network to maintain the Up state any longer. More specifically, the high level of activity during the Up state increases activity-dependent (including calcium [Ca^{2+}]-, sodium [Na^{+}]- and adenosine triphosphate [ATP]-dependent) potassium [K^{+}] conductances (Sanchez-Vives and McCormick, 2000; Cunningham et al., 2006). An increasing outward potassium ion current during the Up state might lead to a failure of the re-enforcing network activity ('disfacilitation') and a hyperpolarisation of the cell (Sanchez-Vives and McCormick, 2000). Neuronal responsiveness to a depolarising current injection is diminished for 3-6 s after the end of the previous Up state, which indicates that no new Up state could occur during this time period, explaining the slow rhythmicity of the SWA (Sanchez-Vives and McCormick, 2000). Potassium channels might also be involved in maintaining the Down state and the associated decreased responsiveness of the single cell to network activity (Cunningham et al., 2006).

In summary, although a minority of cortical neurons can generate bistability intrinsically (Le Bon-Jego and Yuste, 2007), the recruitment of increasing numbers of neurons to a synchronous slow rhythm is dependent on synaptic activity (Crunelli and Hughes, 2010).

Cellular mechanisms of thalamic UDS in vitro

In rats, mice and cats, UDS can be observed in almost all TC and TRN neurons when metabotropic glutamate receptors are activated (Crunelli and Hughes, 2010). Activation of these postsynaptic receptors, located on thalamic neurons, decreases the so-called I_{Leak} current below a certain threshold, and the interplay between I_{Leak} and the 'window' component of the low-threshold Ca^{2+} current, I_T, is thought to the be major factor that renders thalamic cells bistable (Crunelli and Hughes, 2010). Other currents contributing are $I_{CAN,}$ and $I_{h,}$, and in TRN also $I_{K(Ca)}$, $I_{K(Na)}$ (Crunelli and Hughes, 2010). Hence, the intrinsic properties of TC and TRN cells enable rhythmic oscillations in their membrane potential at the slow oscillation frequency (Crunelli and Hughes, 2010), as long as there is some excitatory input from the cortex.

The above description of the synaptic mechanisms of Up and Down states does not, however, explain the strong synchronicity of cortical Up and Down state transitions. Hence, the high synchronicity of UDS in the intact brain must emerge form mutual interactions between thalamus and cortex. Indeed, in combined slice preparations as

well as in the whole animal preparation, firing in TRN neurons and TC neurons is strongly-time locked to the Up state onset, and precedes it by a few milliseconds (Contreras and Steriade, 1995; Rigas and Castro-Alamancos, 2007). Recently it has been shown that a lack of thalamic input to the cortex not only decreased UDS cycle frequency, but also nearly abolished action potential firing during the Up states (David et al., 2013).

Interaction of the three oscillators in vivo

The interaction between the three oscillators (cortex, TRN and TC cells) might be as follows. Up states in deep layer (V/VI) cortical cells are transmitted via cortico-thalamic fibres to the thalamus, where they may activate metabotropic glutamate (mGlu) receptors and induce bi-stability in most thalamic neurons (Crunelli and Hughes, 2010). The strong activity at the beginning of thalamic Up state then induces a new Up state in the cortex, which is sustained by strong synaptic activity in cortical cells (Crunelli and Hughes, 2010).

1.4.6 *SWA as a travelling wave*

When activity is recorded over large cortical areas in humans or rodents, spread of SWA can be observed.

A human high-density EEG study reveals a travelling slow wave originating from prefrontal-orbitofrontal regions and propagating in an anterior-posterior direction (Massimini, 2004).

In one animal study, the direction of spread of SWA was observed to be variable: occurring in both anterior and posterior directions (Volgushev et al., 2006). However, using Up state-associated features like increased multi-unit activity (Ruiz-Mejias et al., 2011) or an increase in LFP gamma activity to mark Up state onset (Sheroziya and Timofeev, 2014), the travel of Up state onset in anterior-posterior direction has been confirmed in other animal studies.

It seems that mainly the Up state onset can spread in the form of a travelling wave. The Down state onset, however, appears to be completely synchronous across the cortex

(Sheroziya and Timofeev, 2014), which has been ascribed to cortical recruitment of the thalamus (Volgushev et al., 2006), but see also section 6.2.2.

1.4.7 *Slow waves and nested oscillations*

Three rhythms define the slow wave sleep LFP: these are SO (< 1 Hz); delta (1-4 Hz) oscillations; and spindle (7-15 Hz) oscillations (Steriade, 2006). Faster activity (> 20 Hz) characteristically occurs on the SWA Up state (Steriade, 2006). These faster rhythms, largely in the gamma (30-80 Hz) and high gamma (80-200 Hz) range, are thought to originate in the cortex (Steriade, 2006). I shall discuss the types of activity that occur nested on the Up state and the following paragraphs, and discuss their possible function in section 1.4.9.

Delta (1-4 Hz)

Delta oscillations occur as several ill-defined peaks between 1 and 4 Hz in the human sleep EEG (Steriade, 2006). In cortical cells, activity in the delta range occurs during the Up state as membrane potential fluctuations, but also during the Down state as clock-like action potential firing at delta frequency (Steriade et al., 1993c).

Steriade (2006) initially proposed that delta rhythm generation is associated with a cortical and a thalamic component. The thalamic component is generated in thalamo-cortical neurons through two currents, the hyperpolarization-activated cation current I_h and a low-threshold transient Ca^{2+}current, I_T.

Cortical delta, however, can survive thalamectomy (Steriade et al., 1993c) and can be generated in cortical slices *in vitro* under a low-dopaminergic and low-cholinergic tone (Carracedo et al., 2013), where it originates in layer V. Therefore, thalamo-cortical connections are not necessary for delta rhythm generation, but delta can be generated purely within the cortex.

Spindle (6-15 Hz)

A sleep spindle is a 0.5–3 second long episode of oscillatory activity at ~6-15 Hz (sometimes called ‘sigma-band’). The five to twenty voltage deflections occurring during this period gradually increase in amplitude during the first half and then decrease

during the second half of the spindle episode (a so-called "waxing and waning pattern", that is, however abolished by some anaesthetics (Contreras et al., 1997).

Spindles are generated in the TRN and transmitted to the cortex via thalamo-cortical cells in other thalamic nuclei. (The TRN does not project to the cortex itself – but receives cortical input mainly from primary sensory areas.) The process is described by Lüthi (2014) as follows. During sleep, lack of the depolarising effect of monoamine transmitters decreases the resting membrane potential of TRN cells. This hyperpolarisation activates voltage-gated 'low threshold Ca^{2+} channels', which in turn leads to Ca^{2+} spikes in TRN cells, which quickly depolarize the neuron to the threshold for Na^{+} action potentials. Fast sequences of action potentials (occurring in bursts, with within-burst firing rates >100 Hz) then occur on top of the Ca^{2+} spikes. All TRN cells use the neurotransmitter gamma-aminobutyric acid (GABA), and their inhibitory effect on thalamo-cortical cells produces rhythmic inhibitory post-synaptic potentials (IPSPs) at spindle frequency (Steriade et al., 1993c) as well as rebound-burst discharge.

The initial waxing phase is associated with recruitment of increasing numbers of cells into the rhythm. TC cell bursting can recruit 30% of pyramidal and 80% of fast spiking interneurons (Peyrache et al., 2011). Several intrinsic and synaptic mechanisms are suggested for spindle termination. Lateral inhibition between TRN cells dampens spindle activity. In both thalamo-cortical and TRN cells, accumulated Ca^{2+} triggers intrinsic mechanisms that reduce the likelihood of bursting in these cells (Lüthi, 2014), leading to the 'waning' phase. In thalamo-cortical cells, this is mediated through an activation of hyperpolarisation-activated cation-selective (HCN) channels; in TRN cells, through sequestration of Ca^{2+} and recruitment of Na^{+}-dependent K^{+} channels.

Gamma (30-80 Hz)

Nested high-frequency oscillations in the gamma frequency riding on the cortical Up states have been seen *in vivo* (Steriade et al., 1996; Ruiz-Mejias et al., 2011), *in vitro* (Compte et al., 2008), and in human scalp and intracranial EEG recordings during sleep (Le Van Quyen et al., 2010; Valderrama et al., 2012). Steriade (2006) suggested that cortical fast rhythmic bursting (FRB) neurons (also called 'chattering cells') would be well suited to generate gamma oscillations on the Up state as they are involved in cortical gamma rhythm generation (Cunningham et al., 2004; Cardin, 2005) and they

project to the thalamus, where neuronal firing is in phase with the cortical gamma oscillations.

In vitro, it has been shown that during Up states, inhibitory barrages show higher power in the gamma range than excitatory-dominated barrages, and that inhibitory synaptic potentials often synchronously inhibit pyramidal cells in their vicinity, suggesting a role of inhibitory interneurons in the Up-state associated gamma rhythm (Hasenstaub et al., 2005). Rhythmic trains of $GABA_A$ receptor-mediated IPSPs in pyramidal cells, induced by drive of inhibitory interneurons, are implicated in any gamma rhythm (Whittington et al., 2011), not only in the transient one observed during the Up state. Fast, rhythmic inhibition is enabled by gap-junction mediated communication of several subclasses of interneurons (Whittington and Traub, 2003). Of particular importance for gamma rhythm generation are fast-spiking inhibitory interneurons (Whittington et al., 1995). The involvement of a specific class of inhibitory interneurons, which expresses the Ca^{2+} buffer parvalbumin (PV), has been indicated (Fuchs et al., 2007; Middleton et al., 2008; Carlen et al., 2012) and confirmed using optogenetics (Cardin et al., 2009; Sohal et al., 2009). Specifically *N*-methyl-*D*-aspartate (NMDA) receptors on these PV^+ (PV expressing) interneurons neurons are critically involved in gamma generation (Carlen et al., 2012). Hasenstaub and colleagues (2005) suggest that the activity of fast-spiking interneurons during SWA is driven or enhanced by interactions with chattering cells, which can also generate higher-frequency oscillations (Gray and McCormick, 1996).

Different mechanisms might be involved in generating gamma oscillations at different frequencies. *In vitro*, it has been shown that in rat auditory cortex 30-45 Hz oscillations in supragranular layers are gap junction-dependent, whereas 50-80 Hz oscillations occurring in layer IV are dependent on pyramidal cell-interneuron interactions and strong glutamatergic excitation (Ainsworth et al., 2011).

However, one recent finding contradicts the assumption of cortical origin of gamma activity during the Up state. Thalamic inactivation reduces SWA as well as associated fast (>10 Hz) oscillations (Lemieux et al., 2014). SWA starts to recover after 12 h and nearly fully recovers over a period of 30 hours, but the Up-state associated fast oscillations do not recover over 30 hours (Lemieux et al., 2014). This indicates that the recovered SWA is generated by different mechanisms. Lemieux et al. (2014) suggest

that increased intrinsic oscillations, but also thalamic input is crucial for the occurrence of fast Up state-associated activity in the intact brain *in vivo*, and that no mechanism is in place to recover this fast network activity after thalamic inactivation.

Indeed, cortico-thalamic neurons can oscillate in the gamma frequency band when depolarised beyond -45 mV, as show *in vitro* (Pedroarena and Llinás, 1997), and during early postnatal development, gamma oscillations synchronise thalamus and cortex (Minlebaev et al., 2011).

Oscillatory activity with frequencies >80 Hz

There are many inconsistencies in the literature as to the nomenclature of brain rhythms with frequencies >80 Hz. Most commonly, such rhythms are called 'very fast oscillations' (Traub et al., 2010; Simon et al., 2013) or 'ultra-fast rhythms' (Steriade, 2006). There is then a further subdivision into 'fast gamma' or 'high gamma' (~80-140/150 Hz), and 'ripples' (>140/150 Hz), and sometimes even 'fast ripples' (>250 Hz) are distinguished.

The hippocampal Up state is characterised by ripples (>140 Hz) (Sullivan et al., 2011), and activity in the high gamma/ripple range (80-200 Hz) occurs during the Up state in the neocortex (Grenier et al., 2001). Activity in the high gamma/ripple range (80-200 Hz) is still present in cortical slabs, suggesting a cortical origin (Grenier et al., 2001). $GABA_A$ receptor-mediated inhibition, however, that is critical for generating gamma, breaks down at frequencies above 90 Hz (Traub et al., 1996), hence cannot be involved in the generation of high gamma/ripple activity. FRB cells showed the strongest ripple-associated firing, but also fast spiking neurons (presumed GABAergic interneurons) fired phase-locked with ripples (Grenier et al., 2001). Hence, excitation as well as inhibition is likely to play a role in ripple generation (Grenier et al., 2001). Ripple-associated inhibition may be regulated by $GABA_B$ receptors (Hollnagel et al., 2014).

Excitation may be mediated by electrical coupling between pyramidal cells, as suggested by modelling (Traub et al., 2010). Recently, it has been confirmed that gap junction networks can generate ripple (>150 Hz) oscillations in human cortex (Simon et al., 2013). In hippocampus, it has been shown that fast gamma (90-140 Hz) oscillations share similar mechanisms to ripples (>140 Hz) (Sullivan et al., 2011), and that PV^+ interneurons likely play a role in ripple induction (Klausberger et al., 2003; Chiovini et al., 2014). However, in awake monkeys it has been shown that gamma (30-80 Hz) and

high gamma (80-150 Hz) oscillations are distinct phenomena with a different origin (Ray and Maunsell, 2011).

1.4.8 *Function of SWA*

Slow wave Up states have been described as "fragments of wakefulness" because of their similarity to the awake brain state (Destexhe et al., 2007). It has been suggested that Up states serve internal processing and are involved in memory transfer from the hippocampus to neocortex (Destexhe et al., 2007). Globally-occurring UDS are thought to provide a "temporal frame for the dialogue between the neocortex and subcortical structures that is necessary for redistributing memories for long-term storage" (Diekelmann and Born, 2010). The dialogue between different brain structures during the Up state might occur via coordinated spiking activity (Ji and Wilson, 2007), or via oscillatory activity (Siapas and Wilson, 1998; Sirota et al., 2003), or a combination of both.

Reactivation in hippocampus and cortex

Many studies have shown that spike sequences that occur during wakefulness (e.g. during a behavioural task) are replayed in the subsequent sleep or rest periods in hippocampus (Wilson and McNaughton, 1994; Skaggs and McNaughton, 1996; Shen et al., 1998; Nádasdy et al., 1999; O'Neill et al., 2008) and neocortex (Hoffman and McNaughton, 2002). Many rodent studies report replay of task-related activity during sleep in the prefrontal cortex (Euston et al., 2007; Peyrache et al., 2009; Johnson et al., 2010).

Reactivation dialogue between hippocampus and cortex

Spike-oscillatory coupling has been reported between cortex and hippocampus: Replay of spike sequences in the PFC seems to occur preferentially during hippocampal ripples (Peyrache et al., 2009). Cortex and hippocampus also show cross-frequency coupling of oscillations, with neocortical spindles and hippocampal fast ripples occurring simultaneously during sleep (Siapas and Wilson, 1998; Sirota et al., 2003). In addition, cortical spike sequences are replayed in coordination with hippocampal spiking activity. Ji and Wilson (2007) show that firing patterns seen during awake experience are replayed in hippocampus and visual cortex in a coordinated manner.

Coordinated activity between hippocampus and cortex can be observed using different measures, but which area is driving this dialogue? Prefrontal cortex spindles occur simultaneously with hippocampal ripples (Siapas and Wilson, 1998; Sirota et al., 2003). Prefrontal Up state-associated multi-unit activity (MUA), precedes sharp wave-ripples in the hippocampus (Mölle et al., 2006). Conversely, recordings from naturally sleeping animals show that hippocampal CA1 (*Cornu Ammonis* 1) pyramidal cell firing precedes mPFC cell firing, and that this spike-timing relationship only exists during SWS, not during REM sleep (Wierzynski et al., 2009). PFC replay occurs during hippocampal sharp-wave-ripples, peaking 40 ms after their occurrence, and preceding prefrontal spindles by 1 s (Peyrache et al., 2009). Another study finds that the mPFC response to hippocampal sleep spindles is layer- and cell-type specific, as interneurons are more strongly affected than pyramidal neurons (Peyrache et al., 2011). Hence, PFC and hippocampus strongly interact during sleep, likely with interactions in both directions.

Ji and Wilson (2007), looking at visual cortex and hippocampus, have shown that a change in either area can precede a change in the other area, and thus suggest a bi-directional model, where cortical UDS trigger hippocampal UDS, during which the "memory trace" replay occurs, which is then transferred back to the cortical region (Ji and Wilson, 2007),

Internal processing

Slow wave sleep appears to be a network behaviour that might favour internal processing over the processing of inputs from the environment. Whisker stimulation during the Up state results in a smaller amplitude of sub-threshold response than during the Down state and sensory evoked action potentials are supressed in the Up state (Petersen et al., 2003) . It seems that the "sensory periphery competes with intra-cortical processing" (Petersen et al., 2003). This is confirmed by another study finding that Up states decrease responsiveness to whisker deflection (compared to Down states, Hasenstaub et al., 2007). Hasenstaub and colleagues (2007) argue that during the Up state the responsiveness of GABAergic neurons is higher compared to that of pyramidal cells, which means that thalamic inputs can activate GABAergic interneurons (Hasenstaub et al., 2007). Prolonged stimulation, however, decreased responsiveness during the Up state (Hasenstaub et al., 2007).

UDS and plasticity

A more active role for UDS than just blocking out thalamic input, has been proposed by Destexhe and colleagues (2007). He suggests that bursts in TC neurons not only trigger Up states in cortical neurons, but also synaptic plasticity. Indeed, some years later it was shown that evoked potentials in the somatosensory cortex induced by thalamic stimulation at 1 Hz are potentiated after a period of SWS (Chauvette et al., 2012) *in vivo*. The authors investigated the mechanisms behind this effect *in vitro*, showing that the effect is a calcium-dependent post-synaptic process involving co-activation of α-amino-3-hydroxy-5-methyl-4-isoxazolepropionic acid (AMPA) and NMDA glutamate receptors (Chauvette et al., 2012). Because these components are also involved in post-synaptic long-term potentiation, the authors argue that long-term potentiation occurs during SWA (Chauvette et al., 2012).

Which SWA features are related to replay?

A temporal relation between replay of spindles and ripples has already been described. But are there particular characteristics of SWA that might facilitate replay? A recent study shows that certain features of slow wave sleep correlate with several measures of reactivation (Johnson et al., 2010). These measures assess similarity between activity during a task and a subsequent sleep period. The number of Down states and the number of high-voltage spindles in the mPFC correlate positively with two independent replay measures in each animal.

SWA features and memory performance in humans

The link between SWA and memory consolidation has been investigated in many human EEG studies. Slow oscillation amplitude and Up state length (Heib et al., 2013) are positively correlated with declarative memory improvement, as is power in the sigma (12-16 Hz) band (Holz et al., 2012), which is the frequency at which spindles occur. SWA and sigma band activity have also been linked to procedural memory (Huber et al., 2004; Holz et al., 2012).

Cortical SWA can also be experimentally manipulated in humans. Immobilisation of the arm (which should induce synaptic depression in the corresponding areas in motor cortex) decreases SWA (Huber et al., 2006), whereas trans-cranial direct current

stimulation (tDCS) can enhance SWA as well as spindle activity in the frontal cortex and lead to memory improvements (Marshall et al., 2006).

1.4.9 *Function of nested fast oscillations during SWA*

The link between SWA and memory is supported by strong evidence. Which part the slow oscillation itself plays, and what the role of the nested fast oscillations are, is not yet known. Most research so far has focused on sleep spindles.

Function of sleep spindles

Spindles play a crucial role in sensory gating. As already described, spindles recorded in the cortex are generated in the thalamus (Lüthi, 2014), which is the brain's sensory relay region, through which all sensory information needs to pass before it reaches the cortex. Cortical activation in response to sensory stimulation is strongly decreased when stimuli are applied during cortical spindles, compared to spindle-free NREM sleep (Dang-Vu et al., 2011; Schabus et al., 2012), suggesting that the thalamus can determine when sensory information reaches the cortex.

As spindles mostly occur during Up states (Mölle et al., 2002; Sirota et al., 2003; Isomura et al., 2006; Mölle et al., 2006; Steriade, 2006), it has been suggested that the cortex (more specifically, the cortical Up state onset) might trigger spindle initiation in the thalamus (Lüthi, 2014). Spindle length, however is dependent on the thalamic network state (Barthó et al., 2014), suggesting that, while the cortex might trigger the closing of thalamic gates, the thalamus determines for how long the gates are shut. However, Up states have also been shown to protect the cortex from thalamic inputs (Watson et al., 2008). Indeed, a recent study investigating responses to auditory stimuli during NREM sleep shows that responses in higher cortical areas, such as the temporal gyrus are diminished or abolished by both spindles and the negative deflection of the slow oscillation (Schabus et al., 2012). In contrast, in the primary sensory cortex, only spindles, but not the slow oscillation phase modulate the response to auditory stimuli (Schabus et al., 2012).

In summary, spindles are involved in sensory gating, but care has to be taken when interpreting such results, as spindles occur during the Up state, which can also reduce responses to thalamic or sensory stimulation in some brain regions.

Several studies have linked spindles to plasticity and memory. Spindles can induce long-term potentiation (LTP) in cortex (Rosanova and Ulrich, 2005) and thalamus (Astori and Lüthi, 2013), and have been linked to improvements in declarative memory performance (Gais et al., 2002; Schabus et al., 2004). Many studies report relations between spindle activity and visuomotor learning (Fogel et al., 2007; Tamaki et al., 2008) and motor sequence learning (Morin et al., 2008; Tamaki et al., 2013).

Spindle activity is reduced in schizophrenia (Ferrarelli et al., 2007; 2010; Keshavan et al., 2011; Wamsley et al., 2012) and cortical spindle timing in relation to hippocampal activity is disrupted in an animal model of schizophrenia (Phillips et al., 2012). Disruption of sleep spindle activity in schizophrenia patients is correlated with deficits in attention and reasoning (Keshavan et al., 2011) as well as the lack of overnight-improvement in a motor task (Wamsley et al., 2012), suggesting a relation to the cognitive deficits in this disorder.

Function of gamma and high gamma activity

The role of the transient gamma and high gamma activity that occurs during NREM sleep on the Up state is not yet clear. However, gamma and high gamma oscillations serve important cognitive functions during wakefulness, and have been linked to memory encoding and retrieval.

Gamma oscillations during wakefulness are associated with sensory processing (Cardin et al., 2009), object recognition (Martinovic et al., 2007; 2008), attention (Tiitinen et al., 1993; Debener et al., 2003; Sokolov et al., 2004; Bauer et al., 2006) and working memory (Howard, 2003; Haenschel et al., 2009). Human hippocampal gamma (30-100 Hz) activity has recently been linked to encoding of novelty in the environment (Park et al., 2014). Gamma activity is implicated in memory encoding (Fell et al., 2003; Osipova, 2006; Jutras et al., 2009; Tort et al., 2009) and memory retrieval (Montgomery and Buzsáki, 2007). In rats, slow gamma (20-50 Hz) activity has been linked to hippocampal memory replay during rest (Carr et al., 2012). Subsequently, fast gamma activity (60-100 Hz) has been associated with retrospective coding (reflecting retrieval), and slow gamma activity (25-55 Hz) with prospective coding (reflecting encoding) in the hippocampus (Bieri et al., 2014).

High gamma activity during wakefulness has been implicated in encoding and recall of recognition memory (Kucewicz et al., 2014) as well as in working memory

(Yamamoto et al., 2014). High gamma band (80-150 Hz) activity has also been related to selective attention (Ray et al., 2008).

Hence, gamma and high gamma activity are strongly implicated in memory encoding and retrieval during wakefulness. As gamma and high gamma activity also occur on the slow wave Up state, the facilitatory effect of SWA on memory processes, might partly be linked to these faster oscillations.

In summary, the link between SWA and memory is supported by strong evidence, and the Up state-associated fast oscillations might be involved in coordinating the reactivation of brain regions (Fries, 2005). The frequency and power of oscillations are known to be related to the level of neuromodulators, such as acetylcholine (Keita et al., 2000) and the monoamines dopamine, noradrenaline and serotonin (Wójtowicz et al., 2009). It is plausible that, through their actions on oscillations, neuromodulators might be able to influence information transfer during sleep (Destexhe et al., 2007). Dopamine is a potent modulator of PFC activity. In the following, dopamine pathways and the effects of dopamine in the brain will be described.

1.5 Dopamine

1.5.1 *Dopamine pathways of the brain*

Dopaminergic neuromodulation in the brain is predominantly based around three major pathways, all originating in the midbrain: the nigrostriatal, the mesolimbic and the mesocortical pathway. The *nigrostriatal pathway* originates in the substantia nigra (SN), terminates mainly in the dorsal striatum, and is involved in functions such as movement initiation and sensory motor integration. The *mesolimbic pathway* originates in the ventral tegmental area (VTA) and SN and supplies limbic structures such as ventral striatum, hippocampus and amygdala, and septum. The *mesocortical pathway* extends from the VTA (and to some extend from SN) to the temporal, parietal and prefrontal cortices. Mesolimbic and mesocortical pathways are involved in functions such as motivation, attention and reward (Abi-Dargham et al.,2003).

In rats, the dopaminergic innervation of the PFC mainly originates in the VTA (Björklund and Dunnett, 2007), so I will focus on this region in the following.

The VTA can fire in two distinct modes: regular firing and burst firing (Bunney et al., 1973). A change from regular firing to burst firing is associated with increased dopamine release from VTA neurons (Schultz, 2007).

1.5.2 *Projections from the VTA to the mPFC*

The VTA sends ipsilateral and contralateral projections to the mPFC (Oades and Halliday, 1987). The entire mPFC is innervated by dopaminergic fibres, mainly targeting layers III-VI (Descarries et al., 1987; Van Eden et al., 1987). The densest innervation is observed in layer VI of the ventral mPFC (IL and DP) (Van Eden et al., 1987). The dorsal VTA projects to the ventral mPFC, and the ventral VTA to the dorsal mPFC (Deutch, 1993).

Sixty percent of neurons in the VTA are dopaminergic neurons (Gu, 2010), with the remainder consisting of GABAergic (Carr and Sesack, 2000) and glutamatergic (Yamaguchi et al., 2007; Gorelova et al., 2012) neurons. Dopaminergic fibres from the VTA to the cortex are unmyelinated, whereas non-dopaminergic fibres are myelinated, leading to different conduction velocities (Seamans and Yang, 2004) from VTA to the PFC. In addition, co-release of glutamate from dopamine terminals has also been reported (Stuber et al., 2010).

1.5.3 *Dopamine receptors*

Once released, dopamine can act on five different types of dopamine receptor (D_1-D_5), all of them being G-protein coupled metabotropic receptors. Dopamine receptors are classified into two groups, which differ in structure and biochemical properties: D_1-like receptors (D_1 and D_5) and D_2-like receptors (D_2, D_3, D_4). All dopamine receptors can be located post-synaptically; D_2 and D_4 receptors can also be located presynaptically and act as autoreceptors, downregulating dopamine release.

Dopamine receptors are heterogeneously distributed in the brain, which leads to regional differences in dopamine effects. In the cortex, the D_1 receptor is the most ubiquitous receptor, followed by D_2, D_4 and D_5 receptors, which are all expressed at low levels (Tritsch and Sabatini, 2012). In rat, cortical expression of D_4 receptors is higher than expression of D_2 and D_3 receptors (Ariano et al., 1997). Similar results have been

obtained in monkey PFC, where D_4 receptor expression is particularly high in PV^+ cells (~60% of PV^+ cells express D_4 receptors, as opposed to ~20% of PV^+ cells express D_2 receptors) (de Almeida and Mengod, 2010). D_1 receptors are expressed in 30-60% of layer II to VI interneurons, in 20-40% of layer V/VI pyramidal cells, and in less that 20% of layer II/III pyramidal cells (Tritsch and Sabatini, 2012). D_2 receptors are expressed in 25% of layer V/VI pyramidal cells, in 20% of layer II to VI interneurons, and in less than 10% of layer II/III pyramidal neurons (Tritsch and Sabatini, 2012).

1.5.4 *Effects of dopamine in the brain*

Dopamine initiates intracellular signalling cascades

Activation of dopamine receptors triggers a wide range of different intracellular signalling cascades (described in great detail in Missale et al., 1998). The D_1 and D_2 family of receptors activate different G-proteins.

D_1-like receptors activate $G\alpha_s$ and $G\alpha_{olf}$, which activate the enzyme adenylyl cyclase, leading to cyclic adenosine monophosphate (cAMP) production, and activation of protein kinase A (PKA). PKA in turn exerts effects on ionotropic glutamate and GABA receptors, as well as on K^+, Na^+ and Ca^{2+} channels (Tritsch and Sabatini, 2012).

D_2-like receptors, once activated, activate $G\alpha_i$ and $G\alpha_o$. These G-proteins inhibit adenylyl cyclase, hence reducing cAMP and PKA. There are, however, also cAMP/PKA-independent pathways, through which dopamine can act on Ca^{2+} and K^+ channels, which will not be described here (for a description see Tritsch and Sabatini (2012).

Through these intracellular signalling cascades, dopamine affects synaptic communication at different stages. Firstly, dopamine can alter the probability of neurotransmitter release from the pre-synaptic terminal (Figure 1.7). Second, dopamine can control number and properties of several post-synaptic receptors, hence influence the response strength in the post-synaptic neuron (Figure 1.7). Third, dopamine can affect excitability of the pre-and post-synaptic membranes (Figure 1.7).

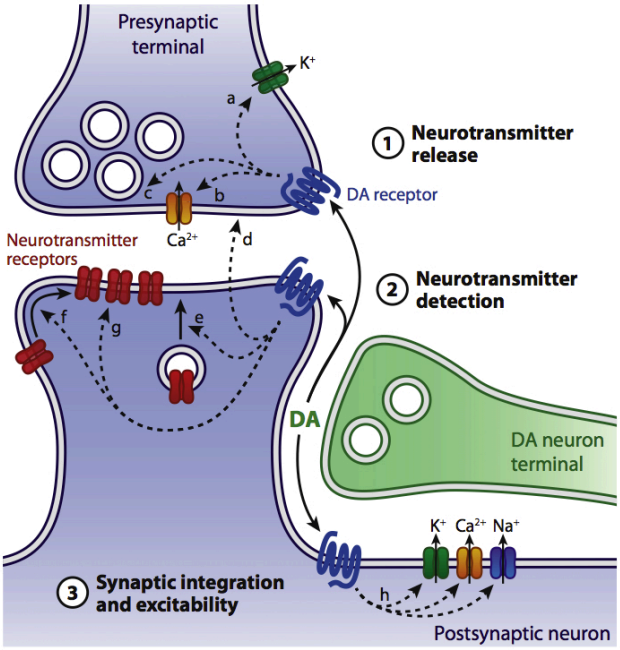

Figure 1.7. Modulation of synaptic transmission by dopamine.
Dopamine affects neurotransmitter release by regulating the excitability of the presynaptic terminal (a), Ca^{2+} influx (b), and effects on the vesicular release machinery (c). This can be mediated via presynaptic as well as postsynaptic receptors as postsynaptic receptors can induce release of retrograde signaling molecules (d). Dopamine also affects neurotransmitter action at the postsynaptic membrane. This can be achieved by modulation of receptor insertion into the membrane (e), recruitment of receptors to the synapse (f), or through effects on the properties of receptors that are already located in the synaptic membrane (g). Dopamine also affects the excitability of pre- and post-synaptic membranes by its effects on ion channels that control resting potential, Ca^{2+} influx, and action potential properties (h). Figure and legend adapted from Tritsch and Sabatini (2012).

Modulation of neurotransmitter release

Dopamine receptors can be expressed in pyramidal cells and fast-spiking interneurons (Tritsch and Sabatini, 2012). Dopamine's effects on neurotransmitter release have been investigated at synapses between these cells, and so far dopamine has been found to decrease release of other neurotransmitters at the investigated cortical synapses, mediated by D_1-like and D_2-like receptors (Tritsch and Sabatini, 2012).

Modulation of synaptic responses

Through its various effects on the receptor composition at the post-synaptic membrane, dopamine is a powerful modulator of post-synaptic responses. *In vitro*, dopamine increases NMDA receptor-mediated excitatory post-synaptic currents (EPSCs) and GABA inhibitory post-synaptic currents (IPSCs), when applied at low concentrations, via D_1-like receptors. Conversely, dopamine reduces these currents, when applied at high concentrations, via $D_{2,3}$ receptors (Seamans and Yang, 2004). D_4 receptor agonist application decreases NMDA receptor-mediated EPSC amplitude (Wang et al., 2003), and $GABA_A$ currents in isolated and cultured PFC pyramidal cells (Wang et al., 2002). D_4 receptor activation decreases AMPA-mediated EPSCs in PFC interneurons (Yuen and Yan, 2009).

Modulation of neuronal excitability

Dopamine affects neuronal excitability via several ionic mechanisms, including a slowly inactivating/persistent Na^+ current (I_{NaP}), a slowly inactivating (outward) K^+ current, which regulates the firing threshold of PFC neurons, and various Ca^{2+} currents (Seamans and Yang, 2004). In most studies, dopamine enhances excitability of pyramidal cells and fast spiking interneurons (Tritsch and Sabatini, 2012).

Modulation of firing rates

Dopamine's effects can also be observed as changes in neuronal firing rates. *In vivo*, iontophoretic dopamine application into the mPFC as well as stimulation of the VTA, inhibits firing in the PFC. Both effects could be blocked by a $D_{2,3}$ receptor antagonist as well as a $GABA_A$ antagonist (Pirot et al., 1992) in most cases, suggesting involvement of local inhibitory interneurons, as well as GABAergic VTA neurons (Pirot et al., 1992). However, it is thought that the VTA stimulation-induced decrease in firing is not dopamine D_2 receptor-mediated, but is due to GABA release. The D_2 receptor block, however, might increase excitability and in turn obstruct the inhibitory effect of GABAergic inputs (Seamans and Yang, 2004).

The interaction between these various effects of dopamine on the synapse can lead to the plethora of effects that dopamine can induce. For example, $D_{1,5}$ receptor activation on fast spiking interneurons leads to suppression of a K^+ leak current (Gorelova et al., 2002) which depolarised the membrane potential of these cells and thus increases their excitability. The increased excitability of fast spiking interneurons might explain the increase in IPSPs observed in pyramidal cells and finally the decrease pyramidal cell firing rate (Gorelova et al., 2002).

Dopamine can also affect local field potential oscillations, which will be discussed in more detail in the introduction of Chapter 5. Finally, it is worth noting that dopamine receptors exist not only in the brain and dopamine has a number of peripheral effects, for example on the peripheral vascular system (Missale et al., 1998).

1.5.5 *PFC functions regulated by dopamine*

In the PFC, dopamine regulates executive functions (spatial working memory (Sawaguchi and Goldman-Rakic, 1991; 1994), behavioral flexibility (Floresco et al., 2006), decision making (Floresco and Magyar, 2006), feeding behaviour (Land et al., 2014), learning (Puig and Miller, 2012) and attention (Kennerley and Wallis, 2009).

Several studies have clarified differential receptor involvement in executive functions. It has been suggested that working memory is mainly D_1 receptor-mediated; behavioural flexibility is mediated by interactions between D_1 and D_2 receptors; and decision making is mediated by D_2, D_3 and D_4 receptors (Floresco and Magyar, 2006).

Stimulus-response learning involves D_1 and D_2 receptors (Puig and Miller, 2012; 2014), whereas emotional associative learning involves activation of D_4 receptors (Laviolette, 2005). However, although dopamine signalling controls attention during working memory, it is not thought to transmit any actual information about the memory content (e.g prediction error) – rather this is thought to be glutamate-dependent (Seamans and Yang, 2004).

1.5.6 *Features of dopamine action*

Dopaminergic modulation has got many interesting features, which are described in detail in (Seamans and Yang, 2004). The most important features are briefly summarised here:

1.) The dependence of performance on D_1 receptor activation is described by an 'inverted U function', with an intermediate level of stimulation being beneficial for performance, but not enough or too much stimulation having adverse effects on performance (Goldman-Rakic et al., 2000; Chen and Yang, 2002).

2.) Dopamine can have biphasic effects, for example an initial decrease in a response measure, followed by an increase in the same measure.

3.) Dopamine can exert opposing effects, via a single receptor and different cell types, but also via different receptors on the same cell type.

4.) Dopamine can have different effects depending on the 'dopaminergic tone' (background level of endogenous dopamine).

Dopamine's effects on sleep as well as on oscillatory activity will be discussed in the introductions to chapters 4 and 5, respectively.

1.5.7 *Dopamine disorders and sleep disturbances*

Dopamine dysfunction is implicated in many disorders, such as Parkinson's disease (PD), attention deficit-hyperactivity disorder (ADHD), schizophrenia (SCZ), and Tourette's syndrome. All of these disorders are associated with sleep deficits (Rye, 2004; Adler, 2005; De Cock et al., 2008; Suzuki et al., 2011; Krystal, 2012; Ganelin-Cohen and Ashkenasi, 2013; Ghosh et al., 2014). Most commonly these consist of difficulties in initiating and maintaining sleep (insomnia), with excessive daytime sleepiness. Often (in PD and SCZ), sleep disturbances precede the onset of 'classical' symptoms (Adler, 2005; Krystal, 2012).

In SCZ, specific sleep abnormalities have been linked to specific symptoms. 'Positive symptoms', such as hallucinations and delusions are associated with shorter REM latency, longer sleep onset latency, and decreased sleep efficiency (time asleep/time in bed), whereas 'negative symptoms', such as emotional flattening, poverty of speech and attention problems, have been linked to lower slow wave EEG amplitude during NREM sleep.

1.6 Thesis overview

In Chapter 2, I describe the animal preparation for electrophysiological experiments performed in urethane anaesthetised rats, the histological procedures used to verify electrode position, and data analysis methods used for this thesis.

The rat mPFC is a heterogeneous region, with four sub-regions that have different structure, projections and serve different functions. However, few studies account for these sub-regional differences. In Chapter 3, I present a detailed characterisation of SWA in the mPFC of urethane-anaesthetised rats and compare the mPFC sub-regions with respect to their slow and fast oscillations during SWA.

Recently, it has been shown in rats that neuronal activity in the VTA increases at the transition from SWS to REM sleep (Dahan et al., 2006), and that tonic dopamine levels are increased during REM sleep in the PFC (Léna et al., 2005). In chapter 4 I investigate how electrical VTA stimulation affects mPFC SWS. I will show that electrical stimulation of the VTA can evoke a transition from SWA to REM sleep-like forebrain activity in anaesthetised rats.

Dopamine modulates fast mPFC oscillations during wakefulness, however, few studies have investigated how dopamine might affect nested fast oscillation during SWA. In chapter 5 I present my results from experiments, in which amphetamine and dopaminergic agonists were injected systemically to investigate their effects on the fast nested oscillations occurring during SWA.

I will discuss details regarding dopaminergic modulation of sleep-wake states and dopaminergic modulation of fast network oscillations in the introductions to Chapter 4 and 5, respectively.

Chapter 2. Methods

Data presented in this thesis stem from *in vivo* experiments in anaesthetised rats. All surgical procedures were performed according to the UK [Animals (Scientific Procedures) Act, 1986, and revised European Directive 2010/63/EU]. All experiments presented in this thesis were performed by myself, initially being trained by my supervisors Sasha Gartside, Adrian Rees and Fiona LeBeau, and later supported when necessary.

2.1 Animals

Male Hooded Lister rats were supplied by Charles River laboratories (Margate, Kent, UK), and housed at Newcastle University's Comparative Biology Centre in a temperature- and humidity-controlled environment. Rats were kept in an enriched environment under a 12 hour light:dark cycle and had access to food and water *ad libitum*. Experiments were performed during daytime hours (the light phase in the animal facility, which the rats spent mostly sleeping). Rats were housed in cages of two to four and were usually allowed a week of acclimatisation before the experiment.

2.2 Electrophysiological recordings under anaesthesia

2.2.1 *Anaesthesia*

Rats weighing 250-330 g were anesthetised with urethane (Sigma-Aldrich). An initial dose of 1.5-1.9 g/kg was administered by intraperitoneal injection (i.p.). A top-up dose of 0.5 g/kg i.p. was given every half an hour until a deep anaesthesia level (confirmed by absence of the pedal withdrawal reflex) was achieved. This anaesthesia level induced continuous slow wave sleep-like activity without sleep state changes. However, if state changes occurred spontaneously, or in response to a pedal pinch or an injection, during the experiment, an additional dose of urethane was administered (0.25 mg/kg urethane i.p.).

2.2.2 *Surgery*

After induction of anaesthesia and confirmation of sufficient depth of the anaesthesia, the animal was fixed in a stereotaxic frame (Kopf, Tujunga, CA, USA). A heating pad with a feedback temperature controller (Harvard apparatus, Holliston, MA, USA) maintained the core temperature of the rat at 36.8°C. In later experiments, a pulse oximeter was attached to the animal's foot and blood oxygen saturation was monitored (Physiosuite, Kent Scientific, Torrington, CT, USA). To achieve an oxygen saturation

of above 90%, medical oxygen (BOC Industrial Gases, UK) was supplied through a tube mounted to the nosebar of the stereotactic frame.

A skin incision was made above the skull using a scalpel. Lidocaine was then applied to the area of incision and fibrous tissue and the periosteum were scraped off the skull to expose bregma. Coordinates were taken and a small circular craniotomy was drilled (RS precision PCB drill/World Precision Instruments IDEAL micro drill) over the area of interest (coordinates given below).

Initial experiments were performed using a single-channel glass-coated tungsten electrode (technical details are given below). Before insertion of this fine electrode, the dura mater was cut with a hypodermic needle. The electrode was lowered with a remote-controlled custom made stepper-motor microdrive.

In the majority of experiments, 16-channel silicon probes (Atlas Neuroengineering, Leuven, Belgium) were used (technical details are given below). These electrodes were able to penetrate the dura. Before insertion, the silicon probes were covered with a fluorescent dye, DiI ($DiIC_{18}(3)$, Molecular Probes, Eugene, Oregon, USA), which was dissolved (1.5-2.5 mg/ml in dimethyl sulfoxide [DMSO]) and dripped on the back side of the silicon probes using a pipette. The electrode was covered with the dye twice, with ten minutes in between for drying, and at least ten minutes drying before insertion into the brain. The electrode was carefully lowered using a one-axis oil-filled hydraulic micromanipulator (Narishige, Japan).

2.2.3 *Recording electrodes and coordinates*

Medial prefrontal cortex recordings

- For single-channel recordings, borosilicate glass-coated tungsten electrodes (Baldwin et al., 1965; Merrill and Ainsworth, 1972) were used with the following coordinates: AP +2.4-2.7, ML 0.6, DV 3-4 mm.
- For unilateral multichannel recordings a single-shank 16-channel silicon probe (part number E16-250-S01-L8.0, Atlas Neuroengineering, Leuven, Belgium) was implanted using the coordinates AP +2.4-2.7, ML 0.6, DV 5.4-5.5 mm. The inter-site spacing of these electrodes is 250 μm, so that 16 electrodes cover a distance of 3.75 mm.

- For bilateral multichannel recordings a dual shank 16 channel silicon probe (part number E16-500-S02-1000-L7.5, Atlas Neuroengineering, Leuven, Belgium) was implanted into the medial prefrontal cortex (coordinates: AP +2.3-2.5, ML +/-0.5, DV 5.3 mm). The inter-site spacing of these electrodes is 500 μm, so that 8 electrodes cover a distance of 3.5 mm.

The Atlas silicon probes used in this thesis are shown in Figure 2.1.

Initially, the coordinates used were based on those in the literature. The exact location used was refined (as described above) based on actual electrode locations seen on histological samples processed as the experiments proceeded.

All data for Chapters 3 and 5 were obtained using the Atlas dual-shank silicon probe. The probe was lowered to a depth of 5.3 mm, so that recording sites covered depths from DV 1.8 mm to 5.3 mm, hence the entire mPFC (Figure 2.2 C, D).

The electrodes were cleaned after each experiment with a solution of an enzymatic detergent in distilled water.

2.2.4 *Data acquisition*

Single channel recording system

The signal was amplified (×1000) and filtered (0.1 Hz-10 kHz) using a preamplifier (Dam-8, World Precision Instruments). The signal was filtered for the local field potential (LFP; low pass 500 Hz), using a TDT system 2 (Tucker Davis Technologies) and digitised by a Micro-1401 (Cambridge Electronic Design, Cambridge, UK) at a sampling rate of 2000 Hz (LFP), and monitored and stored using Spike2 software (Cambridge Electronic Design, Cambridge, UK).

Multi-channel recording system

The 16-channel extracellular signal passed through two 8-channel unity-gain headstages (Plexon, Texas, USA), then was amplified (×1000) and filtered (0.07-300 Hz for LFP) by a Plexon preamplifier (Plexon, Texas, USA). The LFP was digitised at 1000 Hz and recorded on a PC (DELL Intel 4-core) running Plexon software (Sort Client).

A

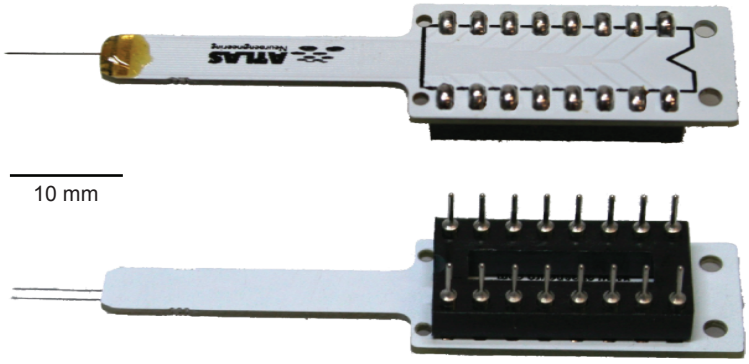

B

Atlas E16-250-S01-L8.0: Single shank electrode with 16 contacts.

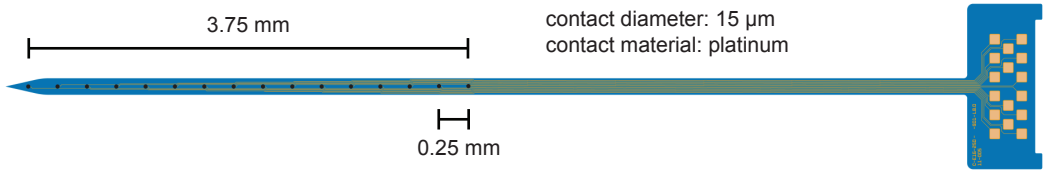

C

Atlas E16-500-S02-L7.5: Dual shank electrode with 16 contacts, 8 contacts per shank.

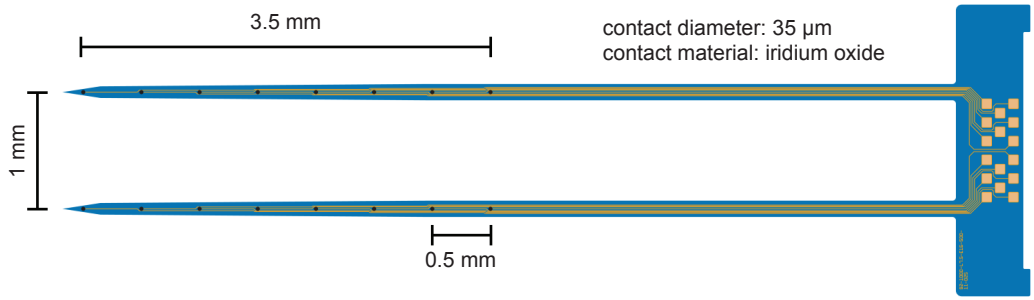

Figure 2.1. Silicon probes used to aquire most of the data presented in this thesis. (A) Silicon probe assembly with PCB providing the 16 channel single and dual shank probes and dual in-line (DIL) header. (B) Single 16-channel silicon probe. (C) Dual shank 16-channel silicon probe.

In addition, some analogue channels were extracted from the Plexon break-out box and monitored during the experiment. These signals were passed through a Hum Bug 50 Hz noise eliminator (Quest Scientific Instruments Inc., BC, Canada) and digitised using a Micro-1401 (Cambridge Electronic Design, Cambridge, UK). Traces were monitored and recorded using Spike2 software (Cambridge Electronic Design, Cambridge, UK).

2.2.5 *Histological verification of recording site position*

Sectioning and staining of the brains from all experiments carried out for this thesis was performed by me.

After the recording session, the rat was sacrificed with Euthatal (dose: ~0.5 ml, pentobarbitone 200 mg/ml). The brain was removed from the skull and stored in 4% paraformaldehyde (PFA) 0.1M phosphate buffer solution (PBS). Two different sectioning and staining protocols were used for prefrontal cortex sections:

1.) Verification of the position of the tungsten electrode in the mPFC

Brains were transferred from PFA to sucrose and left in sucrose until they sank (~2 days) and then stored in a -80°C freezer. Sections (60 μm thick) were cut on a cryostat (Microm HM560, MICROM Int., Walldorf, Germany), and mounted onto gelatine-coated microscope slides (Fisher Scientific UK Ltd., Loughborough, UK) and then stained with cresyl violet.

Cresyl violet staining protocol:

- 5 min distilled water
- 20 min Cresyl violet
- dip in 70% ethanol
- dip in 95% ethanol
- dip in 100% ethanol
- 2 min in 100% ethanol
- 2 min in Histoclear1 (National diagnostics, Atlanta, GA, USA)
- 2 min in Histoclear 2 (National diagnostics, Atlanta, GA, USA)

The slides, still wet, were cover-slipped using Entellan (Merck KGaA, Darmstadt, Germany) mounting medium and left to dry.

Photographs of cresyl violet-stained sections were taken using a monochrome camera (model XC-75CE, Sony), mounted on a MZ6 microscope (Leica) above a light source. Photos were captured using Scion image software (Scion corporation, Frederick, Maryland, USA).

2.) Verification of the multichannel silicon probe position in the mPFC

After the recording session, the rat was sacrificed with Euthatal and the brain was removed from the skull and stored in 4% paraformaldehyde 0.1M PBS in the fridge for a minimum of 12 hours. The brain was then transferred to a 30% sucrose solution for a maximum of 24 hours. Coronal sections (60-100 µm) were cut on a cooled vibratome (vibratome: Zeiss hyrax V50, cooling: Zeiss Hyrax CU65, Zeiss, Oberkochen, Germany) and collected in 0.1M PBS. Sections were then stained in the well using either of the following fluorescent stains to visualise the cytoarchitecture.

- NeuroTrace 500/525 green fluorescent Nissl stain (Molecular probes by life technologies, Eugene, Oregon, USA) at a concentration of 1:300-1:150 (the staining quality seemed to deteriorate over time, so the concentration was increased).
- bisBenzimide H33258 (Sigma) at a concentration of 2.5 µg/ml PBS
- Vectashield HardSet mounting medium with DAPI (Vector Labs LTD., Peterborough, UK)

The following short and long staining protocols were used for bisBenzimide H33258 and the NeuroTrace 500/525 staining:

<u>Short staining protocol used for bisBenzimide H33258 and NeuroTrace 500/525:</u>

- 5 min wash PBS
- 20 min – 2 h fluorescent counterstain (the staining quality seemed to deteriorate over time, so that the duration of staining was increased)
- 5 min wash PBS

<u>Long staining protocol used for bisBenzimide H33258 and NeuroTrace 500/525:</u>

- 40 min PBS
- 10 min PBS + 0.1% Triton X-100
- 5 min wash PBS
- 5 min wash PBS

- 20 min – 2 h fluorescent counterstain (the staining quality seemed to deteriorate over time, so that the duration of staining was increased)
- 10 min PBS + 0.1% Triton X-100
- 5 min wash PBS
- 5 min wash PBS
- leave 2 h at room temperature or overnight at 4 degrees (fridge) in PBS

After staining with either of the fluorescent counterstains, sections were mounted and left to dry. The sections were then coverslipped using Vectashield HardSet mounting medium (Vector Labs Ltd., Peterborough, UK) and stored in the fridge.

Photographs were taken using an Axio Imager Z2 microscope (Zeiss, Oberkochen, Germany) and AxioVision 4.8 software (Zeiss). Tiled pictures were taken using the mosaic setting, with 2.5× magnification. The Rhodamine filter was used for the DiI staining of the electrode tract, and the fluorescein isothiocyanate (FITC) filter was used for the green fluorescent Nissl background stain. An overlay image was produced by the microscope software.

Example sections of mPFC with three different stains are shown in Figure 2.2 A, C and D.

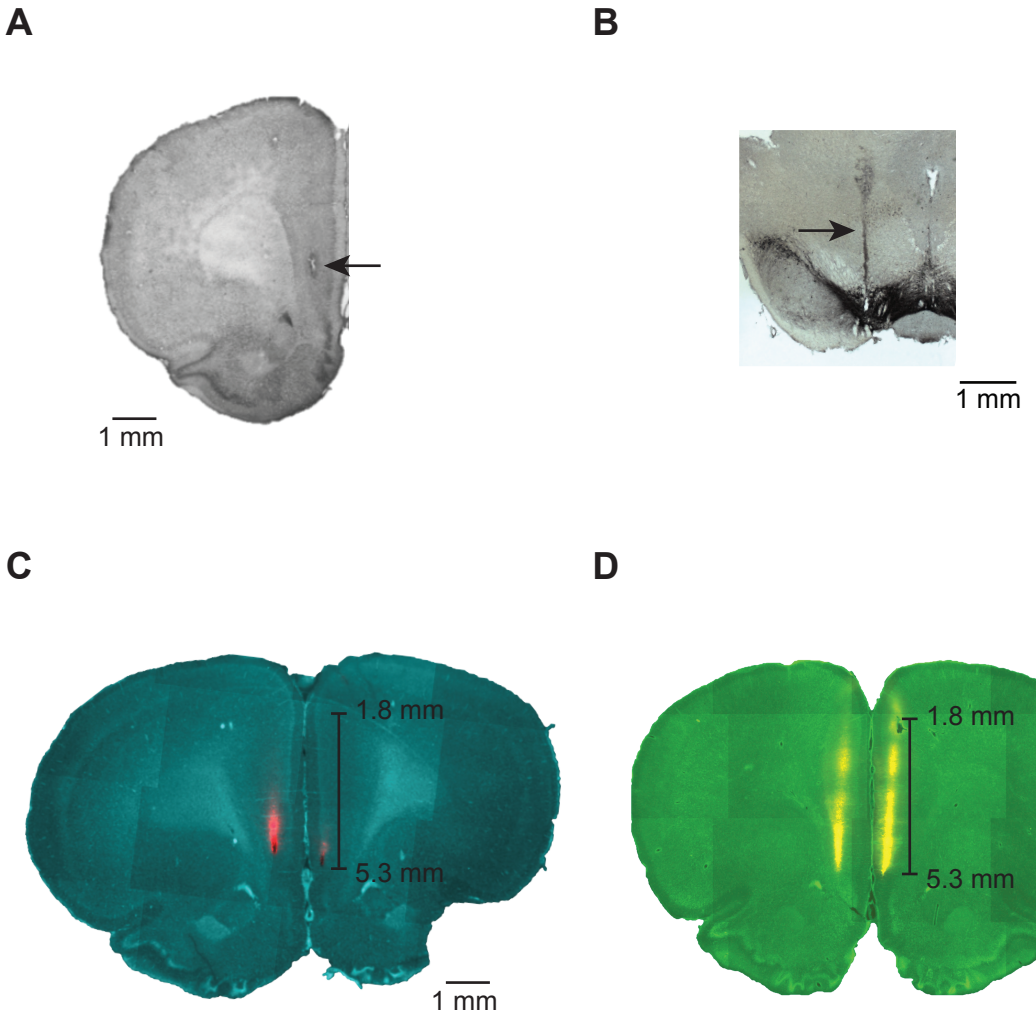

Figure 2.2. Stainings used for the verification of the positions of recording and stimulating electrodes. *(A)* Cresyl violet staining of mPFC coronal section with lesion indicating the position (arrow) of the glass-coated single channel tungsten electrode. *(B)* TH staining for visualisation of dopaminergic neurons in the VTA, to verify position of stimulation electrode (arrow). *(C)* bisBenzimide H33258 staining of coronal section through mPFC to verify position of the dual shank silicon probe (visualised by DiI stain). *(D)* Coronal mPFC section stained with green fluorescent Nissl stain NeuroTrace 500/525 to verify the position of the dual shank silicon probe (visualised by DiI stain). The black lines in (C) and (D) indicate the DV coordinates covered with recording sites (DV 1.8 to 5.3 mm)

2.3 Experimental interventions

2.3.1 *Electrical stimulation of the ventral tegmental area*

Electrical stimulation

A concentric bipolar stimulating electrode (NE-100 concentric bipolar electrode 50 mm, Rhodes Medical Instruments, Carpinteria, CA, USA) was attached to the manipulator of the stereotaxic frame and inserted into the brain (surgery as described above). The coordinates used for the stimulation electrode were AP -5.8, ML 0.6, DV 8 mm (left hemisphere). The dura was cut for the electrode insertion. Stimulation patterns were programmed on a Master-8 stimulator (A.M.P.I, Jerusalem, Israel) and delivered via an Iso-Flex stimulus isolator (A.M.P.I, Jerusalem, Israel). The stimulation protocols are described in the methods section of Chapter 4. The given stimulation pulses were recorded for subsequent data alignment.

Verification of stimulation site

The caudal part of the brain (containing the VTA) was sectioned and stained using either cresyl violet (as described above) or tyrosine hydroxylase immunocytochemistry, as described below. Tyrosine hydroxylase is the enzyme that catalyses the conversion of tyrosine to L-tyrosine to L-dopa, which is itself the precursor of dopamine. After a maximum of eight hours in PFA, brains were cryoprotected in 30% sucrose until they sank and then frozen rapidly in the -80°C freezer. 40 µm thick sections were cut on a freezing microtome (Leitz, Wetzlar, Germany), collected into PBS and tyrosine hydroxylase antibody staining was performed

<u>Tyrosine hydroxylase (TH) immunohistochemistry:</u>

- Wash once in PBS
- Rocking platform (on intensity setting 35).
- Incubate in 0.3% H_2O_2 for 30 min (1:100 dilution of 30% stock in PBS)
- Permeabilise with 1 % Triton (100 µl/10ml) for 20 min
- Incubate with TH antibody (mouse α TH-16, Sigma Aldrich) at 1: 10,000 in 'diluent' solution
    - 'diluent' solution: 3% BSA (Albumin bovine BSA cohn fraction V (Sigma), 1.8% L-lysine in PBS

    - α-TH is stored diluted 1/10 in -20 °C freezer, further dilute 10 ul aliquot to 10 ml diluent solution for 1:10,000
- Leave on rocking platform in cold room (4 °C) overnight
- The following morning, leave sections out of fridge for an hour to bring to room temperature (on rocking platform on 35)
- Wash 3x in PBS for 10 min
- Incubate in the secondary antibody (biotinylated conjugated horse α mouse IgG, Vector laboratories) at 1:100 in diluent solution at room temperature for 2 h, on rocking platform
- Wash 3× in PBS for 10 min
- Incubate in horse radish peroxidase (HRP) strepatavidin (1:300 in PBS) or HRP avidin D (1:100 in PBS) at room temperature
- Wash 3× in PBS for 10 min
- Incubate at room temperature for 5-10 min in Diaminobenzidine (DAB) solution made from gold/silver tablets (Sigma, freezer)
- Wash 3× in PBS for 10 min
- Mount sections on gelatin-subbed slides and allow to dry for 1-2 days
- Dehydrate in ethanol (70%, 95%, 95%, 100%, 100%)
- Defat in Histoclear (National diagnostics, Atlanta, GA, USA)
- Coverslip with Entellan

Photos of TH-stained sections were obtained using an AxioCamHRC (Zeiss, Oberkochen, Germany) mounted on a microscope (model NX60F, Olympus, Tokio, Japan).

An example section of VTA with TH staining is shown in Figure 2.2 B.

2.3.2 *Systemic drug application*

Pharmacological agents were purchased from Tocris/Sigma and dissolved in either saline or DMSO (Table 2.1). All drugs were administered by i.p. injection.

Drug	Action	Dose	Solvent	Supplier
SCH23390 hydrochloride	Selective dopamine D_1-like antagonist (D_1,D_5)	0.3 mg/kg	Saline	Tocris
(*S*)-(-)-Sulpiride	Selective dopamine D_2-like dopamine antagonist (D_2,D_3)	10 mg/kg	DMSO	Tocris
SKF38393 hydrobromide	D_1-like dopamine receptor selective partial agonist (D_1,D_5)	15 mg/kg	DMSO	Tocris
A412997 dihdrochloride	Selective agonist for the dopamine D_4 receptor	10 mg/kg	Saline	Tocris
L745,870	Selective antagonist for the dopamine D_4 receptor	0.5-1 mg/kg	Saline	Tocris
d-Amphetamine sulfate	Induces catecholamine release and blocks catecholamine reuptake	2 mg/kg	Saline	Sigma

Table 2.1. Pharmacological agents used in the experiments in this thesis.

2.3.3 *Data pre-processing*

Filtering for line noise

The raw LFP signal contained 50 Hz noise as well as it's multiples. Hence, prior to any data analysis the LFP signal was notch filtered around 50 Hz, 100 Hz, 150 Hz, 200 Hz, 250 Hz, and 300 Hz. A linear-phase finite impulse response filter (FIR) was used in combination with the MATLAB (Mathworks, Nantick, MA, USA) 'filtfilt.m' function, to prevent phase distortion.

The use of an equiripple FIR filtered ensured minimal amplitude distortion. The filters were created using the MATLAB 'fdatool.m'. Frequency settings were: 49-51 Hz stop band, 48-52 Hz pass band, to reduce noise in the 50Hz band.

Data exporting

Date was recorded in the Plexon ".plx" format and exported to MATLAB ".mat" format using a custom-written script that made use of functions offered in the Plexon

software development kit. During this procedure, the channel numbering was remapped so that channel 1 was the most ventral channel in the right hemisphere, and channel 9 the most ventral channel in the left hemisphere.

2.3.4 *Data analysis*

All data analysis was performed offline using custom scripts I developed.

Spectrograms

Spectrograms (time-frequency representations of the LFP power) were used for visualisation and created either in MATLAB (for example in Figure 3.4) based on the short-time Fourier transform, using the 'spectrogram.m' function with a 0.25 s window with 50% overlap, or exported from Spike2 (512 point fast Fourier transform (FFT) with Hanning window).

During SWA, high-frequency oscillations occur transiently during the Up state, and are absent during the Down state. To investigate these nested oscillations in more detail (as presented in Chapters 3 and 5) it was first necessary to detect Up and Down states, which was achieved as follows.

Up and Down state detection

Up-Down state detection was performed using the phase of the slow oscillation, as described in (Massi et al., 2012). However, with the difference that I used the Hilbert transform to calculate the phase of the slow oscillation, rather than the wavelet transform. The data processing for the Up Down state detection is illustrated in Figure 2.3.

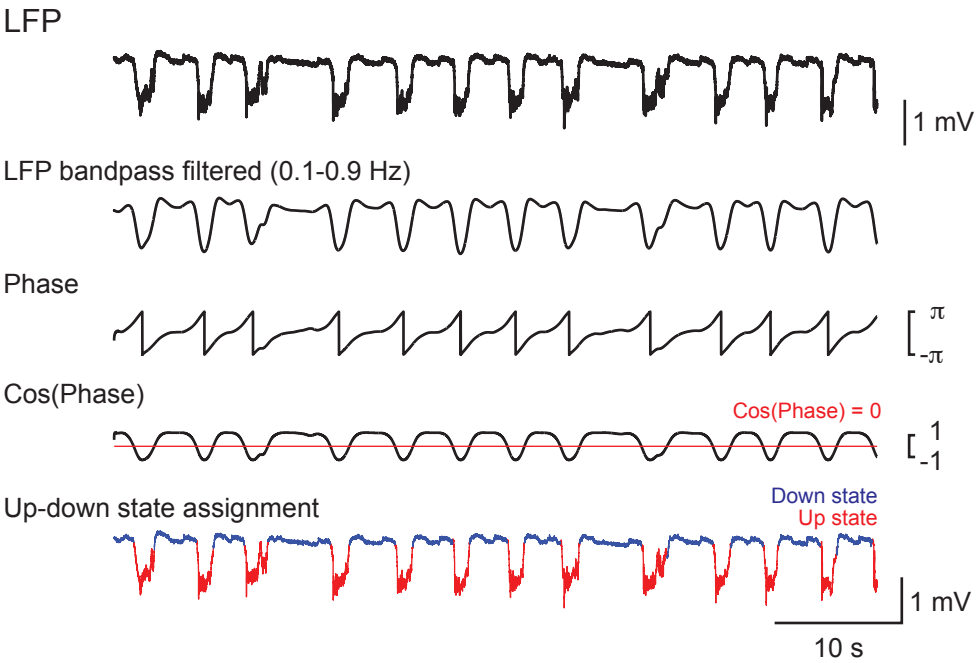

Figure 2.3. Up Down state detection. LFP was filtered for the slow oscillation band (0.1-0.9 Hz). A threshold was set on the cosine of the slow oscillation phase to differentiate Up and Down states. The LFP is shown again, divided into Up states (red) and Down states (blue).

The LFP was first band-pass filtered at 0.1-0.9 Hz (2nd-order Butterworth filter using the MATLAB 'filtfilt.m' function). The analytical signal, $c(t)$,was then calculated using the Hilbert transform, and the slow oscillation phase angle in radians, $\phi(t)$, was calculated as

$$\phi(t) = \text{atan2}\big(\,\text{Im}\big(c(t)\big)\,,\ \text{Re}\big(c(t)\big)\,\big). \qquad \text{(Equation 2.1)}$$

Where atan2 is an arctangent function with two arguments, $\text{Im}(c(t))$ and $\text{Re}(c(t))$, the imaginary and real parts, respectively, of the analytical signal.

A threshold was set at $\cos\big(\phi(t)\big) = 0$, assigning time points with $\cos\big(\phi(t)\big) < 0$ as Up states, and time points with $\cos\big(\phi(t)\big) > 0$ as Down states. Up states shorter than 300 ms were not accepted as such and assigned to Down state. Thus, each time point was either assigned to Up or Down state.

As the analysis methods were further developed during the time course of this work, an additional criterion was added in chapter 5. In chapter 5, Up states also had to fulfil an additional amplitude threshold, as it was observed that some Up states occurred only on approximately half of the recorded channels. The average amplitude over all channels had to be larger than 0.5 mV. Cycles containing Up states with cross-channel average amplitude <0.5 mV were removed from the analysis (Figure 2.4). Cycles following such a cycle were also removed from analysis, as it is not clear where the Down state of the next cycle starts.

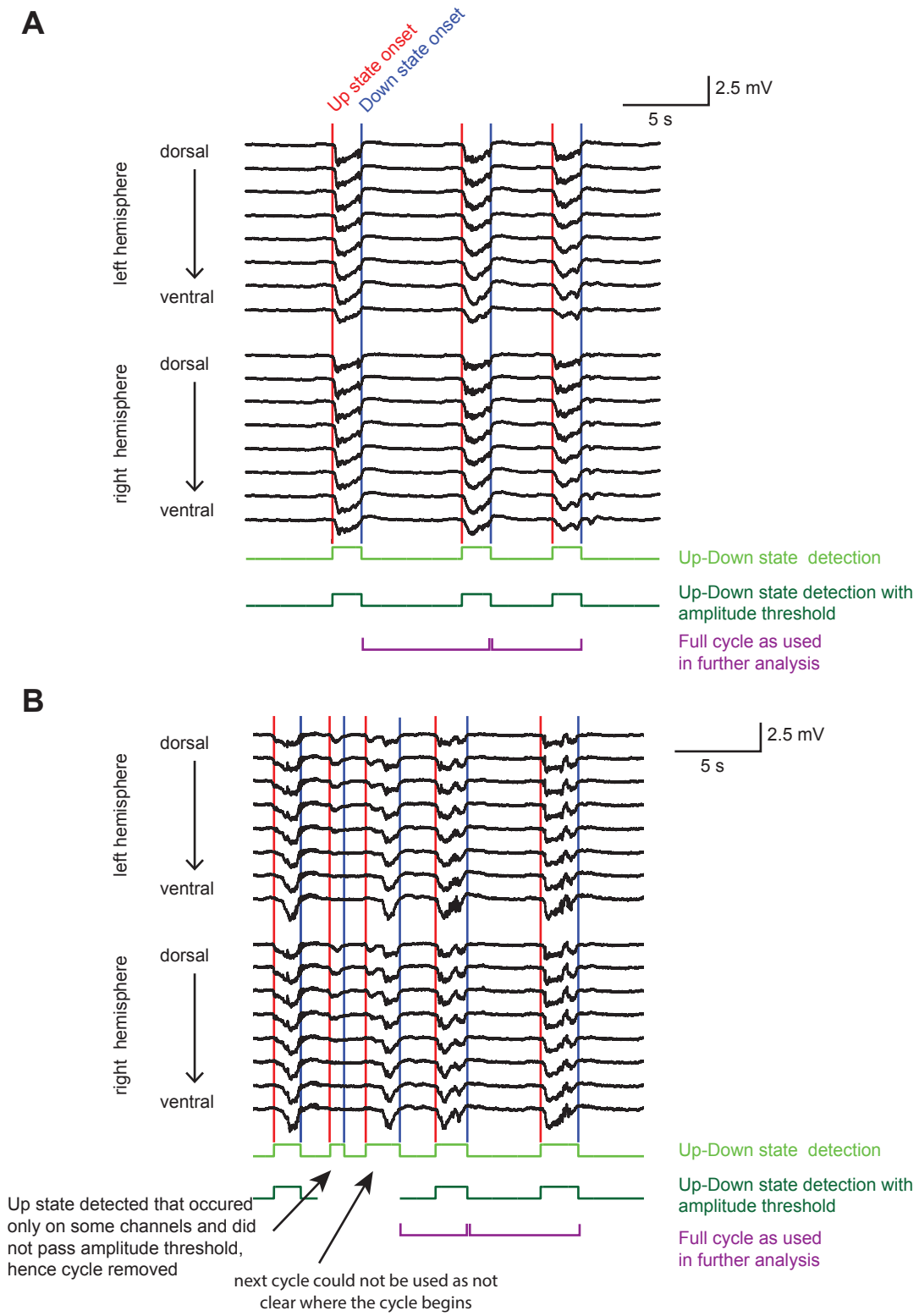

Figure 2.4. Determination of full Down state - Up state cycles for further analysis. *(A)* Example LFP recording (from all 16 recording sites in both hemispheres) from an experiment in which all Up states occured on all channels. *(B)* Example LFP recording (from all 16 recording sites in both hemispheres) from an experiment during which some detected Up states occured on all channels, but others only on some channels in the dorsal mPFC. Cycles containing these Up states have been removed from the analysis in chapter 5 together with the following cycle, by using an amplitude threshold.

Calculation of instantaneous power for higher frequencies

The high-frequency components (6-150 Hz) in the LFP during SWA occur as transient increases in LFP power, with a rapid onset and offset. As fast oscillations have got shorter cycle lengths, the onset of faster oscillations is expected to occur more rapidly then slower oscillations. Hence, the use of classical short-time FFT, with its fixed window size would lead to a low time-resolution in the higher frequencies within the band. In contrast, wavelet analysis uses shorter time windows for higher-frequencies and longer windows for lower frequencies, enabling optimal time-frequency resolution. The basic principle of wavelet transform is that scaled versions of a 'mother wavelet' (a waxing and waning oscillation with limited duration with certain properties) are shifted along the signal and similarity with the signal is assessed. Large scales (creating stretched wavelets) correspond to low frequencies, and small scales correspond to high frequencies.

For the spindle, gamma and high gamma band, an instantaneous band power was calculated using the wavelet transform. Again, the procedure was adapted from Massi and colleagues (2012). For each frequency band, a continuous wavelet transform (MATLAB function 'cwt.m') was performed on the LFP data using a complex Morlet wavelet with band width parameter 1 and center frequency 1.5 Hz (MATLAB wavelet 'cmor1-1.5') and linearly spaced wavelet scales, which could subsequently be converted to equivalent (logarithmically spaced) 'pseudofrequencies' (using MATLAB function 'scal2frq.m').

The continuous wavelet transform of a signal $x(t)$ is defined as

$$CWT(a,b) = \int_{-\infty}^{\infty} x(t)\psi_{a,b}^{*}(t)dt$$

(Equation 2.2)

where

$$\psi_{a,b} = \frac{\psi(\frac{t-b}{a})}{\sqrt{a}}$$

(Equation 2.3)

is the scaled and shifted version of the 'mother wavelet' $\psi(t)$, and $*$ denotes the complex conjugate. The parameters $a \in \mathbb{R}_+$ and $b \in \mathbb{R}$ define the scale and the time shift, respectively.

The power at scale i and time j, p_{ij}, was calculated from the wavelet coefficient c_{ij} as $\sqrt{Re(c_{ij}c_{ij})^2 + Im(c_{ij}c_{ij})^2}$, and was then normalized by dividing by the scale. The normalization step ensured that two sine waves with the same amplitude, but different frequency, had the same power (Liu et al., 2007). The resulting time-frequency representation is shown in Figure 2.5 A ("wavelet scalogram").

The instantaneous area power was then calculated using trapezoidal numerical integration (MATLAB function 'trapz.m') over all frequencies in the band (Figure 2.5 A, green trace). Note that because of the non-linear spacing of the frequencies in the wavelet transform, this equated to integrating over the frequency dimension of the time-frequency matrix, with non-uniform spacing.

To assess the oscillatory power with respect to the UDS, where the UDS cycles have got different lengths, the instantaneous power was aligned to a 'normalised' Down state- Up state cycle, as in (Massi et al., 2012). The procedure used is described below.

Calculation of the UDS phase vector

Time points of state transitions were calculated from the UDS detection logical vector. A cycle always consisted of a Down state and an Up state and contained three transitions: transition 1: Up-to-Down; transition 2: Down-to-Up; transition 3: Up-to-Down (see Figure 2.4 for indication of a full cycle). A phase vector was calculated that assigned -100 to the time point of transition 1, 0 to the time point of transition 2, and 100 to the time point of transition 3. The time points in between were filled with linearly spaced intermediate values, so that a phase vector was achieved with linear phase progression during the Down state, and linear phase progression during the Up state (Figure 2.5 B). As the Up state was shorter than the Down state, but the same range of values was applied to Up and Down state, the phase progression was faster during the Up state (Figure 2.5 B). Up and Down state were then divided into 40 bins per state. Because of the faster phase progression during the Up states, bins were smaller during the Up state (Figure 2.5 B).

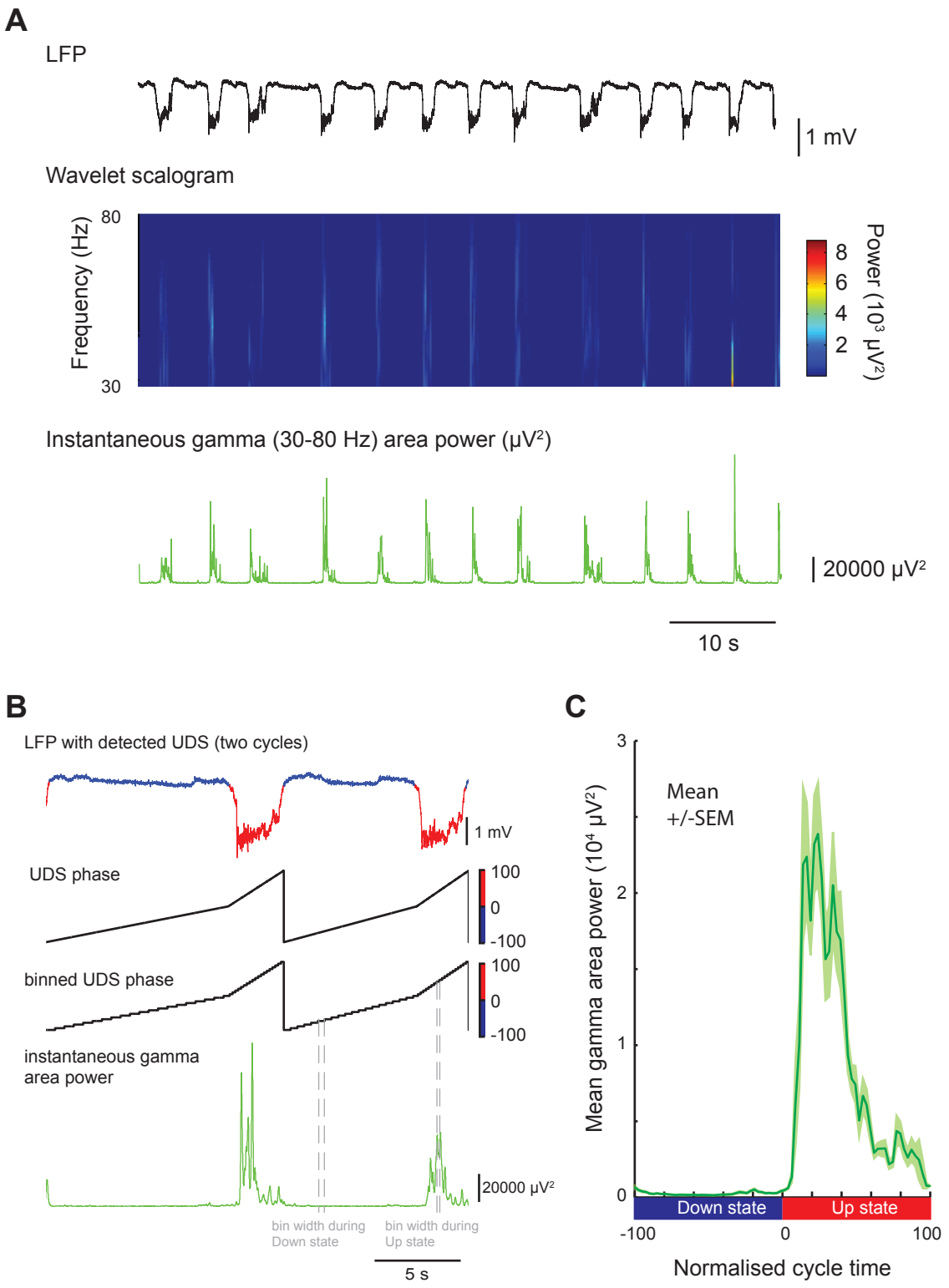

Figure 2.5. Calculation of Down state-Up state cycle aligned mean gamma power. *(A)* Calculation of instantaneous gamma area power using wavelet transform. LFP trace (black) and the time-frequency representation of gamma power calculated using wavelet transform. *(B)* Calculation of mean gamma power aligned to the normalised Down state-Up state cycle. To align the instantaneous gamma power to the normalised cycle, an UDS phase vector is calculated from the UDS detection. This vector is then binned into 40 phase bins per state which is then used to calculate gamma power for each cycle. *(C)* Alignment of the instantaneous gamma power to the normalised cycle.

extreme values (Chapter 3, Chapter 5), or the most extreme value that was not considered an outlier (Chapter 4). In Chapter 4, outliers were values more extreme than 1.5× the IQR.

As a box plot can be difficult to interpret when showing repeated-measures data, I additionally plot the mean ranks showing the comparison intervals used in the multiple comparison test.

A Wilcoxon signed rank test was used to compare two related samples regarding one factor. A Friedman's test was used to compare >2 related samples with respect to one factor (a non-parametric alternative to the one-way non-parametric analysis of variance [ANOVA]), and reported as chi-squared values with degrees of freedom, i.e. χ^2 (df). Tukey post-hoc tests at 0.05 overall significance level were used for post-hoc comparisons. The Wilcoxon signed rank test and Friedman's test were performed in MATLAB (MathWorks Inc. Natick, MA, USA).

Two-and three- way non-parametric ANOVAs were used when several factors and their interactions were investigated. These were performed using the 'aligned rank transform' (ART) tool provided by Wobbrock and colleagues (2011). This was necessary because multi-factorial ANOVA performed on simply ranked data leads to inaccurate results for interaction effects (Richter, 1999). This can be avoided by using the aligned rank transform which reports accurate main and interaction effects (Salter and Fawcett, 1993; Richter, 1999). The ART tool aligns and ranks multifactorial data, resulting in a ranking for each effect (main effects and interaction effects). The output can then be subjected to a standard ANOVA, including all factors. Only the results of the effect for which the data was aligned before ranking are extracted. In the case of a two-way ANOVA, that means that three full-factorial ANOVAs would be performed to receive F-ratios for the two main effects, and the interaction effect. The ANOVAs were performed in Sigmaplot 11.0 (Systat Software Inc., San Jose, California, USA). Two-way ANOVA results were reported as F-values with degrees of freedom, i.e. $F_{(df\ factor,\ df\ residual)}$. Holm-Sidak tests at overall significance level 0.05 were used for post-hoc comparison, either to perform all pairwise comparisons, or the baseline was compared with all other values.

Chapter 3. Characterisation of medial prefrontal cortex slow wave activity under urethane anaesthesia

3.1 Introduction

3.1.1 *Sub-regional differences in sleep oscillations within mPFC*

As discussed in Chapter 1, SWA is highly synchronous across a distance of up to 12 mm apart in cats (Volgushev et al., 2006), although across the whole cortex, a travelling wave occurs in anterior-posterior direction (Massimini, 2004; Ruiz-Mejias et al., 2011; Sheroziya and Timofeev, 2014). The fast oscillations on the Up state, however, are only locally synchronised (Destexhe et al., 1999), hence might differ between cortical areas or even between mPFC subareas.

Indeed, large-scale differences in nested fast oscillations during SWA have been observed between different cortices in mice and humans. Differences in fast beta and gamma oscillations have been observed during SWA in anaesthetised mice between brain regions, with the mPFC showing higher Up state gamma power than visual, somato-sensory and motor cortices (Ruiz-Mejias et al., 2011). Several human studies using either EEG or intracranial depth electrodes have confirmed large-scale regional differences in slow (Riedner et al., 2007) and fast spindle (Andrillon et al., 2011) and gamma (Le Van Quyen et al., 2010) oscillations during sleep.

Small-scale sub-regional differences in persistent fast oscillations have been observed between the mPFC sub-regions *in vitro*. Differences between mPFC sub-regions in beta band oscillations have been observed between PrL and IL (van Aerde et al., 2008). And *in vitro* data from our lab have also confirmed a gradual change in fast oscillation power along the dorsal-ventral gradient (Glykos, 2013). Whether the mPFC sub-regions differ with regard to their oscillations *in vivo*, however, is not known.

As described in section 1.2, the four sub-regions of the mPFC differ significantly in their laminar structure, and possess differential afferent and efferent connections with other brain regions. Hence, mPFC sub-regions might also differ with respect to the oscillatory activity they can produce. As discussed in section 1.4.8, the rat PFC is highly active during SWS and engages in coordinated activity with the hippocampus. Hence, sleep-like activity (such as the SWA seen under urethane anaesthesia) in the rat

represents an interesting *in vivo* model to study differences between the mPFC sub-regions.

3.1.2 *Laminar differences within the mPFC*

As well as having dorso-ventral sub-regions, the mPFC also shows laminar variation in cell type and density. Moreover, each layer has different and characteristic connections with particular brain areas (section 1.2.3). Hence, laminar variation in oscillatory properties is likely.

Deep cortical layers seem to be where SWA originates in cats and rodents (Sanchez-Vives and McCormick, 2000; Chauvette et al., 2010; Beltramo et al., 2013). Deep and superficial layers of rodent mPFC can produce similar continuous fast oscillations when isolated *in vitro* (van Aerde et al., 2009). However, results from our lab have shown that in an *in vitro* cortical slice preparation containing all mPFC layers, the power of induced fast network oscillations is highest in layers V/VI in PrL as well as in IL (Glykos, 2013).

To our knowledge, a detailed analysis of laminar differences of slow and fast sleep oscillations in the rat mPFC has not been undertaken.

3.2 Aims

The aims of this chapter were thus to:

1.) determine the basic properties of UDS in the rat mPFC under urethane,
2.) investigate sub-regional differences of UDS in the rat mPFC under urethane,
3.) investigate laminar differences of UDS in the rat mPFC under urethane.

3.3 Methods

3.3.1 *Dataset*

The animals were anaesthetised and prepared as described in section 2.2 and mPFC LFP activity was recorded using a dual-shank 16-channel silicon probe, implanted with one shank (8 channels) in each hemisphere (for details on electrode specifications and coordinates, see section 2.2.3). The data included in this chapter had to fulfil the following requirement on electrode placement:

(1) The placement of the tip of the dual shank 16-channel silicon probe was confirmed to be at a depth of 5.5 mm in both hemispheres (so that the deepest recording site was at a depth of 5.3 mm which corresponded to the ventral DP, above the dTT).

For the *analysis of basic UDS properties* and the *sub-regional profiles*, a second requirement needed to be fulfilled:

(2) The shanks were equidistant from the midline, so that the laminar position of the shank was the same in both hemispheres. With this positioning both shanks were located in layer III of the mPFC (see Figure 3.1).

In nine experiments, the electrode placement fulfilled these criteria, but in one of these experiments the Up state amplitude was too small to reliably detect Up Down states. Thus, eight experiments were used for the analysis of the basic UDS properties and the sub-regional comparison in this chapter. The left hemisphere was analysed for the sub-regional profiles. Plots are provided to show that there was no difference between left and right hemisphere.

In ten other animals, (1) was fulfilled, but the laminar position differed between the two hemispheres of the mPFC. Data from these ten experiments were used to perform a laminar comparison of mPFC UDS activity, using data from both hemispheres. These ten experiments were divided into two groups: In the first group (n=5), the electrode placement was such that the shank in the left hemisphere was in the superficial layers (layers I and II) and the shank in the right hemisphere in the deep layers (layers III and V), see Figure 3.2 A. This dataset was called ‘RdeeperL’. In the other group (n=5), the shank in the left hemisphere was in the deep layers (layers III and V) and the shank in the right hemisphere in the superficial layers (layers I and II), see Figure 3.2 B. This dataset was called ‘LdeeperR’.

For each experiment, a single 120 s data segment without artefacts was selected from the first 30 minutes of the experiment during which no intervention occurred. This data segment was selected so that it did not include an episode of broadband increased LFP power that occurred regularly during our recordings under urethane anaesthesia. We are not aware of a description of this phenomenon in the literature, thus we call it the ‘very slow modulation of broadband LFP power’ (VSMP), and it will be discussed in more detail in the results section of this chapter.

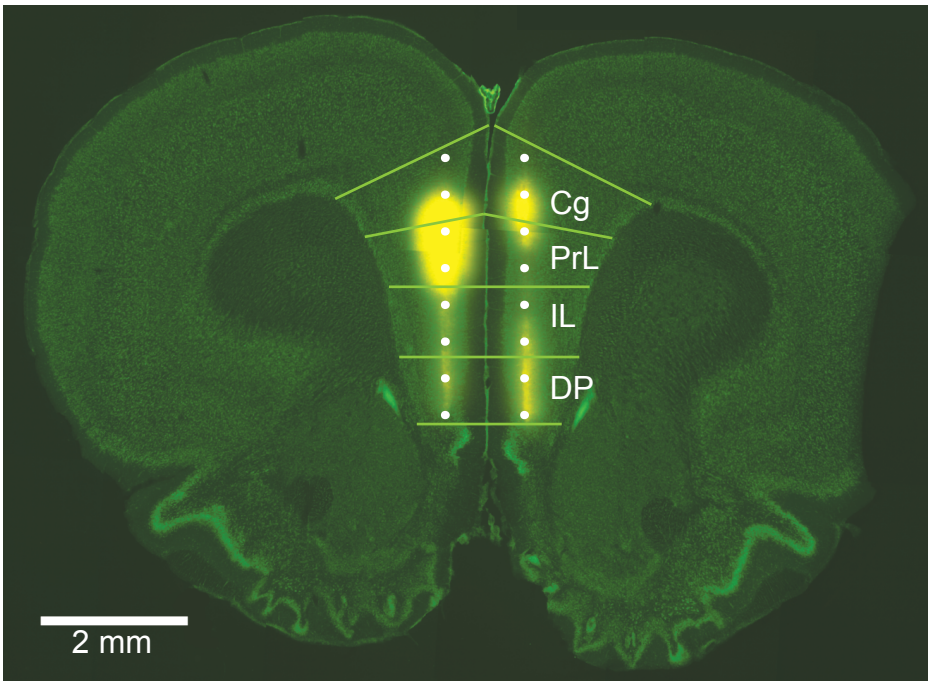

Figure 3.1. Coronal section through the rat mPFC indicating an electrode placement with both shanks equidistant from the midline (as used for the regional comparison). The white dots indicate the approximate position of the recording sites on the two shanks of the 16-channel silicon probe. The yellow stain is the fluorescent dye DiI which was applied to both shanks of the silicon probe before insertion into the brain. The cytoarchitecture is visualised with a green fluorescent Nissl stain. Note that the position of the the two shanks of the silicon probe is equidistant from the midline and both shanks are located in layer III. The light green lines indicate the borders of the mPFC subregions, cingulate cortex (Cg), prelimbic cortex (PrL), infralimbic cortex (IL) and dorsal peduncular cortex (DP). Part of the right hemisphere was trimmed during the slice preparation process for subsequent identification.

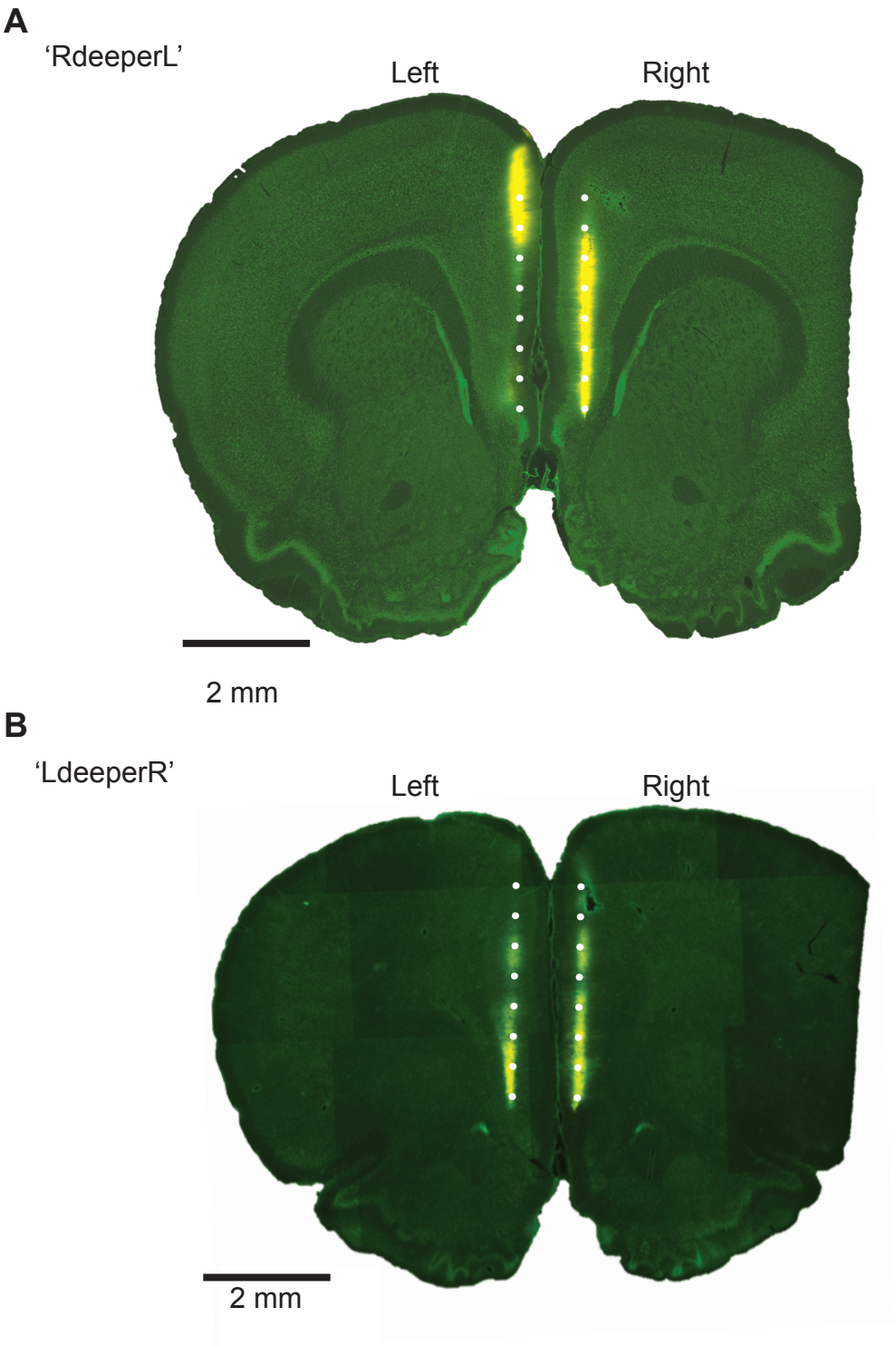

Figure 3.2. Coronal sections through the rat mPFC indicating electrode placements with the two shanks differing in distance from the midline (as used for the the laminar comparison). *(A)* 'RdeeperL' electrode placement: The dual shank 16 channel multichannel silicon probe was positioned so that the left shank was in the superficial layers (layers I-II) and the right shank in the deep layers (layers III-VI) of the mPFC. *(B)* 'LdeeperR' electrode placement: The dual shank 16 channel multichannel silicon probe was positioned so that the left shank was mainly in the deep layers (layers III-VI) and the right shank in the superficial layers (layers I-II). The yellow stain is the fluorescent dye DiI which was applied to both shanks of the silicon probe before insertion into the brain. The cytoarchitecture is visualised with a green fluorescent Nissl stain. The right hemisphere was trimmed during the preparation of the sections for subsequent identification.

Alignment of instantaneous power the normalised UDS cycle

For each cycle, the mean power per bin was calculated, leading to the alignment of the band power to a normalized cycle. This compensated for the variable lengths of UDS cycles within a particular data segment, and thus allowed a mean instantaneous power and standard error (e.g. Figure 2.5 C) to be calculated for each recording channel in a particular animal.

Chapter-specific analysis methods will be explained in the method sections of Chapters 3-5.

2.4 Data grouping

For the results in this thesis, different features of Up states were analysed. Segments of analysed data contained either ~ 48 or ~ 240 Up states per animal for each recording site, depending on the length of data analysed (120 second segments in Chapter 3 and 10 min segments in Chapter 5, respectively).

Up states recorded in the same animal are likely to be more similar to each other than Up states recorded in different animals (due to differences in anaesthesia depth, electrode positioning, and variation between animals). This is a classic case of a nested design, where ignoring this interdependency of certain observations would lead to clusters of observations that are not independent from each other, which can then lead to false-positive results. See (Aarts et al., 2014) for an elaboration on the problem of dependency in nested experimental designs.

One strategy to avoid violating statistical independence assumptions is to average within the cluster. Thus, in our case, all parameters were averaged within animal, yielding a mean value for each animal and each recording site, and each experimental condition (or time point). Statistical analysis was then performed on these mean values.

2.5 Statistical analysis

Because of small sample numbers ($n<10$ animals) for all experimental procedures, normality could not be reliably assessed (and could not be assumed). Hence, non-parametric statistical methods were used throughout this thesis. In figures, group data was typically presented using box plots, in which the median is plotted as a line, the box constitutes the inter-quartile-range (IQR), and the whiskers represented either the most

3.3.2 *Analysis methods*

Cross-correlation

Synchrony between two signals can be measured using *cross-correlation*. One of the signals is shifted relative to the other, and for each shift, or 'lag', the similarity between the signals is calculated. Cross-correlation values can be between -1 (the signals are perfectly anticorrelated) and 1 (the signals are perfectly correlated, i.e. identical). If there is a correlation peak that does not occur at a lag of zero seconds, the time lag to that peak gives a measure of time lag between the two signals.

For the slow oscillation cross-correlation analysis, the two signals to compare were band-pass filtered for the slow oscillation range (0.1-0.9 Hz), using a 2^{nd} order Butterworth filter. The cross-correlation between the two time series was calculated (using MATLAB function 'xcorr.m') and normalised (so that autocorrelations at zero lag are 1). The time lag between the two signals was calculated as the time lag at the peak of the cross-correlation.

Coherence

Another measure for synchrony is *spectral coherenc*e, which is a normalised cross-power spectral density. It is a linear measure of correlation in the frequency domain as opposed to cross-correlation, which assesses similarity in the time domain. Coherence measures consistency of phase relationships between two signals. Coherence values are bounded between 0 and 1, where 1 indicates that any phase differences that exist between the frequency components of two signals are fixed for the entire duration of the analysed signals, and a value of 0 indicates that these phase differences between the two signals are entirely random.

To calculate the slow oscillation coherence, the magnitude squared coherence (MATLAB function 'mscohere') between two LFP signals was computed, and the mean coherence in the slow oscillation band (0.1-0.9 Hz) was calculated.

Alignment of SO amplitude and nested fast oscillation power

For the results in section 3.4.2 and in section 3.4.3, UDSs were detected on the most dorsal recording site (Cg) in the left hemisphere, and all data are then reported relative to the timing of UDS from this 'reference' electrode. In all cases, time zero corresponded to the start of the Up state on this 'reference' electrode, but data were aligned in one of two ways:

i) For UDS amplitude analysis, and analysis of the power of nested fast oscillations, I compensated for the variable lengths of Up and Down states, by mapping the time points of each cycle (consisting of a Down state followed by an Up state) to a normalised time scale with the following correspondences: –100, beginning of the Down state; 0, transition from Down state to Up state; 100, end of the Up state. This alignment method was adapted from Massi and colleagues (2012).

ii) For analysis of latencies of LFP features during the UDS, I simply aligned the data to the start of the Up state (as defined on the 'reference' electrode), retaining the absolute time scale. For this analysis, which was performed on the nested fast oscillations, the UDS-aligned oscillation power was additionally smoothed with a 400 ms rectangular window.

Amplitude

The slow oscillation amplitude was calculated by filtering the LFP for the slow oscillation range (0.1-0.9 Hz), and aligning the slow oscillation trace to the normalised Down-Up state cycle (as described in section 2.3.4). The average (mean) of this 'UDS cycle state-triggered slow oscillation' was calculated, and the slow oscillation amplitude was defined as the peak-to-peak amplitude of this average waveform.

3.4 Results

3.4.1 *Basic properties of medial prefrontal cortex slow wave activity under urethane anaesthesia*

Different frequency components of SWA

The LFP during SWA consisted of several frequency components (see Figure 3.3). Its main characteristic was a large amplitude (~1-3 mV) slow oscillation at frequencies between 0.1 and 0.9 Hz (corresponding to UDS). It also contained spindle activity in the range of 6 to 15 Hz as well as wide-band gamma activity (30-80 Hz). High gamma activity (80-150 Hz) was also observed. In accordance with the literature, the fast oscillatory activity was modulated by the slow oscillation (see example in Figure 3.4). Thereby, the high frequency activity occurred nested within the slow oscillation trough – the Up state – as is typical for such recordings. Note that the Up state, recorded intracellularly is a depolarization (positive deflection), whereas in the LFP, which is recorded in the extracellular space, the Up state typically is a negative deflection. We

have, however, noticed a polarity inversion above the mPFC, where the polarity can be as seen in the EEG (Up state as a positive deflection).

Sleep-like state changes during urethane anaesthesia

As already discussed in section 1.4.1, rodent sleep is subdivided into two sleep states (REM sleep and SWS) and, in contrast to humans, is more fragmented. Sleep-state changes (between a REM-like and a SWS-like state) can be observed under urethane anaesthesia in rats (Clement et al., 2008) and mice (Pagliardini et al., 2013). These sleep-state changes have been reported to occur with a period of approximately 11 minutes (range 7-14 minutes), and are thought to resemble the sleep state transitions between REM sleep and SWS during natural sleep (Clement et al., 2008), which occur with a similar period (Clement et al., 2008).

I observed similar sleep-state transitions in my experiments. A REM-like state was observed, during which the LFP was characterised by a low amplitude (<1 mV) activity with no obvious changes in the frequency components over time in the spectrogram (Figure 3.5 A). The SWA LFP on the other hand, was characterised by large amplitude (1-3 mV) fluctuations, occurring at frequencies below 1 Hz. The spectrograms show that high-frequency activity was modulated by the amplitude fluctuations, with high-frequency activity transiently occurring during the negative deflection of the LFP (Figure 3.5 B). During SWA, the large-amplitude fluctuations and, to an even greater extent, the transient high-frequency activity periods, occurred synchronously in Cg and DP, indicating strong synchrony within the mPFC (Figure 3.5 B, red dotted lines).

In this study, state transitions were avoided by applying high does of urethane. If a REM-like state was observed at the beginning of the recording, or if state transitions occurred, a urethane top-up dose was administered to achieve stable SWA, which then lasted for several hours.

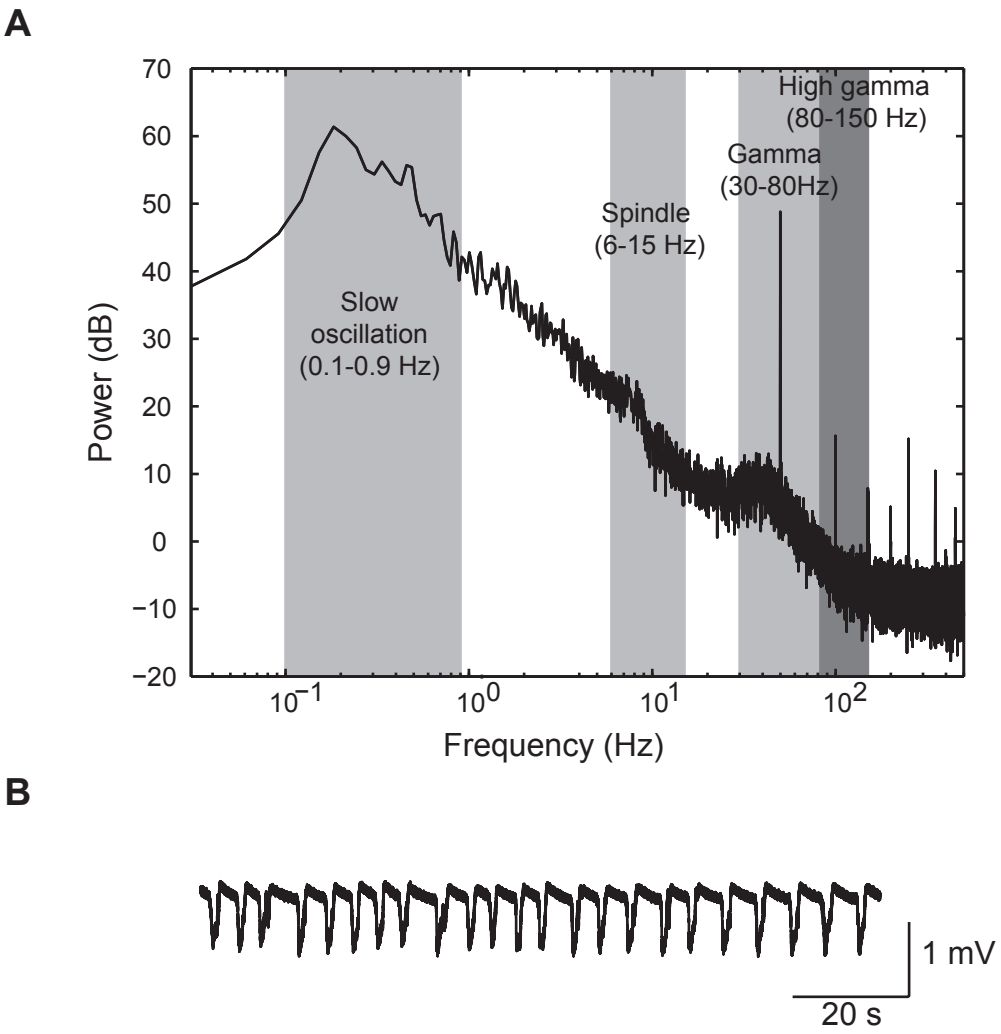

Figure 3.3. Frequency components of the slow oscillation LFP. *(A)* Power spectrum of the 120 s unfiltered LFP trace in (B), showing the frequency components of the slow oscillation. *(B)* Unfiltered (no 50 Hz line-noise filter) 120 s LFP trace (recorded in the Cg) used to calculate the power spectrum in (A).

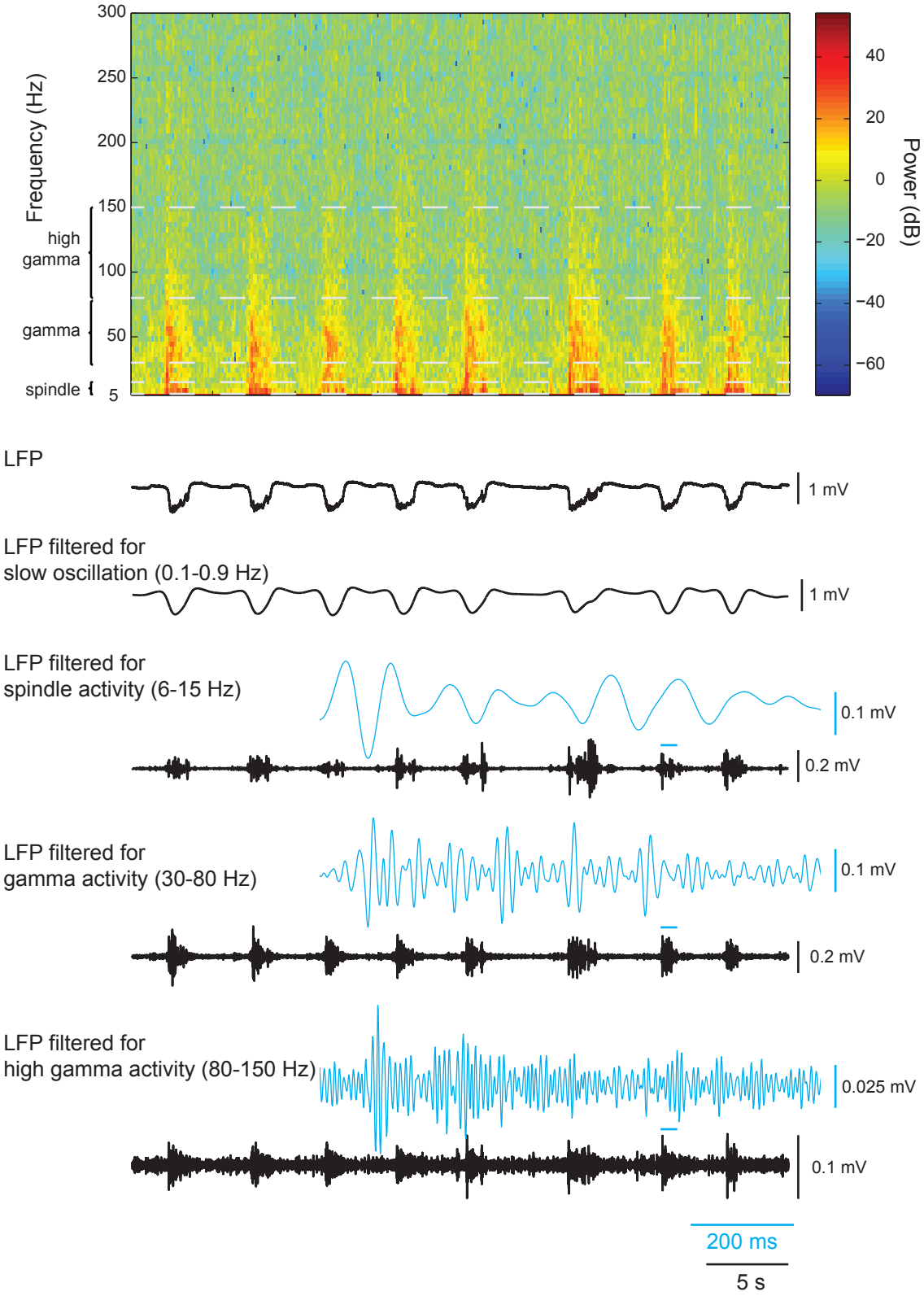

Figure 3.4. High frequency activity occured within the slow oscillation trough. Example spectrogram shows a time-frequency representation of a 40 s LFP segment recorded in the cingulate cortex (Cg). The corresponding (line-noise filtered) LFP trace is shown beneath. The main components of the slow wave signal are shown by bandpass filtering of the LFP for the slow oscillation, spindle, gamma and high gamma activity. Note that the high frequency activity occurs during the negative deflection (i.e. the Up state) of the extracellularly recorded slow oscillation. The insets (blue) show the fast oscillations during one Up state (indicated with a blue line above the black trace) on a different scale.

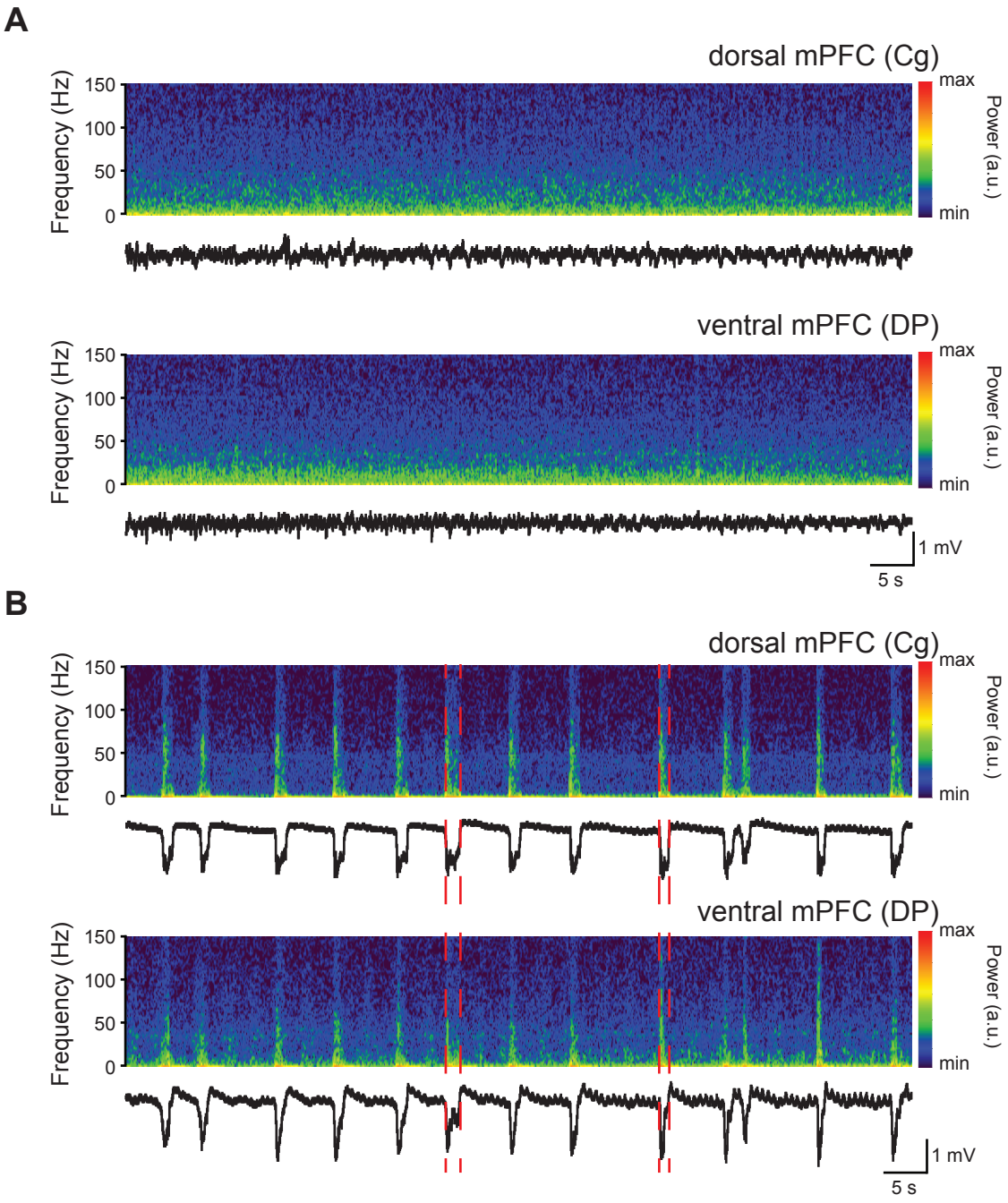

Figure 3.5. REM-like state and SWA could be observed during urethane anaesthesia. LFP (black) and spectrograms of LFP recorded in dorsal mPFC (Cg) and ventral mPFC (DP) simultaneously. *(A)* The REM-like state under urethane anaesthesia was characterised by low amplitude fast fluctuations in dorsal and ventral mPFC. *(B)* SWA was characerised by large amplitude fluctuations occuring with a frequency of < 1 Hz. Dotted red lines are plotted to emphasise the synchrony of the Up state during SWA, especially of the high-frequency content in the spectrogram. Data in (A) and (B) are from the same animal, during different brain states. SWA in (B) was achieved by administration of an additional dose of urethane (the LFP trace starts 90 seconds after injection).

The 'very slow modulation' of LFP power (VSMP)

Although I observed state changes between a REM-like state and SWA occasionally, they were never as regular as described previously in rats (Clement et al., 2008). Instead of the 7-14 minute periods observed in cortex and hippocampus in (Clement et al., 2008), state changes from SWA to the REM-like state would spontaneously occur after several hours of SWA, and could last for >20 minutes. As I was mainly interested in SWA, in these cases a urethane top-up was administered to achieve the return to SWA. After administration of the urethane top-up dose, SWA would continue for several hours. However, we observed another phenomenon that occurred with the periodicity described by (Clement et al., 2008). A broad increase in LFP power occurred spontaneously with a period of 4-11 minutes, during the REM-like state (Figure 3.6 A) as well as during SWA (Figure 3.6 B). This 'very slow modulation' of LFP power (VSMP) was observed during all experiments performed for this thesis, and was stronger in the ventral mPFC compared to the dorsal mPFC, during both the REM-like state and during SWA (Figure 3.6 A, B). The VSMP was very regular in some experiments (as in Figure 3.6 A), less regular in others. Usually, the 'high power state' of the VSMP was shorter than the 'low power state' (Figure 3.6 A, B). The 'high power state' of the VSMP lasted ~1-2 minutes, whereas the 'low power state' lasted ~2-9 minutes. The onset of the 'high power state' seemed to be sharp, often accompanied by a marked increase in the spindle/beta band (~14-16 Hz) power (Figure 3.6 A, B). A magnification of the SWA LFP including a high-power state is shown in Figure 3.7. The 'high power state' was usually detectable by eye in the spectrograms from Cg and DP (Figure 3.7), but could not be observed in the Cg LFP trace (Figure 3.7). Conversely, the transition to the 'high power state' could clearly be detected by eye from LFP recordings from the DP (Figure 3.7).

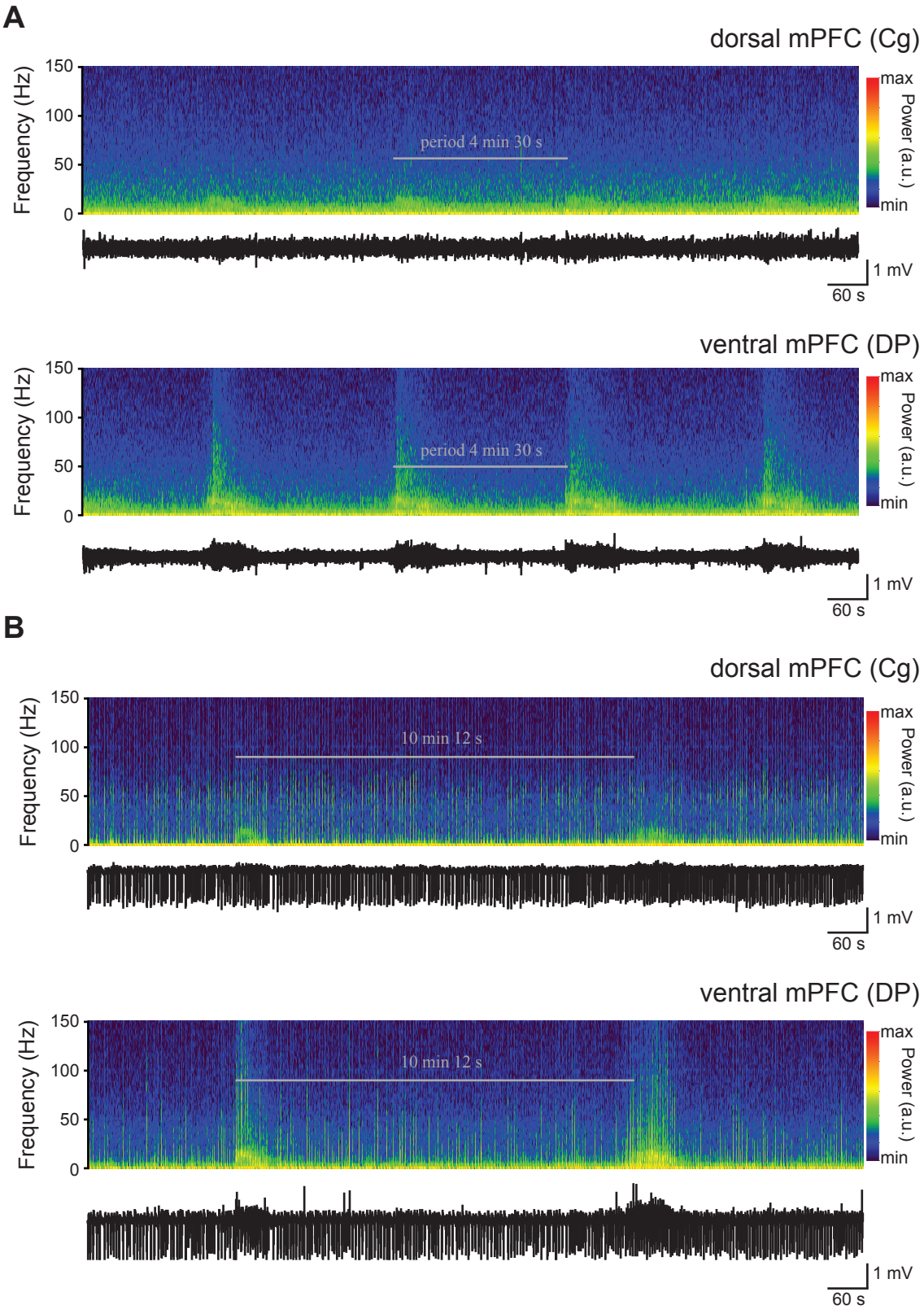

Figure 3.6. The very slow modulation of LFP power (VSMP) during the spontaneous REM sleep-like state and during SWA . LFPs (black) and spectrograms of LFP recorded in Cg and DP under baseline conditions. *(A)* The very slow modulation of LFP power (VSMP) during the desynchronised, REM sleep-like state. The VSMP period in this example was 4 min 30 s. *(B)* The very slow modulation of LFP power (VSMP) during SWA. The VSMP period in this example was 10 min and 12 s. Data in (A) and (B) are from the same animal, during different brain states, SWA in (B) was achieved by administration of an additional dose of urethane.

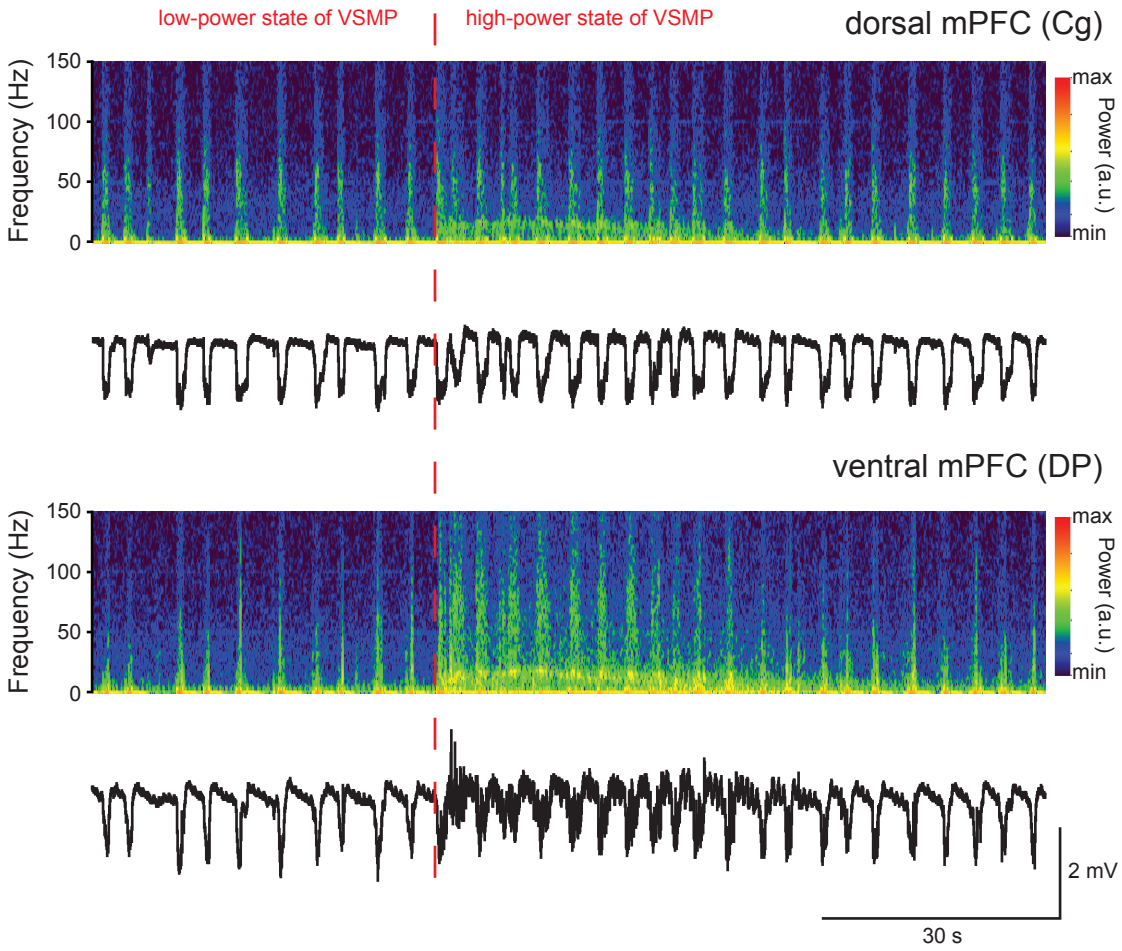

Figure 3.7. The very slow modulation of LFP power (VSMP) during SWA - high power state and low power state. LFPs (black) and spectrograms of LFPs recorded in Cg and DP under baseline conditions (data from the same animal as Figure 3.6). The rapid onset of the high power state was accompanied by a marked increase in power at 16 Hz (spindle/beta band). After ~30 s, the LFP changed from 'high power state' of the VSMP back to 'low power state' of the VSMP. Note that in the Cg recording, the 'high power state' of the VSM can can be identified from the spectrogram, but is not visible in the LFP. Conversely, in the DP recording, the 'high-power state' of the VSM is characterised by marked changes in the spectrogram as well as in the LFP.

In this chapter, as fast oscillations on the Up state appeared to be affected by the VSMP, and to avoid biasing the analysis towards one of the states, short segments that did not contain any increased power state of the VSMP were chosen (length of data segments: 120 s). In Chapters 4 and 5, where the analysis needed to be performed with regard to a reference time point (drug injection or electrical stimulation), very long data segments (10 minutes) were analysed, so that each data segment contained both states of the VSMP.

Synchrony of the slow oscillation

The rat mPFC is unique in that it is a piece of cortex that extends from the dorsal cortical surface in a ventral direction along the medial wall, almost to the ventral surface of the brain. Hence, we first sought to find out how synchronous the slow oscillation was in the rat mPFC. First, the intra- and inter-hemispheric synchrony of the slow oscillation (0.1-0.9 Hz) was investigated using coherence and cross-correlation analysis.

Data from the eight animals with electrode placement equidistant to the midline were used to analyse the synchrony of the slow oscillation.

Synchrony of the slow oscillation – Coherence

The slow oscillation coherence was calculated between the most dorsal channel in the left hemisphere (reference channel) and all other recording sites. Coherence decreased with increasing distance from the site used as a reference, but was high in the entire mPFC (0.86 on the most distant channel on the ipsilateral side, Figure 3.9 A). The coherence between the two hemispheres was calculated at each depth (D-V), and was slightly lower in the most dorsal and most ventral parts of the mPFC (dorsal: 093; ventral: 0.95; in between: 0.96-0.99; Figure 3.9 B). Hence, the slow oscillation is characterised by a consistent phase-relationship in the mPFC.

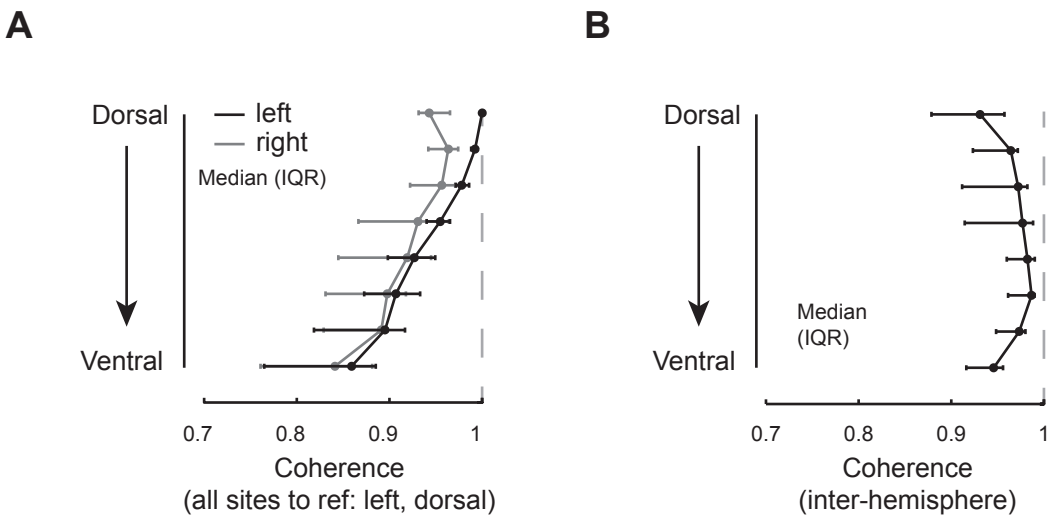

Figure 3.8. Synchrony of the mPFC slow oscillation - coherence.
*(A) C*oherence in the slow oscillation band between the most dorsal site (Cg) in the left hemisphere and all other recording sites (median with IQR-error bars, n=8). *(B)* Inter-hemispheric coherence in the slow oscillation band (median with IQR-error bars, n=8).

Synchrony of the slow oscillation – Cross-correlation

Cross-correlation was calculated to calculate the time delay between dorsal and ventral mPFC. An example of a slow oscillation cross-correlation between the most dorsal and most ventral channel from one animal is shown in Figure 3.9 A.i,ii. The time lag between the slow wave signal on the most dorsal channel (located in Cg) and the most ventral channel (located in DP) was calculated as the time lag at the peak of the cross-correlation. This dorsal-to-ventral time lag (reference: dorsal) was not different from zero ($p>0.05$, Wilcoxon signed-rank test, median: 19 ms, IQR: -0.5 – 80.5, n=8, Figure 3.9 A.iii). The same cross-correlation analysis was performed on the most dorsal channel of the left and right hemisphere (example in Figure 3.9 B.i,ii). The inter-hemispheric cross-correlation (reference: left) of the most dorsal recording site was not different from zero ($p>0.05$, Wilcoxon signed rank test, median: -0.5 ms, IQR: -24.5 – 3.5, n=8, Figure 3.9 B.iii). Hence, neither the lag between the most dorsal and the most ventral channel in the left hemisphere, nor the lag between the right and left hemisphere was significant, which means that the slow oscillation occurred rather synchronous in both hemispheres and along the entire dorsal-to-ventral axis within the mPFC. Note, however, that for the dorsal-to-ventral comparison there was a high between-animal variability, with some animals showing a positive, others a negative lag.

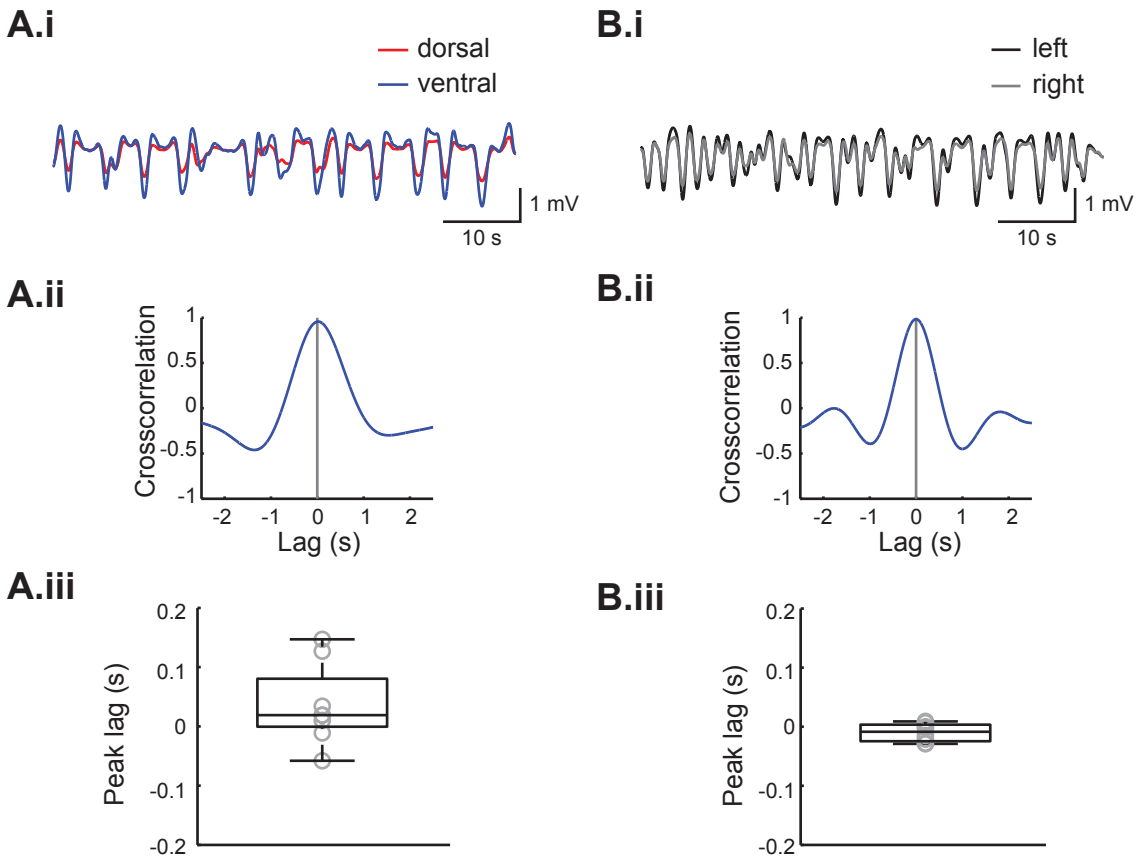

Figure 3.9. Synchrony of the mPFC slow oscillation - cross-correlation.
(A) Slow oscillation cross-correlation between the most dorsal and most ventral recording sites. *(A.i)* Example of 60 s LFP traces from the most dorsal (Cg) and most ventral (DP) recording sites filtered for the slow oscillation. *(A.ii)* Cross-correlation of the two traces in (A.i.) *(A.iii)* Box plot showing peak lag of cross-correlation, grey circles show peak lags from all experiments. Peak lags were not different from zero ($p>0.05$, Wilcoxon signed-rank test, n=8) *(B)* Cross-correlation between left and right hemisphere. *(B.i)* Example of 60 s LFP traces from left and right most dorsal recording site (Cg), filtered for the slow oscillation. *(B.ii)* Cross-correlation of the traces in (B.i.) *(B.iii)* Box plot showing peak lag of inter-hemispheric cross-correlation, grey circles show peak lags from all experiments. Peak lags were not different from zero ($p>0.05$, Wilcoxon signed-rank test, n=8).

Up-Down state parameters

Data from the eight animals with electrode placements equidistant to the midline were used to determine the basic features of the slow oscillation, characterized as Up-Down states. Because of the strong inter- and intra- hemispheric synchrony of the slow oscillation, meaning that UDS frequency and state lengths are the same for all channels, data from one channel were analysed (which was from the Cg region in the left hemisphere). Up-Down states were detected as described in section 2.3.4 and their basic parameters (Up state length, Down state length and Up-Down cycle frequency) calculated (Figure 3.10 A). These UDS parameters for all experiments are shown in Figure 3.10 B. Up-Down states occurred with a median frequency of 0.26 Hz (IQR: 0.21-0.29 Hz, n=8). The median Up state duration was 1.56 s (IQR: 1.32-1.64 s, n=8). Down states had a median duration of 2.51 s, which was longer than Up states (IQR: 1.94-3.26 s, n=8).

Having found that UDS occurred highly synchronously in the entire mPFC, in both hemispheres, I sought to investigate the hypothesis that there might be fine differences in the characteristics of the UDS – and associated fast oscillations – between the mPFC sub-regions, owing to local variations in architecture and connectivity.

It is first worth pointing out that, because the slow oscillation occurred in synchrony across the entire mPFC and I define UDS using the phase of the slow oscillation, no differences in UDS frequency, or length of Up or Down states could occur, by definition. However, I was able to study differences in UDS amplitude and, more importantly, in the characteristics of the nested fast oscillations.

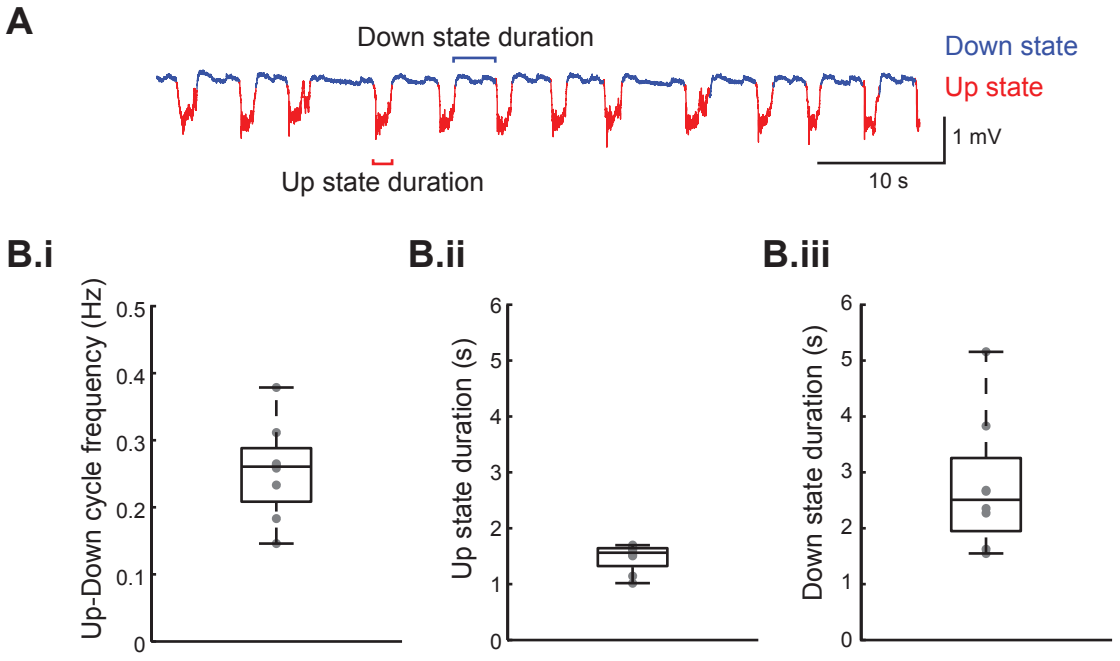

Figure 3.10. Medial prefrontal cortex Up-down state parameters. *(A)* Example LFP trace (recorded in Cg) with indication of detected Up- and Down states and illustration of the parameters Up state length and Down state length. *(B)* Box plots showing the basic Up-Down state parameters (n=8), with individual data points shown as grey dots. *(B.i)* Up-Down cycle frequency, *(B.ii)* Up state duration, *(B.iii)* Down state duration, n=8.

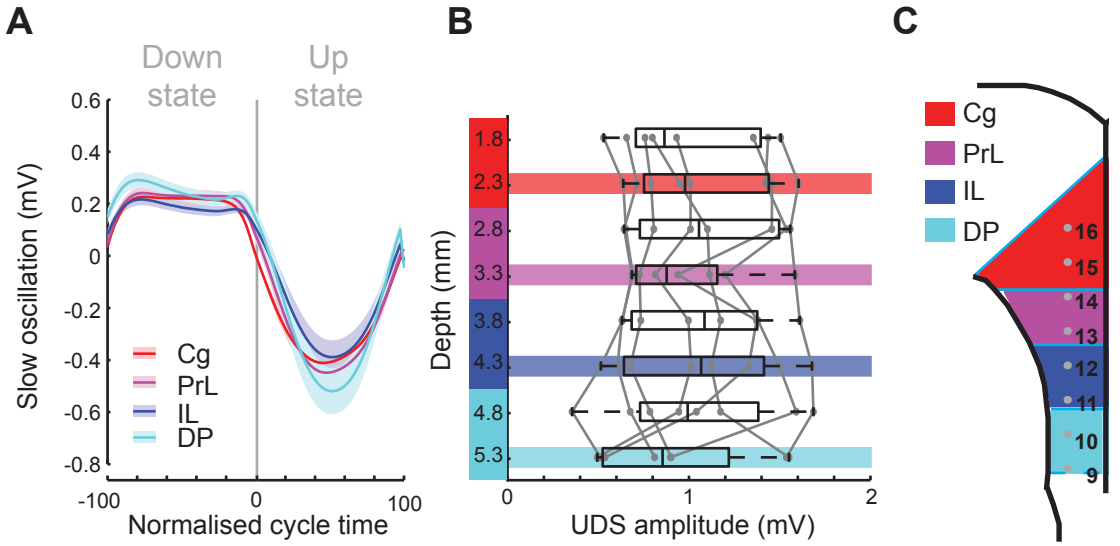

Figure 3.11. Amplitude of mPFC Up-Down states. *(A)* Example of the slow oscillation (LFP, band-pass filtered 0.1-0.9 Hz) aligned to the normalised Down state-Up state cycle. Data from one experiment (mean +/- SEM over all Up states in the data segment) shown for four mPFC subregions. *(B)* Box plot showing the UDS amplitude, i.e. slow oscillation peak-to-peak amplitude |Min SO Up state - Max SO Down state|, grey dots represent individual data points. Coloured shading indicates the recording sites the example data in (A) is from. There was no amplitude difference between the sub-regions ($\chi^2(7)=6.25$, $p>0.05$, Friedman's test, n=8). *(C)* Schema of mPFC indicating the recording sites (grey) in the left hemisphere used to calculate peak-to-peak amplitudes in (B). The mPFC sub-regions are colour-coded.

3.4.2 *Sub-regional profile of Up-Down state amplitude*

The UDS amplitude was measured as the peak-to-peak amplitude of the slow oscillation, aligned to the normalised Down-Up state cycle. An example for the alignment of the slow oscillation is shown in Figure 3.11 A. Figure 3.11 B shows the group data of UDS amplitude for different depths in the mPFC. Figure 3.11 C shows the corresponding recording sites in the left hemisphere of the mPFC. Two recording sites covered each mPFC sub-region (Figure 3.11 C). Depths of 1.8 and 2.3 mm (in Figure 3.11 B) corresponded to Cg, 2.8 and 3.3 mm to PrL, 3.8 and 4.3 mm to IL, and 4.8 and 5.3 mm to DP. Across all animals, the UDS amplitude was not dependent on the mPFC sub-region ($\chi^2(7)=6.25$, $p>0.05$, Friedman's test, n=8, Figure 3.11 B).

3.4.3 *Sub-regional profile of nested fast oscillation power*

Next, the nested fast oscillations within the Up states were investigated for sub-regional differences. For the spindle, gamma and high gamma band, an instantaneous band power was calculated for the selected 120 s LFP trace (detailed explanation in Chapter 2. Methods) and each UDS was aligned to a normalised Down-Up state cycle. Taking the mean across UDSs during this period gave mean power as a function of normalised cycle time for each frequency band, at each recording site in each animal.

To get a single value representative of a particular recording site in a particular animal, the mean power across normalised time during the Up state was then calculated. Thus a sub-regional profile of mean Up state power was calculated for each animal.

Sub-regional profile of mean Up state gamma power

Up state gamma power varied depending on the sub-region. A schema of the mPFC indicating the recording sites in the left hemisphere and the corresponding mPFC sub-regions is shown inFigure 3.12 A. The cycle-aligned gamma power for four recording sites (one from each sub-region, Figure 3.12B) illustrates how there are clear differences between the four mPFC sub-regions.

Group analysis of the mean Up-state power across recording sites (Figure 3.12 C.i) showed that there was a sub-regional difference in gamma power ($\chi^2(7)=52.04$, $p<0.001$, Friedman's test, n=8). Note that I use the term 'sub-regional difference' to report the results in this section, although the statistical analysis was performed on all 8 recording sites (i.e. depths, Figure 3.12 C.i), and two recording sites were always in the same sub-region (as indicated inFigure 3.12 A).

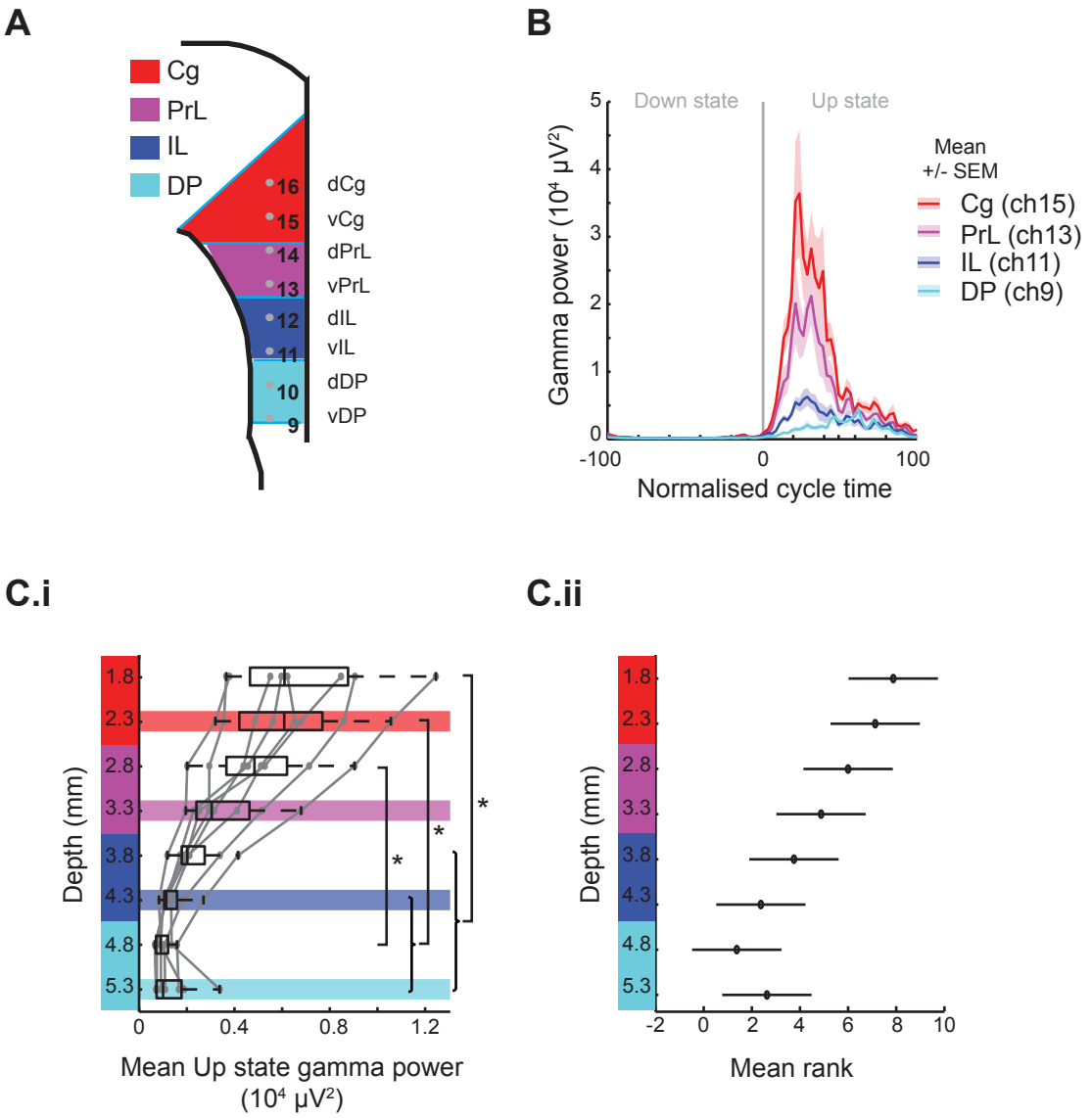

Figure 3.12. Sub-regional profile of Up state gamma (30-80 Hz) power.
(A) mPFC schema indicating the subregions with recording sites in the left hemisphere. *(B)* Example of mean gamma power from four channels aligned to the normalised Down-Up state cycle (mean over all Up states during 120 s recording from one animal). *(C.i)* Boxplot showing sub-regional profile of mean Up state gamma power, n=8; grey dots show individual data points. There were sub-regional differences in mean Up state gamma power ($\chi^2(7)=52.04$, $p<0.001$, Friedman's test, n=8). * indicates significance in a Tukey post-hoc test. *(C.ii)* Mean ranks (circles) for data in (C.i) with whiskers showing comparison intervals for Tukey post-hoc tests.

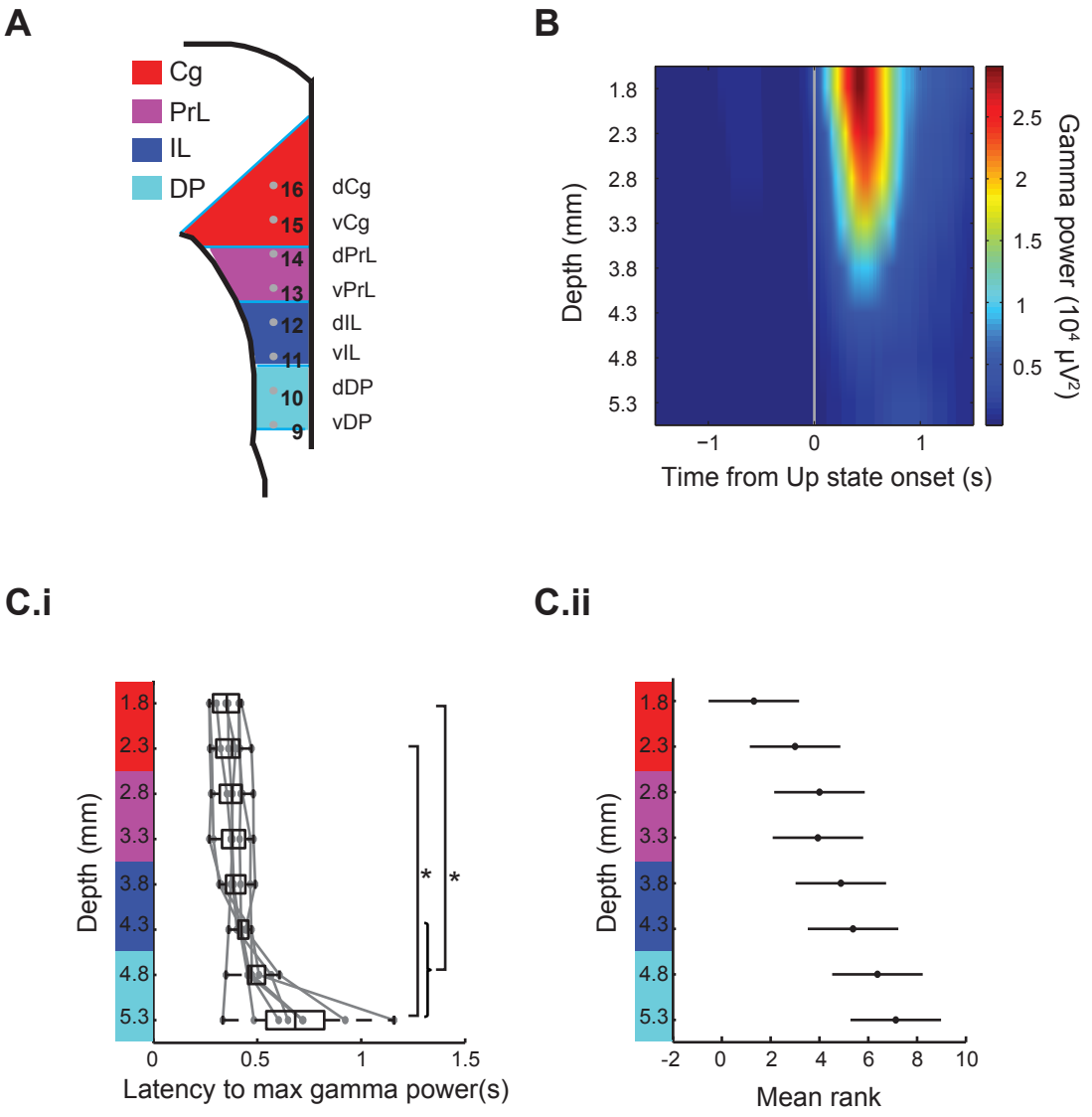

Figure 3.13. Latencies to peak gamma (30-80 Hz) power.
(A) mPFC schema indicating the subregions with recording sites in the left hemisphere. *(B)* Typical subarea profile of Up state onset-aligned smoothed gamma power (data from one animal). *(C.i)* Boxplot showing latencies from Up state onset to maximal gamma power across the mPFC, n=8; individual data points shown as grey dots. There were sub-regional differences in the latency to peak gamma power ($\chi^2(7)=32.42$, $p<0.01$, Friedman's test, n=8). * indicates significance in a Tukey post-hoc test. *(C.ii)* Mean ranks for data in (C.i) and comparison intervals for Tukey post-hoc test.

The dorsal Cg differed from IL and DP; the ventral Cg differed from vPrL and DP; and the dorsal PrL differed from the dorsal DP (Tukey post-hoc test). A box plot can be difficult to interpret when showing repeated-measures data, hence a plot of the mean ranks is shown to visualise how the Up state gamma power changes along the dorsal-to-ventral gradient. The plot of the mean ranks showed that there was a smooth, gradual decrease in gamma power from dorsal to ventral sites, with a slight increase again on the most ventral recording site (Figure 3.12 C.ii).

Sub-regional profile of latency to peak gamma power

Figure 3.13 B is based on the same example data as Figure 3.12 B, but this time, gamma power is smoothed and plotted on an absolute time scale. Gamma power from all 8 recording sites is shown, indicating a marked decrease in gamma power on ventral sites, as well as an apparent increase in peak latency, particularly on the most ventral site. Group analysis revealed that the gamma peak latency varied significantly with sub-region (χ^2 (7)=32.42, $p<0.01$, Friedman's test, n=8, see Figure 3.13 C.i). The median latency was 0.35 s (IQR: 0.29-0.41) at the most dorsal recording site (dorsal Cg), increasing to 0.68 s (IQR: 0.54-0.82) in DP. The latency differed between the dCg and the ventral regions (vIL, DP) as well as between the vCg and DP (Tukey post-hoc tests). The mean rank plot indicates a gradual increase in latency from dorsal to ventral mPFC (Figure 3.13).

Sub-regional profile of mean Up state high gamma power

Up state high gamma power also varied depending on recording depth. An example high gamma profile for all recording channels shows a clear dorsal-to-ventral difference in Up state high gamma power (Figure 3.14 B). In this example, Cg and PrL show similar Up state power levels, whereas in IL and DP the Up-state associated increase in high gamma power is very small, and occurs later during the Up state.

The group data confirmed a sub-regional difference in Up state high gamma power (χ^2 (7)=47.5, $p<0.01$, Friedman's test, n=8, Figure 3.14 C.i). Cg and dorsal PrL differed from ventral IL and DP, and ventral PrL differed from dorsal DP (Tukey post-hoc test). The statistical results revealed that, for high gamma power, there was mainly a strong dorsal-to-ventral difference, rather than a gradual transition in high gamma power (mean ranks plot in Figure 3.14 C.ii), with higher power in the dorsal regions (Cg, PrL) than in the ventral regions (vIL, DP), and an intermediate value in the dorsal IL (Figure 3.14 C.ii).

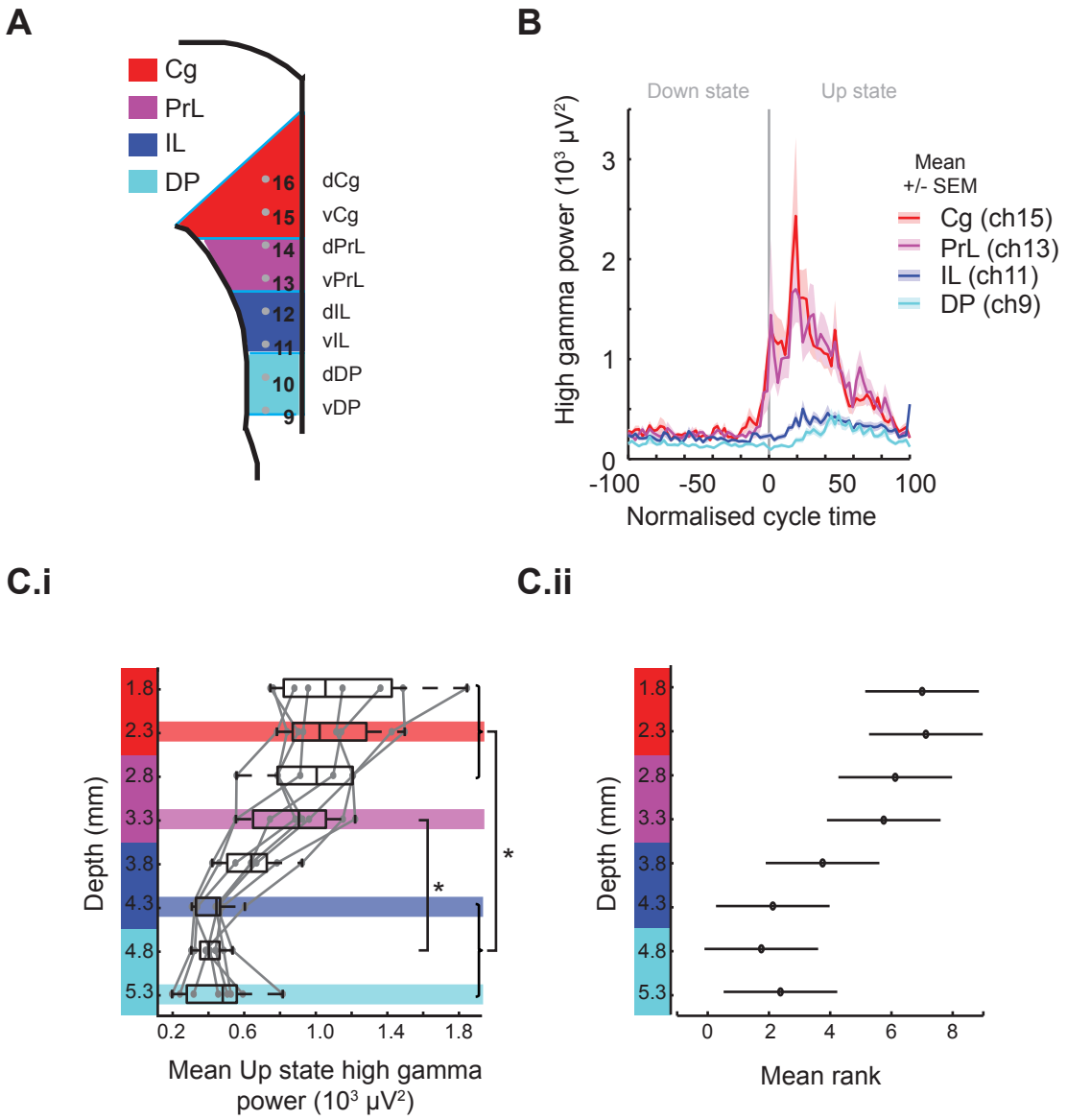

Figure 3.14. Sub-regional profile of Up state high gamma (80-150 Hz) power. *(A)* mPFC schema indicating the subregions with recording sites in the left hemisphere. *(B)* Example of mean high gamma power from four channels aligned to normalised Down state-Up state cycle (mean over all Up states during 120 s recording from one animal). *(C.i)* Boxplot showing sub-regional profile of mean Up state high gamma power, n=8; grey dots show individual data points. There were sub-regional differences in mean Up state high gamma power ($\chi^2(7)=47.5$, $p<0.01$, Friedman's test, n=8). * indicates significance in a Tukey post-hoc test. *(C.ii)* Mean ranks for data in (C.i) and comparison intervals for Tukey post-hoc tests.

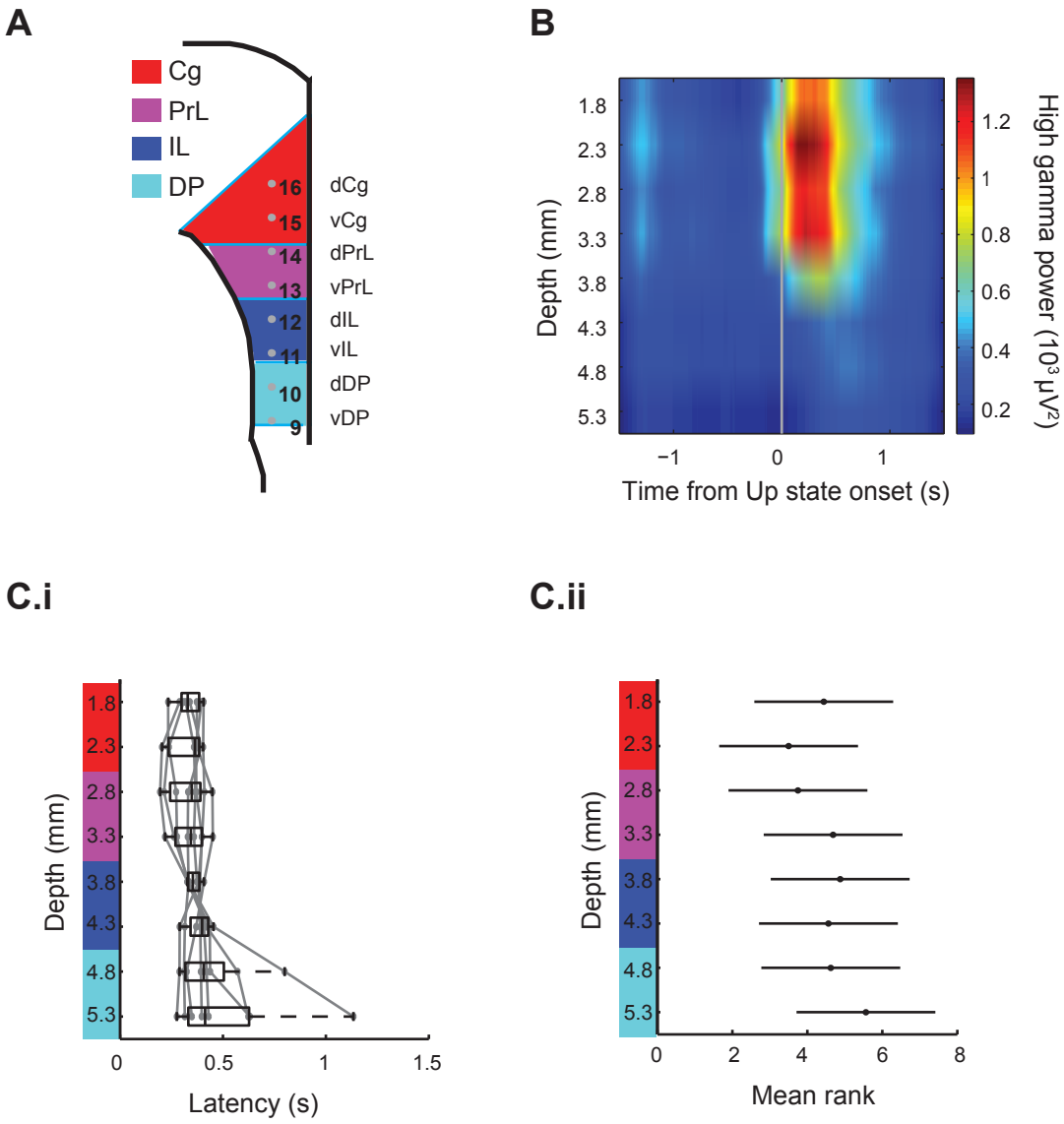

Figure 3.15. Latencies to peak high gamma (80-150 Hz) power.
(A) mPFC schema indicating the subregions with recording sites in the left hemisphere. *(B)* Typical subarea profile of Up state onset aligned smoothed high gamma power (data from one animal). *(C.i)* Boxplot showing latencies from Up state onset to maximal high gamma power across the mPFC (n=8); individual data points shown in grey. There was no sub-regional difference in the latency to the peak high gamma power ($\chi^2(7)=3.87$, $p=0.79$, Friedman's test, n=8). *(C.ii)* Mean ranks for data in (C.i).

Sub-regional profile of latency to peak high gamma power

Figure 3.15 B shows an example profile of Up state onset-aligned high gamma power on an absolute time scale for latency analysis.

Group analysis showed that the high gamma peak latency did not vary significantly with sub-region (χ^2 (7)=3.87, p>0.05, Friedman's test, n=8, Figure 3.15 C.i). The median latency was 0.33 s (IQR: 0.30-0.38) in the CG and 0.41 s (IQR: 0.33-0.63) in the DP.

Sub-regional profile of mean Up state spindle power

A sub-regional difference was also found for spindle power. The example spindle power profile over the normalised Down-state-Up-state cycle shows higher spindle power dorsally compared to ventrally, with the highest power in ventral Cg and dorsal PrL (Figure 3.16 B). Spindle power seemed to peak at different times during the Up state, with sub-regional differences. In the example in Figure 3.16 B, the peaks in Cg became smaller with progression of the Up state, but in DP, the spindle peaks became larger with progression of the Up state. Group analysis (Figure 3.16 C.i) confirmed a sub-regional difference in mean Up state spindle power (χ^2 (7)= 32.21, p<0.001, Friedman's test, n=8). The Cg and ventral PrL differed from the ventral IL, and the ventral Cg differed from the dorsal IL (Tukey post-hoc test). The mean rank plot (Figure 3.16 C.iii) shows high spindle power in the three most dorsal regions (Cg and ventral PrL), then a decrease from dPrL to vIL, and an increase again in DP, nearly reaching the level of the dorsal mPFC.

Sub-regional profile of latency to peak spindle power

A clear latency difference in spindle power was found between the dorsal and ventral mPFC. Figure 3.17 B shows an example sub-regional profile of Up state-onset aligned spindle power. The group data plot (Figure 3.17 C.i) shows that in all experiments, the latency to spindle power peak was increased on the most ventral channel. The latency was constant from depth -1.8 mm (which corresponded to Cg) to -3.8 mm (corresponding to the dorsal IL), with a median latency of 0.25 s (IQR: 0.22-0.26) in the Cg and 0.27 s (IQR: 0.25-0.29) in the dorsal IL. A higher latency was found in the DP with a median latency of 0.34 s (IQR: 0.28-0.87 s) in the dorsal DP (depth 4.8 mm), and a median latency of 0.82 s (IQR: 0.64-1.03 s) in the ventral DP (depth 5.3 mm).

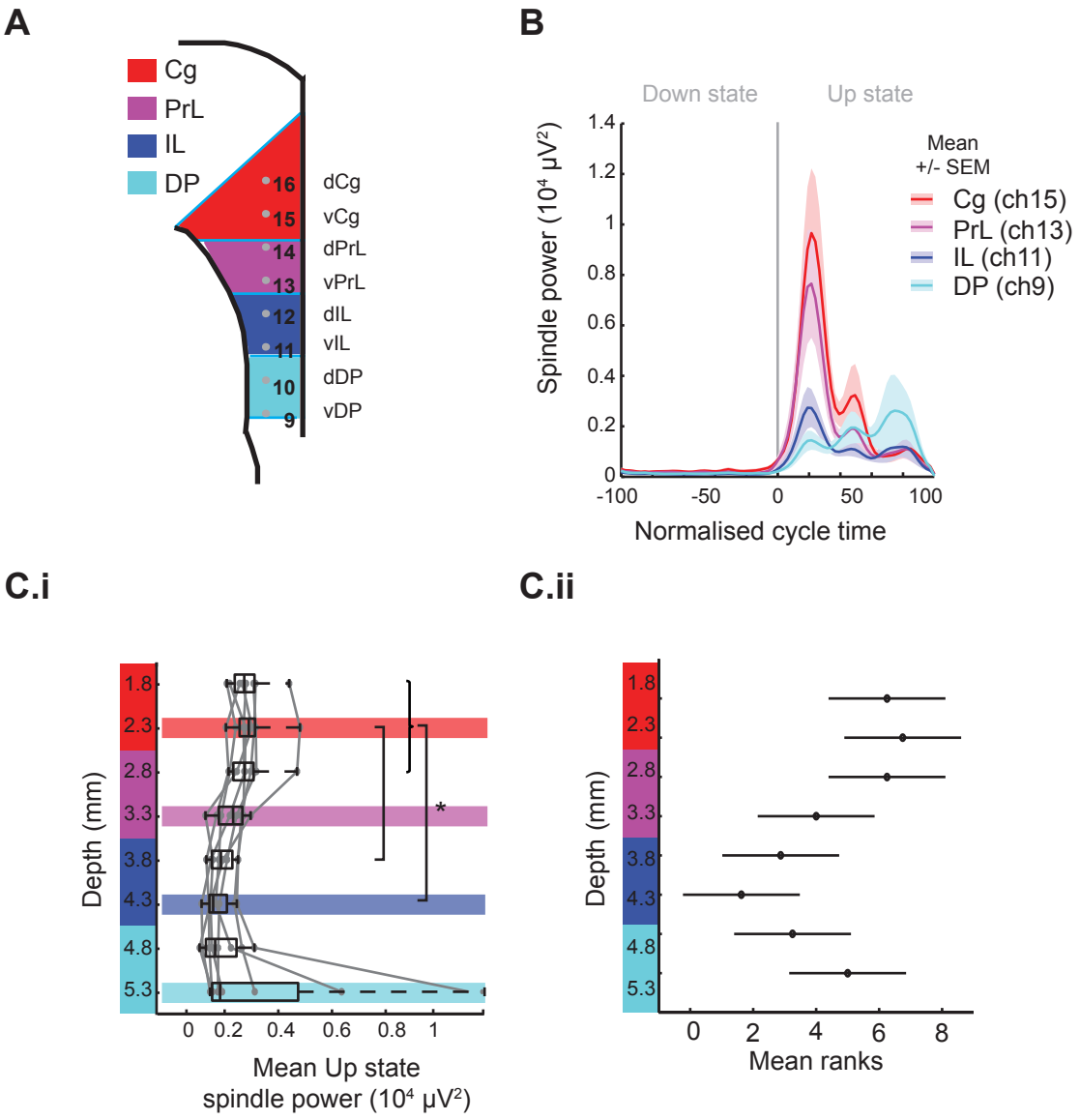

Figure 3.16. Sub-regional profile of Up state spindle (6-15 Hz) power.
(A) mPFC schema indicating the subregions with recording sites in the left hemisphere. *(B)* Example of mean spindle power from four channels aligned to normalised Down-Up state cycle (mean over all Up states during 120 s recording from one animal). *(C.i)* Boxplot showing sub-regional profile of mean Up state spindle power (n=8); grey dots show individual data points. There were sub-regional differences in mean Up state spindle power ($\chi^2(7)=32.21$, $p<0.001$, Friedman's test, n=8). * indicates significance in a Tukey post-hoc test. *(C.ii)* Mean ranks for data in (C.i) and comparison intervals for Tukey post-hoc tests.

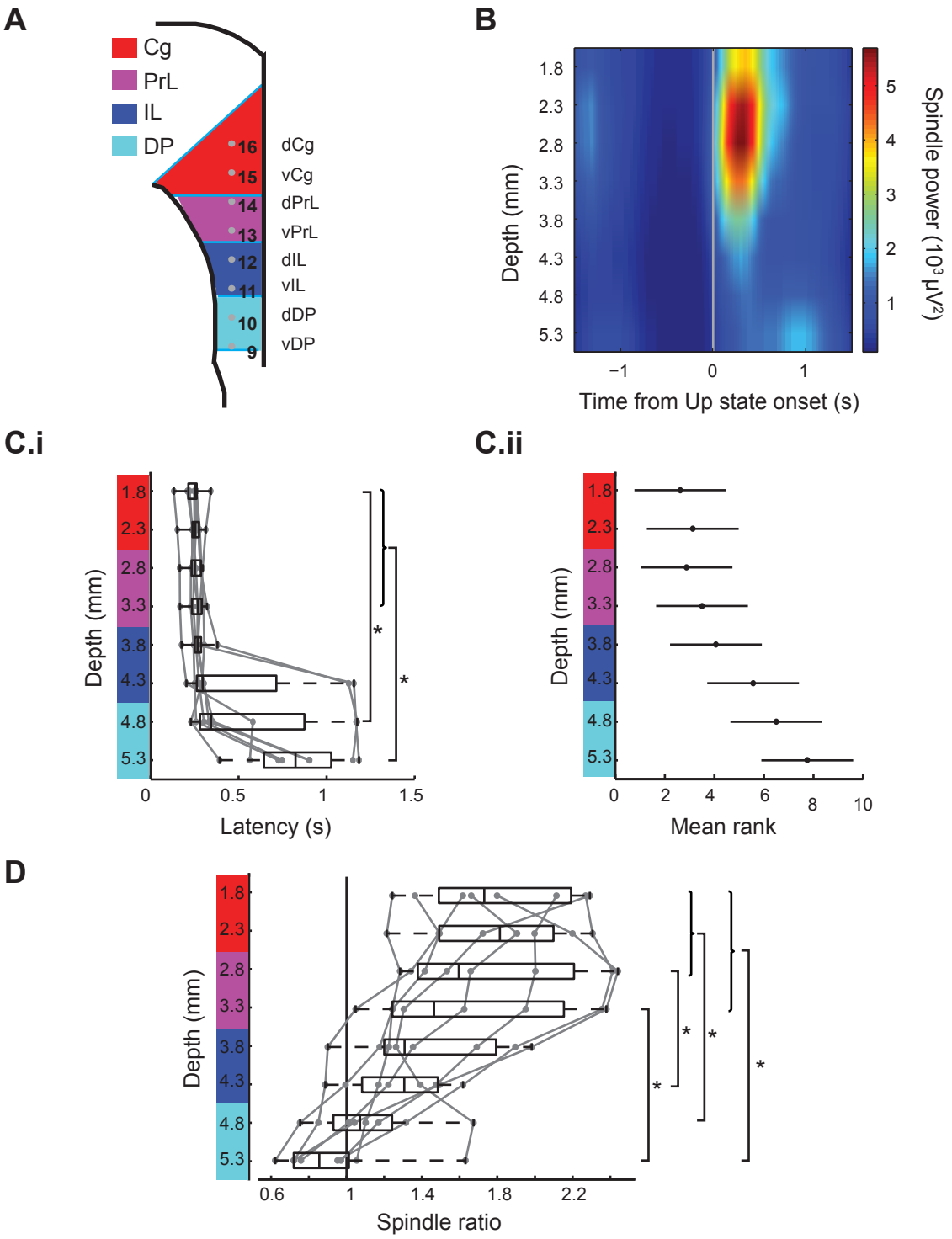

Figure 3.17. Latencies to peak spindle (6-15 Hz) power.
(A) mPFC schema indicating the sub-regions with recording sites in the left hemisphere. *(B)* Typical subarea profile of Up state onset aligned smoothed spindle power (data fom one animal). *(C.i)* Boxplot showing latencies from Up state onset to maximal spindle power across the mPFC (n=8); individual data points shown in grey. There were sub-regional differences in latency ($\chi^2(7)=33.34$, $p<0.001$, Friedman's test, n=8).
* indicates significance in a Tukey post-hoc test. *(C.ii)* Mean ranks for data in (C.i) and comparison intervals for Tukey post-hoc test. *(D)* Box plot showing the spindle ratio (n=8), which is the spindle power in the 1st Up state half divided by the spindle power in the 2nd Up state half. There was a sub-regional difference in spindle ratio ($\chi^2(7)=39.7$, $p<0.001$, Friedman's test, n=8). * indicates significance in a Tukey post-hoc test.

Statistical analysis revealed that the latency to the spindle power peak was dependent on the sub-region (χ^2 (7)= 33.34, p<0.001, Friedman's test, n=8). The latency in dCg differed from the latency in dDP. And the latencies in Cg and PrL differed from the latencies observed in vDP (Tukey post-hoc tests). The mean rank plot shows the sub-regional profile (Figure 3.17 C.ii.).

As mentioned above, spindle power seemed to increase several times during the Up states, forming distinct peaks, reaching a maximum early during the Up state in Cg, but late in DP (Figure 3.16 A). Hence, an additional analysis was performed to compare spindle power in the first Up state half, to spindle power in the second Up state half. Figure 3.17 D shows a box plot of the ratio of mean Up state power in the first half of the Up state over mean Up state power in the second half. Values > 1 indicate that the power is higher in the first half of the Up state, whereas values < 1 indicate that the power is higher in the second half of the Up state. Looking at the dorsal-to-ventral profile, it becomes clear that in the dorsal regions the spindle power is higher in the first half of the Up state in all experiments, then going into ventral direction, the spindle power ratio gets closer to one, meaning the spindle power is the same in the first and second half of the Up state, whereas at the most ventral site it is higher in the second half of the Up state in nearly all experiments. Indeed, the spindle ratio was dependent on dorso-ventral depth (p<0.001, χ^2 (7)= 39.7, Friedman's test, n=8).

3.4.4 *Sub-regional SWA profile: additional analysis and figures*

In the previous sections, analysis was performed on data from the left hemisphere. In this section I am showing data for the left and right hemisphere, to confirm that there was no difference in the amplitude and nested fast oscillation profiles between the hemispheres. In addition, some additional analyses were performed to further demonstrate robustness of the results.

Up-Down state amplitude in right and left hemisphere

As expected, the sub-regional profile of Up-Down state amplitude did not differ between the left and the right hemisphere (Figure 3.18).

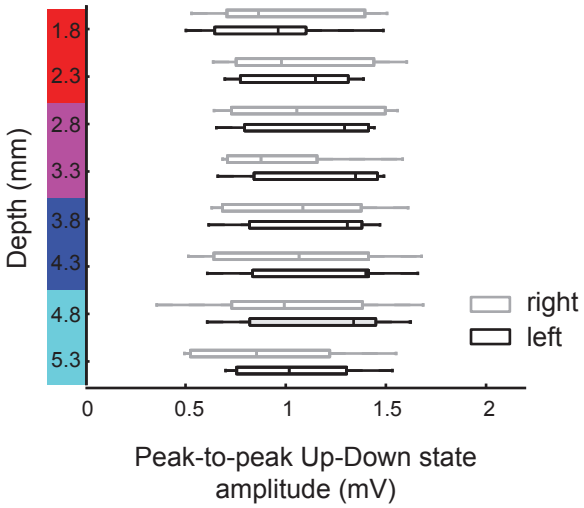

Figure 3.18. Sub-regional profile of Up-Down state amplitude in left and right hemisphere. No obvious difference in Up Down state amplitude between right and left hemisphere was observed when comparing data that was obtained from layer III in right and left hemisphere.

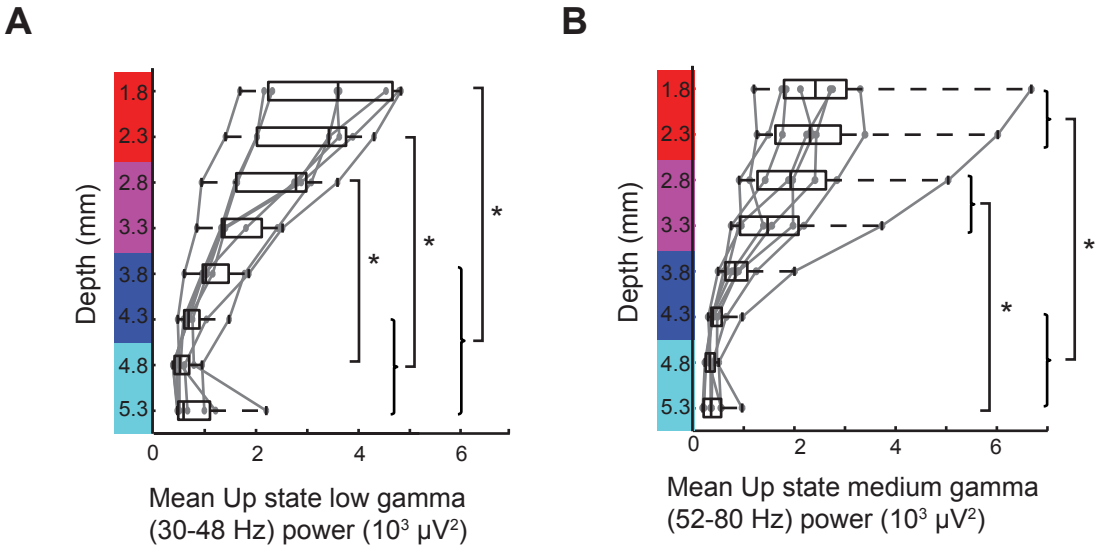

Figure 3.19. Sub-regional profile of Up state low gamma (30-48 Hz) and medium gamma (52-80 Hz) power in the left hemisphere.
(A) Sub-regional profile of mean Up state low gamma power. There were sub-regional differences in mean Up state low gamma power ($\chi^2(7)=50.08$, $p<0.001$, Friedman's test, n=8). *(B)* Sub-regional profile of mean Up state medium gamma power. There were sub-regional differences in mean Up state medium gamma power ($\chi^2(7)=50.67$, $p<0.001$, Friedman's test, n=8). In both ranges, the sub-regional distribution shows the same shape as the distribution of the gamma (30-80 Hz) power. * indicates significance in a Tukey post-hoc test.

Up state mean low and high gamma power

In the literature, the gamma band is sometimes divided into two bands (Belluscio et al., 2012; Bieri et al., 2014), with varying limits, usually around 50 Hz or 60 Hz (which has the advantage of avoiding mains noise, but also has functional implications (Bieri et al., 2014). Hence I performed the regional comparison again, for the 'low gamma (30-48 Hz) and 'medium gamma' (52-80 Hz) bands, to see if the observed differences were driven by a more specific frequency band. However, mean Up state power in these sub-bands showed a similar profile over the sub-areas to the gamma band (Figure 3.19 A and B). For both frequency bands, there was a significant difference between the subareas (low gamma: χ^2 (7)=50.08, p<0.001, medium gamma: χ^2 (7)=50.67, p<0.001, Friedman's test, n=8).

Up state maximum power

To determine whether the observed sub-regional differences in the *mean* Up state power did not occur simply because of a shorter duration of the gamma rhythm during the Up state, the sub-regional comparison was also performed on the *maximum* power during the Up state, for all three frequency bands.

The maximal Up state gamma power differed between the sub-regions (χ^2(7)=53.25, p<0.01, Friedman's test, n=8, Figure 3.20 A). The maximal Up state high gamma power also depended on the sub-regions (χ^2 (7)=49.96, p<0.001, Friedman's test, n=8, Figure 3.20 B), as did the maximal Up state spindle power (χ^2 (7)=27.96, p<0.001, Friedman's test, n=8, Figure 3.20 C). In all cases, the power was larger in dorsal compared to ventral regions. These results are in agreement with the previous analyses on Up state mean power.

Up state mean gamma power – local referencing

As I did not use local referencing during the experiments, it could be argued that the observed activity in the high-frequency bands might be global rather than local activity. To underpin the local source of this activity, post-hoc local referencing was performed by subtracting the LFP on channel 9 from the other LFPs. Figure 3.21 shows the sub-regional Up state gamma profile for the locally-referenced LFP. After subtraction, gamma activity is left on the channels dorsal to the reference channel, and the sub-regional distribution of gamma power is comparable to the one in Figure 3.12. Hence, local referencing yields similar results indicating local differences in gamma activity.

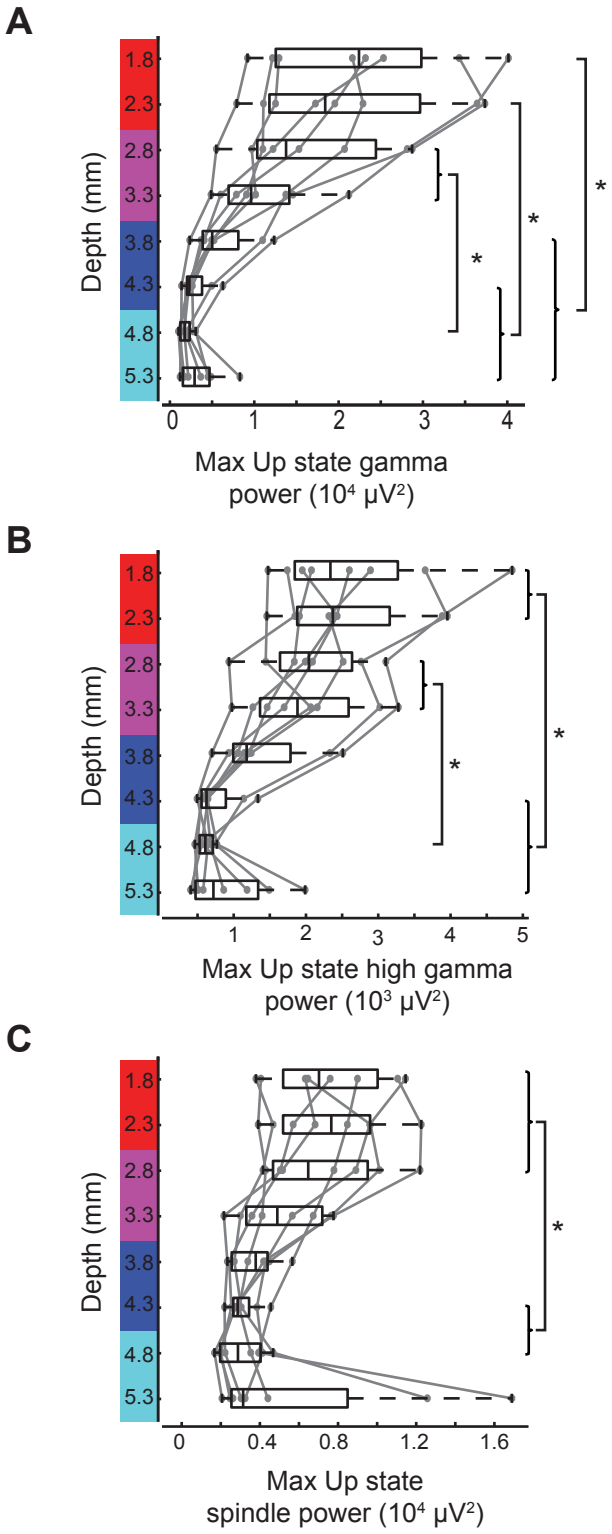

Figure 3.20. Sub-regional profile of maximum Up state power in the gamma, high gamma and spindle ranges. *(A)* Sub-regional profile of maximum Up state gamma power. There were sub-regional differences in maximal Up state gamma power ($\chi^2(7)=53.25$, $p<0.01$, Friedman's test, n=8). *(B)* Sub-regional profile of maximum Up state high gamma power. There were sub-regional differences in maximum Up state high gamma power ($\chi^2(7)=49.96$, $p<0.001$, Friedman's test, n=8). *(C)* Sub-regional profile of maximum Up state spindle power. There were sub-regional differences in maximal Up state spindle power ($\chi^2(7)=17.96$, $p<0.001$, Friedman's test, n=8). In (A), (B), and (C), * indicates significance in a Tukey post-hoc test.

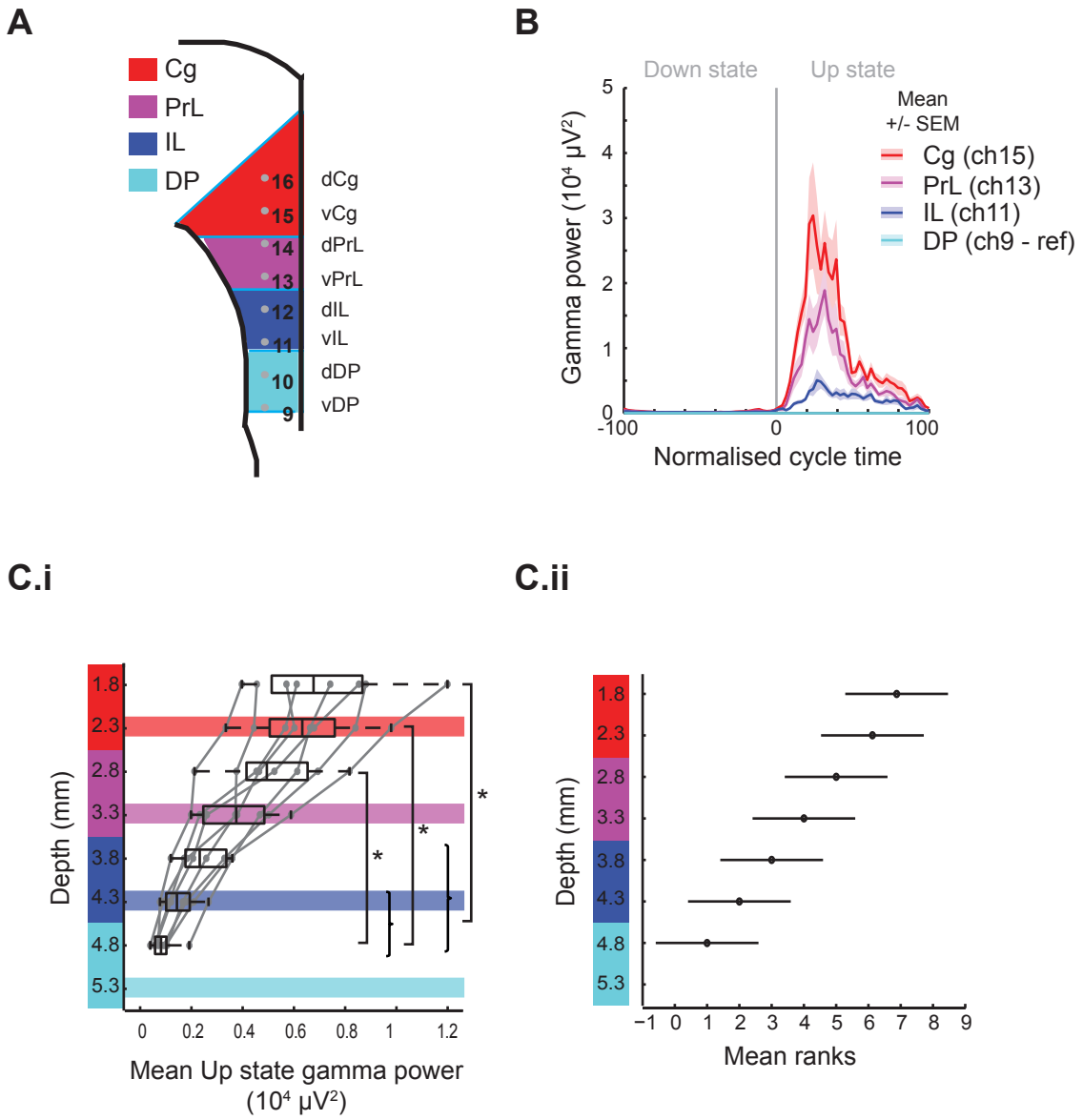

Figure 3.21. Sub-regional profile of Up state gamma (30-80 Hz) power of locally-referenced LFP data (channel 9 as reference). *(A)* mPFC schema indicating the sub-regions with recording sites in the left hemisphere.*(B)* Example of mean gamma power from four channels aligned to the normalised Down-Up state cycle (mean over all Up states during 120 s recording from one animal). *(C.i)* Boxplot showing sub-regional profile of mean Up state gamma power, n=8; grey dots show individual data points. There were sub-regional differences in mean Up state gamma power ($\chi^2(6)=47.62$, $p<0.001$, Friedman's test, n=8). * indicates significance in a Tukey post-hoc test. *(C.ii)* Mean ranks for data in (C.i) and comparison intervals for Tukey post-hoc tests.

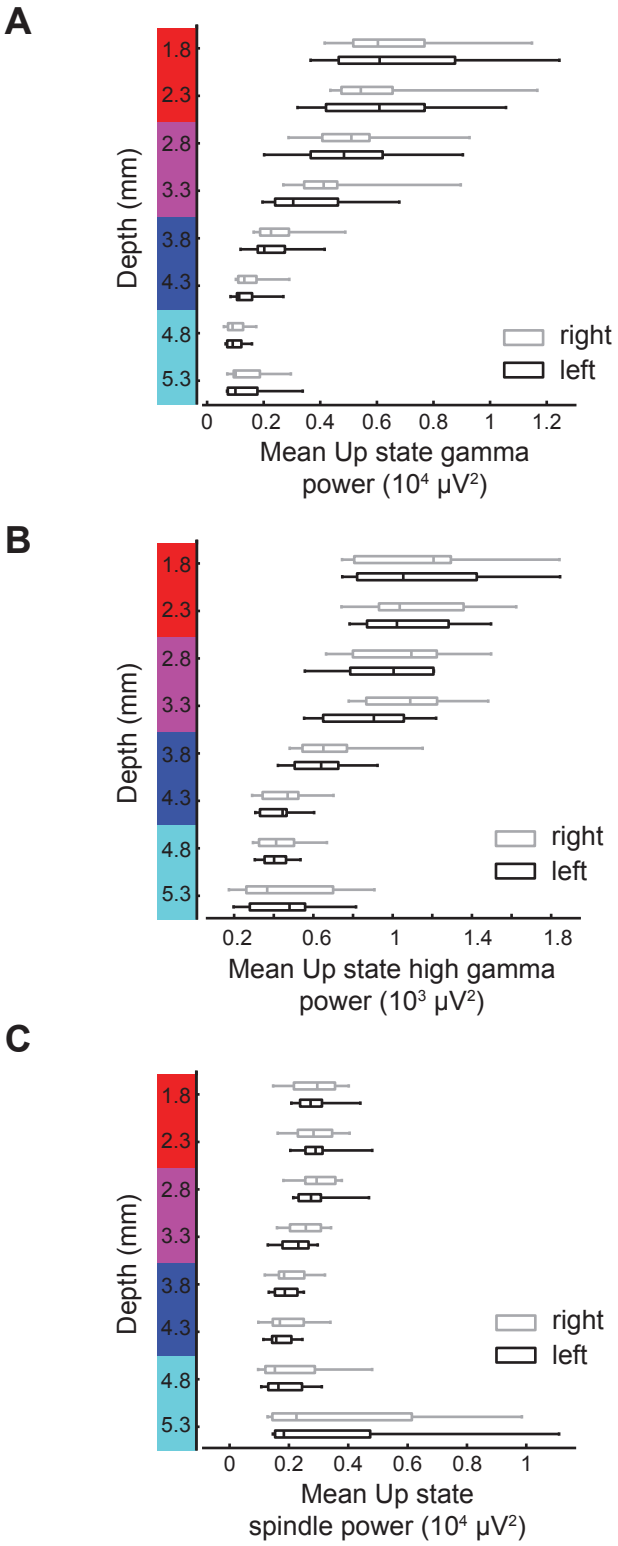

Figure 3.22. Sub-regional profile of mean Up state power in right and left hemisphere. *(A)* Mean Up state gamma power profile in the right and left hemisphere. *(B)* Mean Up state high gamma power profile in the right and left hemisphere. *(C)* Mean Up state spindle power profile in the right and left hemisphere. No differences were observed in Up state gamma, high gamma, or spindle power between the right and left hemisphere when data was obtained from layer III in both hemispheres.

Nested fast oscillation mean power during the Up state in right and left hemisphere

The analysis of the mean Up state fast oscillation power was performed in the left hemisphere. Here, I show the data for both hemispheres to show that the right and left hemisphere did not differ in these experiments, where the laminar position was the same in both hemispheres.

Mean Up state gamma power (Figure 3.22 A), mean Up state high gamma power (Figure 3.22 B) and mean Up state spindle power (Figure 3.22 C) showed very similar profiles between the hemispheres.

3.4.5 *Laminar profile of SWA – introductory remarks*

In this section, I report differences between cortical laminae within the mPFC. Several studies in rats (Sanchez-Vives and McCormick, 2000), mice (Beltramo et al., 2013) and cats (Chauvette et al., 2010) have found that the slow oscillation originates in deep cortical layers. However, a study in naturally sleeping humans has found that the slow oscillation, as well as the high frequency activity during the Up state, originates in the superficial layers (Csercsa et al., 2010).

Here, I sought to investigate laminar differences in the UDS amplitude as well as high-frequency oscillation power during the Up state, as this might give a clue regarding the origin of the UDS and nested fast network activity. Note however, that for the data used in this chapter, the superficial layer data are recorded in one hemisphere, and the deep layer data in the other hemisphere, within the same animal. To account for possible differences between the left and the right hemisphere, analysis was performed on two different datasets. The 'RdeeperL' dataset consisted of experiments in which one electrode shank was placed in the superficial layers of the left hemisphere, and the other in the deep layers of the right hemisphere (Figure 3.23 A). The 'LdeeperR' dataset, on the other hand, consisted of experiments in which one electrode shank was placed in the superficial layers of the right hemisphere, and the other in the in deep layers of the left hemisphere (Figure 3.23 B). Factors investigated in the statistical analysis are '*Laminar depth*' and depth in dorso-ventral direction ('*D-V depth*').

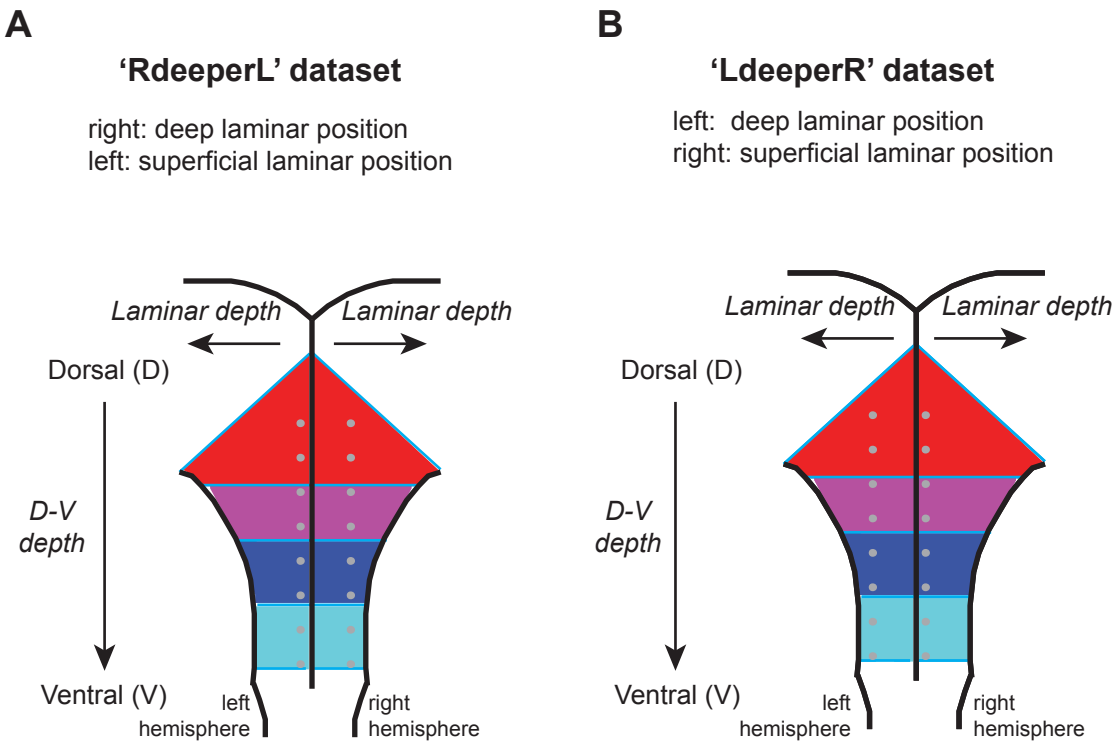

Figure 3.23. Electrode positioning in the mPFC for the 'RdeeperL' and 'LdeeperR' datasets with indication of the ANOVA factors '*Laminar depth*' and '*D-V depth*'. *(A)* mPFC schema indicating the electrode site location in the 'RdeeperL' dataset. *(B)* mPFC schema indicating the electrode site location in the 'LdeeperR' dataset. The ANOVA-factors '*Laminar depth*' and '*D-V depth*' are indicated with arrows.

3.4.6 *Laminar profile of Up-Down state amplitude*

My results showed that the UDS amplitude was dependent on the cortical lamina from which the LFP was recorded. In addition, within layer I/II and within layer III-VI data, there was a sub-regional difference in UDS amplitude across the dorso-ventral axis of the mPFC. This contrasts with my results from the layer III dataset (Section 3.4.2), where no sub-regional difference in amplitude was seen.

'RdeeperL' dataset: The UDS amplitude was significantly larger in deep layers compared to superficial layers (main effect of *Laminar depth*, $F_{(1,28)}$=22.07, p<0.01, two way RM ANOVA (two factor repetition), n=5, Figure 3.24 A). In contrast to the results obtained for layer III (section 3.4.2), the UDS amplitude was also dependent on *D-V depth* ($F_{(7,28)}$=4.72, p<0.01, n=5). There was an interaction between laminar depth and D-V depth (*Laminar depth*D-V depth* $F_{(7,28)}$=7.00, p<0.001, n=5), but no individually significant differences were found between laminar depths at specific D-V depth (Holm-Sidak post-hoc test). Conversely, the sub-regional amplitude difference was significant for three comparisons in the superficial layers, but only one comparison in the deep layers (Figure 3.24 A). This indicates that in both, superficial and deep layers, there was a sub-regional difference in UDS amplitude, and that this sub-regional difference might be more pronounced in superficial layers.

'LdeeperR' dataset: In this dataset, the finding of a sub-regional difference in UDS amplitude was confirmed. The UDS amplitude was significantly larger in deep compared to superficial layers (*Laminar depth* ($F_{(1,28)}$=30.46, p<0.01, two way RM ANOVA (two factor repetition), n=5, Figure 3.24 B). And again, the UDS amplitude was dependent on the *D-V depth* ($F_{(7,28)}$=3.66, p<0.01, n=5). There was no interaction between laminar depth and D-V depth (*Laminar depth*D-V depth* $F_{(7,28)}$=0.45, p>0.05), indicating that the difference in UDS amplitude between deep and superficial layers was not dependent on the position in D-V direction in the mPFC.

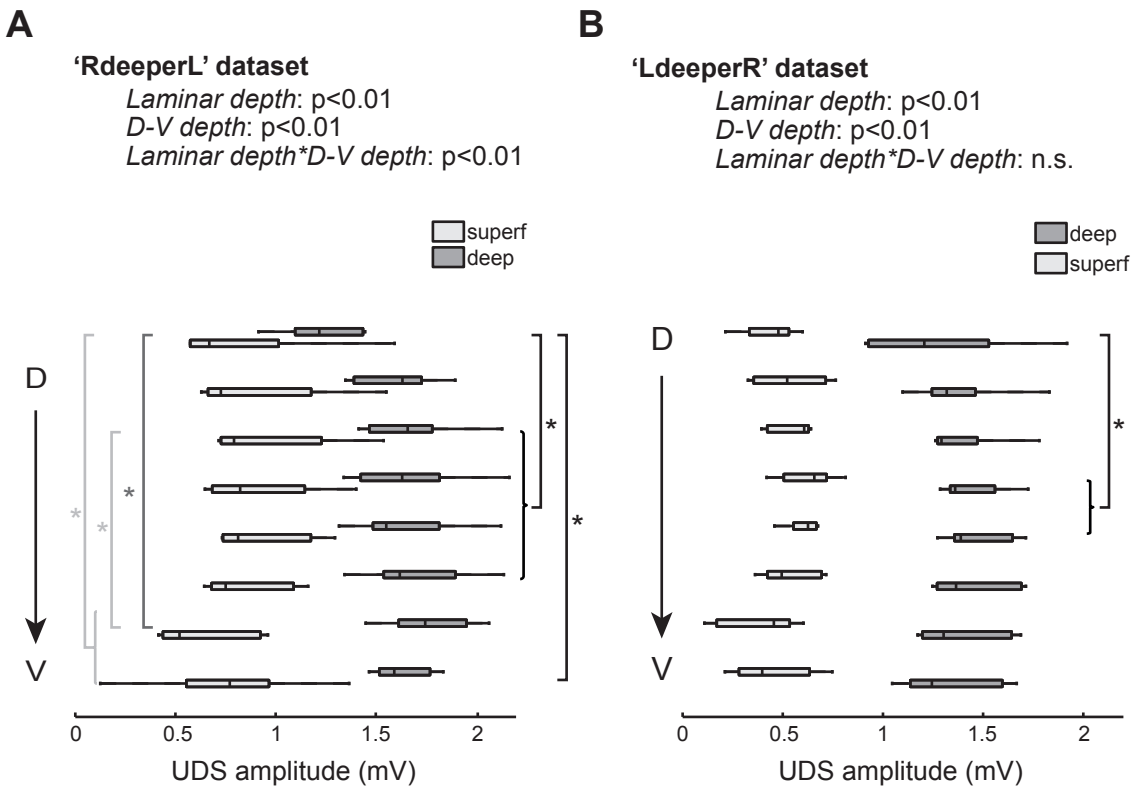

Figure 3.24. Laminar profile of Up-Down state amplitude.
(A) Box plot showing the UDS amplitude in deep laminar position (in the right hemisphere) and superficial laminar position (in the left hemisphere). *(B)* Box plot showing the UDS amplitude of the slow oscillation in deep laminar position (in the left hemisphere) and superficial laminar position (in the right hemisphere). * in A and B indicates significance in Holm-Sidak post-hoc test after a significant main effect of *Laminar depth* in two-way RM ANOVA, n=5. * in A indicates significance of *D-V depth* difference within the deep layers in Holm-Sidak post-hoc test. * in A indicates significance of *D-V depth* difference within the superficial layers in Holm-Sidak post hoc test.

3.4.7 *Laminar profile of nested fast oscillation power*

Laminar comparison of mean Up state gamma power

A laminar difference in mean Up state gamma power was found in both datasets, with higher power in the deeper laminar position. In addition, the sub-regional difference in mean Up state gamma power observed in layer III (section 3.4.3) was confirmed for layers I/II and III-VI.

'RdeeperL' dataset: In this dataset, mean Up state gamma power was significantly higher in deep compared to superficial layers (main effect of *Laminar depth:* $F_{(1,28)}$=74.77, p<0.001, two way RM ANOVA (two factor repetition), n=5, Figure 3.25 A). Consistent with the results for the layer III dataset used in the previous sub-section for the sub-regional comparison (section 3.4.3), mean Up state gamma power was higher in the dorsal compared to the ventral mPFC (main effect of factor *D-V depth* $F_{(7, 28)}$=36.68, p<0.001, n=5). The interaction between laminar depth and D-V depth was also significant (*Laminar* depth***D-V depth* $F_{(7,28)}$=22.50, p<0.001, n=5). Post-hoc tests revealed that the mean Up state gamma power was higher in the deep than in the superficial layers in most of the mPFC (vCg, PrL, vIL, and DP, Holm-Sidak, Figure 3.25 A).

'LdeeperR' dataset: In this dataset, the above observation was confirmed. Again, mean Up state gamma power was dependent on *Laminar depth* ($F_{(1,28)}$=37.01, p<0.01, two way ANOVA (two factor repetition), n=5, Figure 3.25 B) and again, sub-regional differences could be confirmed ($F_{(7,28)}$=70.22, p<0.001, n=5). There was an interaction between laminar depth and D-V depth (*Laminar depth*D-V depth* $F_{(7,28)}$= 9.09, p<0.001, n=5), hence a post-hoc test was performed to see, which sub-regions exhibited a laminar difference. Again, the laminar difference was significant in most of the mPFC (vCg, dPrL, vIL and DP, Holm-Sidak test, Figure 3.25 B).

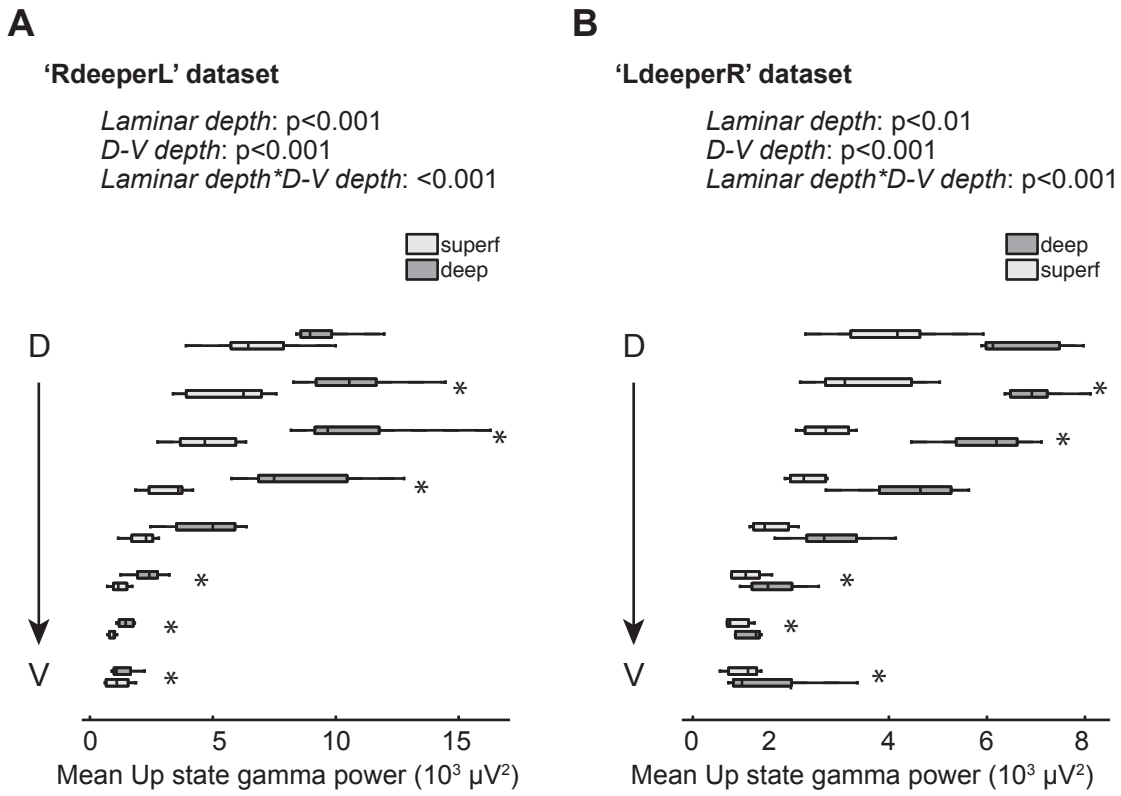

Figure 3.25. Laminar profile of mean Up state gamma (30-80 Hz) power.
(A) Box plot showing the mean Up state gamma power in deep laminar position (in the *right* hemisphere) and superficial laminar position (in the *left* hemisphere). *(A)* Box plot showing the mean Up state gamma power in deep laminar position (in the *left* hemisphere) and superficial laminar position (in the *right* hemisphere). * in (A) and (B) indicates significance in Holm-Sidak post-hoc test (*Laminar depth* within *D-V depth*) after a significant *Laminar depth*D-V depth* interaction in a two-way RM ANOVA, n=5.

Laminar comparison of mean Up state high gamma power

Mean Up state high gamma power was higher in the deep layers in both datasets. In addition, the sub-regional difference in Up state high gamma power observed in layer III (section 3.4.3) was confirmed for layers I/II and III-VI.

'RdeeperL' dataset: The mean Up state high gamma power was significantly higher in the deep layers compared to superficial layers (main effect of *Laminar depth* ($F_{(1,28)}$=46.94, p<0.01, two way RM ANOVA (two factor repetition), n=5, Figure 3.26 A). The mean Up state high gamma power was also significantly higher in dorsal compared to ventral mPFC (main effect of *D-V depth* ($F_{(7,28)}$=24.60, p<0.001, n=5). There was also a significant interaction between laminar depth and D-V depth (*Laminar depth*D-V depth* $F_{(7,28)}$=9.56, p<0.001, n=5), and the laminar difference was significant in most of the mPFC (PrL, vIL, DP, Holm-Sidak post-hoc test, Figure 3.26 A).

'LdeeperR' dataset: Again, the mean Up state high gamma power was significantly larger in deep compared to superficial layers (main effect of *Laminar depth* ($F_{(1,28)}$=8.46, p<0.05, two way RM ANOVA (two factor repetition), n=5, Figure 3.26 B). The mean Up state high gamma power was also dependent on *D-V depth* ($F_{(7,28)}$=53.96, p<0.001). The interaction between laminar depth and D-V depth was significant (*Laminar depth*D-V depth* $F_{(7,28)}$= 12.61, p<0.001), and the laminar difference was significant in half of the recording sites (associated with the regions dPrL, vIL, DP, Holm-Sidak post-hoc test, Figure 3.26 B).

Laminar comparison of mean Up state spindle power

Mean Up state spindle power was dependent on laminar depth in both data sets. In addition, the sub-regional difference in mean Up state spindle power observed in layer III (section 3.4.3) was confirmed here for layers I/II and III-VI in both data sets.

'RdeeperL' dataset: The mean Up state spindle power was significantly larger in deep compared to superficial layers (main effect of *Laminar depth* ($F_{(2,28)}$=30.24, p<0.01, two way RM ANOVA (two factor repetition), n=5, Figure 3.27 A). In addition, mean Up state spindle power was dependent on *D-V depth* ($F_{(7,28)}$=9.59, p<0.001, n=5). However, for spindle power, the difference in laminar depth was not dependent on D-V depth (*Laminar depth*D-V depth* $F_{(7,28)}$=1.95, p>0.05).

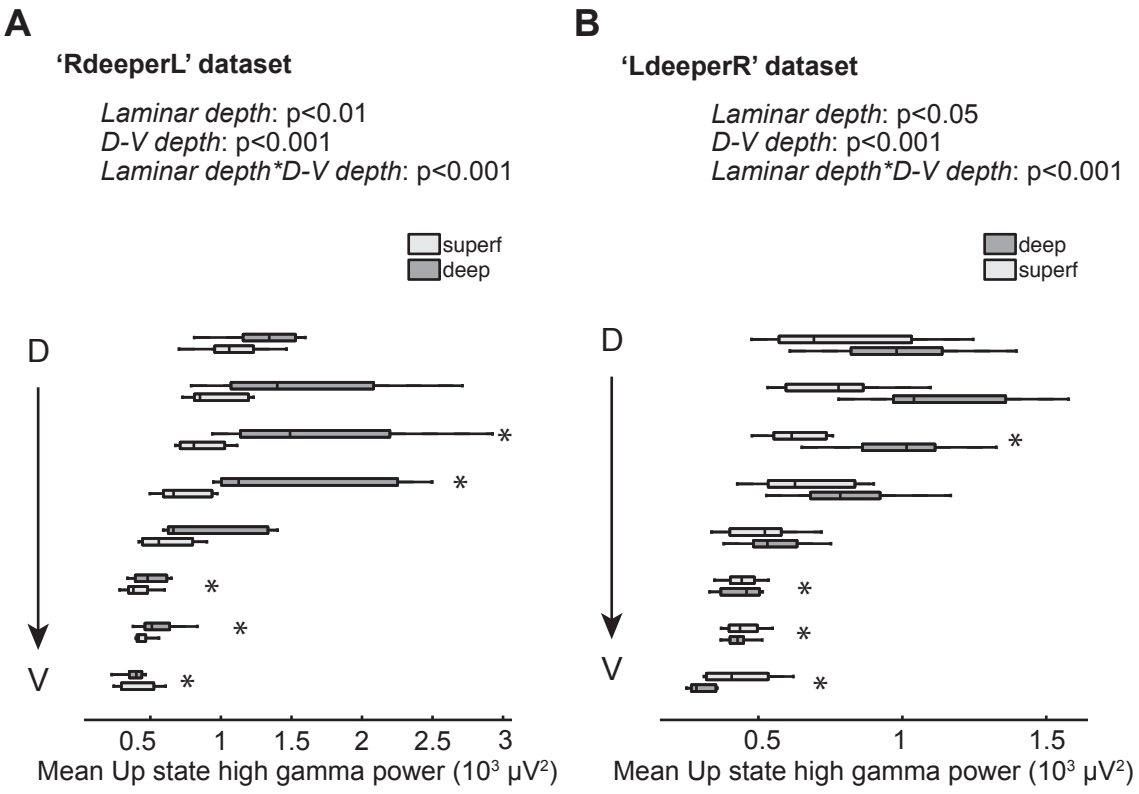

Figure 3.26. Laminar profile of mean Up state high gamma (80-150 Hz) power. *(A)* Box plot showing the mean Up state high gamma power in deep laminar position (in the *right* hemisphere) and superficial laminar position (in the *left* hemisphere). *(B)* Box plot showing the mean Up state high gamma power in deep laminar position (in the *left* hemisphere) and superficial laminar position (in the *right* hemisphere). * in (A) and (B) indicates significance in Holm-Sidak post-hoc test (*Laminar depth* within *D-V depth*) after a significant interaction of *Laminar depth*D-V depth* in two-way RM ANOVA, n=5.

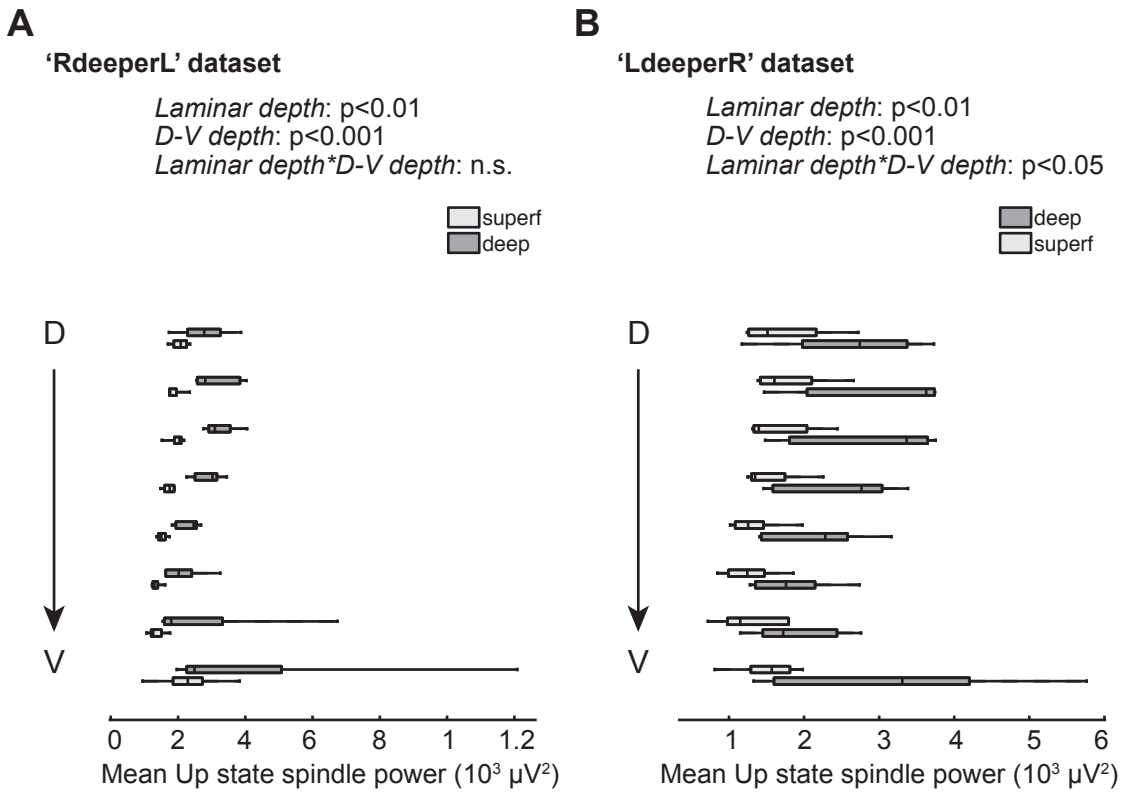

Figure 3.27. Laminar profile of mean Up state spindle (6-15 Hz) power.
(A) Box plot showing the mean Up state spindle power in deep laminar position (in the *right* hemisphere) and superficial laminar position (in the *left* hemisphere). *(B)* Box plot showing the mean Up state spindle power in deep laminar position (in the *left* hemisphere) and superficial laminar position (in the *right* hemisphere). None of the post-hoc tests were significant.

'LdeeperR' dataset: Mean Up state spindle power was dependent on *Laminar depth* ($F_{(1,28)}$=30.45, p<0.01, two way RM ANOVA (two factor repetition), n=5, Figure 3.27 B) and *D-V depth* ($F_{(7,28)}$=5.35, p<0.001, n=5). The interaction between laminar depth and D-V depth was significant (*Laminar depth*D-V depth* $F_{(7,28)}$=2.37, p<0.05, n=5). However, none of the post-hoc comparisons were significant (Holm-Sidak).

Hence, in contrast to the laminar difference in mean Up state gamma and high gamma power, the laminar difference in mean Up state spindle power was less dependent on the D-V position in the mPFC.

Analysis of latencies to peak power was not performed on this data. As the data used for the laminar comparison stems from two different hemispheres, an analysis of latencies would not be meaningful as the latencies would not be between neighbouring deep and superficial layers, but between deep and superficial layers in different hemispheres, separated by the medial wall.

3.5 Discussion

3.5.1 *Summary of results*

Investigating SWA in the mPFC of urethane-anaesthetised rats, we found the following properties of SWA:

Up-Down states

- The slow oscillation (< 1 Hz) was characterized by a high degree of synchrony across the entire mPFC (dorsal-to-ventral) within each hemisphere, and also between the two hemispheres.
- Up-Down states could be detected from the slow oscillations and occurred at a median frequency of 0.26 Hz, with a median Up state duration of 1.56 s and a median Down state duration of 2.51 s.
- The UDS amplitude did not differ between the mPFC sub-regions in layer III.
- The UDS amplitude showed some sub-regional variation in layers I/II and III-VI.
- UDS amplitude was larger in deep (III-VI) compared to superficial layers (I/II).

Nested fast activity

- Up state gamma power gradually decreased in the dorsal to ventral direction in the mPFC.
- Up state high gamma power was higher in the dorsal mPFC than in the ventral mPFC.
- Up state spindle power was highest in Cg, decreases gradually in PrL and IL, and was very variable in the ventral DP.
- Latencies between Up state onset and peak power were sub-region-dependent for gamma and spindle oscillations, with longer latencies in the ventral mPFC.
- Peak spindle activity occurred at the beginning of the Up state in the dorsal mPFC, and towards the end of the Up state in the ventral mPFC.
- For all frequency bands, Up-state nested fast oscillations had higher power in the deep layers of mPFC.

The results in this thesis were obtained in rats under urethane anaesthesia, a widely used model to investigate SWA. However, it is not clear how far the features of SWA observed in this thesis apply to SWA during natural SWS, especially as SWA during natural SWS is associated with memory-related processes, which might not necessarily occur during anaesthesia. In Chapter 6, I discuss the similarity between SWA in anaesthetised animals and naturally sleeping humans, and discuss the applicability of the results to SWA during human SWS.

3.5.2 *SWA was synchronous across the entire mPFC in both hemispheres*

SWA has been previously shown to be highly synchronous across the dorsal cortical surface. The mPFC in rats does not extend along the dorsal brain surface, but extends along the medial wall, almost from the dorsal to the ventral surface of the brain. Our findings show that, despite this obvious anatomical difference, the slow oscillation in the mPFC is very synchronous, as in the rest of the cortex (Volgushev et al., 2006; Sheroziya and Timofeev, 2014). This result is perhaps to be expected, given that mPFC regions are all highly interconnected (Heidbreder and Groenewegen, 2003), and also that they all receive strong thalamic inputs (Berendse and Groenewegen, 1991).

In addition, I found the slow oscillation to be very synchronous between the two hemispheres. This is in agreement with the literature as, using voltage sensitive dye recordings of the entire cortex in anaesthetised and quiet awake mice, strong inter-

hemispheric activity correlation of SWA has been shown (Mohajerani et al., 2010). In the same study, the experiments were repeated in a genetic mouse model lacking callosal connections, which showed SWA was no longer coordinated between the two hemispheres. Hence, the strong inter-hemispheric synchrony we observed may be mediated partly by trans-callosal mPFC connection, but also because of common thalamic inputs.

3.5.3 *The parameters of the detected Up-Down state were similar to those in the literature*

The UDS we observed under urethane anaesthesia occurred with a median frequency of 0.26 Hz, with a median Up state duration of 1.56 s and a median Down state duration of 2.51 Hz. These values are similar to what has been observed in urethane-anaesthetised cats by (Steriade et al., 1993d), who found frequencies between 0.3 and 0.4 Hz, Up states lasting 0.8-1.5 s and longer Down states. In the hippocampus of urethane anaesthetised rats the slow oscillation occurred at 0.17 Hz (Sharma et al., 2010). Both of these studies found that the slow oscillation frequency is lower under urethane compared to other anaesthetics.

3.5.4 *The very slow modulation of LFP power*

During all recordings performed for this thesis, the very slow modulation of broadband LFP power was observed under baseline, and after drug application. The 'high power state' of the VSMP lasted ~1-2 minutes, whereas the 'low power state' lasted ~2-9 minutes. The complete cycle, consisting of a 'low power state' and a 'high power state' lasted ~ 3-11 minutes. A comparison with similar findings in the literature was attempted in the following:

Cyclic brain state alternations (REM sleep-NREM sleep)

Cyclic brain state alternations, between REM sleep and NREM sleep-like states, with a similar cycle length have been observed in mice (Pagliardini et al., 2013) and rats (Clement et al., 2008) under urethane anaesthesia. In rats, these cyclic alternations occur with a cycle length of ~11 min (Clement et al., 2008). The characterising feature of these REM sleep-NREM sleep alternations is a fluctuation of power in the slow oscillation range, which is ~1 Hz (Figure 3.28 B and C, adapted from (Clement et al., 2008).

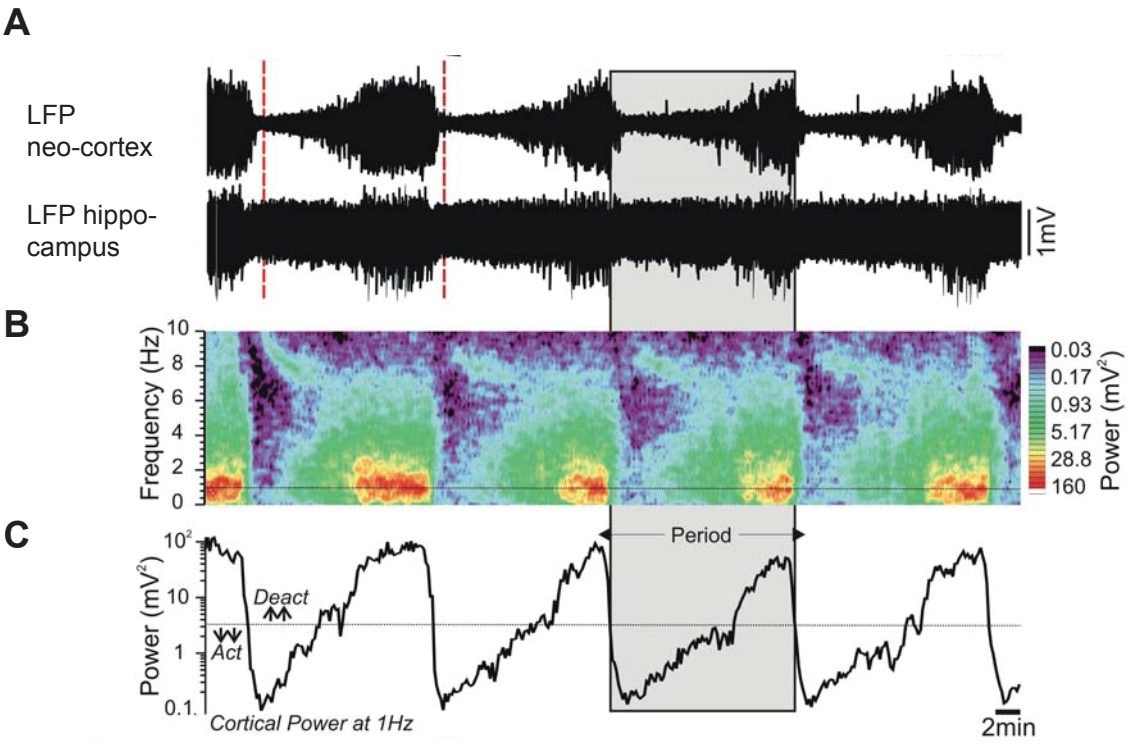

Figure 3.28. Sleep state-like transitions between REM sleep and NREM sleep under urethane anaesthesia as observerved in (Clement et al., 2008) show cyclic fluctuations in slow oscillation power. *(A)* Neocortical and hippocampal LFP recorded under urethane anaesthesia, showing cyclic brain state alternations. *(B)* The most prominent power fluctuation in the cortical LFP occured at 1 Hz. *(C)* Cortical power at 1 Hz from spectrogram in (B). The cortical power at 1 Hz shows cyclic amplitude fluctuations with a ~9 minute period. Figure adapted from (Clement et al., 2008).

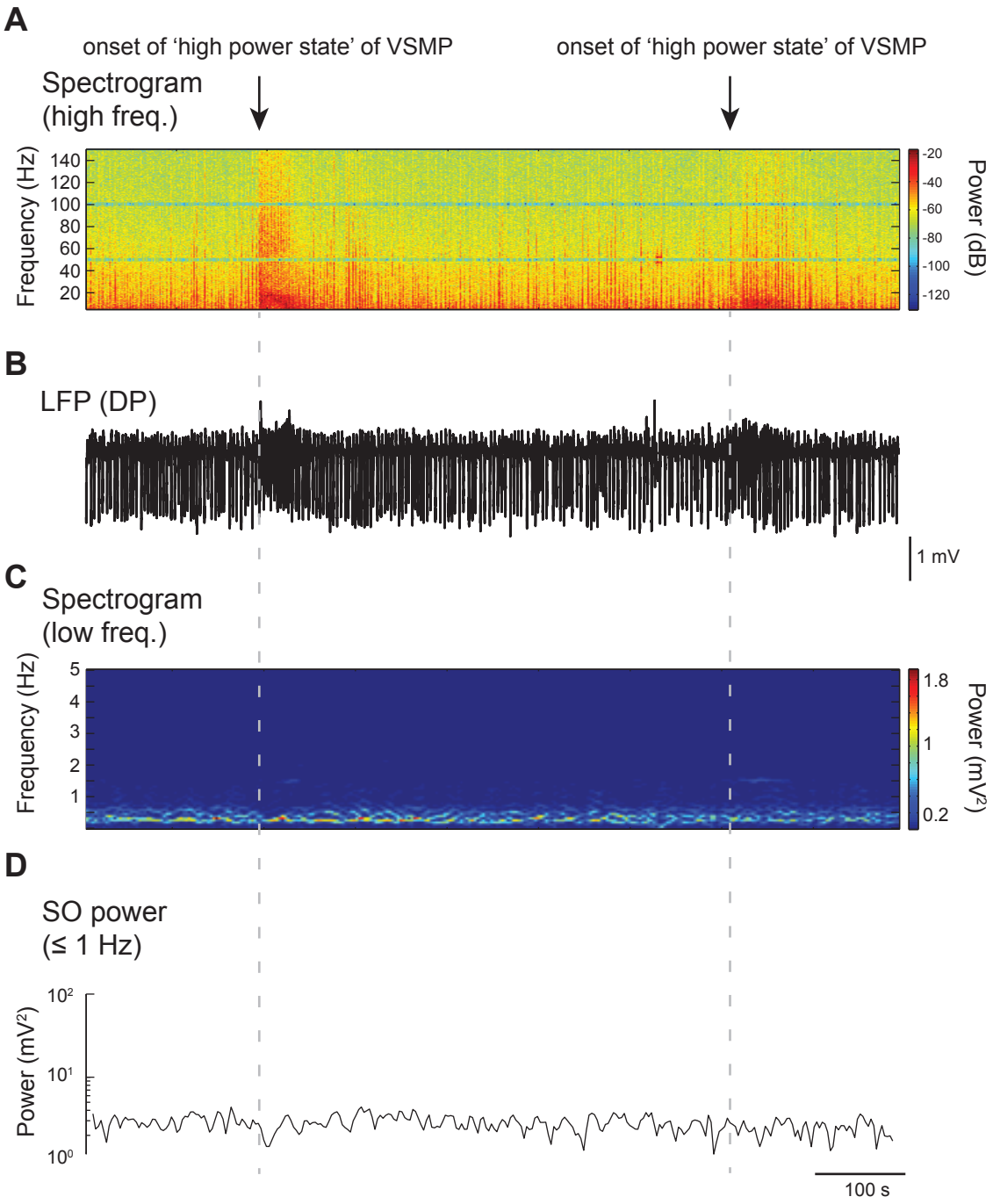

Figure 3.29. The very slow modulation of LFP power did not exhibit changes in the power of the slow oscillation. *(A)* Spectrogram showing high frequencies, of a 15 min DP LFP shown in (B), including two 'high power states' of the VSMP. *(B)* 15 min LFP recorded in ventral mPFC (DP). *(C)* Spectrogram showing power in the low frequencies of LFP in (B). The slow oscillation frequency occurs as a band of increased power in 0.2-0.8 Hz range. *(D)* Slow oscillation (≤ 1 Hz) power calculated from the spectrogram in (C). Grey, dashed lines indicate the onset of the 'high power states' of the VSMP (detected by eye from the spectrogram in (A). The power in the SO range does not fluctuate between the 'high power state' and the 'low power state' of the VSMP.

The 'high power state' of the VSMP in my experiments, however, still exhibited the slow oscillation (SO), as can be seen from the LFP traces in Figure 3.7. To confirm that the VSMP was not characterised by changes in SWA power, I repeated the analysis performed in (Clement et al., 2008) on a 15 minute LFP recording from the DP region (Figure 3.29), where the VSMP was strongest. There was no clear variation in SO amplitude visible in the LFP (Figure 3.29 B), which is in contrast to the cortical recording of (Clement et al., 2008), shown in Figure 3.28 A, where there are marked fluctuations in SO power. Thus, to be able to identify the 'high power states' of the VSMP, a spectrogram showing the high-frequency (>5 Hz) components of the LFP is shown Figure 3.29 A. Two 'high power states' can be seen in the spectrogram (Figure 3.29 A). In this example, a spectrogram using longer time windows showed the low frequency components (<5 Hz) of the signal, and the slow oscillation (SO) could be seen as a continuous band at ~0.2-0.8 Hz. The sum of the LFP power in the SO range (≤1 Hz) in Figure 3.10 D showed no fluctuations in the SO power. Hence, the VSMP reported here was different from REM sleep-NREM sleep transitions observed under anaesthesia by Clement et al. (2008).

However, the anaesthesia level chosen for this thesis was very deep, to ensure stable SWA activity without spontaneous switching to the REM-like state. Hence, it might be that the VSMP is a different expression of the REM sleep-SWA cycling observed in (Clement et al., 2008). Note, however, that the VSMP in my experiments was observed during both the REM-like state and during SWA (Figure 3.6), indicating that the VSMP is a background-rhythm present during both main sleep stages.

Cyclic alternating pattern of human NREM sleep

Another phenomenon that shows some similarity with the VSMP observed in my experiments is the occurrence of periodic micro-arousal states that have been observed in human EEG during NREM sleep, which have been termed 'cyclic alternating pattern' (CAP) (Terzano et al., 1985; Terzano and Parrino, 1993; 2000; Terzano et al., 2002; Parrino et al., 2006). CAP consists of a less activated state (state B) and a more activated state (state A) (Figure 3.30). Each state is 2-60 s long (Terzano et al., 2002), and the two states alternate at a frequency of ~0.047 Hz (Terzano and Parrino, 2000)(i.e. cycle length 21 s). In healthy humans, CAP occurs only during NREM sleep (Terzano et al., 2002), however in patients with periodic, REM-selective sleep apnoea, CAP can occur during REM sleep (Terzano et al., 2002). Abnormal sleep behavior,

such as periodic limb movements (PLM), sleep bruxism (excessive teeth grinding), sleep walking and disordered breathing, occur selectively during the activated phase A (Parrino et al., 2006).

Interestingly, in PD patients who suffer from REM sleep behavior disorder (RBD), which means that they show abnormal movements during REM sleep, these REM-associated movements do not have the PD features (De Cock et al., 2007). However, movements occurring during NREM sleep, during the A phase of CAP, are parkinsonian in nature. (Parrino et al., 2006).

Although the cycle length of CAP in humans is different to the cycle length of the VSMP, similarity exists between the 'high power state' of the VSMP in this study and the A phase of CAP, especially when it occurs in the form of an increased high-frequency content (Figure 3.30, phase A3).

Ultra-slow (0.025 Hz) modulation of 16 Hz LFP power in hippocampus of anaesthetised and awake rats

Another type of activity that is similar to the VSMP observed in my experiments are rhythmically occurring oscillations at 16 Hz in the hippocampus in rats anaesthetized with urethane (Penttonen et al., 1999). These oscillations occur every 40 seconds, and do not abolish the underlying slow oscillation (Figure 3.31). Although the frequency of this modulation (cycle length 40 s) is faster than the VSMP (cycle length 3-11 min), the pattern observed by (Penttonen et al., 1999) is strikingly similar to the VSMP in two ways: first, the fast oscillation frequency observed is the same as the frequency observed during the 'high power state' in the DP; second, the slow oscillation is consistently present (Figure 3.31.), as it is during both states of the VSMP (Figure 3.29). Hence, the VSMP is most similar to the ultra-slow modulation observed by (Penttonen et al., 1999). The frequency difference could be explained by the fact that a different rat strain was used, or differences in anaesthesia depth (my recordings are performed under very deep urethane anaesthesia). Interestingly, (Penttonen et al., 1999) found the slow oscillation also in behaving rats, as a rhythmic increase in interneuron firing every 25-45 s, indicating preservation across brain states.

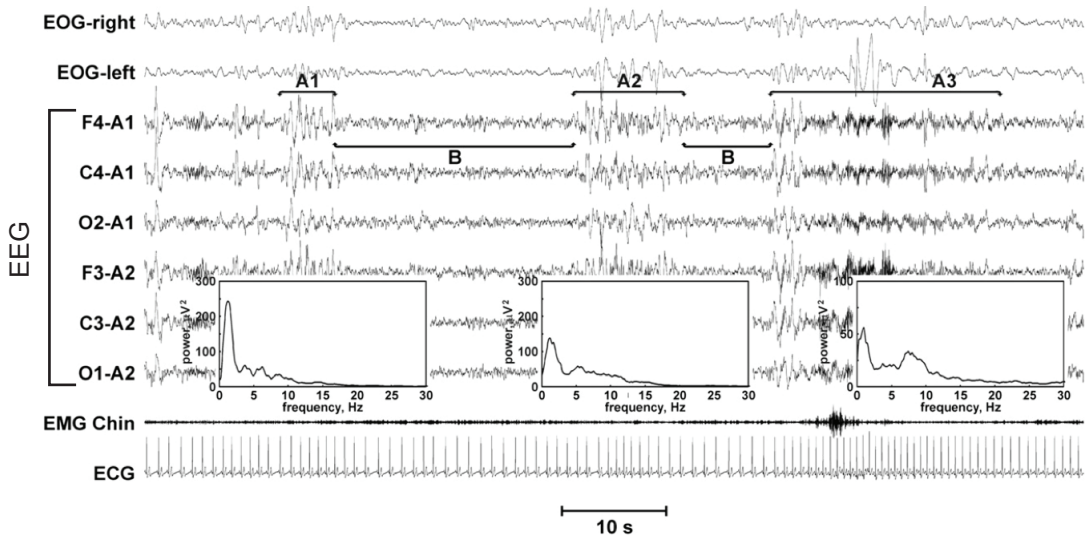

Figure 3.30. The cyclic alternating pattern (CAP) of human NREM sleep. Human sleep recording consisting of EEG, EOG (electro-oculogram) and EMG (electro-myogram) and ECG (electro-cardiogram) recording containing several activated (A-phases) and less activated periods (B-phases) of CAP. A1 is an active phase with mainly low frequency content (<2.5 Hz), A2 is an active phase with a mixture of low and high (>5 Hz) frequencies, A3 has more high-frequency content (see inset spectrograms). Figure adapted from (Parrino et al., 2012).

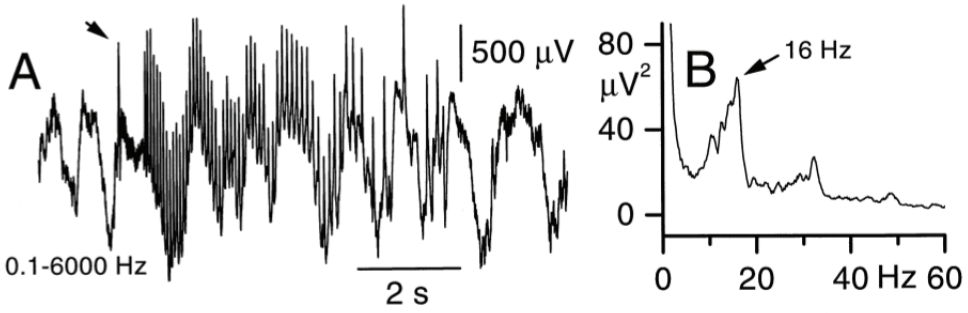

Figure 3.31. Ultra-slow oscillation (0.025 Hz) in rat hippocampus. *(A)* Wide-band LFP from pyramidal layer of CA1 showing the LFP activation that occurred every 40 s. *(B)* Power spectrum of the LFP in (A) showing the strong 16 Hz component of the LFP signal (32 and 48 Hz peaks are harmonics). Figure adapted from (Penttonen et al., 1999).

Note that while very slow oscillations (< 0.1 Hz) have also been observed directly in LFP recordings (Aladjalova, 1957; Filippov, 2005; Filippov et al., 2008), most people's filter setting cut off frequencies below 0.1 Hz, so that activity at frequencies below 0.1 Hz can only be observed when it modulates firing rates or faster oscillations. Slow modulations of this kind might be difficult to spot during the recording, unless an online-spectrogram is monitored.

The very slow modulation of LFP power occurred during NREM sleep and REM sleep

The human CAP is associated with NREM sleep only, and the hippocampal ultra-slow oscillation (0.025 Hz) has been observed during SWA under urethane. The VSMP, however, could be observed during REM sleep and NREM sleep, suggesting that it is entrained by a pace-maker that is conserved across sleep stages. Periodic occurrence of EEG arousal during NREM sleep as well as REM sleep (McNamara et al., 2002), has been observed in infants (2-10 weeks old). The periodicity was again in the minute range, and faster during REM sleep (one arousal every 1.9 min) than during NREM sleep (one arousal every 3.5 min) (McNamara et al., 2002). Slow (0.1 Hz) fluctuations in brain activity, that are retained during REM sleep and NREM sleep oscillations have also been observed using reflected light imaging of neural activity (Mayhew et al., 1996), hence might represent changes in cerebral blood flow. This is in line with human studies, consistently finding oscillations <0.1 Hz in the resting state BOLD signal (for a review see Fox and Raichle, 2007). These resting state BOLD oscillations have recently been shown to correlate with EEG fluctuations (Hiltunen et al., 2014). Hence, the underlying mechanism might be conserved not only during NREM sleep-REM sleep transition, but even in wakefulness, as also suggested by the data in (Penttonen et al., 1999).

3.5.5 *Sub-regional differences in UDS amplitude were layer-dependent*

When analysing data from layer III (section 3.4.2), the UDS amplitude was consistent across mPFC sub-regions. However, when analysing data from layers I/II and layer III-VI (section 3.4.6), the UDS amplitude differed between mPFC sub-regions, with higher amplitude in the medial (D-V depth-wise) part of the mPFC (PrL, IL). The fact that a sub-regional difference in amplitude was found in superficial and deep layers, but not in layer III might be due to the fact that the laminar structure of mPFC undergoes the most changes on the outer parts of the mPFC (layers I/II and V/VI). At

least in one dataset, the sub-regional amplitude difference seemed to be driven by the superficial layers, which is plausible as the superficial layers I/II undergo marked changes along the D-V axis of the mPFC, moving in the medial-lateral direction, as can be seen from the electrode positioning in Figure 3.2 A. The linear electrode array might cross layers when positioned in superficial layers, and be partly located in layer I, partly in layer II. This might explain why a sub-regional amplitude difference was found when data from layers I/II was included ('RdeeperL' and 'LdeeperR' datasets), but not when data from layer III was analysed (as for the sub-regional comparison).

3.5.6 *Sub-regional differences in nested fast oscillations*

Nested fast oscillations in all three investigated frequency bands were stronger in the dorsal mPFC, and the latency to the peak power decreased in the dorsal-to-ventral direction.

Contrast to in vitro results

In contrast to the *in vitro* results of (van Aerde et al., 2008) and the results obtained in our lab by Vasileios Glykos (Glykos, 2013), who found higher oscillatory power in ventral compared to dorsal mPFC sub-regions, we found the opposite sub-regional pattern for fast oscillations during Up states during urethane-induced SWA: higher power in the dorsal compared to ventral regions. This sub-regional pattern occurred for all investigated frequency bands.

What might explain these opposite findings? The main difference between the *in vivo* and the *in vitro* preparation is that the *in vitro* preparation lacks input from other brain regions, hence *in vitro* oscillations may not be truly representative of *in vivo* oscillations in the intact animal. Another possible explanation for the difference between my *in vivo* results and the previous *in vitro* results might be that the *in vitro* results are based on persistent (Glykos, 2013) or non-persistent (van Aerde et al., 2008) (beta band) oscillations, whereas I have been looking at transient oscillations in the spindle, gamma and high gamma range. In addition, the *in vitro* oscillations were induced by pharmacological activation of cholinergic receptors (van Aerde et al., 2008) or kainate plus cholinergic receptors (Glykos, 2013), thus could represent a different sensitivity to these agents (van Aerde et al., 2008). Although urethane also has some receptor-mediated pharmacological effects in the brain, it has small affects on multiple receptors, rather than a strong effect on one receptor (Hara and Harris, 2002). Hence,

sub-regional differences observed under urethane anaesthesia are most likely not related to different sensitivities to receptor activation.

In addition, persistent fast network oscillations lasting for several hours, as observed *in vitro,* might be generated through different mechanism than the transient fast oscillations during SWA. Hence, a comparison of my results for SWA during anaesthesia to SWA during natural sleep would be desirable.

Possible explanation for the observed sub-regional differences in fast oscillations

To further discuss my finding that nested fast oscillations have higher power in the dorsal mPFC, it is worth comparing this trend to the histological features of the mPFC. Differences in oscillatory power might be related to differences in laminar structure, cell type profile or connectivity might also explain the sub-regional differences.

Any oscillation observed in the LFP will, to some extent, depend on the *laminar structure* of the brain region that produces it. Fast LFP oscillations, particularly in the gamma and high gamma range are local network phenomena caused by mutual interactions between spatially well-arranged pyramidal cell and interneuron networks, possibly also involving gap junction coupling. Hence, the reflection of fast oscillations in the LFP is heavily dependent on a clear laminar structure, with large populations of regularly-arranged neurons producing large, synchronous extracellular dipoles, and hence large LFP oscillations (van Aerde et al., 2008). In this way, the dorsal mPFC may produce higher power LFP oscillations because of its more organised laminar arrangement and higher cell number per layer. Hence, my results might reflect the laminar structure of mPFC.

Differences in the *cell type profile* might also explain the sub-regional differences. My results clearly show that gamma power was very low particularly in the ventral part of IL and the dorsal part of DP. This could be explained by a lack of parvalbumin-positive (PV^+) interneurons in this region, which is indicated by reduced PV^+ labelling (Paxinos et al., 1999; Jones et al., 2005). As already discussed in section 1.4.7, PV^+ interneurons are strongly implicated in the generation of cortical gamma rhythms (Fuchs et al., 2007; Middleton et al., 2008; Cardin et al., 2009; Sohal et al., 2009; Carlen et al., 2012).

Spindles occurred later, with lower power, during the Up state in the ventral mPFC compared to the dorsal mPFC. My results of spindle activity occurring at the beginning and the end of the Up state are consistent with findings that the likelihood of spindle occurrence is increased twice during the slow oscillation cycle (Valencia et al., 2013). In addition, two kinds of fast-spiking interneurons have been distinguished in PFC, either firing early or later during the Up state (Puig et al., 2008), with the early-firing ones being coupled more strongly to the spindles than the late-ones. Mölle and colleagues (2011) found that the time of occurrence of spindles during the Up state was linked to its frequency content: fast spindles (12-15 Hz) occurred at the beginning of the Up state, whereas slow spindles (9-12 Hz) occurred towards the end of the Up state. I have not analysed the frequency content of early and late spindles in this thesis, but this is something that can be explored. In humans, the source of slow spindle activity seems to be the frontal cortex, and the source of the fast spindle activity, which spreads across the parietal cortex, the precuneus (Anderer et al., 2001). Because the two spindle patterns occur in sequence, it has been suggested that they might be linked to succeeding steps in sleep-dependent memory processing, e.g. cortico-hippocampal versus cortico-cortical information transfer (Mölle et al., 2011). I am the first to link the spindle timing difference in the mPFC between the beginning and the end of the Up state to different sub-regions of the mPFC.

Differences in thalamic *connectivity* might also explain the observed differences in spindle timing between the mPFC sub-regions. As explained in section 1.4.7, spindle oscillations are induced in the cortex by thalamo-cortical neurons which fire a rebound burst following the release from inhibitory input from the TRN. The entire mPFC receives thalamic inputs, but with different thalamic nuclei targeting different mPFC sub-regions (Berendse and Groenewegen, 1991).

The *central medial nucleus* (CMN) of the thalamus projects to layers I and III of the dorsal mPFC (Berendse and Groenewegen, 1991), which is where I observed the highest spindle power in mPFC. The CMN might be important for goal-directed behaviour, as it could integrate the activity of PFC, striatum and amygdala (Vertes et al., 2012). More specifically, it has been suggested that the CMN "may promote the temporary storage of information (working memory) at the PFC, its evaluation at the amygdala and nucleus accumbens, and preparation for actions at the striatum" (Vertes et al., 2012). The *nucleus reuniens* targets layer VI of the entire mPFC, layer I of Cg and

PrL, and all layers in DP, with a particularly dense innervation into layer I (Vertes, 2006). The nucleus reuniens has been described as the link between mPFC and hippocampus (Vertes et al., 2007), and it has been suggested that limbic information might primarily reach mPFC and hippocampus through the nucleus reuniens (Vertes, 2006). The *rhomboid nucleus* targets selectively layer I in the DP (Berendse and Groenewegen, 1991), with dense innervation in the superficial layers. The reuniens and rhomboid nuclei (i.e. the ventral midline thalamus) have been linked to long-term memory consolidation of spatial working memory (Loureiro et al., 2012).

Spindle activity could thus be induced in different sub-regions of the mPFC, depending on the projection target of the spindle-inducing nucleus. I have shown that for spindles in the dorsal mPFC, spindle power is highest during the first half of the Up state, whereas in the ventral mPFC, spindle power is highest during the second half of the Up state. Hence, it could be that the CMN may induce the mPFC spindles that occur early during the Up state, in the dorsal mPFC, possibly synchronised between mPFC and striatum or amygdala. On the other hand, the ventral midline thalamic nuclei may trigger mPFC spindles that occur late during the Up state in the ventral mPFC, possibly synchronised with the hippocampal ripples. Indeed, some hippocampal ripples take place at the end of the Up state (Peyrache et al., 2011). Thus, I suggest that the spindles at the beginning of the Up state, with the highest power in the dorsal mPFC, might serve a different function to the spindles occurring at the end of the Up state in the ventral mPFC.

The early and late spindles could also originate in different laminae and reflect a thalamo-cortico-thalamic feedback loop. It has been reported that some cells in the TRN and in the ventral anterior (VA) and ventral medial (VM) nuclei of the thalamus (projecting to middle layers of the cortex) preferentially fire at the beginning of the cortical Up state, whereas some deep layer frontal cortico-thalamic cells fire at the end of the cortical Up state (Ushimaru et al., 2012).

3.5.7 *Laminar differences in slow and nested fast oscillations*

In addition to the sub-regional differences, laminar differences of mPFC SWA were revealed.

My results show that the amplitude of UDS was higher in deep mPFC layers than in superficial layers, which is in agreement with the previous animal literature, which indicated layer V as the origin of cortical UDS activity (Sanchez-Vives and McCormick, 2000; Chauvette et al., 2010; Beltramo et al., 2013).

Gamma and high gamma power were greater in deeper layers compared to superficial layers and the same holds for spindle power, which gives some indication that the origin of the fast activity during the Up state might be in deep cortical layers.

Conversely, human depth recordings show that during natural sleep, Up state gamma power is highest in cortical layers II and III and that slow, as well as fast, oscillations originate from these 'supra-granular' layers (Csercsa et al., 2010).

In summary, it seems that during natural sleep in humans, the slow oscillation as well as fast nested activity might originate in superficial layers, whereas in urethane-anaesthetised rats, SWA as well as fast nested activity might originate in deep layers. This difference in laminar origin might be due to differences between human and animal (rat/cat) cytoarchitecture (Csercsa et al., 2010) or connectivity, or differences between anaesthesia and natural sleep (Csercsa et al., 2010).

3.6 Conclusions and future research

The results presented in this chapter provide a detailed characterisation of UDS in the mPFC. We could confirm our hypothesis of laminar differences in UDS and nested fast oscillations. Deep layers were identified as the likely driver of UDS as well as the fast oscillatory activity occurring on the Up states. Strong-sub-regional differences were found between the mPFC subareas, which could serve as an orientation for future studies.

More direct evidence for layer V as the originator of UDS and nested fast activity could be supplied by CSD analysis of within-hemisphere recording from deep and superficial layers with closely-spaced shanks.

It would be interesting to further clarify the link between nested fast oscillations, and the profile of certain cell types, e.g. PV^+ interneurons, in the mPFC, for example by targeting these neurons with a toxin.

Parallel recordings from mPFC and different thalamic nuclei, or mPFC and hippocampus and amygdala/striatum could be performed to confirm the hypothesis that early and late Up state spindles might represent different connectivity of the mPFC with other brain regions.

Chapter 4. The effects of stimulation of VTA afferents to the mPFC on slow wave activity under urethane anaesthesia

As discussed in section 1.5.5, dopamine is a powerful modulator of PFC function during wakefulness. In addition, disorders associated with a dysfunction of the dopaminergic system, such as PD, SCZ, and ADHD, are accompanied by sleep deficits (section 1.5.7). Hence, an aim of this thesis was to investigate how dopamine might affect SWA in the mPFC. In this chapter, I describe my results regarding the effect of electrical stimulation of the VTA and subsequent dopamine release on mPFC SWA in urethane anaesthetised rats. In the following, I will give a brief overview of the role of dopamine in the modulation of sleep and wake states.

4.1 Introduction: Dopamine and sleep-wake states

Dopamine was originally assumed to be the only monoamine not involved in sleep-wake state regulation, because early studies of VTA dopamine neurons in rats and cats during the sleep-wake cycle did not detect any state-dependent changes in firing rate (Miller et al., 1983; Trulson and Preussler, 1984). Since these early studies, a role for dopamine in arousal and wakefulness has been established and a role for dopamine in the modulation of sleep stages (REM sleep versus SWS) has been suggested.

4.1.1 *Dopaminergic modulation of wakefulness (wake vs sleep)*

Genetic knockout and toxin studies suggest wake-promoting effect of dopamine

Dopamine transporter (DAT) knockout mice, which have chronically increased synaptic dopamine levels, develop an altered sleep architecture, showing a 20% increase in wakefulness (Giros et al., 1996; Wisor et al., 2001). Drugs that enhance dopamine levels such as amphetamine and cocaine also increase wakefulness, and decrease sleep (REM sleep and NREM sleep) (Giros et al., 1996; Wisor et al., 2001). In Parkinson's disease, loss of dopaminergic neurons leads to various sleep-related symptoms such as excessive daytime sleepiness, insomnia and REM sleep behaviour (Lima, 2013). D_2 receptor knockout mice also spent more time asleep (REM sleep and NREM sleep) at the expense of wakefulness (Qu et al., 2010).

Systemic application of dopaminergic agents affect wakefulness

Modulation of sleep-wake states in rats mediated by the dopamine receptors D_1R and D_2R have been summarised by Monti and Monti (2007). This body of work suggests that, in rats, systemic application of agents acting at D_1 and D_2 receptors modulates wakefulness (wake versus sleep), but does not differentially affect the time spent in REM sleep versus time spent in SWS (Monti and Monti, 2007). Specifically, D_1R agonists increase wakefulness, and decrease SWS as well as REM sleep, whereas D_1R antagonists have the opposite effect. In contrast, small doses of D_2R agonists, systemically administered, increase sleep (SWS and REM sleep) and decrease wakefulness through D_2 autoreceptor action. Finally, systemic administration of large doses of D_2R agonists have the opposite effect, they decrease sleep and increase wakefulness through postsynaptic dopamine receptors.

The VTA is probably not the source of the wake-promoting effect of dopamine

Two lines of evidence point against the VTA as a mediator of dopamine's waking influence. First, neurotoxic lesion of the VTA does not decrease wakefulness, in fact it does the opposite (Lai et al., 1999). Second, VTA burst firing does not increase during wakefulness compared to sleep (Dahan et al., 2006).

Wake-promoting influence of dopamine might originate in the ventral periaqueductal grey

As neurotoxic lesion of the VTA does not decrease wakefulness (Lai et al., 1999), the effect of dopamine on wakefulness has been suggested to be mediated by a population of wake-active dopamine neurons in the ventral periaqueductal grey matter (vPAG) (Lu, 2006). Killing most of these neurons by injection of 6-hydroxydopamine increases daily sleep by ~20% (Lu, 2006).

It is thought that the dopamine neurons in the vPAG exert their waking influence via their inhibitory projections to the ventrolateral preoptic area (VLPO), which is an important sleep-promoting center. Dopamine inhibits VLPO neurons *in vitro*, however, this effect might be mediated by an adrenergic, not a dopamine receptor. Loss of dopaminergic neurons in the vPAG (Jellinger, 1999) has been linked to the excessive daytime sleepiness in PD (Matheson and Saper, 2003).

A subpopulation of VTA neurons show circadian rhythmicity

Although the VTA seems not to be the major driver of dopamine's waking effect, a subpopulation of VTA neurons is selectively active during the active phase of the circadian rhythm (Luo et al., 2008). Anatomical confirmation was provided a year later by the same group, showing that the suprachiasmatic nucleus (SCN), which is a circadian pacemaker, projects to the VTA via the medial preoptic nucleus (MPON) (Luo and Aston-Jones, 2009), a center of sleep-active neurons. As neurons in the MPON are sleep active, it has been suggested that VTA neurons are inhibited by the MPON neurons during the rest phase (Luo and Aston-Jones, 2009).

In summary, although dopamine has a potent waking effect, the VTA is not a waking-center. Instead, a number of studies have indicated that dopamine from the VTA might play a role during REM sleep.

4.1.2 *Dopaminergic modulation of sleep architecture (REM sleep vs SWS balance)*

In contrast to selective dopamine agonists/antagonists, which do not influence the REM sleep-SWS balance, evidence suggests that dopamine itself does affect sleep architecture. Reduced dopamine function leads to a reduction in REM sleep activity, and a corresponding facilitation of SWS. 'Dopamine active transporter' (DAT)-knockout mice, which have chronically increased synaptic dopamine levels, develop an altered sleep architecture with increase in wakefulness and a decrease in SWS, leaving REM sleep unaffected (Wisor et al., 2001). On the contrary, a selective decrease in the time in REM sleep was found in WT mice after treatment with alpha-methyl-*para*-tyrosine (αMT) (Dzirasa et al., 2006), an irreversible inhibitor of TH that impedes dopamine production (Watanabe et al., 2005). Moreover, complete depletion of dopamine achieved by treating DAT-knockout mice with αMT leads to complete abolishment of REM sleep such that animals display slow large amplitude activity even during wakefulness (Dzirasa et al., 2006). Furthermore, opposing effects of dopamine neuron loss on the two sleep stages have been observed in cats, where treatment with the Parkinson-inducing dopaminergic neurotoxin 1-methyl-4-phenyl-1,2,3,6-tetrahydropyridin (MPTP) (Javitch et al., 1985) has been shown to selectively decrease REM sleep and increase SWS (Pungor et al., 1990). All of these results point towards a REM-facilitatory role of dopamine.

4.2 Aims of this chapter

Whereas the VTA does not seem to play a major role in dopamine's waking effect, it might play a role in dopamine's effects on sleep architecture.

Two studies investigating dopamine neuron activity and dopamine levels during the sleep-wake cycle indicate a role for the VTA in REM sleep. First, VTA dopamine neurons are most active during REM sleep (compared to SWS and wakefulness) (Dahan et al., 2006). Second, a microdialysis study found increased dopamine levels during REM sleep compared to SWS in the mPFC and nucleus accumbens (which are the main target regions of the VTA) of unanaesthetised rats (Léna et al., 2005). What might be the role of the increase in VTA activity and subsequent dopamine release in PFC and nucleus accumbens at the transition from NREM sleep to REM sleep?

Some evidence suggests that the VTA might be able to induce REM sleep. Firstly, tonic high-frequency electrical stimulation of the VTA induces hippocampal theta (Orzeł-Gryglewska et al., 2012) in anaesthetised rats, which is a marker of REM sleep (Pace-Schott and Hobson, 2002). Unfortunately, no neocortical activity was recorded in that study. Secondly, electrical stimulation of the VTA with a burst pattern during SWA in anaesthetized rats was shown to induce a prolonged membrane potential depolarization in prefrontal cortex pyramidal cells (Lewis and O'Donnell, 2000), which might, if happening in many cells, support a REM-like forebrain activation as characteristic for REM sleep (see section 1.4.1). However, whether VTA stimulation can induce a REM-like activated LFP state in the mPFC has not been investigated.

Hence, the aim of this chapter was to investigate the effect of electrical stimulation of the VTA on the SWA LFP in the mPFC of anaesthetised rats.

4.3 Methods

4.3.1 *Electrical stimulation and electrophysiological recording*

Electrophysiological experiments in rats were performed under urethane anaesthesia. A stimulation electrode was implanted into the VTA, and a recording electrode (either a single-channel tungsten electrode or a 16-channel silicon probe), into the mPFC. A more detailed description of animal preparation, as well as electrode specifications and coordinates are given in Chapter 2.

Group data presented in this chapter were recorded from the ventral mPFC (ventral PrL, IL and DP), predominantly from layers III-V, which are the areas with most dense dopaminergic innervation (section 1.5.2). Data recorded with single-channel tungsten electrodes was combined with data recorded with silicon probes, by choosing one recording site that was located in the ventral mPFC. Some examples are shown of multichannel data from the entire mPFC obtained using silicon probes.

The stimulation parameters were chosen as in Orzeł-Gryglewska and colleagues (2012), where tonic electrical stimulation of the VTA at 50 Hz for 30 s was shown to induce hippocampal theta. Each stimulus consisted of a continuous train of 1500 biphasic pulses delivered at 50 Hz (equating to a 30 s period). At the start of each experiment, the current was slowly increased from 0.18 mA in 0.2-0.5 mV steps, until a repeatable response to the stimulation was observed (usually that was between 0.2 and 0.6 mA). The response was a change from the high amplitude-slow wave rhythm to a low amplitude-fast rhythm (LAF) rhythm, which usually began a few seconds after stimulation onset (Figure 4.1). In some cases this rhythm was interrupted by short periods of large amplitude fluctuations (e.g. Figure 4.3 B). Electrical stimulation of the VTA was applied at ten-minute intervals to assess the effects of dopaminergic antagonists.

Electrical stimulation of the VTA was also performed with a range of protocols that more closely mimicked physiological firing patterns produced by VTA dopamine neurons. These burst pattern stimulation protocols also had a duration of 30 s, and consisted of five biphasic pulses per burst, at a frequency of 25 Hz, and an inter-burst-interval of either 0.5 or 1 s. An inter-burst-interval of 0.5 s corresponds to one burst per 0.7 s, similar to that reported for VTA dopamine neurons during REM sleep (Dahan et al., 2006) (n=3). I also tested the effects of tonic stimulation at 10 Hz and 25 Hz with a duration of 30 s (n=3).

4.3.2 *Drug application*

To investigate the receptors mediating the observed stimulation response, the response to the stimulation was assessed during baseline conditions and after systemic (i.p.) administration of dopamine antagonists. The effects of two doses of the $D_{1,5}$ receptor antagonist SCH23390 (0.3 mg/kg, n=7 and 0.6 mg/kg, n=6) were assessed, as

well as the effect of the D_2 receptor antagonist sulpiride (10 mg/kg, n=7). Finally, I tried to mimic the VTA stimulation effect by systemic application of the $D_{1,5}R$ agonist SKF38393 (15 mg/kg, n=7), as well as amphetamine (2 mg/kg, n=4) and the D_4R agonist A412996 (10 mg/kg, n=5).

4.3.3 *Verification of recording sites*

At the end of the experiment, the rat was sacrificed by an overdose of Euthatal, and the brain was collected for sectioning and staining to verify the position of the recording site. Briefly, for verification of the stimulation electrode in the VTA, either a cresyl violet staining protocol or a TH immunohistochemistry protocol was used, as described in section 2.2.5. For the verification of the PFC recording electrode, cresyl violet staining was used to verify the position of single channel tungsten electrodes, and DiI with green fluorescent Nissl was used to verify the position of the silicon probe.

4.3.4 *Analysis*

LFP segments were aligned to the stimulation period and the LAF rhythm induced by VTA-stimulation was detected from the amplitude of the slow oscillation as follows:

LFP segments were filtered using a 0.1-2 Hz 2^{nd} order Butterworth band pass filter. The analytical signal of the filtered LFP was calculated using the Hilbert transform, and an amplitude envelope was calculated as the complex modulus (magnitude) of the analytical signal. The amplitude envelope was smoothed using a moving average filter with a 3 s window. The mean of a one-minute period starting just before the stimulation onset was calculated and the amplitude threshold was set to 50% of that mean so that an LAF rhythm was detected when the amplitude decreased by at least 50% of the mean.

Three parameters were derived from the amplitude envelope using this threshold (Figure 4.1):

1. The time over the stimulation period during which the amplitude was below threshold was used as a measure of the 'time during stimulation spent in LAF rhythm'.
2. The 'onset latency': the time interval from the start of the stimulation period to the first time when the LAF rhythm was detected for at least 3 s continuously.
3. The 'time to return of SWA' was calculated as the time interval between offset of the stimulation period to the first time point in the LFP with an above-threshold amplitude lasting for at least 5 s.

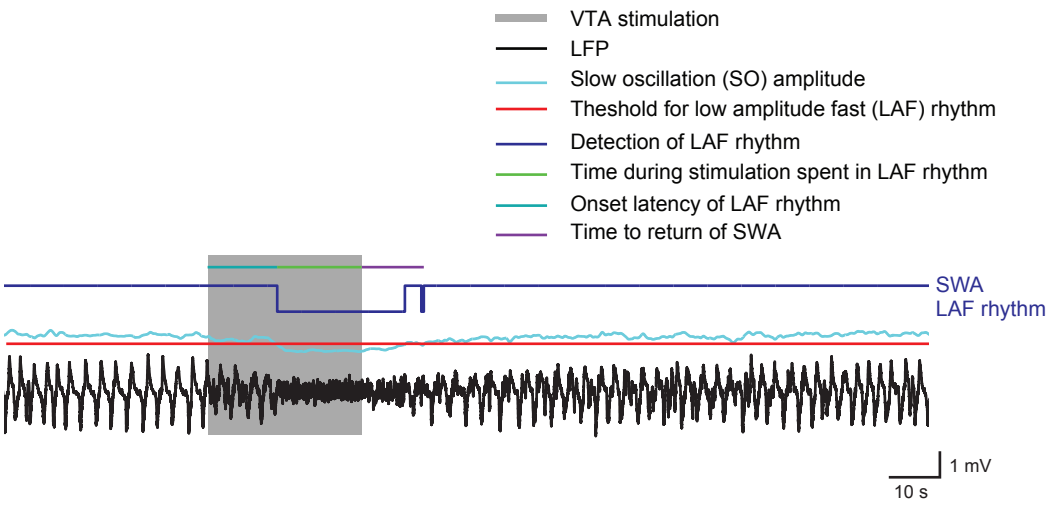

Figure 4.1. Detection of low amplitude fast (LAF) rhythm. LFP response (black trace) to VTA stimulation (grey box) with slow oscillation (SO) amplitude (light blue) and amplitude threshold (red) used for the detection of the LAF rhythm. The output of the detection is shown as a logic level trace in dark blue. High level corresponds to slow wave activity (SWA), low level corresponds to LAF rhythm. The parameters calculated from the LAF rhythm detection are indicated above: the 'onset latency' is the latency from start of stimulation to onset of the LAF rhythm, the total LAF rhythm time is divided into 'time during stimulation in LAF rhythm' and 'time to return of SWA' (time from the end of the stimulation period until the re-appearance of SWA).

Note also that the increase in 'onset latency' and the decrease in the 'time during stimulation in the LAF rhythm' are describing the same effect: namely a shorter LAF rhythm that occurs at longer latency, or block of the LAF rhythm. The 'time in LAF' parameter was chosen because of the interruptions that sometimes occurred during the LAF rhythm, which indicate a weaker response, as does a later onset. However, just the onset latency would not be sensitive to this effect.

4.3.5 *Statistics*

Because of the small sample sizes (less than 10 animals per group), the normality of the data could not be reliably assessed. Hence, non-parametric statistical methods were used in this chapter.

Using the three parameters described above, the baseline condition was compared to the drug condition. For statistical analysis, the third stimulation (the point at which the drug had been applied for 30 min) of each condition was chosen, as this was the time point when the D_1 R antagonist was deemed to have the most consistent effect.

To determine whether the LAF rhythm occurred synchronously in the entire mPFC and occurred with consistent latencies when VTA stimulation was performed repeatedly, the onset latency to the LAF rhythm in three successive stimulations in the most dorsal to the most ventral region in both hemispheres was subjected to a three-way ANOVA with factors *Hemi* (cortical hemisphere), *Depth*, and *Time.*

To determine the effects of the drug application, two-way ANOVAs were run, with factors *Condition* (baseline vs drug) and *Treatment Group* (active drug(s) vs vehicle), after transforming the data using the ART tool as described in section 2.5.

4.4 Results

I first describe the LFP response that was induced by electrical VTA stimulation and then present how the response was affected by dopamine $D_{1,5}$R and $D_{2,3}$R antagonism.

4.4.1 *Tonic high-frequency VTA stimulation induced a low amplitude fast (LAF) rhythm that occurred synchronously across the mPFC and could be repeatedly induced*

Under baseline conditions, tonic stimulation of the left VTA at 50 Hz for 30 s induced a change from high amplitude SWA to a low amplitude fast (LAF) rhythm in the mPFC, similar to previously observed 'activated' or 'desynchronised' cortical states,

induced by stimulation of reticular formation (Moruzzi and Magoun, 1949), locus coeruleus (LC) (Marzo et al., 2014) or pedunculopontine nucleus (PPN) (Steriade et al., 1991; 1996). This stimulation response was observed bilaterally, in the entire mPFC (Figure 4.2). This response could be induced repeatedly with consistent onset latency, time in LAF rhythm and time to return to SWA (Figure 4.3), although in some cases the LAF rhythm was interrupted by a brief slow wave episode (as in Figure 4.3 B).

The onset latency to the LAF rhythm in response to three successive stimulations (given at 10-minute time intervals) in the most dorsal and most ventral region (Cg and DP, respectively), in both hemispheres, was subjected to a three-way ANOVA with factors *Hemi* (cortical hemisphere), *Depth*, and *Time* (Figure 4.4). There was no significant difference in onset latency between the ipsi- and the contra-lateral hemisphere to the stimulation (main effect *Hemi* $F_{(1,60)}=0.61$, $p>0.05$), nor was the onset latency dependent on depth (main effect *Depth* $F_{(1,60)}=0.07$, $p>0.05$). The onset latency was stable with repeated stimulation (main effect *Time* $F_{(2,60)}=0.01$, $p>0.05$). None of the interactions were significant (*Hemi*Depth*: $F_{(1,60)}=0.01$, $p>0.05$, *Hemi*Time*: $F_{(2,60)}=0.03$, $p>0.05$, *Depth*Time*: $F_{(2,60)}=0.01$, $p>0.05$, *Hemi*Depth*Time*: $F_{(2,60)}=0.04$, $p>0.05$).

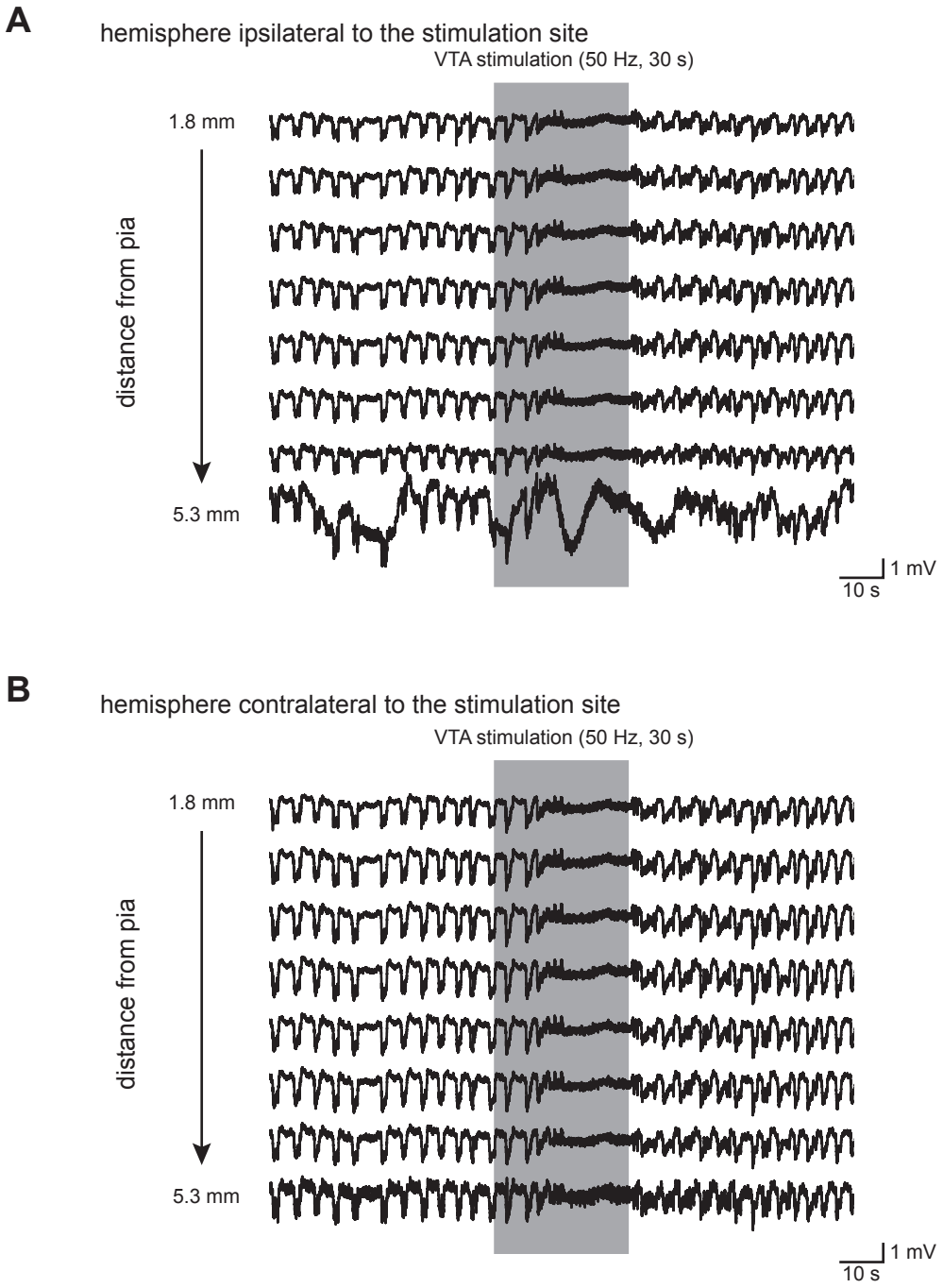

Figure 4.2. The LAF rhythm evoked by VTA stimulation occurred synchronously across the entire mPFC in both hemispheres. *(A)* The LAF rhythm evoked by VTA stimulation occured synchronously across the entire mPFC in the hemisphere ipsilateral to the stimulation site. LFP traces from different depths within the mPFC are shown. *(B)* The LAF rhythm evoked by VTA stimulation occured synchronously across the entire mPFC in the hemisphere contra-lateral to the stimulation site, with the same latency. LFP traces from different depths within the mPFC are shown.

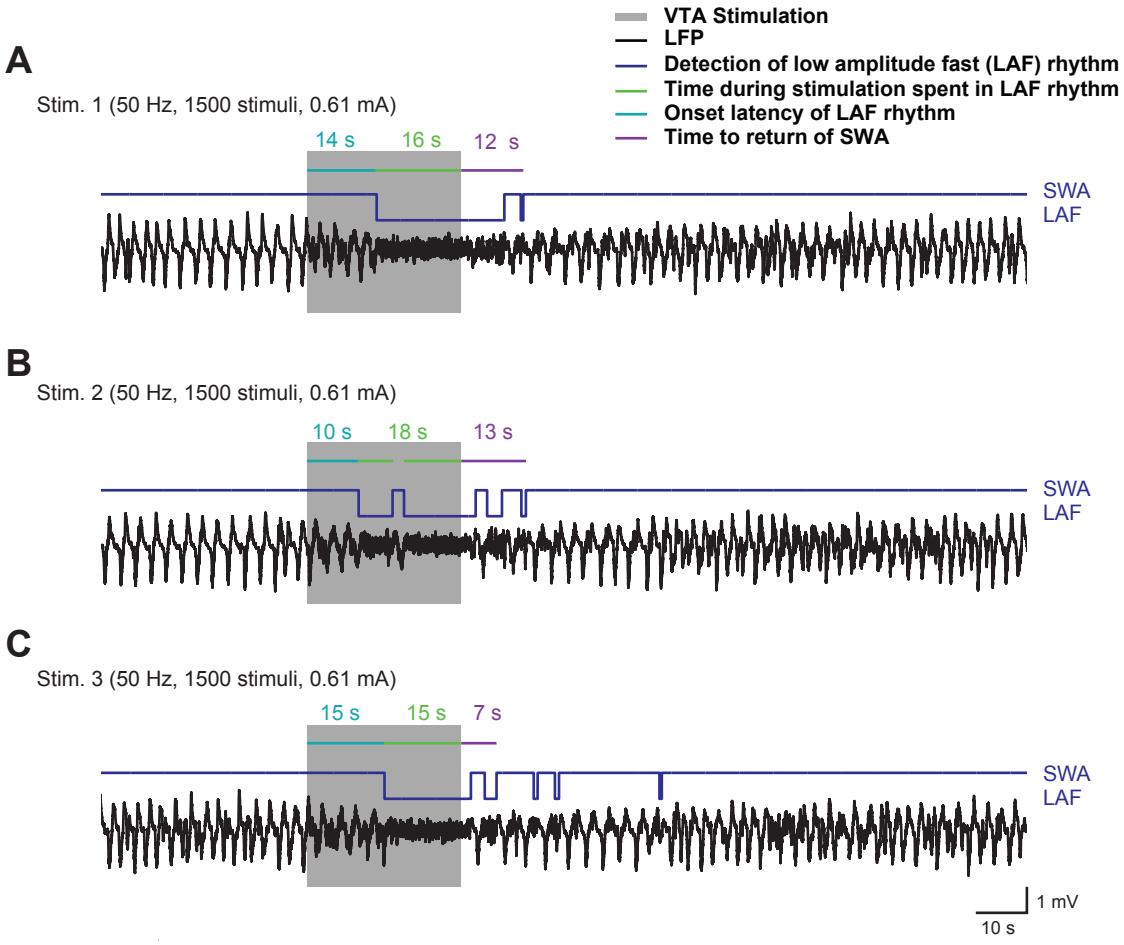

Figure 4.3 The VTA stimulation induced LAF rhythm could be induced repeatedly. Three successive LFP responses to VTA stimulation at 10 minute intervals (black) with the detection of the LAF rhythm (dark blue). The three parameters 'time during stimulation spent in LAF rhythm', 'onset latency' and 'time to return of SWA' are indicated for each response (green, turquoise and purple, respectively).

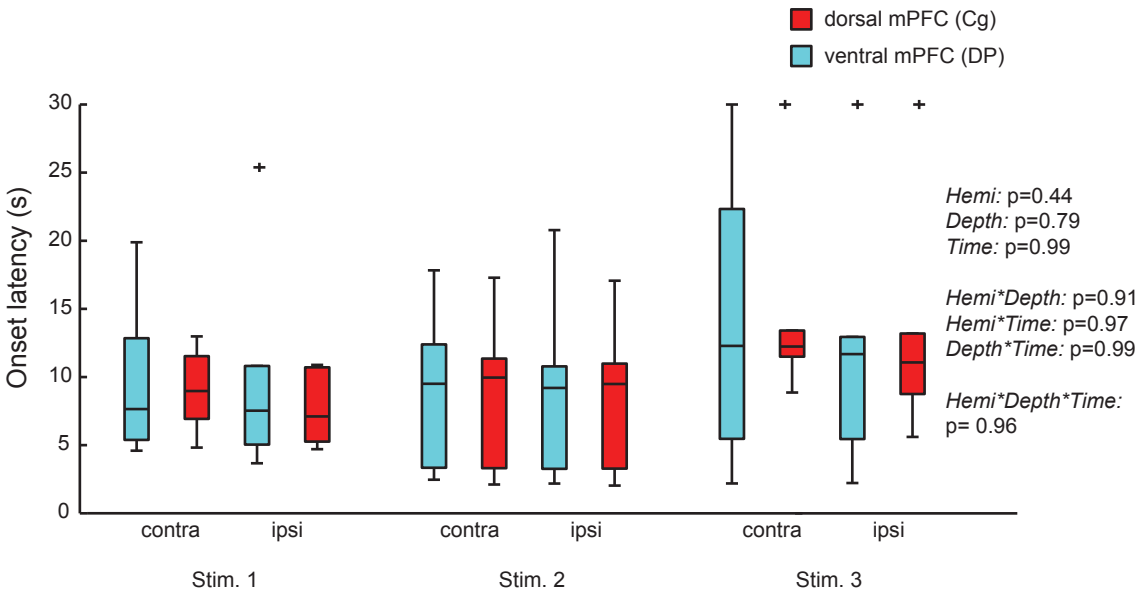

Figure 4.4 The onset of the LAF rhythm was synchronous and the onset latency consistent over repeated stimulations. Box plot shows onset latency for the most dorsal mPFC region (Cg) and most ventral mPFC region (DP), for both hemispheres, for three successive VTA stimulations that were given during baseline conditions, at 10-minute intervals (n=6); **+** represents outliers. p-values on the right of the figure represent results from a three-way RM ANOVA (three-factor repetition).

The VTA stimulation-induced LAF rhythm was similar to the spontaneous LAF rhythm

The induced LAF rhythm was qualitatively similar to the spontaneous 'desynchronised', or 'REM-like' state that was sometimes observed under lighter (overall dose: 2.4 g/kg) urethane anaesthesia (Figure 4.5). The spectral power of the induced LAF rhythm was similar to the power of the spontaneous LAF rhythm (Figure 4.6), with a dominant peak in the delta (1-4 Hz) range (at 1.1 Hz for the spontaneous activation and 1.6 Hz for the induced activation). Both power spectra showed a second peak in the theta (4-10 Hz) range (8.3 Hz for the spontaneous activation and 4.6 Hz for the induced LAF rhythm).

Induction of the LAF rhythm is dependent on stimulation electrode position in the VTA

The ability to induce the LAF rhythm was dependent on the location of the stimulating electrode in the midbrain: stimulation at the same AP and ML coordinates, but in two other brainstem regions outside the VTA did not induce a LAF rhythm in the mPFC (Figure 4.7). Note that the LAF rhythm induced by VTA stimulation in this example started shortly after stimulation onset (Figure 4.7). Typically, such a rapid-onset LAF rhythm was usually interrupted by at least one slow wave episode.

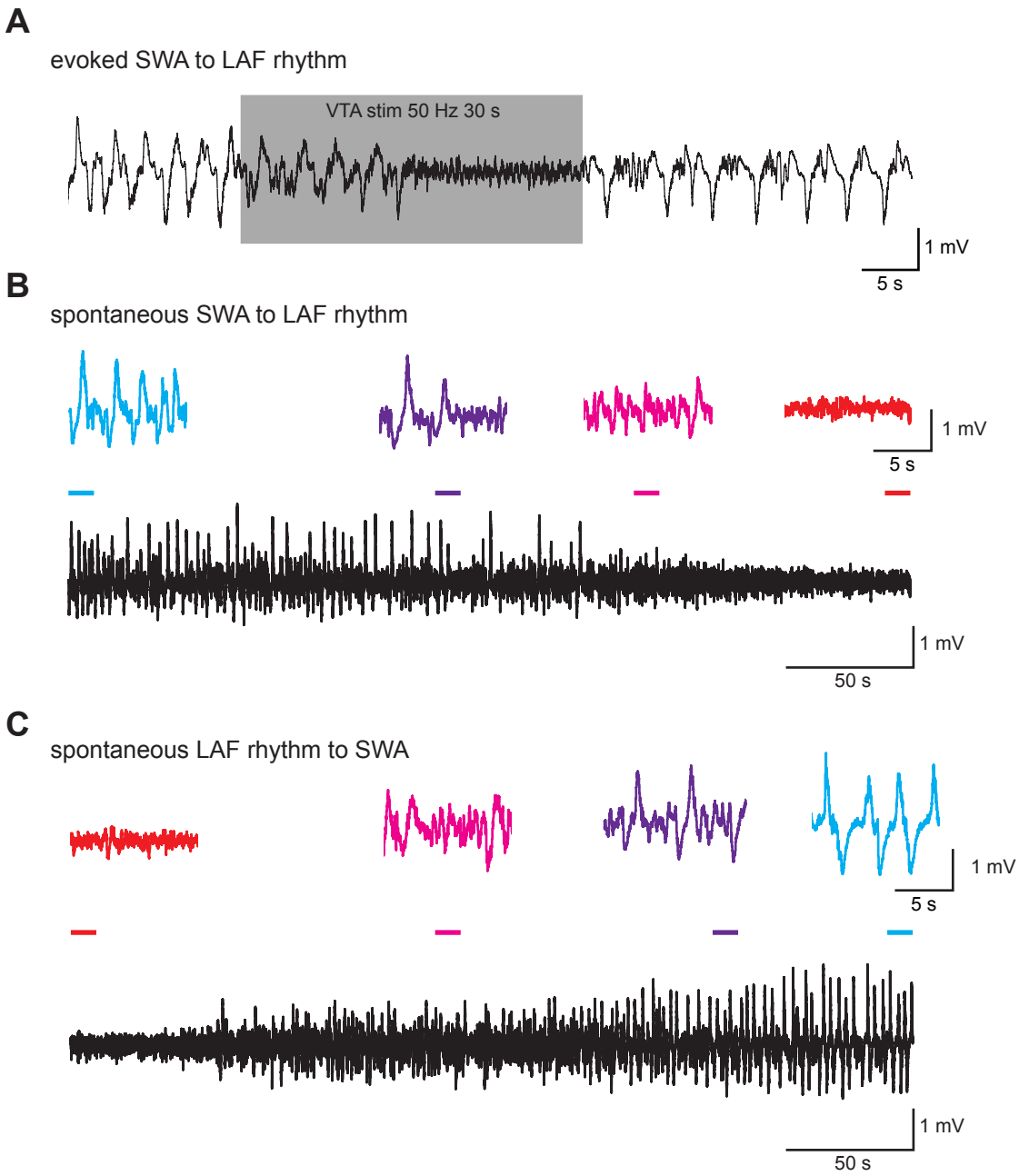

Figure 4.5. The evoked LAF rhythm was similar to the spontaneous LAF rhythm observed during urethane anaesthesia. *(A)* LAF rhythm evoked by VTA stimulation (black: LFP trace, grey box: stimulation period). *(B)* Spontaneous LFP transition from SWA to LAF rhythm (black), *Insets:* coloured traces show magnification of respective 10-second periods indicated by the coloured bar above the main trace. The scale of the magnified traces in (B) is the same as the scale of the trace in A. *(C)* Spontaneous LFP transition from LAF to SWA rhythm (black), *Insets:* coloured traces show magnification of respective 10-second periods indicated by the coloured bar above the main trace. The scale of the magnified traces in (C) is the same as the scale of the trace in (A).

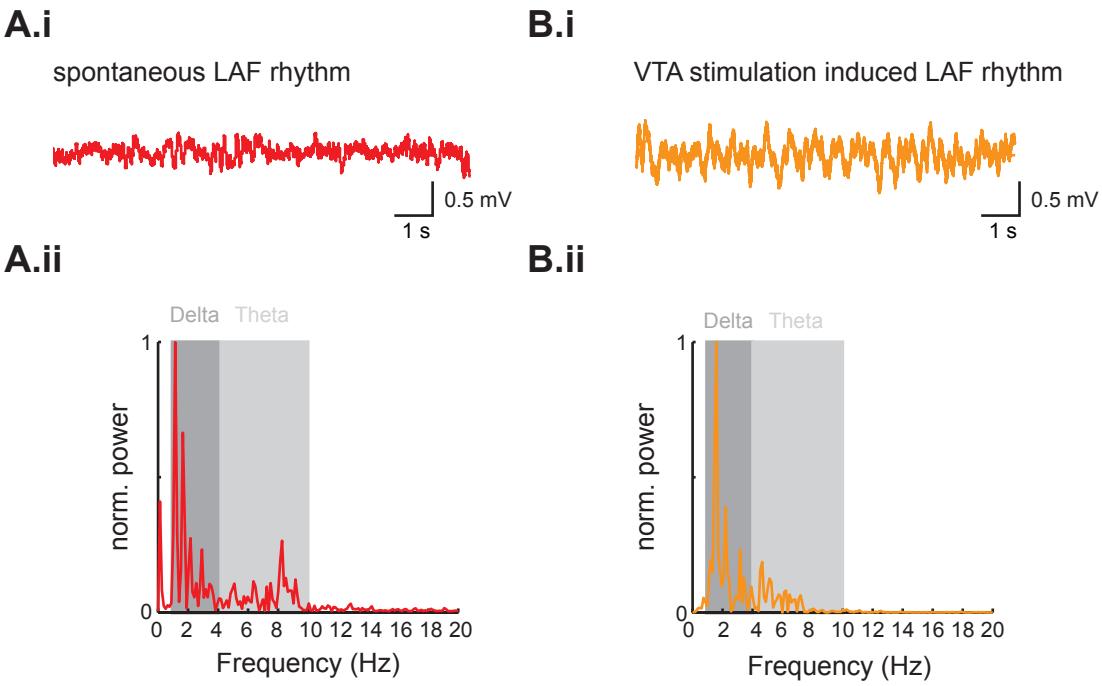

Figure 4.6. Frequency content of the spontaneous LAF rhythm and the induced LAF rhythm. *(A.i)* LFP recording of spontaneous LAF rhythm. *(A.ii)* Power spectrum of the trace in (A.i) *(B.i)* LFP recording of VTA stimulation-evoked LAF rhythm. *(B.ii)* Power spectrum of the trace in (B.i). Both signals contain delta (1-4 Hz) and theta (4-10 Hz) band activity.

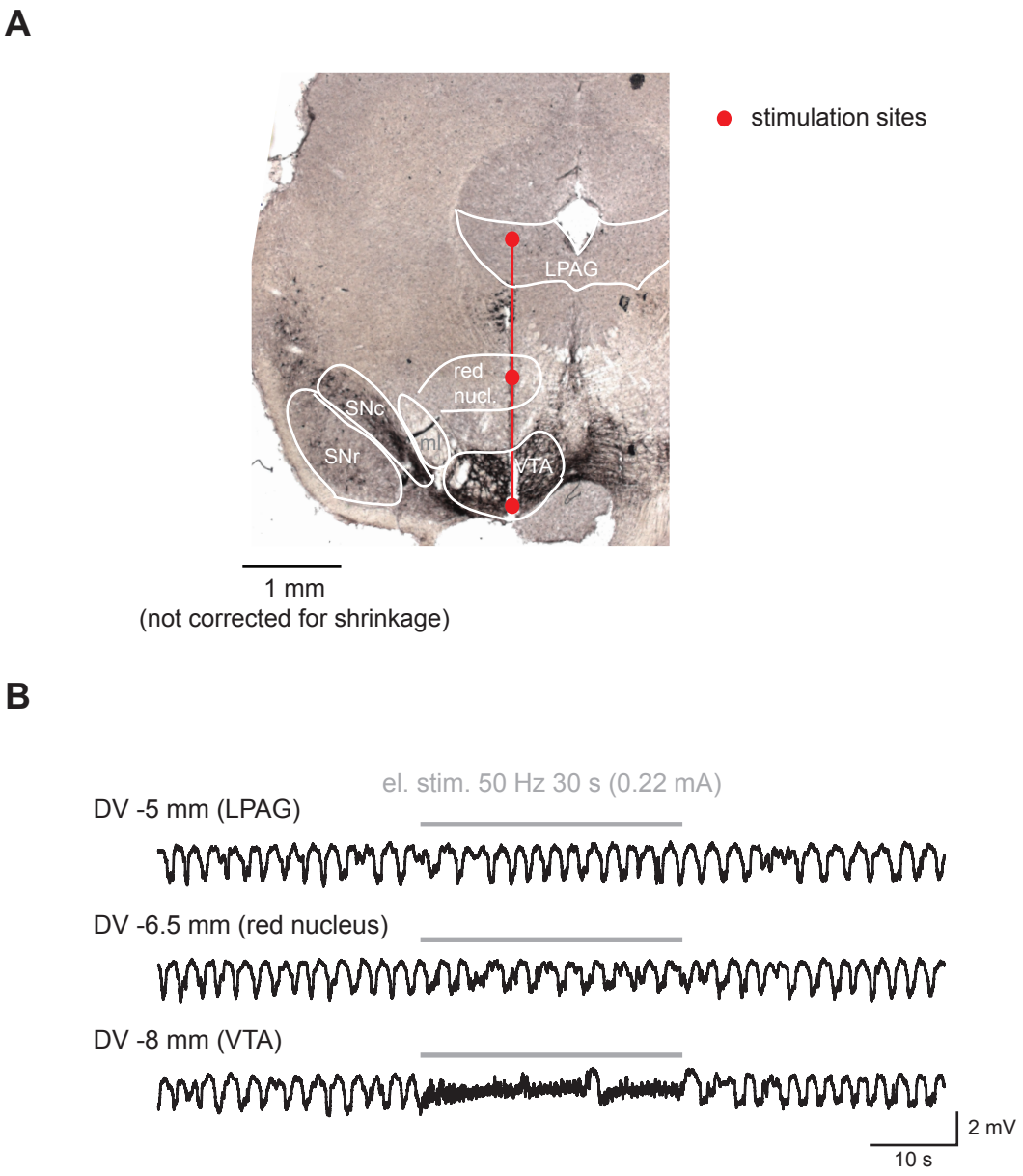

Figure 4.7. Dependency of the induced LAF rhythm on the position of the stimulation electrode in the VTA. *(A)* Coronal section of the rat brain stained with TH hydroxylase immunohistochemistry (as described in Chapter 2) to visualise dopamine neurons. VTA stimulation using the same current was applied to three stimulation sites (indicated with red dots). LPAG: lateral periaqueductal grey, red nulc.: red nucleus, SNc: substantia nigra pars compacta, SNr: substantia nigra pars reticulata, VTA: ventral tegmental area, ml: medial lemniscus. *(B)* LFP responses, recorded in mPFC, to a tonic 50 Hz stimulation are shown for different depths (DV coordinates) in the same animal. Responses to stimlation in the LPAG (lateral periaqueductal grey), the red nucleus and the VTA are shown. Only the stimulation in the VTA induced an LAF rhythm.

The induced LAF rhythm could be reproduced using a burst pattern of stimulation with parameters in the physiological firing range of dopamine neurons

Burst patterns of stimulation were applied in three animals to show that an artificial VTA activation that resembles more closely the natural firing patterns of dopamine neurons could induce a similar response in the mPFC to the one induced with the tonic 50 Hz stimulation pattern. VTA dopamine neurons fire in bursts during REM sleep, with one burst per 0.7 s, ~3.5 spikes per bursts, and a within-burst firing rate of 22 Hz (Dahan et al., 2006). A burst pattern with an overall duration of 30 seconds, five biphasic pulses per burst, at a frequency of 25 Hz, and an inter-burst-interval (IBI) of either 0.5 or 1 s was used. Tonic stimulation of the VTA at a lower frequency (25 Hz), as well as stimulation using a burst pattern, induced an LAF rhythm in the mPFC (Figure 4.8): Tonic stimulation at the lower frequency (25 Hz) induced a LAF rhythm (Figure 4.8 B) with a latency comparable to the latency of the response to the tonic 50 Hz stimulation pattern (Figure 4.8 A). A similar response was also induced with the burst pattern with a within-burst-frequency of 25 Hz and an IBI of 0.5 s (Figure 4.8 C). The interrupted LAF rhythm that was sometimes observed in response to the tonic 50 Hz stimulation was also observed with a bursting pattern stimulation (Figure 4.8 D). Tonic stimulation at 10 Hz never induce an LAF rhythm (n=3, data not shown).

Burst pattern stimulation could entrain UDS

Interestingly, one burst stimulation pattern tested (within-burst frequency 25 Hz, IBI: 1 s) seemed to be able to entrain single Down states followed by Up states (Figure 4.9). This was observed in all three animals in which burst stimulation patterns were tested, and entrainment always occurred with the same (25 Hz; 1 s) stimulation pattern. The amplitude of these entrained Down states was larger in the dorsal mPFC (Cg and PrL) compared to the ventral mPFC (IL and DP).

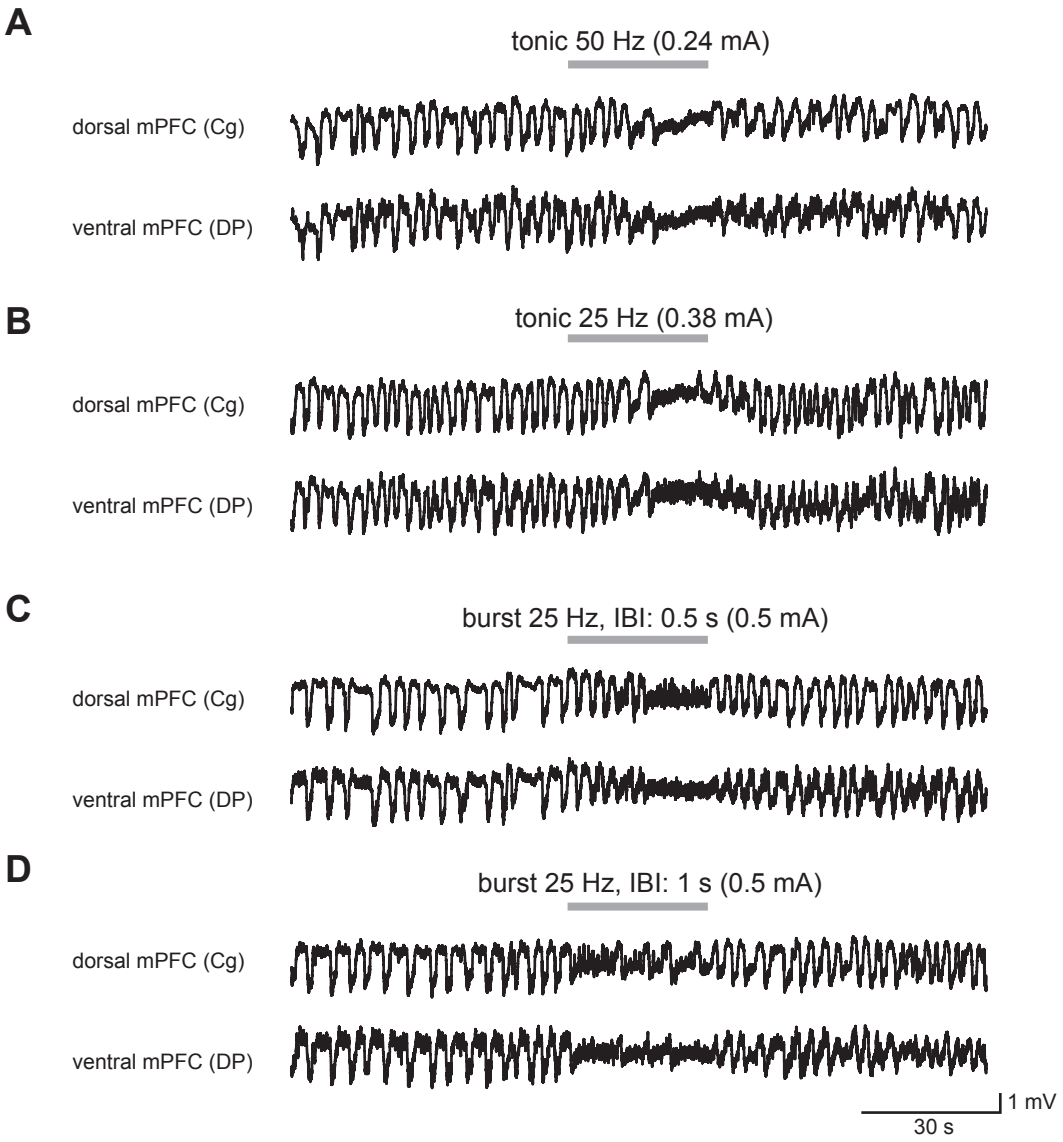

Figure 4.8. VTA stimulation with burst patterns induced similar responses to the tonic 50 Hz pattern. For each LFP response to VTA stimulation, data from the most dorsal and most ventral recording site (which were located in Cg and DP, respectively) are shown (black). The grey bar above indicates the stimulation period which was always ~30 seconds. *(A)* LFP response to continuous stimulation at 50 Hz with 1500 stimuli, at 0.24 mA. *(B)* LFP response to continuous stimulation at 25 Hz, 750 stimuli, 0.38 mA. *(C)* LFP response to burst pattern stimulation, 5 stimuli per burst, at 40 ms intervals (within-burst frequency 25 Hz), inter-burst interval (IBI) 0.5 s (thus burst frequency 2 Hz), at 0.5 mA. *(D)* LFP response to burst pattern stimulation, 5 stimuli per burst, at 40 ms intervals (within-burst frequency 25 Hz), IBI: 1 s (thus, burst frequency 1 Hz), 0.5 mA.

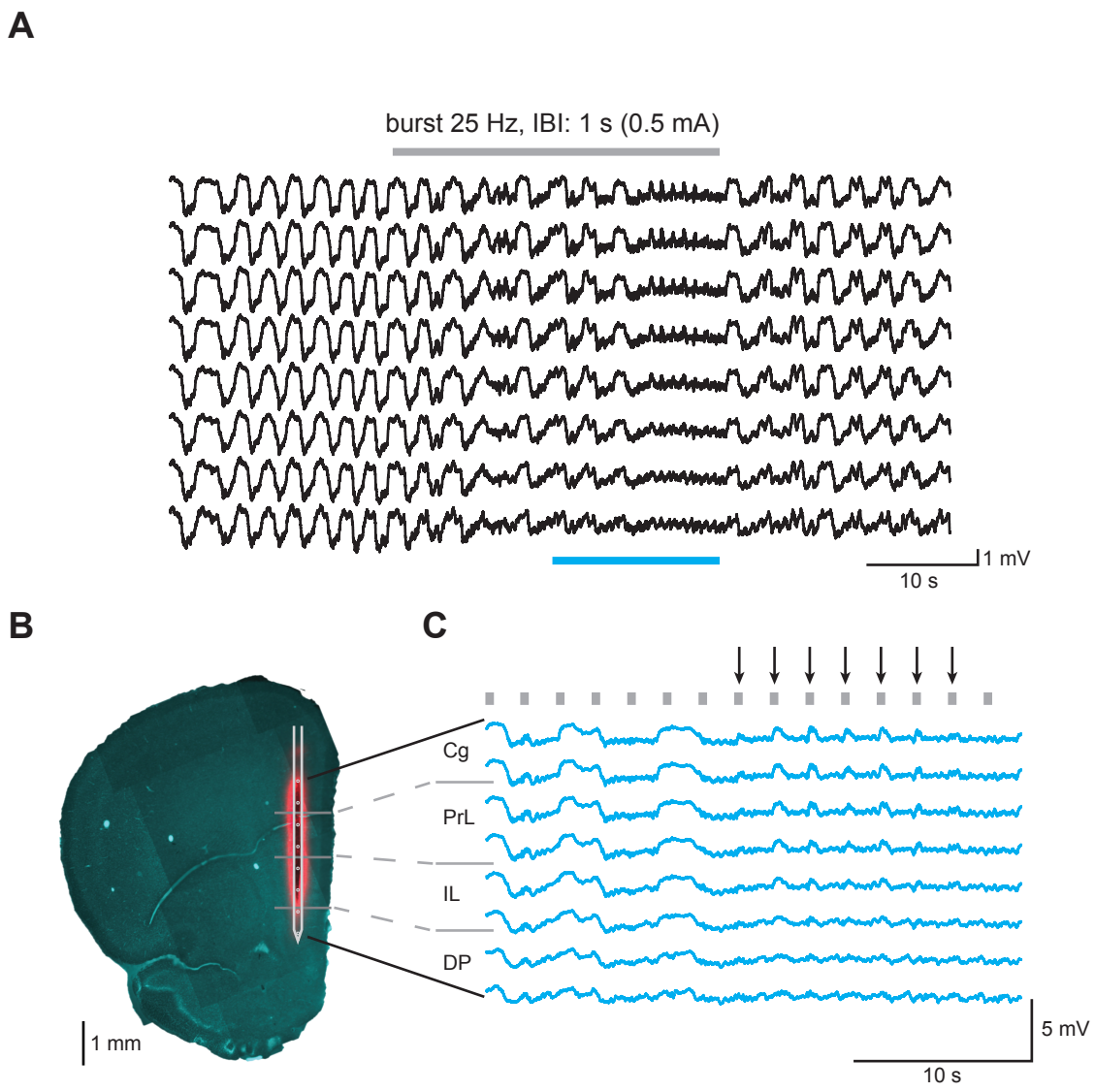

Figure 4.9. VTA stimulation with burst pattern could entrain short Down states
(A) mPFC LFP response to burst pattern stimulation, with 5 stimuli per burst, at 40 ms intervals (within-burst frequency 25 Hz), inter burst interval (IBI): 1 s (burst freqency 1 Hz), at 0.5 mA. Light blue bar below the traces indicates location of magnified traces in (C). *(B)* Coronal section through mPFC showing electrode position (grey schematic); red staining (DiI) indicates the positioning of the silicon probe, turquoise stain is DAPI background stain. Grey lines indicate borders between mPFC sub-regions. *(C)* Magnified LFP (light blue) during the second half of the stimulation period, with indication of the burst pattern of the stimulation (grey blocks). Bursts that entrained Down states are marked with black arrows.

4.4.2 *Dopamine receptor involvement in the VTA stimulation-induced LAF rhythm*

In this subsection I describe the involvement of dopamine receptors in the control of LAF rhythm assessed by systemic application of dopamine antagonists. I record the effects of the antagonists on the LAF rhythm, in particular the three parameters 'onset latency', 'time during stimulation in the fast rhythm', and 'time to return to SWA'. The stimulation pattern used was the 50 Hz tonic stimulation.

The dopamine $D_{1,5}$ antagonist SCH23390 reliably blocked the LAF rhythm

Because of the inverted U-shaped response curve of D_1R mediated effects (section 1.5.6), the effect of two doses, 0.3 mg/kg i.p., n=7 and 0.6 mg/kg i.p., n=6) of the $D_{1,5}R$ antagonist SCH23390 were tested and compared to a vehicle control group (saline, n=8). Two of the animals which received the 0.3 mg/kg dose of SCH23390 group were removed from the analysis. One was removed because – although there was an increase in frequency of the LFP – there was no amplitude reduction in the baseline VTA stimulation response, so the latencies could not be calculated. Another experiment was removed because the single-channel tungsten electrode was histologically verified to be outside the mPFC. Thus, there were five animals included in the 0.3 mg/kg SCH23390 group.

Both doses of SCH23390 blocked the induction of the LAF rhythm (Figure 4.10 B, C). Block of the LAF rhythm 30 minutes after injection was observed in 4/5 animals with 0.3 mg/kg and in 5/6 animals with 0.6 mg/kg. In comparison, in the vehicle (saline) control experiments, only 1/8 VTA stimulation responses were abolished 30 minutes after injection.

The dopamine $D_{2,3}R$ antagonist sulpiride did not reliably block the LAF rhythm

The $D_{2,3}$ antagonist sulpiride was applied in seven experiments at a dose of 10 mg/kg i.p. (n=7) and compared to the effect of a vehicle control (DMSO) injection (n=4).

After sulpiride application, the LAF rhythm was blocked in 3/7 cases after 30 minutes. Thus, in the majority of cases the $D_{2,3}R$ antagonist sulpiride did not abolish the LAF rhythm (example shown in Figure 4.10. D). In comparison, 30 minutes after DMSO injection, the VTA stimulation was abolished in 0/4 animals (no example shown).

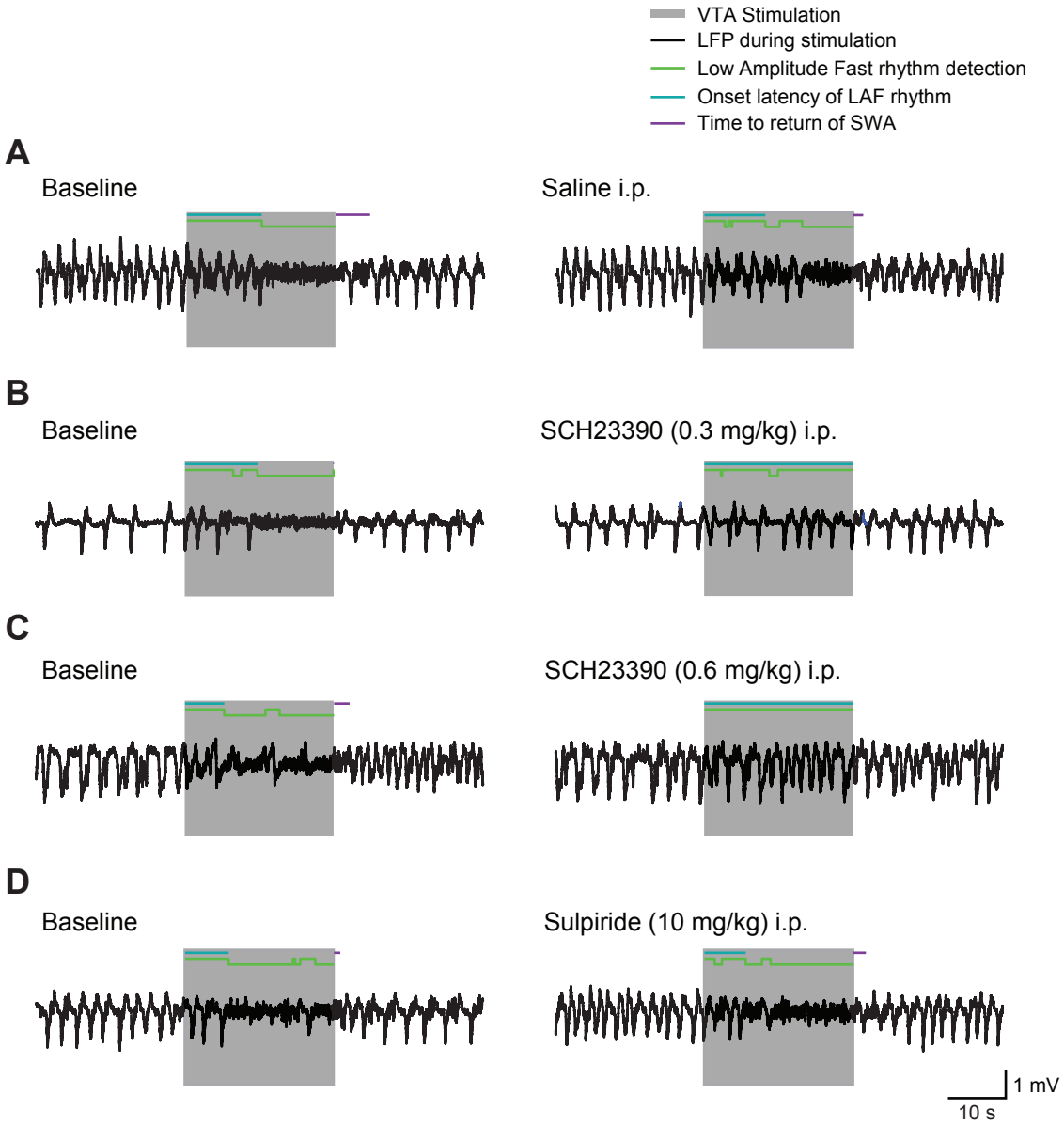

Figure 4.10. Example traces illustrating the effects of the $D_{1,5}$R antagonist SCH23390 and the $D_{2,3}$R antagonist sulpiride on the LAF rhythm. LFP traces from four experiments are shown under baseline and drug condition, illustrating the responses to VTA stimulation in the four treatment groups. *(A)* VTA stimulation response to the third baseline stimulation (*left*) and to a stimulation applied 30 minutes after saline injection (*right*). *(B)* VTA stimulation response to the third baseline stimulation (*left*) and to a stimulation applied 30 minutes after $SCH23390_{low\ dose}$ injection (*right*). *(C)* VTA stimulation response to the third baseline stimulation (*left*) and to a stimulation applied 30 minutes after $SCH23390_{high\ dose}$ injection (*right*). *(D)* VTA stimulation response to the third baseline stimulation (*left*) and to a stimulation applied 30 minutes after sulpiride injection (*right*).

To analyse these data quantitatively, three parameters were assessed, the 'onset latency to the LAF rhythm', the 'time during stimulation spent in the LAF rhythm' and the 'time to return of SWA'. Note that the former two of these parameters are limited by the duration of the VTA stimulation period, which was 30 s.

In cases where no LAF rhythm was induced, values ('onset latency to the LAF rhythm' and 'time to return of SWA') were excluded. For the statistical analysis, which was based on time points 'baseline stimulation 3' or 'drug stimulation 3', any experiment in which no LAF rhythm occurred at one or both of these time points was excluded from the statistical analysis.

4.4.3 *Modulation of the latency to the onset of the fast rhythm by dopamine antagonists*

In the experimental groups in which the SCH23390 was applied, the VTA-stimulation induced LAF rhythm was blocked at 20 and 30 minutes after drug injection in most cases (SCH23390 0.3 mg/kg: at 20 min: block in 3/5 experiments, at 30 min: block in 4/5 experiment; SCH23390 0.6 mg/kg: at 20 min: block in 6/6 experiments, at 30 min: block in 5/6 experiments). Hence, the onset latency to the LAF rhythm was not investigated.

The effect of the $D_{2,3}R$ antagonist sulpiride on the onset latency to the LAF rhythm was not different from the effect of the vehicle DMSO.

There was an apparent decrease in onset latency after sulpiride as well as DMSO injection (Figure 4.11 A). The third stimulation during baseline and drug condition were compared statistically (Figure 4.11 B). A two-way ANOVA revealed that there was a difference between the groups (main effect *Treatment Group* $F_{(1,9)}=11.11$, $p<0.05$), a drug effect (main effect *Condition* $F_{(1,9)}=6.085$, $p<0.05$), but no interaction between treatment group and condition (*Treatment Group*Condition* $F_{(1,9)}=0.0219$, $p>0.05$).

Median onset latency as well as IQRs are presented in Table 4.1.

	Time during stimulation in LAF (s)	
Group	**Baseline condition**	**Drug condition**
DMSO	16.50 (13.07 – 22.14)	9.53 (4.76 – 14.49)
Sulpiride (10 mg/kg)	11.40 (9.29 – 20.48)	1.43 (0.84 – 5.05)

Table 4.1: Onset latency (Median and IQR) for DMSO and Sulpiride groups.

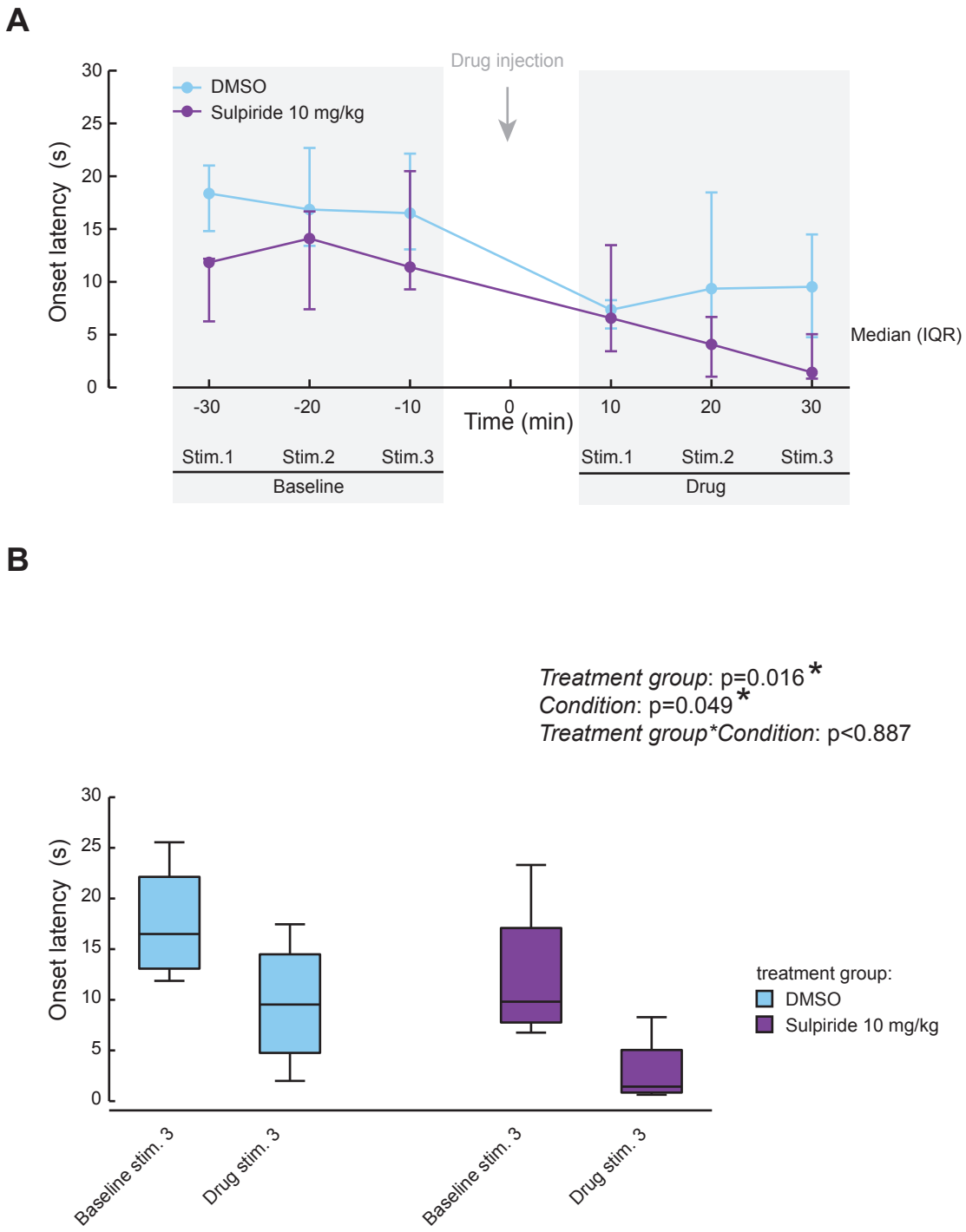

Figure 4.11. The effect of the $D_{2,3}R$ antagonist sulpiride on the onset latency was not different from the effect of the vehicle DMSO. *(A)* Line plot showing the median onset latency with IQR-errorbars for three baseline VTA stimulations and three VTA stimulations after drug injection (10, 20 and 30 minutes) for the two treatment groups (DMSO n=4, sulpiride group n=7). *(B)* Box plot showing onset latency for the third stimulation during baseline and drug conditions for the two treatment groups (DMSO group n=4, sulpiride group n=4). p-values on the right indicate results from two-way RM ANOVA (one-factor repetition).

4.4.4 *Modulation of the time during the stimulation spent in LAF rhythm by dopamine antagonists*

Some LFP responses to the VTA stimulation started immediately with the onset of the stimulation, but the LAF rhythm did not last during the whole stimulation period- but was interrupted by short slow-wave sequences. This could not be detected by the parameter 'onset latency to the LAF rhythm', thus an additional parameter was investigated, the 'time during the VTA stimulation spent in the LAF rhythm'. Again, this parameter is limited by the stimulation duration of 30 s. Generally, an increase in onset latency corresponds to a decrease in time spent in the LAF rhythm.

The $D_{1,5}R$ antagonist SCH23390 decreased the time in the LAF rhythm

The time in the LAF rhythm was relatively stable for the three (baseline) stimulations. The two doses of SCH23390 decreased the median time in the fast rhythm dose-dependently (Figure 4.12). The 0.3 mg/kg dose of SCH23390 lead to a sharp decrease in time in LAF rhythm 20 minutes after injection, whereas the 0.6 mg/kg dose decreased the time in LAF rhythm 10 minutes after the drug injection.

A two-way ANOVA revealed no difference in the time spent in the LAF rhythm between the groups (main effect of *Treatment Group* $F_{(2,16)}=0.85$, $p>0.05$). There was a difference between the baseline period and the drug period (main effect of *Condition* $F_{(1,16)}=34.26$, $p<0.001$) and the effect differed between the treatment groups (*Treatment Group*Condition* $F_{(2,16)}=11.50$, $p<0.001$). Post-hoc analysis revealed that the time in the LAF rhythm was significantly decreased in the saline group and in the 0.6 mg/kg SCH23390 group, but not in the 0.3 mg/kg SCH23390 group (post-hoc Holm-Sidak test after significant interaction). As for the 'onset latency', for the median time during stimulation in the LAF rhythm, the drug effect was larger than the saline effect. The median time in LAF rhythm and IQRs are shown in Table 4.2**.**

	Time during stimulation in LAF (s)	
Group	**Baseline condition**	**Drug condition**
Saline	16.37 (6.44 – 18.72)	12.07 (9.30 -14.66)
SCH23390 (0.3 mg/kg)	16.93 (11.28 – 21.54)	1.91 (0 – 7.19)
SCH23390 (0.6 mg/kg)	20.47 (17.18 – 28.72)	0 (0-0.09)

Table 4.2: Time in LAF rhythm (Median and IQR) for Saline and SCh23390 groups.

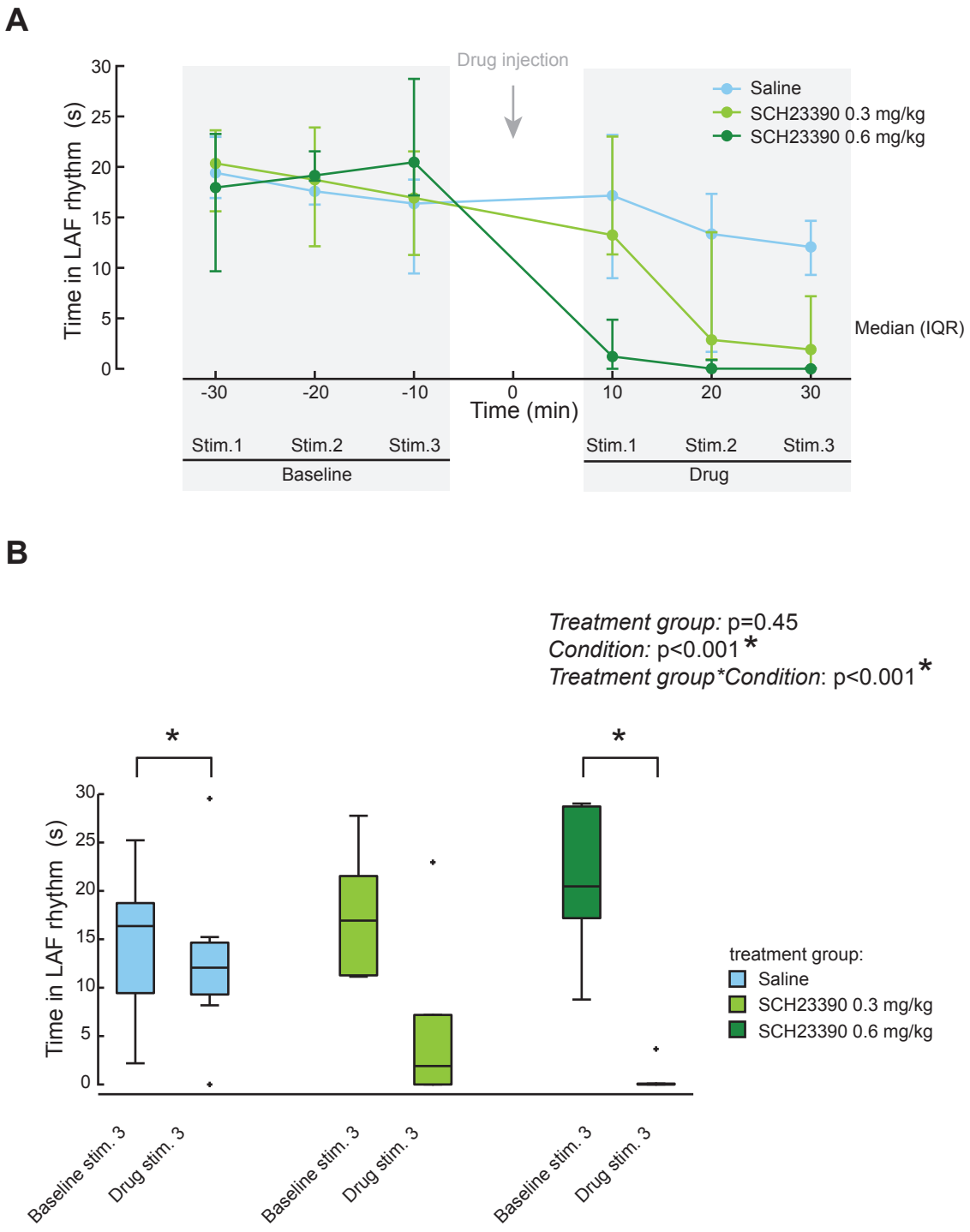

Figure 4.12. The $D_{1,5}$ receptor antagonist SCH23390 and saline decreased the time in the LAF rhythm. *(A)* Line plot showing the median time during stimulation in LAF rhythm with IQR-errorbars for three baseline VTA stimulations and three VTA stimulations after drug injection (10, 20 and 30 minutes) for the three treatment groups (Saline group n=8, 0.3 mg/kg SCH23390 group n=5, 0.6 mg/kg SCH23390 group n=6). *(B)* Box plot showing the time in the LAF rhythm for the third stimulation during baseline and drug conditions for the three treatment groups. ⁺ indicates outliers, p-values on the right indicate results from two-way RM ANOVA (one-factor repetition). * indicates significance in post-hoc Holm-Sidak test after significant interaction *Treatment group*Condition*.

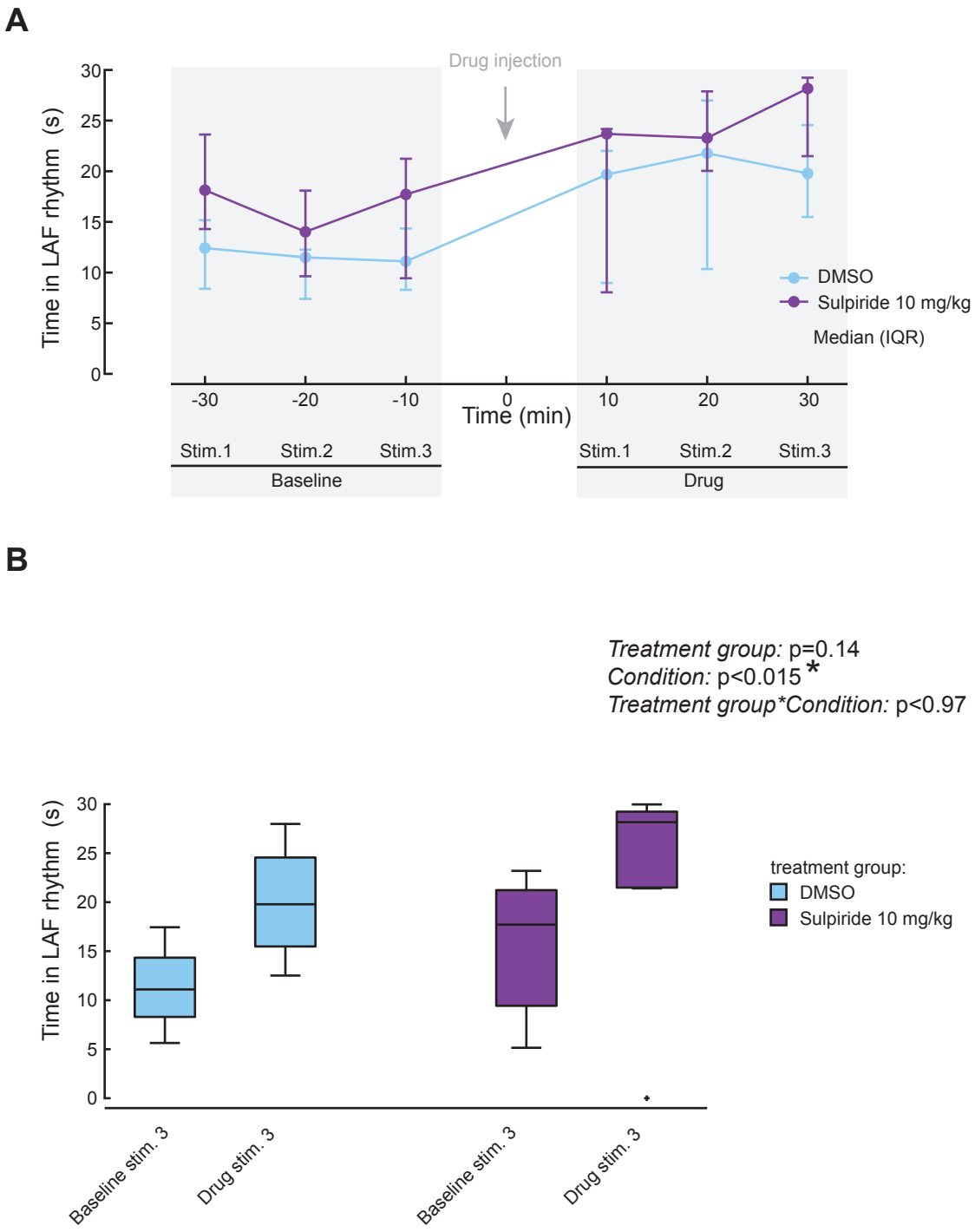

Figure 4.13. The $D_{2,3}$ receptor antagonist sulpiride and the vehicle DMSO increased the time in the LAF rhythm. *(A)* Line plot showing the median time during stimulation in LAF rhythm with IQR-errorbars for three baseline VTA stimulations and three VTA stimulations after drug injection (10, 20 and 30 minutes) for the two treatment groups (DMSO n=4, sulpiride group n=7). *(B)* Box plot showing the time in the LAF rhythm for the third stimulation during baseline and drug conditions for the three treatment groups. + indicates outliers. p-values on the right indicate results from two-way RM ANOVA (one-factor repetition).

The $D_{2,3}$ R antagonist sulpiride but also the vehicle increased the time in the LAF rhythm

Intraperitoneal injection of vehicle (DMSO) and sulpiride both led to an increase in the time spent in the LAF rhythm (Figure 4.13 A). The group data used in the statistical comparison is shown in Figure 4.13 B. A two-way ANOVA revealed that there was no difference between the two groups (main effect of *Treament Group* $F_{(1,9)}$=2.62, p>0.05). The baseline condition differed from the drug condition (main effect of *Condition* $F_{(1,9)}$=8.93, p<0.05). However the effect was not dependent on the group (interaction *Treament Group*Condition* $F_{(1,9)}$=0.00, p>0.05). Thus, sulpiride did not have an effect that was different from the effect of the vehicle. The median time in the LAF rhythm and IQRs are shown in Table 4.3.

	Time during stimulation in LAF (s)	
Group	**Baseline condition**	**Drug condition**
DMSO	11.10 (8.30 – 14.35)	19.79 (15.48 – 24.56)
Sulpiride (10 mg/kg)	17.71 (9.44 – 21.23)	28.16 (21.49 – 29.23)

Table 4.3: Time in LAF rhythm (Median and IQR) for DMSO and sulpiride groups.

4.4.5 *Modulation of the time to the return of SWA by dopamine antagonists*

The third parameter used to describe the response was the 'time to return to SWA' after the VTA stimulation-induced LAF rhythm. The 'time to return to SWA' ranged between 0 and 46 seconds under baseline conditions.

As described in section 4.4.3, the SCH23390 blocked the VTA stimulation induced LAF rhythm in nearly all cases, hence the effect of SCH23390 on the time to return to SWA was not investigated.

The effect of the $D_{2,3}$R antagonist sulpiride on the time to the return of SWA was not different from the effect of the vehicle DMSO.

The time to the return of the SWA was variable, but seemed to increase after drug injection in both groups (Figure 4.14 A). The third baseline stimulation was compared to the third drug stimulation (Figure 4.14 B).

There was no difference between the groups (main effect *Treatment group* $F_{(1,9)}$=0.03, p<0.05). There was a treatment effect (main effect *Condition* $F_{(1,9)}$=6.4, p<0.05) which was not dependent on the treatment group (interaction *Treatment*

*Group*Condition* $F_{(1,9)}$=0.617, p>0.05). Hence, although the 'time to return of SWA' was longer during drug compared to baseline conditions, there was no difference in this effect between the DMSO and the sulpiride group. The median time to return of SWA and IQRs are listed in Table 4.4.

	Time to return of SWA (s)	
Group	**Baseline condition**	**Drug condition**
DMSO	1.07 (0.28 – 5.72)	7.06 (1.06 – 29.79)
Sulpiride (10 mg/kg)	0.56 (0.09 – 1.44)	5.80 (1.88 – 35.99)

Table 4.4: Time to SWA return (Median and IQR) in DMSO and sulpiride groups.

To gain further insight into dopamine receptor involvement in the generation of the LAF rhythm, an attempt was made to mimic the VTA stimulation with pharmacological activation of dopamine receptors and induce an LAF rhythm in the mPFC.

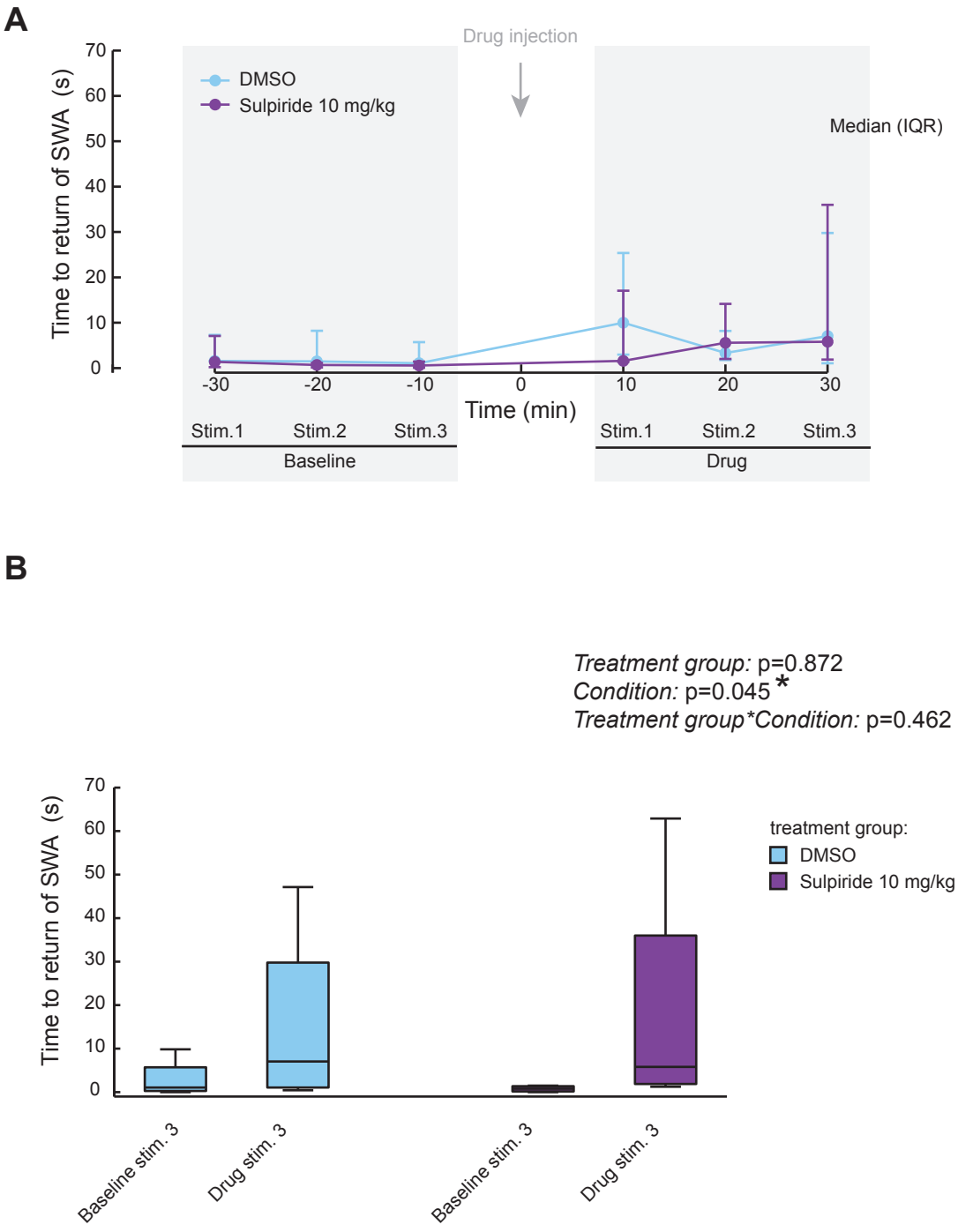

Figure 4.14. The effect of the $D_{2,3}$R antagonist sulpiride on the time to the return of SWA was not different from the effect of the vehicle DMSO. *(A)* Line plot showing the median time to return of SWA with IQR-errorbars for three baseline VTA stimulations and three VTA stimulations after drug injection (10, 20 and 30 minutes) for the two treatment groups (DMSO group n=4, sulpiride group n=7). *(B)* Box plot showing the time to the return of SWA of the third stimulation during baseline and drug conditions for the two treatment groups DMSO group n=4, sulpiride group n=4). p-values on the right indicate results from two-way ANOVA (one-factor repetition).

4.4.6 *The Dopamine $D_{1,5}$R agonist SKF38393 did not mimic the effect of the VTA stimulation*

As the $D_{1,5}$ receptor antagonist SCH23390 blocked the ability of VTA stimulation to induce the LAF rhythm in the mPFC, a likely candidate for mimicking the VTA stimulation effect was a $D_{1,5}$ receptor agonist. However, administration of the dopamine $D_{1,5}$ R agonist SKF38393 (15 mg/kg i.p.) failed to reliably induce LAF. A brief LFP desynchronisation similar to the LAF rhythm was seen in two out of seven rats. However, there was no change in SWA in the other five animals up to ~40 minutes post injection (data not shown).

4.4.7 *Increase of dopamine levels by amphetamine application did not mimic the effect of the VTA stimulation*

Amphetamine increases dopamine release and inhibits its reuptake, and therefore might be more likely to be effective than specific agonists. However, amphetamine (2 mg/kg i.p.) only induced a brief LAF-like rhythm in one out of four animals, with a very short latency of 160 seconds after injection.

In summary, neither dopamine $D_{1,5}$R activation, nor increased dopamine levels induced by amphetamine administration, could reliably induce an LAF rhythm as seen after VTA stimulation.

4.4.8 *D_4R activation could induce an LAF rhythm*

Systemic application of the D_4 receptor agonist A412997 (10 mg/kg) could induce an LAF rhythm in all sub-regions of the mPFC. Figure 4.15 A shows data from the most dorsal region, cingulate cortex (Cg), and the most ventral region, dorsal peduncular (DP). This change to the LAF rhythm occurred during the 'high power state' of the VSMP. As described in section 3.4.1, the VSMP could be observed in the spectrogram during baseline conditions and occurred with a period of several minutes and was most pronounced in the DP region of the mPFC (Figure 4.15 A). During baseline conditions, the LFP during the 'high power state' of the VSMP was still characterised by a large amplitude SWS-like rhythm (Figure 4.15 B.i and B.iii). However, after A412997 injection, the LFP during 'high power state' of the VSMP was a low amplitude fast LAF rhythm (Figure 4.15 B.ii and B.iv), similar to the LAF rhythm observed in response to the VTA stimulation. This change to an LAF rhythm during the 'increased power state' of the VSMP, occurred in four out of five animals following injection of

A412997. This drug-induced LAF rhythm was present during the 'high power state' of the VSMP for 30-40 minutes in three experiments, and up to 80 minutes after A412997 injection in one experiment. Figure 4.16 shows data from the same experiment as Figure 4.15, but over a longer time period to show the regular occurrence of the LAF rhythm before and after A412997 injection, which was accompanied by a decrease in amplitude, or rather a shift in the LFP towards a more positive level.

More generally A412997 reduced the LFP amplitude (Figure 4.15 A), as can also be seen by comparing LFP segments of the 'low power state' of the VSMP from before and after A412997 (Figure 4.15, pre injection: C.i, C.iii, post injection: C.ii, C.iv).

In two out of five experiments the response to A412997 was biphasic: Initially, the regularly occurring periods of increased power were abolished for 15-18 minutes (Figure 4.17), after which, in one experiment, the VSMP re-occurred with a LAF rhythm, for up to 40 minutes after drug injection. In the other experiment, the slow modulation was abolished for 18 minutes and a permanent (as opposed to nested in the 'high power state' of the VSM) REM-like rhythm occurred lasting for 30 minutes, still interrupted by a few slow wave cycles (data not shown).

In light of the fact that the D_4R agonist A421997 induced a transient LAF rhythm, similar to the LAF rhythm induced by the VTA stimulation, a block of the VTA stimulation-induced LAF rhythm with the D_4R antagonist L745,870 (0.5 and 1 mg/kg i.p.) was attempted (n=2). In one experiment, L745,870 seemed to strengthen the response to the VTA stimulation, in the other L745,870 seemed to weaken it. So the role of the D_4R was not further investigated, because of the strict time limit of this study.

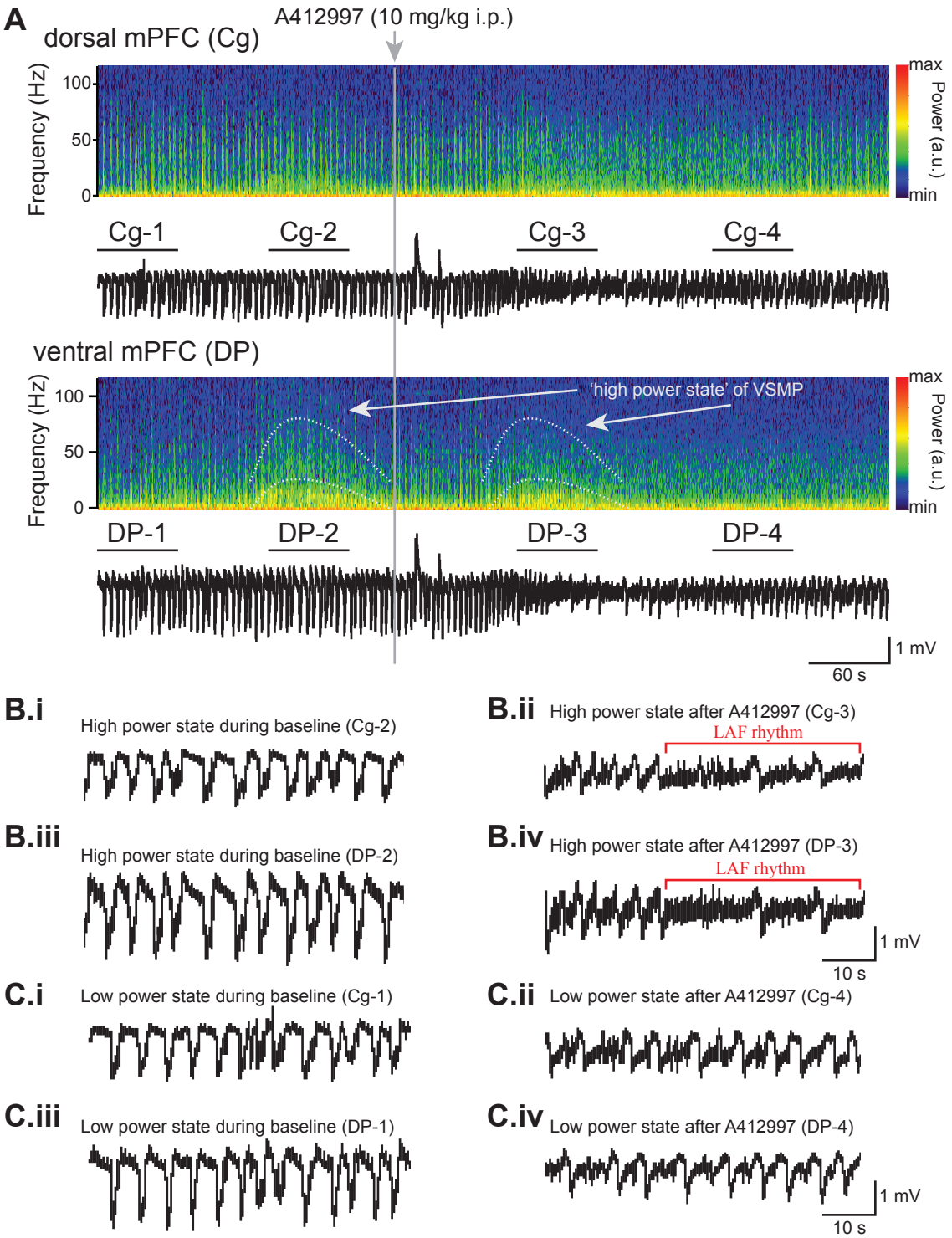

Figure 4.15. The D_4 receptor agonist A412997 induced a change in the LFP similar to the LAF rhythm during the 'high power state' of the VSMP. *(A)* LFP (black) and spectrogram of LFP recorded from cingulate cortex and dorsal peduncular cortex showing time around the injection of the D_4 agonist A412997. High power states of the VSMP occured before and after drug injection (highlighted in dashed, light grey line). Only after the injection of A412997, an LAF rhythm could be observed during the high power state. *(B)* Magnified LFP traces showing the LFP during the 'high power state' of the VSMP before (B.i: Cg, B.iii: DP) and after (B.ii: Cg, B.iv: DP) injection of the D_4 agonist A412997, where an LAF rhythm occurred. *(C)* Magnified LFP traces showing the 'low power state' of the VSMP before (C.i: Cg, C.iii: DP) and after injection of the D_4 agonist A412997 (C.ii: Cg, C.iv: DP), where the LFP amplitude was also reduced, but not as much as during the 'high power state'.

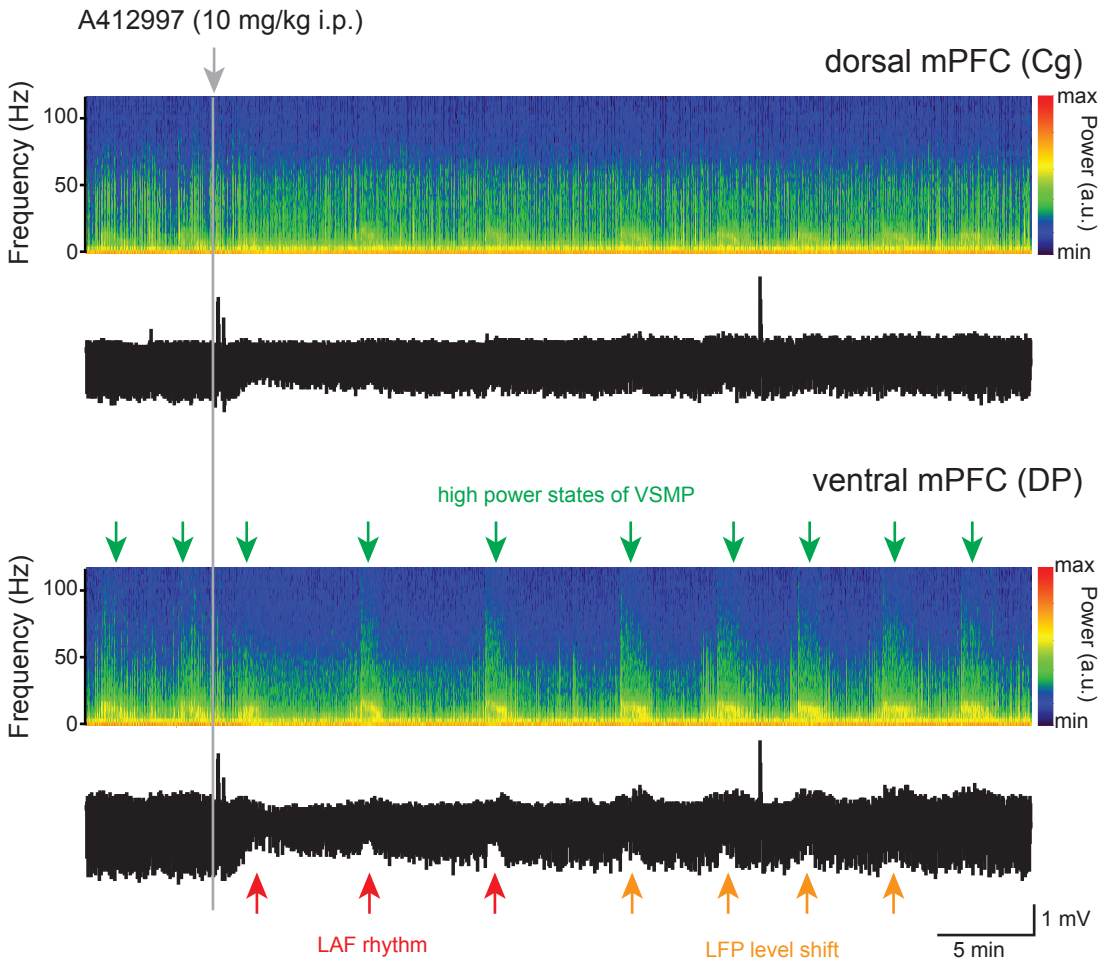

Figure 4.16. The LAF rhythm-induced by the D_4 receptor agonist A412997 occurred repeatedly during the high power state of the very slow modulation of LFP power (VSMP). LFP (black) and spectrogram of LFP recorded from Cg and DP (from the same experiment as Figure 4.17) showing time interval around the injection of the D_4R agonist A412997. After application of A412997, the high power states of the VSMP (green arrows) are accompanied by either an LAF rhythm (red arrows; visible in the LFP trace from the ventral mPFC as an amplitude reduction), or as a shift in the LFP level (orange arrows) to a more positive level.

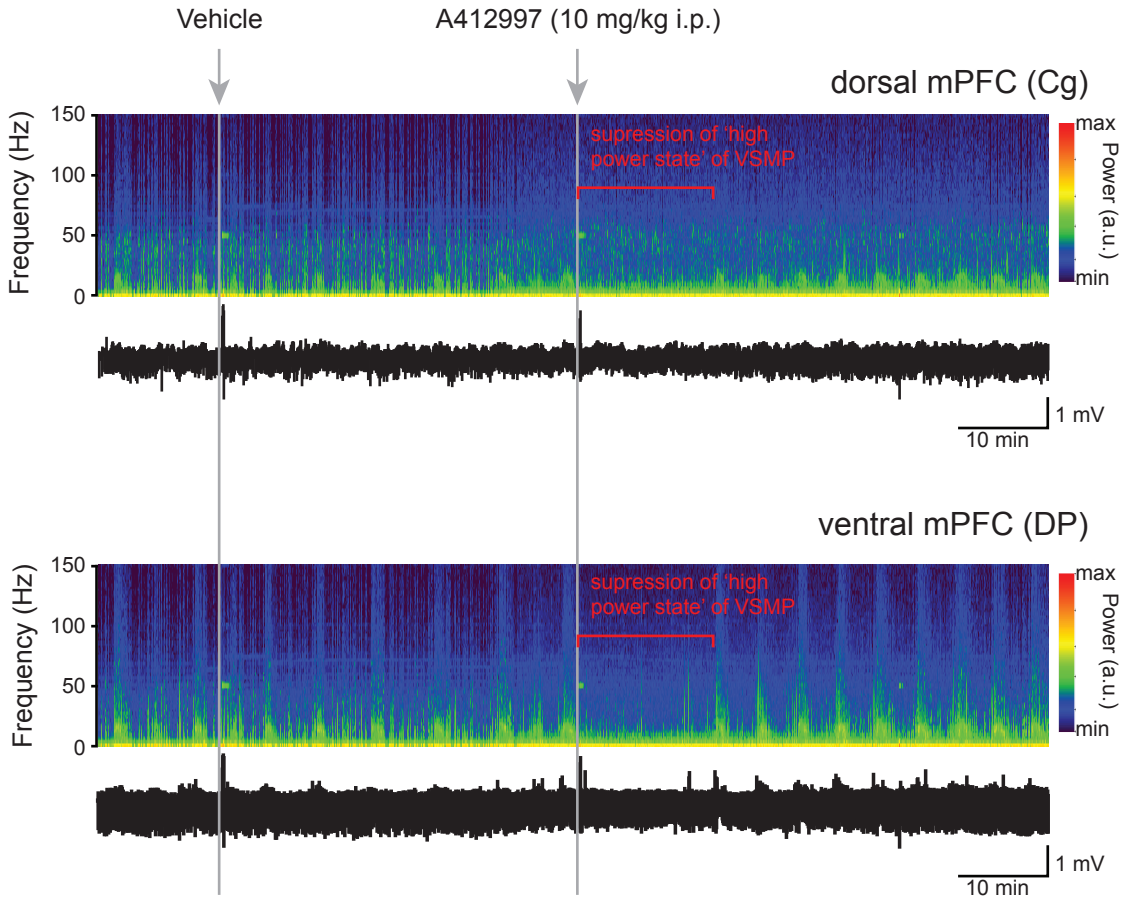

Figure 4.17. Transient suppression of the 'high power' state of the very slow modulation of LFP power (VSMP) by the D_4 receptor agonist A412997. LFP (black) and spectrogram of LFP recorded from Cg and DP from a different animal than the data shown in Figures 4.17 and 4.18. A time interval around the injection of the vehicle and the D_4 agonist A412997 is shown. In this experiment, the VSMP was abolished for ~ 15 minutes after the injection of A412997, but not after vehicle injection.

4.5 Discussion

4.5.1 *Summary of results*

In this chapter I have shown that:

- High-frequency electrical VTA stimulation induces a transition from SWA to a LAF rhythm within mPFC, an LFP pattern similar to the spontaneous REM-like state observed under urethane anaesthesia. The latency between onset of the stimulation and the onset of the LAF rhythm was several seconds.
- This transition to this LAF rhythm was unaffected by a D_2R antagonist but was completely blocked by a dopamine D_1R antagonist in a dose- and time-dependent manner.
- The VTA stimulation effect could not be mimicked by systemic injection of a D_1R agonist.
- A D_4R agonist could induce repeated transitions to an LAF rhythm during the VSMP.
- Electrical stimulation of the VTA with a burst pattern can also induce a LAF rhythm, but can induce Down state transitions, when a burst pattern with a within-burst-frequency of 25 Hz and IBI 1 s is applied.

4.5.2 *VTA-stimulation induced LAF rhythm and $D_{1,5}R$ involement*

I have shown that VTA activation consistently induced a REM-like mPFC activation pattern (LAF rhythm) with a latency of ~10 s. The latencies I observed were similar to the time period by which increased VTA bursting precedes REM sleep (10-20 s) (Dahan et al., 2006), indicating the physiological relevance of the effect observed in this thesis. In the study by Dahan and colleagues (2006), REM sleep onset was detected as muscle atonia and increased cortical theta rhythm synchronisation in the EEG. It has already been shown that VTA stimulation induces theta activity in the hippocampus (Orzeł-Gryglewska et al., 2012). As I used the same stimulation pattern as Orzeł-Gryglewska and colleagues (2012), I can compare our results to theirs regarding the observed latencies. Interestingly, VTA stimulation induces hippocampal theta immediately (Orzeł-Gryglewska et al., 2012). Together, these findings suggests that increased VTA bursting might immediately induce hippocampal theta, but produce muscle atonia and cortical (including mPFC) activation 10-20 seconds later.

However my results differ from (Lewis and O'Donnell, 2000), who induced an *immediate* prolonged Up state in PFC pyramidal cells with a short burst of electrical VTA stimulation. In my experiments, however, mPFC LFP responses occurred with a delay in the range of several seconds. Another difference is that, in (Lewis and O'Donnell, 2000), the VTA stimulation-induced depolarisation could not be blocked by SCH23390 at a similar dose to the one used in this thesis, only decreased in duration. However, in my study, the VTA stimulation did not induce an LAF rhythm when SCH23390 was administered. These differences between the results might be explained by the different methodology, i.e. intracellular versus LFP recordings. Another explanation might be that (Lewis and O'Donnell, 2000) used higher currents (up to 1 mA), in contrast to ~0.18-0.6 mA used in my study. Indeed, the long latency to the LAF rhythm observed in my experiments could be decreased and an almost immediate response could be observed if the stimulation was applied using a higher current (data not shown).

Support for D_1 receptor involvement in the VTA stimulation response can be found by combining the following findings. VTA stimulation failed to induce a hippocampal theta rhythm after septum inactivation (Orzeł-Gryglewska et al., 2012), indicating that indirect pathways from the VTA to the HPC via the septum are mediating this effect. Interesingly, VTA stimulation can induce theta burst firing in medial septal neurons (Fitch, 2006) and it has been suggested that a tonic level of D_1 receptor activation is necessary to enable medial septal neurons to fire in the theta burst mode (Fitch, 2006).

The VTA stimulation induced LAF rhythm occurred bilaterally in the entire mPFC. The VTA sends dopaminergic projections to the entire mPFC (Descarries et al., 1987; Van Eden et al., 1987), explaining the extent of the response within the mPFC in one hemisphere. However, VTA projections mainly target the ipsi-lateral side (Oades and Halliday, 1987). So for most structures, only 1-10% of connections cross to the contralateral hemisphere (Oades and Halliday, 1987). In rats, only 11-12% of VTA projections target frontal cortical areas in the contralateral side (Swanson, 1982). However, despite this, strong bilateral responses to unilateral VTA manipulation have been observed elsewhere (Orzeł-Gryglewska et al., 2010; Kunori et al., 2014). It is possible that the bilateral effect is induced through a polysynaptic pathway via another brain region.

In primary motor cortex (M1), where electrical VTA stimulation induces a bilateral response, it has been shown that the bilateral response was mediated by parallel fibres from the VTA, more specifically, via glutamate co-release from dopaminergic VTA neurons (Kunori et al., 2014). The authors ruled out that the bilateral response was mediated via connections between the two motor cortices (Kunori et al., 2014) or via activation transmitted to the contralateral side near the stimulation site (Kunori et al., 2014), as it was shown for bilateral effects produced by locus coeruleus stimulation (Marzo et al., 2014). As ~12% of VTA-M1 connections are contralateral (Hosp et al., 2011), which is the same percentage as contralateral VTA-frontal cortex connections (Swanson, 1982), the bilateral mPFC response observed in this thesis is likely also mediated via parallel VTA-PFC projections.

Most likely, the effect we observed is not restricted to the mPFC. The site of stimulation in the VTA used in this thesis contains projections not only to the mPFC, but also to the ventral striatum, amygdala, septum (which mediates effect on hippocampal theta), and perirhinal cortex (Björklund and Dunnett, 2007). Electrical stimulation might also spread to neighbouring areas such as the substantia nigra, which projects mainly to the dorsal striatum. Bypassing fibres will be stimulated as well. In view of the many projection targets of VTA and SN neurons, the fact that only a few VTA-PFC projections project to the contralateral side, is of minor importance. In addition, it has been shown that strong activation is not needed to induce a global brain state change. To the contrary, burst spiking of a single cortical neuron is sufficient to induce a global transition from SWS to REM sleep (Li et al., 2009).

It should also be noted that because an effect can be blocked by a dopaminergic antagonist, does not mean that the effect is mediated by activation of that specific receptor. Dopamine is a particularly complicated neurotransmitter in this regard, as it has many interactions with other neurotransmitters (Tseng, 2004), and the dopaminergic ‘tone’ affects the physiology of PFC neurons (Seamans and Yang, 2004). Thus, a change in dopaminergic tone can uncover or cover the action of another neurotransmitter.

4.5.3 *$D_{2,3}$ receptor involvement in the VTA-stimulation induce LAF rhythm*

Systemic administration of the $D_{2,3}$R antagonist did not have an effect on the LAF rhythm that was different from the vehicle (DMSO). The dose used in this thesis (10 mg/kg i.p.) was twice as high as the 5 mg/kg i.v. dose that has been found to be effective under anaesthesia (Floresco et al., 2001; Belujon and Grace, 2008). Note that the i.p. route is less direct, thus higher doses need to be chosen. Thus, D_2-like receptors seem not to be involved in the VTA-stimulation induced PFC activation.

Our findings are in contrast to the findings of (Dzirasa et al., 2006), which suggest a role for D_2-like receptors in REM generation. However their study was performed in animals "completely depleted" of dopamine (DAT-knockout treated with αMT), in which REM sleep could be recovered with a $D_{2,3}$R agonist. Chronic alteration of the dopamine system, as in genetic DAT-knockout models, might induce adaptive changes leading to different dopamine system function than in naïve animals. These animals could, for example, have supersensitive D_2 receptors, possibly inducing an effect that might not be related to REM mechanisms in healthy animals.

My findings suggest that $D_{2,3}$ receptors are not involved in the induction of the REM-like rhythm in the mPFC, which is consistent with data showing that pharmacological agents targeting the D_2 receptors in rodents have no selective effect on REM vs SWS (reviewed in Monti and Monti (2007)).

4.5.4 *Amphetamine and the $D_{1,5}$ R agonist SKF38393 did not mimic the VTA stimulation response*

The $D_{1,5}$R agonist SKF38393 was unable to induce a LAF rhythm as observed after VTA stimulation. The $D_{1,5}$ R agonist dose used (15 mg/kg) was three-times the dose that is behaviourally effective *in vivo* (de Lima et al., 2011; Lejeune et al., 2013). In one experiment an additional dose of 30 mg/kg was administered at the end of the experiment, which was also not effective.

The fact that systemic application of a $D_{1,5}$ receptor agonist did not mimic the VTA stimulation effect is surprising, as antagonism of $D_{1,5}$ receptors was able to block it. However, this failure of the $D_{1,5}$ receptor agonist is consistent with the failure of $D_{1,5}$

receptor agents to selectively modulate sleep states (SWS/REM) in rodents (Trampus and Ongini, 1990; Trampus et al., 1991; 1993).

Amphetamine also failed to mimic the VTA stimulation response. The dose of amphetamine used in this thesis (2 mg/kg) has been shown to be effective in anaesthetized rats in the prefrontal cortex (it decreases firing rate) (Mora et al., 1976).

The VTA-stimulation induced LAF rhythm might involve activation of several dopamine receptors, possibly D_1 and D_2-like receptors. Hence activation of just one receptor type might not be sufficient to change PFC activity from SWA to the LAF rhythm. Using systemic injection, it also cannot be predicted how much of the drug will arrive in the mPFC. Effects in other brain regions might counteract and occlude possible mPFC effects. It is also possible, that the LAF rhythm induction is not only mediated by dopamine neurons. Using electrical stimulation, all neurons in the vicinity of the electrode will be stimulated. As the VTA contains different populations of neurons, namely dopamine neurons, GABA neurons as well as glutamate neurons (Yamaguchi et al., 2007; Gorelova et al., 2012), electrical stimulation activates all these neuron types. It is also possible that glutamate co-release from dopaminergic terminals in the mPFC plays a part in the response, as it does in the M1 response to VTA stimulation neurons (Kunori et al., 2014). Hence it is likely, that the observed effect contains a dopaminergic and a glutamatergic component.

4.5.5 *D_4R agonist-induced LAF rhythm*

The D_4 receptor agonist could induce regular transitions to an activated REM-like state that occurred with a similar frequency as REM-SWS transitions that have been observed under urethane anaesthesia (Clement et al., 2008). The ability of the D_4R agonist to induce spontaneous re-occurring REM-like states under deep urethane anaesthesia has not been previously described. This finding is consistent with the literature in that a D_4 antagonist has been shown to have a differential influence on REM and SWS (Cavas and Navarro, 2006). The natural rhythmicity of these transitions suggests that a tonic activation of D_4 receptors might be necessary for REM transitions to break through deep SWS, during which REM phases are usually abolished. The transitions from SWS activity to LAF rhythm observed after D_4 receptor activation were

similar to the spontaneous transitions from SWS activity to REM-like desynchronisation observed in rats under urethane aneasthesia (Clement et al., 2008).

I observed the strongest D_4R agonist-induced LAF rhythm near the dorsal tenia tecta (dTT). Moreover, in one experiment the D_4R agonist-induced LAF rhythm occurred only in one hemisphere. In this experiment the laminar position of the two shanks differed between the hemispheres, with the LAF rhythm occurring in the superficial layer II, but not in the deep layers (V/VI) in the other hemisphere. There are no specific studies addressing D_4 receptor expression in the dTT; but in a study of cortical and striatal expression a section containing the tenia tecta was densely stained using polyclonal antibody against D_4 receptors (Wedzony et al., 2000).

Note that the slow modulation of the LFP power (VSMP) was also most pronounced in the ventral mPFC (e.g. Figure 4.15) indicating a link between the slow modulation of the LFP power and the D_4R agonist induced LAF-like rhythm.

4.5.6 *Entrainment of Down states by VTA burst pattern stimulation*

Using a burst pattern with an inter-burst-interval of 1 s we saw an entrainment of a Down state followed by an Up state in response to each stimulation burst. Previously, VTA stimulation has been shown to induce Up states with short latencies, via a non-dopaminergic mechanism (Lewis and O'Donnell, 2000). Sixty percent of VTA neurons contain dopamine (Gu, 2010), but there are also glutamate neurons in the VTA which project to the PFC, with layers V and VI of infralimbic and prelimbic cortex as their main targets (Yamaguchi et al., 2007; Gorelova et al., 2012). Glutamate can also be co-released from dopamine terminals, which has been shown for the shell of the nucleus accumbens (Stuber et al., 2010). Glutamate release might mediate the Up state transitions induced by VTA stimulation, either through release from non-dopaminergic glutamate VTA neurons, or through co-release from dopaminergic neurons.

An Up-to-Down transition induced by VTA stimulation has, to the best of my knowledge, not been reported. However, brief VTA stimulation has been shown to evoke hyperpolarized postsynaptic potentials lasting ~20-30 ms (Lewis and O'Donnell, 2000), indicating an inhibitory component of the VTA stimulation response. This inhibitory component could partly explain the VTA stimulation induce Down states observed in this study.

4.5.7 *Methodological considerations*

Considerations regarding the study of sleep rhythms and the dopaminergic system under urethane anaesthesia are discussed in Chapter 6.

It has also to be noted that the tonic 50 Hz stimulation pattern we have employed for most of this chapter is not in the physiological range of VTA dopamine neuron firing. However, it has been suggested that dopamine release induced by electrical stimulation is mainly due to increased overall activity in dopamine neurons rather than increased bursting (Floresco et al., 2003). Thus, the fact that we used a tonic stimulation, not a burst-pattern stimulation should not be important. To support this argument, we have confirmed that VTA burst pattern stimulation with parameters in the physiological range of dopamine neurons can also induce similar LFP responses.

The strength of the VTA stimulation effect was quantified with three measures, which were 'onset latency', 'time in LA' rhythm, and 'latency to return to SWA'. Note, however, that two of the measures, the increase in 'onset latency' and the decrease in the 'time during stimulation in the LAF rhythm' are describing the same effect: namely a shorter LAF rhythm that occurs at longer latency, or block of the LAF rhythm. The 'time during stimulation in LAF' rhythm parameter was chosen because of the interruptions that sometimes occurred during the LAF rhythm, which indicated a weaker response, as did a later onset. However, just the onset latency would not be sensitive to this effect. An alternative measure would be the absolute duration of the response, which would equate the sum of 'time during stimulation in the LAF rhythm' and 'latency to return of SWA'. This measure would then not be limited to a maximum of 30 s. However, different mechanisms might be involved in initiating and terminating a response like the one observed, which is an argument for using measures to separate these mechanisms.

4.6 Conclusions and future research

The result of the experiments in this Chapter provide further evidence for the role of the mesocortical dopamine pathway in sleep state modulation and indicate the possible involvement of mechanisms mediated by $D_{1,5}$ receptors. However, as drugs were

applied systemically (i.p.), we do not know if the $D_{1,5}$R block of the VTA stimulation effect is mediated by prefrontal receptors. Local drug application by iontophoresis would give more specific data about the source of the effects observed.

In this study, a $D_{2,3}$R antagonist could not block the VTA stimulation induced LAF rhythm. Future experiments could also investigate if other D_2-like receptors are involved in the VTA stimulation induce LAF rhythm induction, for example the D_4 receptor. This seems likely as an LAF-like rhythm similar to that induced by the VTA stimulation was observed after systemic administration of a D_4R agonist.

Interestingly, VTA stimulation could induce varied responses. In contrast to the strong 'activated' LAF rhythm, one of the employed burst stimulation patterns could entrain UDS, seemingly by induction of a Down state by each burst. Hence, it would also be interesting to investigate how VTA stimulation can have such different effects on mPFC UDS. Are the LAF rhythm and the Down state induction mediated by different dopamine receptors, or even by different neurotransmitters?

With electrical stimulation we cannot select for neurons projecting to a specific target regions, thus we stimulate neurons that send axons to many parts of the brain – not only to the mPFC – so dopamine will be released in many other brain regions. Employing techniques such as optogenetics or 'designer receptors exclusively activated by designer drugs' (DREADD), it would be possible to stimulate neurons of a certain type (e.g. dopamine neurons) projecting to a certain brain region (e.g. projecting to the mPFC). After revealing the neuron type involved in these responses using optogenetics or DREADD, local application of specific receptor antagonists could then determine if the effect is induced by the primary neurotransmitter released by that neuron type, or via co-release of another transmitter, as is the case for the VTA-stimulation induced M1 response (Kunori et al., 2014).

Future studies on interactions between PPN and VTA during SWA-REM sleep transitions as well as during SWA could advance our knowledge on sleep-state and Up-Down state generation. Specifically, the interactions between the PPN and VTA neuron subpopulations would be of interest.

I provided further evidence for a latency difference between REM-activity onset in mPFC and hippocampus. An interesting question to investigate would be how the hippocampal theta onset occurred several seconds before the change in cortical (including mPFC) and muscle atonia and what role it could play.

Findings regarding sleep rhythms obtained in anaesthetised animals should be combined with findings in naturally sleeping animals to confirm that similar mechanisms are involved in sleep-state switching during anaesthesia and natural sleep.

Chapter 5. The effects of dopaminergic agents on medial prefrontal cortex slow wave activity under urethane anaesthesia

5.1 Introduction

In chapter 4, I have shown that activation of the intrinsic dopamine release machinery by electrical VTA stimulation leads to a termination of SWA in the mPFC and a transition to a LAF rhythm, similar to the REM-like state. This effect seemed to be predominantly dependent on a high level of D_1 receptor activation, but we cannot exclude the possibility that glutamate also plays a role, as neither pharmacological D_1R activation nor elevation of extracellular dopamine by amphetamine could replicate the effect.

The VTA and dopamine might not only play a role in REM rhythm generation, but also modulate SWA. This seems likely, as the LFP recorded from the VTA exhibits the slow oscillations, synchronized with PFC pyramidal cells, and blocking VTA activity desynchronizes PFC Up states (Peters et al., 2004). In addition, VTA stimulation can induce Up states in the prefrontal cortex (Lewis and O'Donnell, 2000). Indeed, $D_{1,5}$ receptors have been shown to be involved in the modulation of Up state amplitude *in vivo* (West and Grace, 2001) and Up state occurrence *in vitro* (Mayne et al., 2013). Dopamine has also been shown to modulate fast (beta and gamma) LFP oscillations *in vitro* (Weiss et al., 2003; Wójtowicz et al., 2009; Steullet et al., 2014), and amphetamine (Wood et al., 2012) and D_4R activation (Kocsis et al., 2013) modulate gamma activity *in vivo*. Hence, it is likely that tonic dopamine levels might shape the nested fast LFP oscillations occurring on the slow oscillation Up state.

Mechanisms and suggested functions of nested fast oscillations are described in section 1.4.7 and section 1.4.9, respectively. A detailed characterization of Up state spindle, gamma and high gamma range activity during baseline conditions is provided in Chapter 3.

This chapter studies the effects of amphetamine and dopamine receptor agonists on these nested Up state fast oscillations. In the following sections, I briefly review how dopamine modulates persistent fast oscillations, and which receptors have been implicated, as the same receptors might also modulate nested Up state oscillations.

5.1.1 *Dopamine and fast oscillations*

To date, studies on dopaminergic modulation of oscillations have mainly investigated beta- and gamma-band oscillations.

In vivo animal studies using acute application of dopaminergic agents or chronically elevated dopamine levels consistently report increases in gamma power. Systemic amphetamine application increases prefrontal gamma power in freely moving rats (Wood et al., 2012). Acute D_4 receptor activation leads to a rapid onset, long-lasting (~ 2 h) elevation of gamma power in prefrontal cortex and hippocampus (Kocsis et al., 2013). DAT-knockout mice, which have chronic hyper-dopaminergia, exhibit increased hippocampal gamma oscillations when they explore a novel environment (Dzirasa et al., 2006).

In vitro animal studies, however, provide contradictory results about the effect of dopamine on gamma oscillations. Two studies show that application of dopamine *decreases* the power of carbachol- and kainate-induced gamma oscillations in rat hippocampal slices (Weiss et al., 2003; Wójtowicz et al., 2009), via D_1 receptor activation (Weiss et al., 2003). D_3 receptor activation also decreases gamma power in hippocampal slices (Schulz et al., 2012). However, in another study, neither dopamine (at the same concentration) nor $D_{1,5}$ or $D_{2,3}$ receptor activation had an effect on kainate-induced hippocampal gamma oscillations (Andersson et al., 2012b). However, in the presence of a D_1 receptor antagonist, dopamine induced an increase in gamma power, as did bath application of a D_4R agonist. The authors conclude that dopamine's effect on D_4 receptors was counteracted by simultaneous D_1R activation (Andersson et al., 2012b). Recently, it has been shown that dopamine as well as D_1-like and D_2-like receptor activation *increases* carbachol- and kainate-induced beta band (13-28 Hz) oscillation power in slices of mouse anterior cingulate cortex (Steullet et al., 2014).

Human studies investigating genetic polymorphisms of the dopamine D_4 receptor gene (DRD4) and the dopamine transporter gene that are associated with increased dopamine levels, suggest a facilitatory effect of dopamine on gamma activity (Demiralp et al., 2007). In line with these results, the antipsychotic haloperidol, a D_2-like *antagonist* with similarly high affinity for D_2 and D_4 receptors (Roth et al., 1995), reduces the gamma response to an auditory stimulus (Ahveninen et al., 2000).

5.2 Aims of this chapter

As reviewed above, D_1-like receptors have been shown to modulate UDS occurrence and amplitude, and D_1-like receptors, as well as D_2-like receptors (particularly D_4 receptors) modulate persistent gamma activity. However, whether dopamine also modulates fast oscillatory activity that occurs during the Up state in the mPFC, is not known.

This is of relevance, as it is possible that the slow wave Up state reflects a communication time window, during which memory traces can be transferred between hippocampus and neocortex (Destexhe et al., 2007). It has been suggested that the information transfer during the Up state might be aided by neuromodulators (Destexhe et al., 2007), and that neuronal interactions can be modulated by LFP high-frequency synchronisation (Womelsdorf et al., 2007). Differential actions of D_1 and D_4 receptors in the mPFC have already been shown to be behaviourally relevant for information encoding (Lauzon et al., 2009). Hence, dopaminergic modulation of fast oscillations during the Up state might influence information transfer during sleep and thus possibly also support memory consolidation.

Thus, the aim of this chapter was to investigate the role of dopamine and D_1 and D_4 receptors in the modulation of slow and nested fast oscillations during SWA.

5.3 Methods

5.3.1 *Dataset*

LFP data from both hemispheres of the mPFC of 19 animals were acquired and analysed for this chapter. In three animals, slow wave activity was recorded for three hours to see if the parameters of interest (introduced in Chapter 3) were stable over time. In 16 experiments the effect of dopaminergic agents were tested. All drugs were administered intraperitoneally. Thirty to forty minutes before the drug injection, the vehicle (saline/DMSO) was injected via the same route as a within-animal-control.

The following drugs were used:

- *d*-Amphetamine was administered at a dose of 2 mg/kg i.p. (n=4),
- the D_1-like receptor agonist SKF38393 was administered at a dose of 15 mg/kg (n=7), and
- the D_4R agonist A412997 was administered at a dose of 10 mg/kg (n=5).

As shown in section 3.4.4, Up state mean gamma, high gamma and spindle power did not differ between the left and the right hemisphere. However, the power of the nested oscillations did depend on the laminar position of the electrode (section 3.4.7). Hence, in this chapter, the hemisphere with better targeting of layers III and V was identified (using histological verification of the recording sites) and used for subsequent analysis. Data from four LFP channels were used (one channel from each region).

5.3.2 *Data analysis*

Up-Down states were detected as described in section 2.3.4. The Up-Down state parameters as well as the Up state gamma, high gamma and spindle power were calculated as described in section 2.3.4.

Parameters were assessed using ten-minute LFP data segments. This duration was chosen because of the VSMP, which is described in Chapter 3. The cycle lengths of the VSMP was 3-11 minutes, hence a data segment with a length of 10 minutes was considered long enough to contain periods of data both with, and without, a period of increased power.

The point of drug injection was called time 0. The first segment, the pre-injection segment, was from -11 to -1 minutes (and called "-5 min"). A 1-minute distance from the injection time was chosen to avoid artefacts (caused by experimenter manipulation during the injection) appearing in the data segment. The first post-injection segment was from 5 to 15 minutes (and called "10 min"). After that, segments were taken at 10-minute intervals.

5.3.3 *Statistics*

Because of the small sample sizes (less than 10 animals in each group), the normality of the data could not be reliably assumed. Hence, non-parametric statistical methods were used in this chapter, as in the rest of this thesis.

Stability of parameters

The stability of the parameters over time, and with saline injection, were only assessed qualitatively as only three experiments were performed hence not enough to perform a statistical test.

Drug effects on UDS parameters

Up state frequency, Up state duration and Down state duration were assessed using a Wilcoxon signed rank test to compare the percentage change of baseline, 10 minutes after injection, between vehicle and active drug.

Drug effects on nested fast oscillations

Two statistical analyses were performed:

1.) Time course analysis

To see if the drug induced a deviation from the baseline, a two-way RM ANOVA (on aligned ranks) was used on all time points from -5 min $_{drug}$ to the last time point measured after drug injection. The two factors were (sub-)*Region* and *Time*.

2.) Comparison with vehicle

At least 30 minutes separated vehicle from drug injection, making +20 minutes the last possible time point to use for the vehicle effect (+20 denotes the time interval from 15 to 25 minutes after injection). To see if the drug effect was different from the vehicle effect at 20 minutes, a two-way RM ANOVA (on aligned ranks) was performed on the percentage changes 20 minutes after injection of vehicle or drug, with factor *Treatment* (two levels: vehicle or drug) and factor *Region* (four levels: Cg, PrL, IL, DP).

5.4 Results

In three experiments, the parameters Up Down state frequency, Up state duration, Down state duration, as well as the Up state power in the spindle, gamma and high gamma bands (introduced in Chapter 3) were assessed for their stability over time and the effect of an intraperitoneal saline injection. In these three experiments, slow wave activity was recorded for three hours, with a saline injection at 30 minutes.

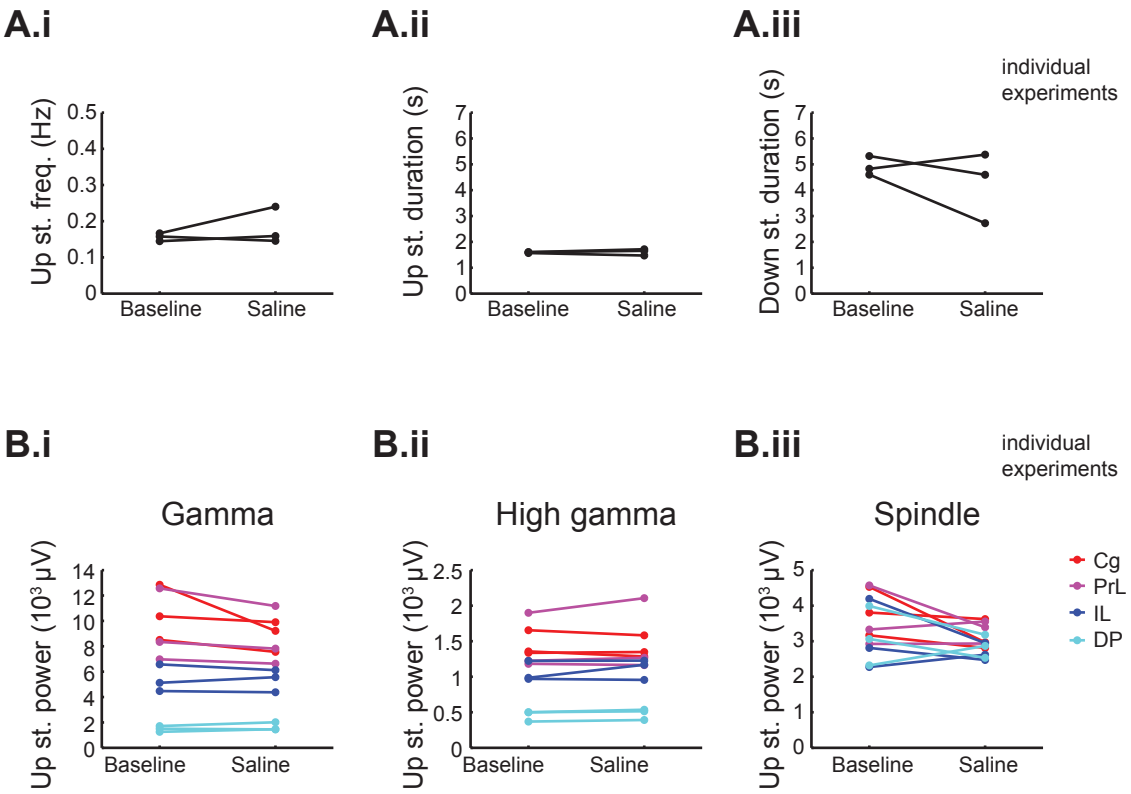

Figure 5.1. Stability of parameters with saline injection. *(A)* Up Down state parameters immediately before and 10 minutes after saline injection (individual experiments shown, n=3). *(A.i)* Up state frequency was not affected by saline, *(A.ii)* Up state duration was not affected by saline injection. *(A.iii)* Down state duration was not affected by saline injection in two out of three experiments. *(B)* Nested oscillation parameters immediately before and after saline injection (individual experiments shown, n=3; one recording channel from each subregion). *(B.i)* Up state gamma power was not affected by the saline injection. *(B.ii)* Up state high gamma was not affected by saline injection *(B.iii)* Up state spindle power showed some changes with the injection, however not in a systematic way.

5.4.1 *Stability of parameters with saline injection*

Figure 5.1 shows how a saline injection 30 minutes after the start of the recording affected the parameters. Up state frequency, Up state duration and Down state duration did not change systematically with the i.p. saline injection (Figure 5.1A.i-A.iii). Up state gamma and high gamma power appeared stable (Figure 5.1 B.i, B.ii), whereas Up state spindle power seemed more variable, however, not in a consistent way (Figure 5.1 B.iii).

5.4.2 *Stability of parameters over time*

Figure 5.2 shows the parameters over the time course of three hours (the saline injection for the above comparison was given at 30 minutes). Up state frequency appeared stable for an hour, but increased considerably over the time course of the next two hours (Figure 5.2 A.i). However, Up state duration was relatively stable over this long time course (Figure 5.2 A.ii). Thus it appears that the change in Up state frequency was predominantly explained by a change in Down state duration, which was highly variable already in the first hour of the experiments, then strongly decreased over the time course of the following two hours (Figure 5.2 A.iii).

Up state gamma, high gamma and spindle power did not systematically change over a three hour time period (Figure 5.2 B.i-iii).

In summary, Up state gamma, high gamma and spindle power were not affected by a saline injection and were stable over the time course of three hours. Thus, the effect of pharmacological manipulations on these parameters could be investigated. However, as the stability of the Up-Down state parameters over the time scale of hours was a concern, effects on these parameters were only analysed if they occurred within ten minutes after injection.

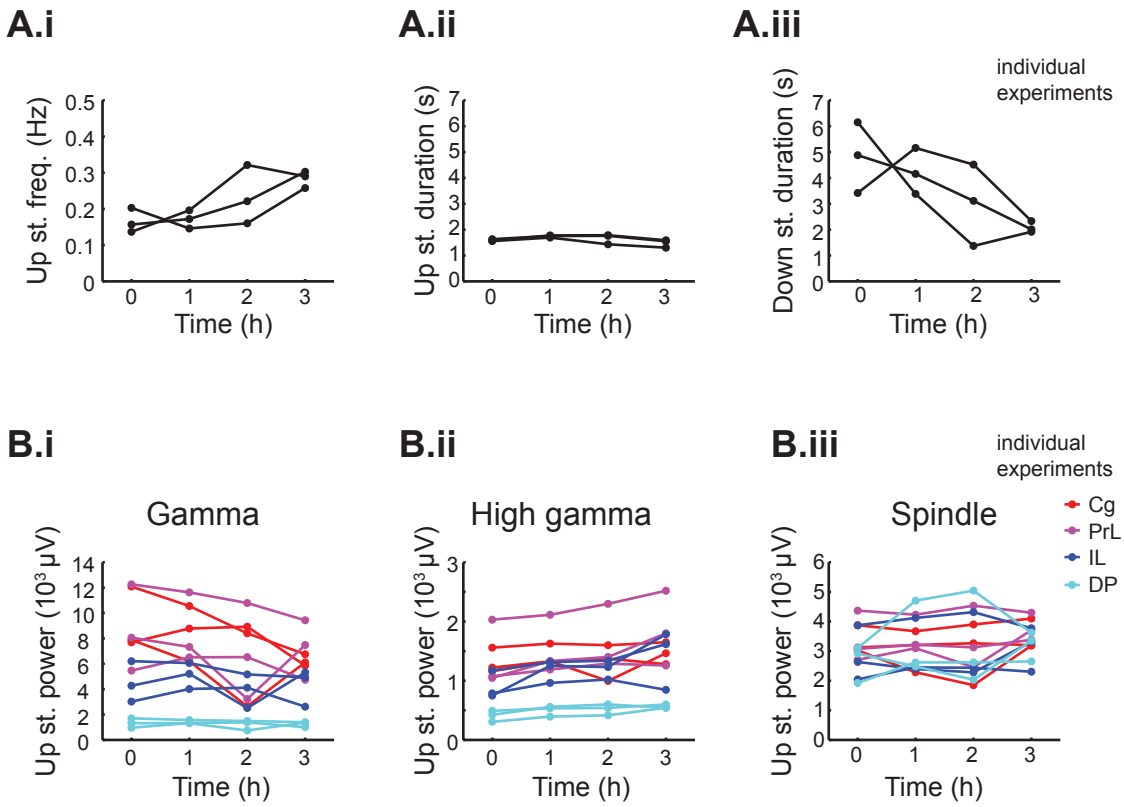

Figure 5.2. Stability of parameters over time. *(A)* Up-Down state parameters over a time course of three hours (individual experiments shown, n=3). *(A.i)* Up state frequency was relatively stable for the first hour, then increased rapidly. *(A.ii)* Up state duration was stable over time. *(A.iii)* Down state duration decreased considerably over time. *(B)* Nested oscillation parameters over time (individual experiments shown, n=3; one recording channel from each subregion for each experiment). *(B.i)* Up state gamma power was variable, but did not change in a systematic way over time. *(B.ii)* Up state high gamma power was stable. *(B.iii)* Up state spindle power showed some variability, however not in a systematic way.

5.4.3 *Effect of systemic administration of the dopamine releasing agent amphetamine on UDS*

Dopamine does not cross the blood-brain barrier, hence cannot be used to investigate effects on the brain when systemic injection is used. Hence, to investigate the effect of non-specific dopamine receptor activation, amphetamine was injected systemically, which increases extracellular dopamine levels (Calipari and Ferris, 2013).

Amphetamine seemed to affect the Up Down state parameters within ten minutes following injection. Thus, the effects on these parameters are shown (Figure 5.3, Figure 5.4). The percentage change induced by amphetamine or the vehicle 10 minutes after injection is shown in Figure 5.3 and Figure 5.4). However, because only four experiments were performed, no statistical test (Wilcoxon signed-rank test) could be performed.

Effect of amphetamine on Up state frequency

There was a trend for amphetamine to increase Up state frequency within 10 minutes after injection (Figure 5.3 A; median change vehicle: -1.11% [IQR: -4.77 – 14.03], amphetamine: 66.77% [IQR: 40.08 – 82.40]). Figure 5.3 B shows that amphetamine strongly increased Up state frequency in three out of four experiments. In one experiment, the increase was slightly less pronounced and there was also an increase following the vehicle. In this experiment, the Up state frequency was already high at the beginning of the experiment (~0.4 Hz), compared to 0.15-0.2 Hz in the other experiments. Amphetamine might have affected this faster Up-down state activity less, as it was possibly already at the upper limit of Up-Down state frequencies that can be generated under urethane anaesthesia.

Effect of amphetamine on Up state duration

Up state duration seemed not to be affected by amphetamine (Figure 5.4 A; median change vehicle: 2.50% [IQR: -5.72 – 3.74], amphetamine: -1.35% [IQR: -4.24 –3.68]).

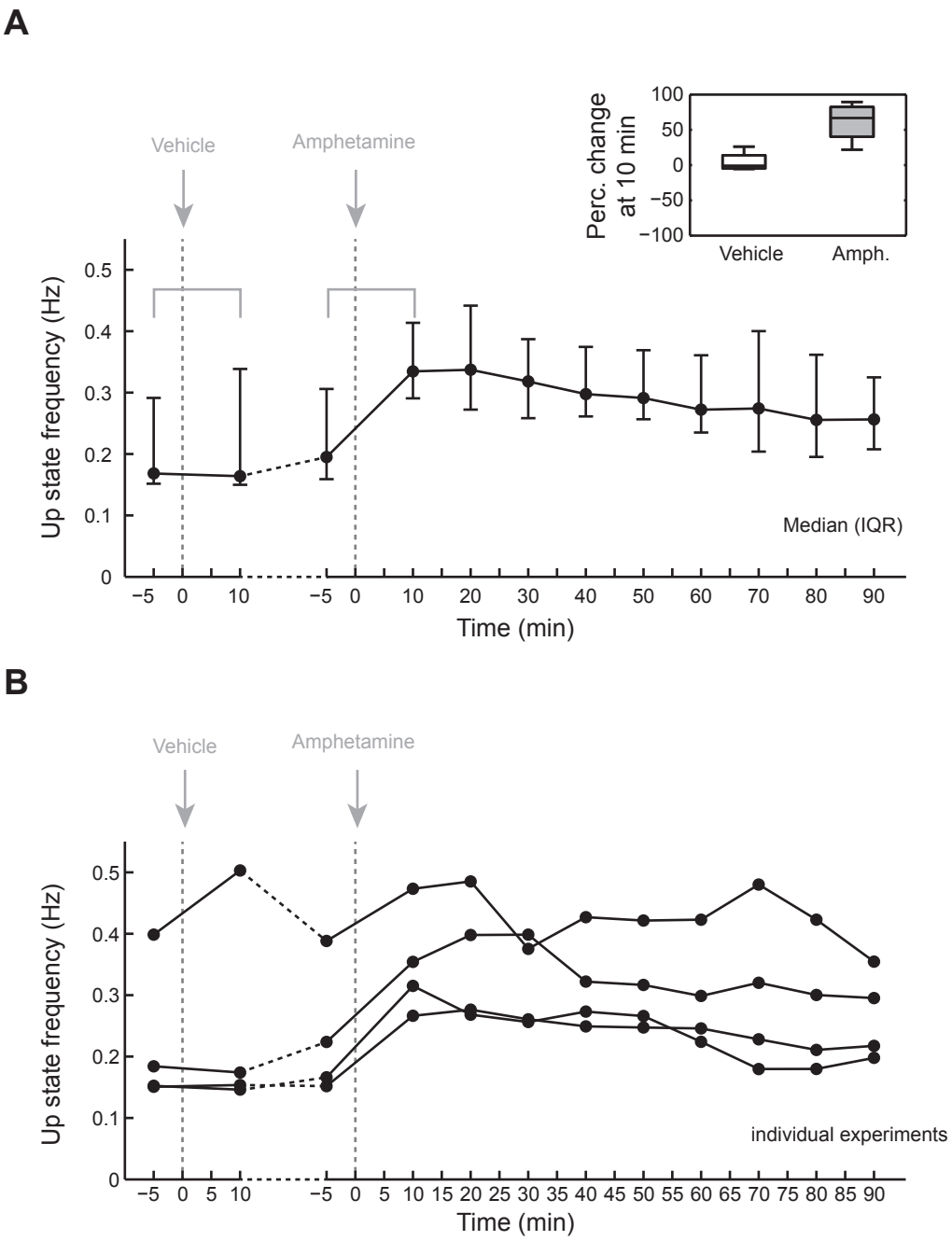

Figure 5.3. Effect of amphetamine on Up state frequency. *(A)* Line plot showing median Up state frequency (error bars represent IQRs) over the time course of the experiment, n=4. *Inset:* Box plot showing percentage change in Up state frequency (10 min post injection compared to pre-injection period) for vehicle and amphetamine injections (n=4). *(B)* Time course of amphetamine action on Up state frequency for all experminents.

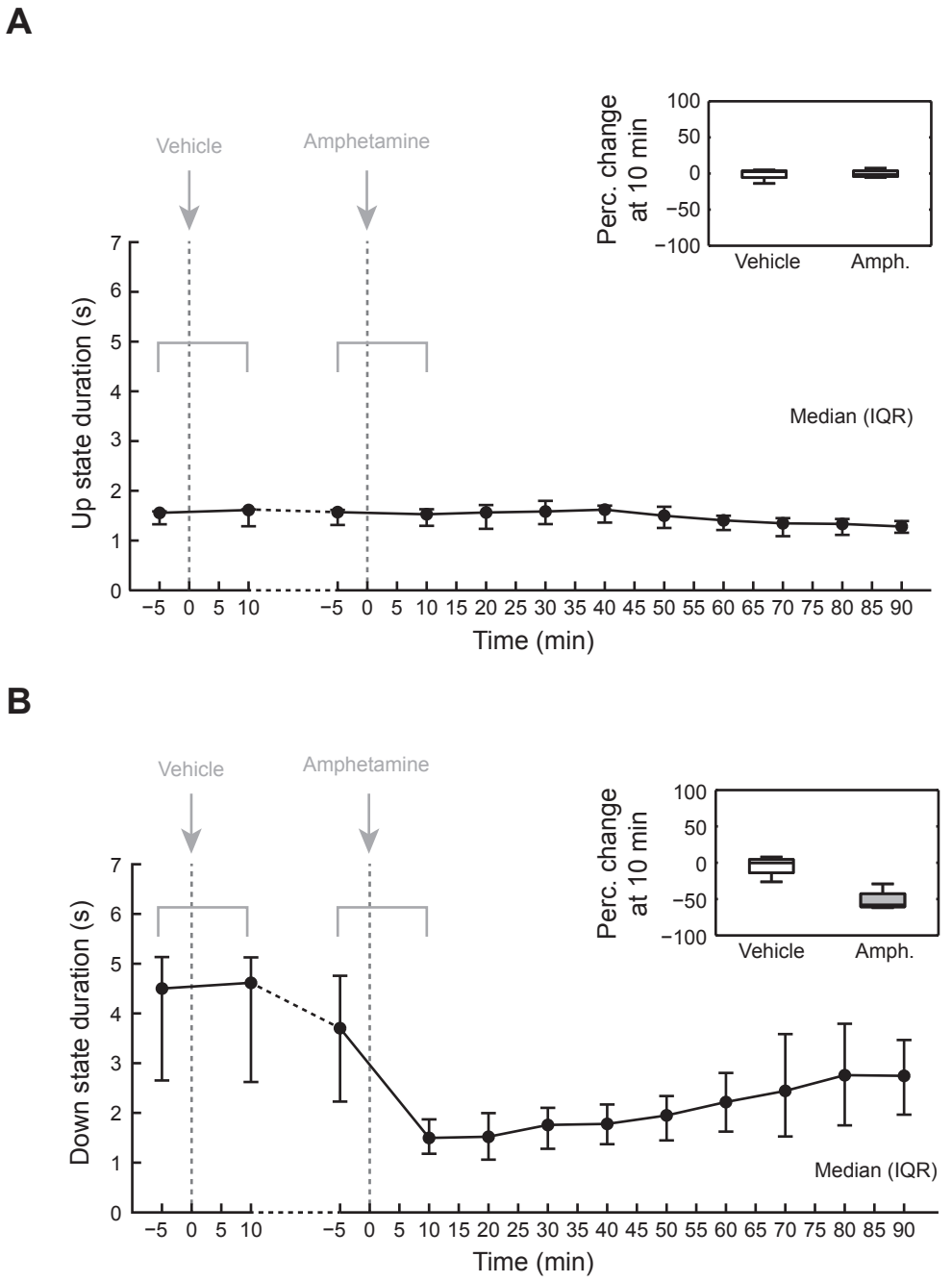

Figure 5.4. Effect of amphetamine on Up and Down state duration. *(A)* Line plot showing median Up state duration (error bars represent IQRs) over the time course of the experiment. *Inset:* Box plot showing percentage change in Up state duration (10 min post injection compared to pre-injection period) for vehicle and amphetamine injections (n=4). *(B)* Line plot showing median Down state duration (with error bars indicating IQRs) over the time course of the experiment. *Inset:* Box plot showing percentage change in Down state duration (10 min post injection compared to pre-injection period) for vehicle and amphetamine injections (n=4).

Effect of amphetamine on Down state duration

In line with the apparent increase in Up-Down state frequency seen in Figure 5.3, there was a trend for the Down state duration to decrease within ten minutes after the amphetamine injection (Figure 5.4 B; median change vehicle: -0.13% (IQR: -13.92 – 4.58), amphetamine: -57.85% (IQR: -60.74 – -42.61)).

5.4.4 *Effect of systemic administration of amphetamine on Up state gamma power*

Figure 5.5 A shows the Up state gamma power in the four mPFC sub-regions (median and IQR) over the time course of the experiment. In agreement with the results in section 3.4.3, the Up state gamma power was higher in dorsal compared to ventral mPFC regions and the decrease in mean Up state gamma power along the dorsal-to-ventral gradient was a gradual change. The vehicle injection at the beginning of the experiment did not notably affect Up state gamma power. Amphetamine, however, decreased Up state gamma power within ten minutes after injection (Figure 5.5 A).

Time course

A two-way RM ANOVA on all time points around the amphetamine injection, from -5 to 90 minutes (with respect to amphetamine injection) was run and revealed an effect of amphetamine on Up state gamma power (main effect of *Time* $F_{(9,81)}=14.98$, $p<0.001$, n=4, Figure 5.5 A) as well as a sub-regional difference (main effect of *Region* $F_{(3,81)}=38.72$, $p<0.001$). The amphetamine effect on Up state gamma power differed between the sub-regions (interaction *Time*Region* $F_{(27,81)}=19.40$, $p<0.001$). Post-hoc tests revealed that the overall effect of amphetamine lasted until 60 minutes after injection (Holm-Sidak test). Post-hoc tests within the specific sub-regions revealed that the amphetamine-induced reduction in Up state gamma power lasted up to 50 minutes after injection in the Cg, 60 minutes in the IL and 80 minutes after injection in the DP. No time point was significantly different from the baseline in PrL.

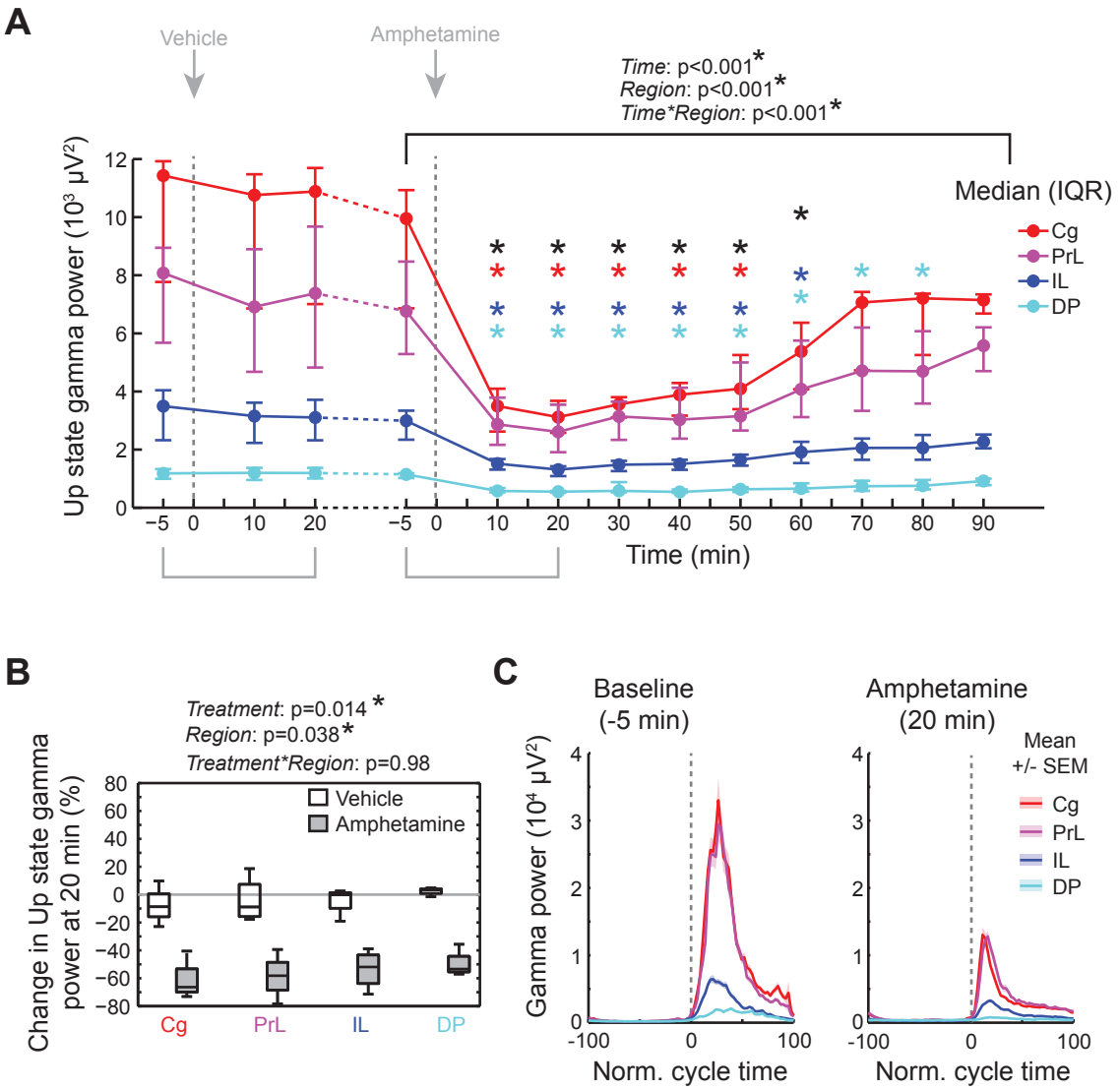

Figure 5.5. Amphetamine decreased Up state gamma power. *(A)* Line plot showing median Up state gamma power (error bars represent IQRs) over the time course of the experiment, for the four mPFC subregions (n=4). p-values are from a two-way RM ANOVA on aligned ranks, using the time points indicated by the black bracket. * indicates time points that were significantly different from the amphetamine baseline (Holm-Sidak post-hoc test after significant main effect of *Time*), * * * indicate time points that were significantly different from the baseline in Cg, IL, and DP, respectively (Holm-Sidak post-hoc test after significant *Time*Region* interaction). Grey brackets under graph mark the time points used for vehicle comparison in (B). *(B)* Box plot showing percentage change in Up state gamma power 20 minutes after vehicle and amphetamine injections (expressed as percent of baseline) for four mPFC sub-regions (n=4 rats). p-values from two-way RM ANOVA on aligned ranks; no post-hoc test was significant. *(C)* Example from one experiment showing gamma power aligned to the normalised Down-Up state cycle (mean +/-SEM over all Up states occurring within the 10 minute data segment). *Left* plot shows aligned gamma power at 5 minutes before amphetamine injection, *right* plot shows aligned gamma power at 20 minutes after amphetamine injection.

Comparison with vehicle

The percentage change (from baseline) in Up state gamma power after 20 minutes induced by amphetamine was compared to the percentage change induced after 20 minutes by the vehicle (Figure 5.5 B). The change in Up state gamma power following amphetamine injection differed from the change following vehicle injection (main effect of *Treatment,* $F_{(1,9)}$=27.04, p<0.05, n=4). Up state gamma power differed between the sub-regions (main effect of factor *Region*, $F_{(3,9)}$=4.89, p<0.05), with a difference between Cg and DP (post-hoc Holm-Sidak test). The percentage change in Up state gamma power was not sub-region-dependent (interaction *Treatment*Region* $F_{(3,9)}$ = 0.06, p >0.05, for percentage change; medians and IQR values are reported in Table 5.1).

Example data

Figure 5.5 C shows the gamma power for one experiment aligned to the normalised Down-Up state cycle. In all sub-regions, gamma power increases sharply at the start of the Up state (Figure 5.5 C). Following amphetamine injection, the rise in gamma power at the beginning of the Up state occurs with a similar steepness, however does not reach the same peak value.

5.4.5 *Effect of systemic administration amphetamine on Up state high gamma power*

Figure 5.6 A shows the Up state high gamma power in the four mPFC sub-regions (median and IQR) over the time course of the experiment. In agreement with the results in section 3.4.3, the Up state high gamma power was higher in dorsal compared to ventral mPFC regions, with the main difference being between Cg/PrL and IL/DP. Neither the vehicle injection at the beginning of the experiment, nor the amphetamine injection seemed to affect the Up state high gamma power (Figure 5.6).

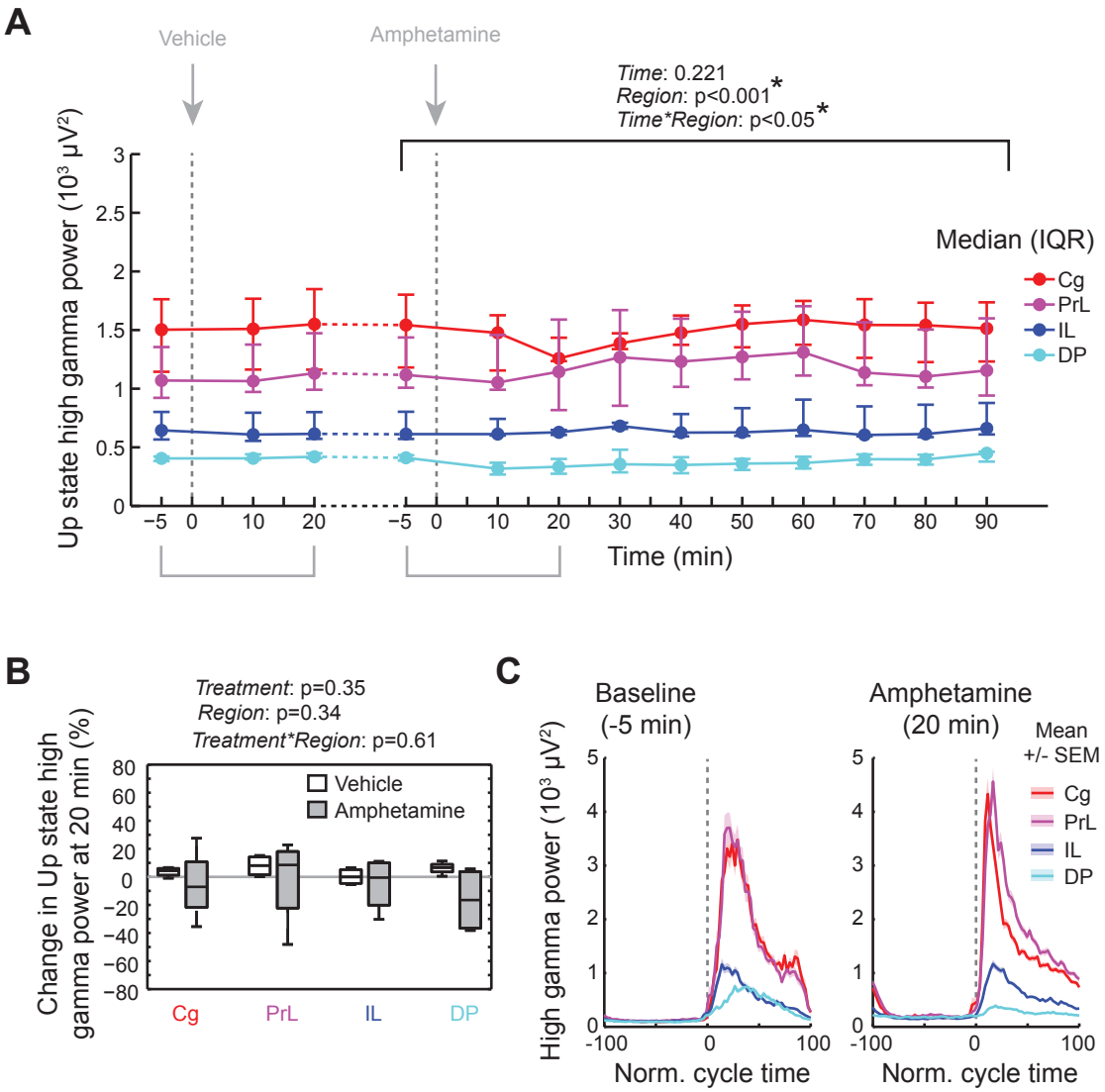

Figure 5.6. Amphetamine did not affect Up state high gamma power. *(A)* Line plot showing median Up state high gamma power (error bars represent IQRs) over the time course of the experiment, for the four mPFC subregions (n=4). p-values are from a two-way RM ANOVA on aligned ranks, using the time points indicated by the black bracket. Grey brackets underneath the figure mark the time points for the comparison with the vehicle. *(B)* Box plot showing percentage change in Up state high gamma power 20 minutes after vehicle and amphetamine injections for four mPFC sub-regions (n=4 rats). p-values are from two-way RM ANOVA on aligned ranks. *(C)* Example from one experiment showing high gamma power aligned to the normalised Down-Up state cycle (mean +/-SEM over all Up states occurring within the 10 minute data segment). *Left* plot shows aligned high gamma power at 5 minutes before amphetamine injection, *Right* plot shows aligned high gamma power at 20 minutes after amphetamine injection.

Time course

The analysis of the time course around the amphetamine injection from (-5 to 90 minutes) revealed no effect of amphetamine (main effect of factor *Time,* $F_{(3,81)}$=1.44, p>0.05, n=4, Figure 5.6). There was a sub-regional difference (main effect of factor *Region,* $F_{(3,81)}$=20.95, p<0.001). There was a *Region*Time* interaction ($F_{(27,81)}$=1.86, p<0.05). However, the effect of amphetamine was not significant in any individual sub-region (post-hoc Holm-Sidak test).

Comparison with vehicle

The percentage changes 20 minute after injection for vehicle and amphetamine are shown in Figure 5.6 B. Medians and IQR values of the percentage change are given in Table 5.1. The percentage change following amphetamine injection was not different from the percentage change following the vehicle injection (main effect of *Treatment* $F_{(1,9)}$=1.25, p>0.05, n=4). There was no regional difference (main effect of *Region* $F_{(3,9)}$=1.27, p>0.05) and no interaction between treatment and region (interaction *Treatment*Region*: $F_{(3,9)}$=0.64, p>0.05).

Example

Figure 5.6 C shows an example of high gamma power from a single experiment aligned to the normalised Down-Up state cycle. Although it looks like the Up state gamma peak appears sharper in the Cg and PrL after the amphetamine injection, the mean Up state gamma power (as reported above) was not changed.

5.4.6 *Effect of systemic administration of amphetamine on Up state spindle power*

Figure 5.7 A shows the Up state spindle power in the four mPFC sub-regions (median and IQR) over the time course of the experiment. In agreement with the results in section 3.4.3, the Up state spindle power showed variation between the sub-regions, which was less pronounced than for Up state gamma and high gamma power. Neither the vehicle injection at the beginning of the experiment, nor the amphetamine injection seemed to affect the Up state spindle power (Figure 5.7 A).

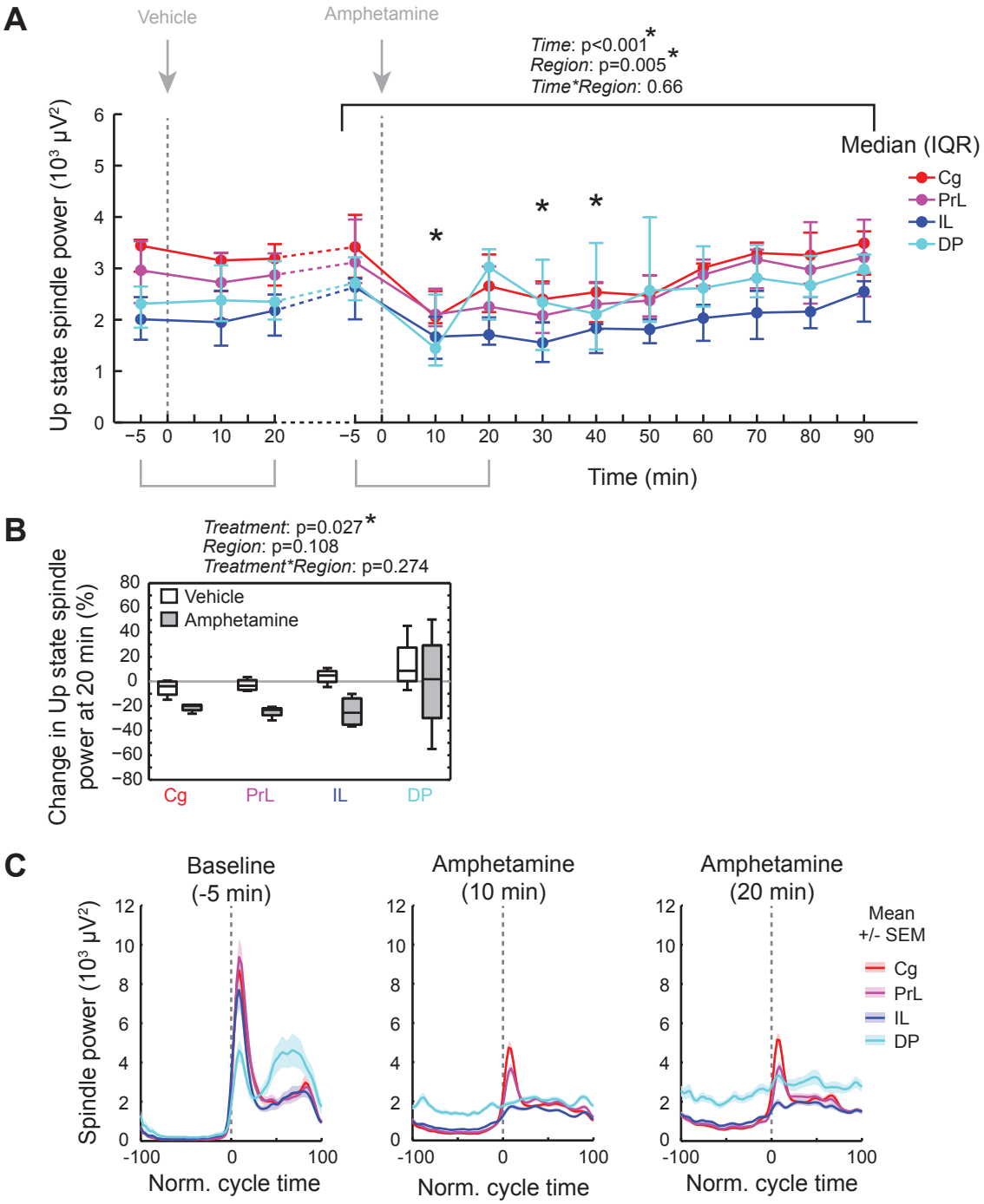

Figure 5.7. Amphetamine decreased Up state spindle power. *(A)* Line plot showing median Up state spindle power (error bars represent IQRs) over the time course of the experiment, for the four mPFC subregions (n=4); p-values are from a two-way RM ANOVA on aligned ranks, using the time points indicated by the black bracket. * indicates time points that were significantly different from the baseline (Holm-Sidak post-hoc test after main effect of factor *Time)*. Grey brackets mark the time points for the vehicle comparison. *(B)* Box plot showing percentage change in Up state spindle power 20 minutes after vehicle and amphetamine injection for the four mPFC subregions (n=4). p-values are from a two-way RM ANOVA on aligned ranks. *(C)* Example from one animal showing spindle power aligned to the normalised Down-Up state cycle (mean +/-SEM over all Up states occurring within the 10 minute data segment). *Left:* aligned spindle power 5 minutes before amphetamine injection. *Middle:* aligned spindle power 10 minutes after amphetamine injection. *Right:* aligned spindle power 20 minutes after amphetamine injection.

Time course

Up state spindle power during the time course of the experiment is shown in Figure 5.7 A. An investigation of the time course around the amphetamine injection from -5 to 90 minutes revealed that the amphetamine effect was significant (main effect of factor *Time* $F_{(9,81)}$=4.72, p<0.001, n=4). Post-hoc tests revealed that data points at 10 minutes, 30 and 40 minutes after amphetamine injection were significantly different from the baseline (Holm-Sidak test). There was a main effect of *Region* ($F_{(3,81)}$=8.80, p<0.01), but no interaction *Time*Region* ($F_{(27,81)}$=0.87 p>0.05).

Comparison with vehicle

Looking at the percentage change after 20 minutes (Figure 5.7 B), the amphetamine effect was significantly different from the vehicle effect (main effect of *Treatment*: $F_{(2,9)}$=16.59, p<0.05, n=4). There was no sub-regional difference (main effect of *Region*: $F_{(3,9)}$=2.71, p >0.05). And the amphetamine did not differ between the sub-regions (interaction *Treatment*Region* $F_{(3,9)}$=1.52, p>0.05). For the medians and IQR values of the percentage change see Table 5.2.

Example data

Figure 5.7 C (*left panel*) shows a representative example of the finer-scale changes in spindle power over the course of the normalised Down-Up state cycle during the baseline condition in an individual animal. Interestingly, the spindle power showed two peaks, one at the beginning, the other at the end of the Up state.

Ten minutes after amphetamine injection Figure 5.7 C (*middle panel*), there was a decrease in Up state spindle power in all four sub-regions. In the dorsal mPFC regions (Cg and PrL), the timing of the spindle peak at the Up state onset was retained, but in the ventral mPFC regions (IL, DP) both spindle peaks during the Up state were completely abolished. In particular, the spindle power in the DP no longer seemed to be modulated by the Down state- Up state cycle.

Twenty minutes after amphetamine injection we saw an overall increase in spindle power in DP during both the Up state *and* Down state (Figure 5.7 C, *right panel*). This was reflected as an increase in the mean Up-state power, and was seen consistently across subjects (as observed in Figure 5.7 A, +20 mins). However, despite this broad increase in spindle power in DP, there was no return of the characteristic double-peaked Up state activity seen in the baseline period. So the increase in spindle power in the DP

observed at 20 minutes in the group data (Figure 5.7 A) does not appear to represent a recovery of Up-state time locked spindle activity.

	Gamma % change 20 min post inj.		*High gamma % change 20 min post inj.*	
	Vehicle	**Amphetamine**	**Vehicle**	**Amphetamine**
Cg	-8.73	-66.37	4.40	-7.09
	(-15.90 – 0.60)	(-69.88 – 53.31)	(1.24 – 6.04)	(-21.77 – 10.73)
PrL	-8.84	-58.20	8.10	8.50
	(-15.78 – 7.37)	(-68.46 – -48.50)	(1.55 – 14.23)	(-22.24 – 18.08)
IL	-0.10	-51.94	-0.05	-0.53
	(-9.77 – 1.45)	(-63.79 – -43.29)	(-4.67 – 5.18)	(-20.16 – 9.98)
DP	3.32	-54.40	6.64	-16.53
	(0.91 – 4.09)	(-55.47 – -44.23)	(3.54 – 8.96)	(-36.62 – 3.73)

Table 5.1. Percentage change (median with IQR in brackets) in Up state gamma and high gamma power 20 minutes after vehicle or amphetamine injection.

	Spindle % change 20 min post inj.	
	Vehicle	**Amphetamine**
Cg	-3.85	-19.94
	(-10.79 – -0.20)	(-23.45 – -19.09)
PrL	-3.55	-23.20
	(-6.76 – 1.09)	(-27.60 – -21.75)
IL	4.78	-25.45
	(-0.37 – 8.33)	(-35.05 – -13.79)
DP	8.72	1.82
	(0.33 – 27.50)	(-29.78 – 29.33)

Table 5.2. Percentage change (median with IQR in brackets) in Up state spindle power 20 minutes after vehicle or amphetamine injection.

5.4.7 *Effects of systemic administration of the $D_{1,5}$R agonist SKF38393 on Up Down state parameters*

The $D_{1,5}$R agonist SKF38393 did not have an immediate effect on the Up-Down state parameters. There was a slow increase in Up-Down state frequency as well as a decrease in Up state duration (data not shown). However, these changes were small compared to the changes that occurred over time (section 5.4.1), so were not further analysed.

5.4.8 *Effects of systemic administration of the $D_{1,5}$R agonist SKF38393 on Up state gamma power*

Time course

Up state gamma power over the time course of the experiment is shown in Figure 5.8 A. Analysis of the time course from -5 to 60 minutes showed that SKF38393 decreased Up state gamma power (main effect of factor *Time* $F_{(6,72)}$=2.81, $p<0.05$, n=5). There was a difference between the sub-regions (main effect of factor *Region* $F_{(3,72)}$=66.65, $p<0.001$), with Cg being different from IL and DP, PrL being different from IL and DP, and IL from DP. There was also an interaction between region and time (*Time*Region*: $F_{(18,72)}$=5.27, $p<0.001$). The decrease in Up state gamma power was significant at 10, 20 and 60 minutes after injection. Post-hoc tests (baseline vs all) revealed that in DP, the same time points were significantly different from the baseline.

Comparison with vehicle

The percentage change (after 20 minutes) in Up state gamma power induced by SKF38393 was different from the vehicle response (main effect of factor *Treatment* $F_{(1,18)}$=40.45, $p<0.001$, n=7, Figure 5.8 B). There was a sub-regional difference in Up state gamma power (main effect of factor *Region* $F_{(3,18)}$=3.98, $p<0.05$), but no significant interaction between treatment and region (*Treatment*Region*: $F_{(3,18)}$=1.12, $p>0.05$). Median and IQR values are shown in Table 5.3.

Example data

Figure 5.8 B shows an example of gamma power from a single experiment aligned to the normalised Down-Up state cycle, showing a decrease in mean Up state gamma power in all sub-regions.

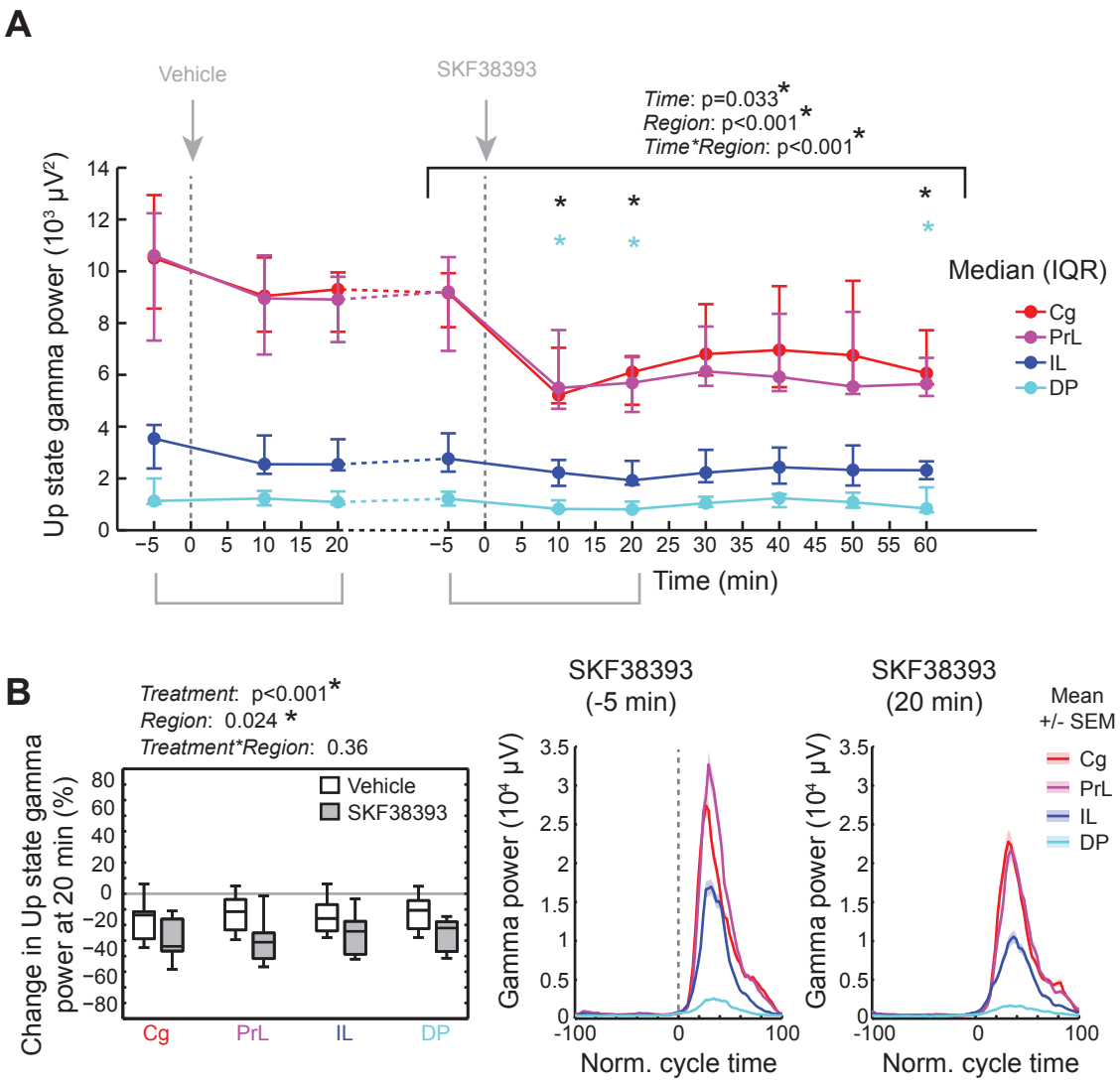

Figure 5.8. The dopamine $D_{1,5}$R agonist SKF38393 decreased Up state gamma power. *(A)* Line plot showing median Up state gamma power (error bars represent IQRs) over the time course of the experiment, for the four mPFC subregions (n=5); p-values are from a two-way RM ANOVA on aligned ranks, using the time points indicated by the black bracket. * indicates time points that were significantly different from the baseline (Holm-Sidak post-hoc test after main effect of factor *Time*. * indicates time points that were significantly different from the baseline within DP (Holm-Sidak post-hoc test after significant *Time*Region* interaction). Grey brackets mark the vehicle comparison in (B). *(B)* Percentage change in Up state gamma power 20 minutes after vehicle and SKF38393 injection for the four mPFC subregions (n=7 animals). p-values are from a two-way RM ANOVA on aligned ranks. *(C)* Example from one experiment showing gamma power aligned to the normalised Down-Up state cycle (mean +/-SEM over all Up states occurring within the 10-minute data segment). *Left:* aligned gamma power at 5 minutes before SKF38393 injection, *right*: aligned gamma power at 10 minutes after SKF38393 injection.

5.4.9 *Effects of systemic administration of the $D_{1,5}R$ agonist SKF38393 on Up state high gamma power*

Time course

Mean Up state high gamma power over the time course of the experiment is shown in Figure 5.9 A. Analysis of the time course from -5 to 60 minutes showed that there was no effect of SKF38393 on Up state high gamma power (main effect of factor *Time* $F_{(6,72)}=2.12$, $p>0.05$, n=5). There was a sub-regional difference ($F_{(3,72)}=24.91$, $p<0.001$), with Cg being different from IL and DP, and PrL being different from IL and DP. There was an interaction between region and time (*Time*Region* $F_{(18,72)}=4.81$, $p<0.001$). However, no post-hoc comparison of time within any of the regions were significant (Holm-Sidak test).

Comparison with vehicle

Comparing percentage change 20 min after SKF38393 injection with the percentage change 20 min after vehicle injection, there was a difference between SKF38393 and vehicle condition in Up state high gamma power (main effect of factor *Time* $F_{(1,18)}=6.98$, $p<0.01$, n=7, Figure 5.9 B). There was no sub-regional difference (main effect of factor *Region* ($F_{(3,18)}=2.14$, $p>0.05$). The effect of SKF38393 was sub-region-dependent (interaction *Time*Region* $F_{(3,18)}=4.06$, $p<0.05$). However, none of the post-hoc test were significant (Holm-Sidak test). Median and IQR values are shown in Table 5.3.

Example data

Figure 5.9 B C shows an example of high gamma power from a single experiment aligned to the normalised Down-Up state cycle. A decrease in Up state high gamma power is apparent 20 minutes after SKF38393, without loss of the timing with respect to the UDS cycle.

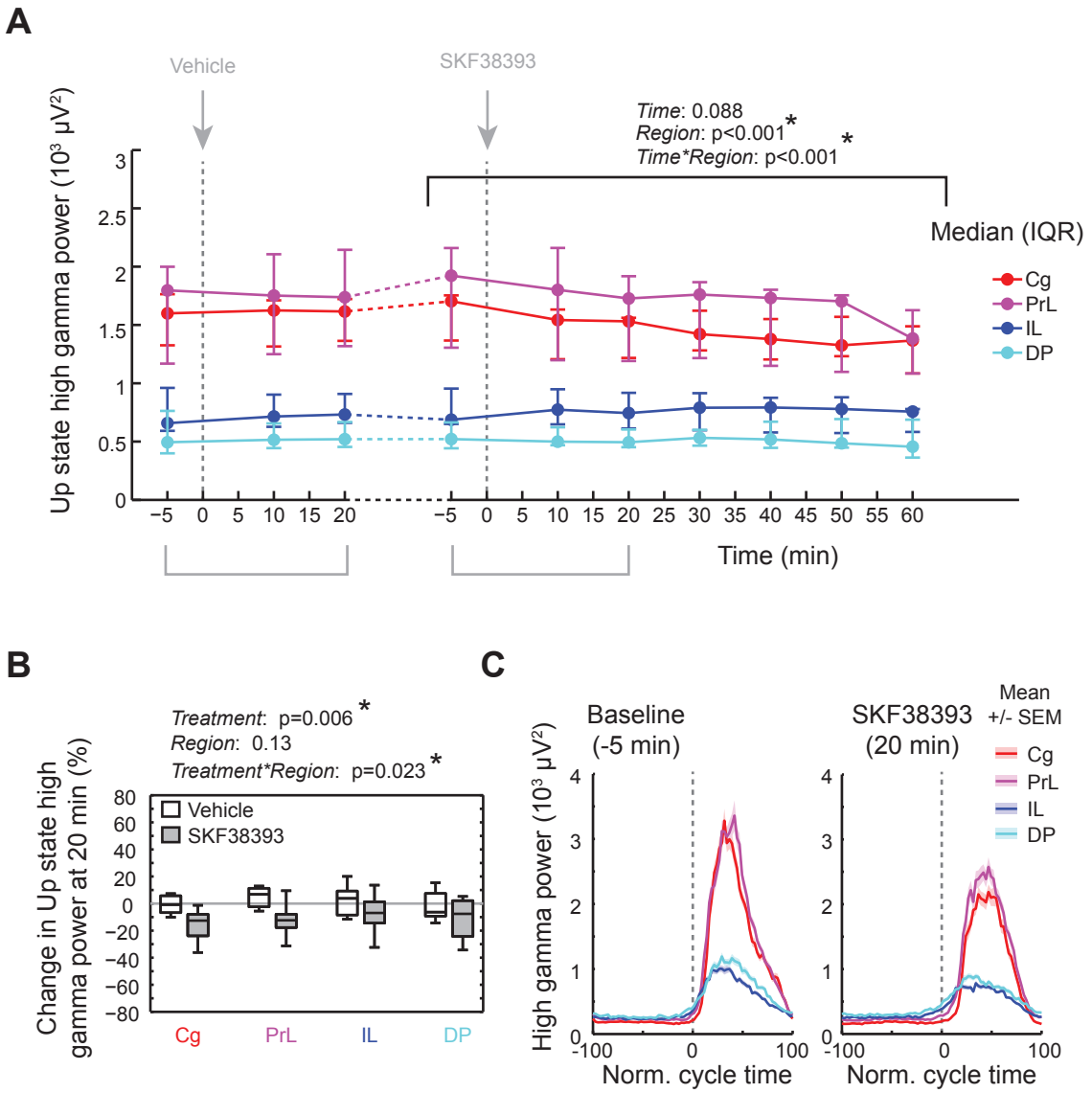

Figure 5.9. The dopamine $D_{1,5}$ receptor agonist SKF38393 decreased Up state high gamma power. *(A)* Line plot showing median Up state high gamma power (error bars represent IQRs) over the time course of the experiment, for the four mPFC subregions (n=5); p-values are from a two-way RM ANOVA on aligned ranks, performed on the time points indicated by the black bracket. Grey brackets mark the timepoints used for the comparison with the vehicle in (B). *(B)* Box plot showing percentage change in Up state high gamma power 20 minutes after vehicle and SKF38393 injection for the four mPFC subregions (n=7); p-values are from a two-way RM ANOVA on aligned ranks. *(C)* Example from one animal showing high gamma power aligned to the normalised Down-Up state cycle (mean +/-SEM over all Up states occurring within the 10-minute data segment). *Left:* aligned gamma power at 5 minutes before SKF38393 injection, *right*: aligned gamma power at 20 minutes after SKF38393 injection.

5.4.10 *Effects of systemic administration of the $D_{1,5}R$ agonist SKF38393 on Up state spindle power*

Time course

The time course of the effect of SKF38393 on Up state spindle power is shown in Figure 5.10 A. Analysis of the time course from -5 to 60 minutes revealed that SKF38393 did not have a significant effect (main effect of *Time* $F_{(6,72)}$=1.06, p>0.05., n=5). There was a sub-regional difference (main effect of factor *Region* $F_{(3,72)}$=5.02, p<0.05) and the interaction *Time*Region* was significant ($F_{(18,72)}$=3.13, p<0.001). However, none of the post-hoc comparisons were significant within the regions.

Comparison with vehicle

The percentage change in Up state spindle power 20 minutes following vehicle (DMSO) and SKF38393 injection is shown in Figure 5.10. There was no difference in percentage change at 20 minutes between SKF38393 and the vehicle (DMSO) (main effect of factor *Time* $F_{(1,18)}$=0.19, p>0.05). There was no regional difference in percentage change at 20 minutes between SKF38393 and the vehicle (main effect of *Region* $F_{(3,18)}$=2.86, p>0.05, n=7). There was no interaction between sub-region and treatment (*Treatment*Region* $F_{(3,18)}$=0.03, p>0.05). Median and IQR values are shown in Table 5.4.

Example data

Two illustrative examples of spindle power (aligned to the normalised Down-Up state cycle) before and after SKF38393 injection are shown in Figure 5.10 C.i and C.ii, respectively. Figure 5.10 C.i shows an example in which the timing of spindle peaks relative to the UDS cycle is retained, however spindle peaks are smaller and wider after SKF38393 injection. Figure 5.10 C.ii shows an example in which the spindle timing with respect to UDS cycle seems to be abolished. In both these examples, the mean Up state spindle power appears unchanged.

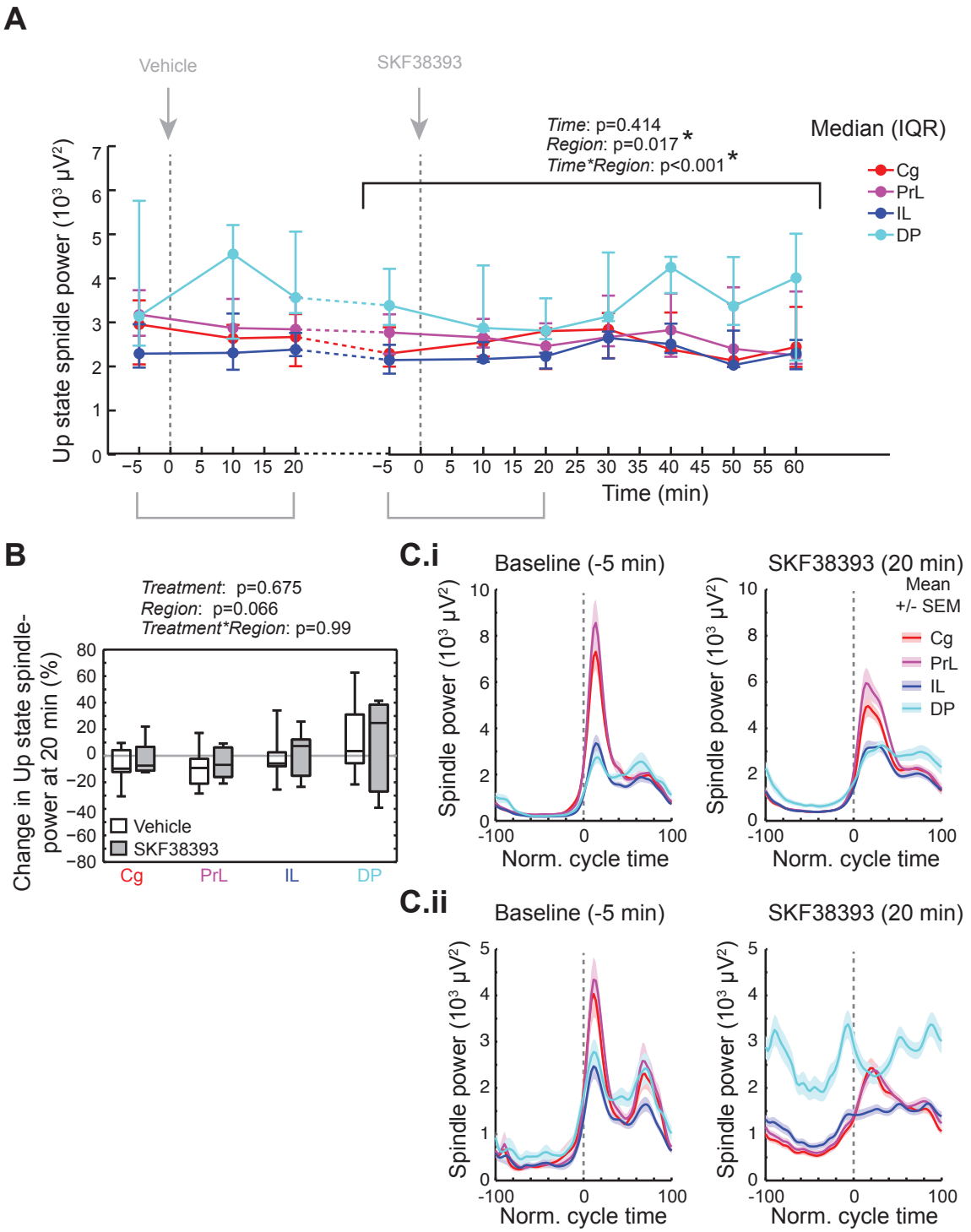

Figure 5.10. The $D_{1,5}$ receptor agonist SKF38393 did not affect Up state spindle power. *(A)* Line graph showing showing median Up state spindle power (error barrs represent IQRs) over the time course of the experiment, for the four mPFC subregions (n=5); p-values are from a two-way RM ANOVA on aligned ranks. *(B)* Box plot showing percentage change in Up state gamma power 20 minutes after injection of vehicle and SKF38393 for the four sub-regions; p-values are from a two-way RM ANOVA on aligned ranks. *(C.i)* Example of cycle-aligned gamma power from one experiment, before and 20 minutes after SKF38393 injection. Although the mean Up state spindle power was comparable for each sub-region, the peak during the Up state appeared wider in this experiment. (*C.ii)* Another example for cycle-aligned spindle power before and 20 minutes after SKF38393 injection. Again, the mean Up state spindle power was comparable, but the timing of spindle power with regard to the UDS cycle was abolished.

	Gamma % change 20 min post inj.		*High Gamma % change 20 min post inj.*	
	Vehicle	**SKF38393**	**Vehicle**	**SKF38393**
Cg	-13.67	-33.71	-0.82	-12.59
	(-28.89 – -11.47)	(-36.70 – -16.24)	(-6.72 – 5.77)	(-23.86 – -8.00)
PrL	-11.41	-31.05	6.78	-12.36
	(-23.19 – 3.63)	(-41.56 – -25.10)	(-2.40 – 11.27)	(-17.73 – -7.89)
IL	-15.82	-24.10	3.81	-6.94
	(-23.83 – -6.93)	(-38.77 – -17.70)	(-8.52 – 9.26)	(-14.43 – 1.27)
DP	-10.61	-22.00	-6.32	-7.61
	(-22.41 – 1.24)	(-37.00 – -18.01)	(-9.30 – 7.51)	(-24.28 – 2.12)

Table 5.3 Percentage change (median and IQR in brackets) in Up state gamma and high gamma 20 minutes after vehicle and SKF38393 injection.

	Spindle % change 20 min post inj.	
	Vehicle	**SKF38393**
Cg	-9.68	-7.39
	(-12.17 – -4.29)	(-11.26 – 6.72)
PrL	-9.17	-6.81
	(-20.99 – -2.33)	(-15.96 – 6.26)
IL	-5.82	7.32
	(-7.93 – 2.58)	(-15.10 – 12.21)
DP	3.56	24.71
	(-5.63 – 31.10)	(-26.86 – 38.54)

Table 5.4 Percentage change (median with IQR in brackets) in Up state spindle power 20 minutes after Vehicle and SKF38393 injection.

5.4.11 *Effects of systemic administration of the dopamine D_4R agonist A412997 on Up Down state parameters*

The D_4R agonist A412997 did not have a strong, immediate effect on the Up-Down state parameters (data not shown). There was an increase in Up-Down state frequency as well as a decrease in Up state duration. However, these changes were small compared to the changes that occurred over time (section 5.4.1), so were not further investigated.

5.4.12 *Effects of systemic administration of the dopamine D_4R agonist A412997 on Up state gamma power*

Time course

The mean Up state gamma power over the time course of the experiment is shown in Figure 5.11. Analysing all time points from -5 to 70 minutes around A412997 injection revealed a significant effect of the drug (main effect of *Time*: $F_{(7,84)}=8.28$, $p<0.001$, n=5), and all time points from 10 to 40 minutes after injection were significantly different from the baseline (Holm-Sidak post-hoc test). There was a sub-regional difference in Up state gamma power (main effect of *Region* ($F_{(3,12)}=55.01$, $p<0.001$). The drug effect was region-specific (interaction *Time*Region* $F_{(21,84)}=5.98$, $p<0.001$), with the 10 to 40 minutes time points being significant for the DP only (Holm-Sidak post-hoc test).

Comparison with vehicle

The percentage changes after 20 minutes that occurred with the vehicle and with A412997 for the four sub-regions are shown in Figure 5.11 B. There was a significant difference between the effect of A412997 and the effect of the vehicle (main effect of *Treatment*: $F_{(1,12)}=159.872$, $p<0.001$, n=5). There was no sub-regional difference in Up state gamma power (main effect of *Region* $F_{(3,12)}=2.64$, $p>0.05$). Although there was a regional component to the A412997 effect (interaction *Treatment*Region* $F_{(3,12)}=6.434$, $p<0.01$), none of the post-hoc comparisons were significant (Holm-Sidak test). The median percentage change and IQR values are shown in table Table 5.5.

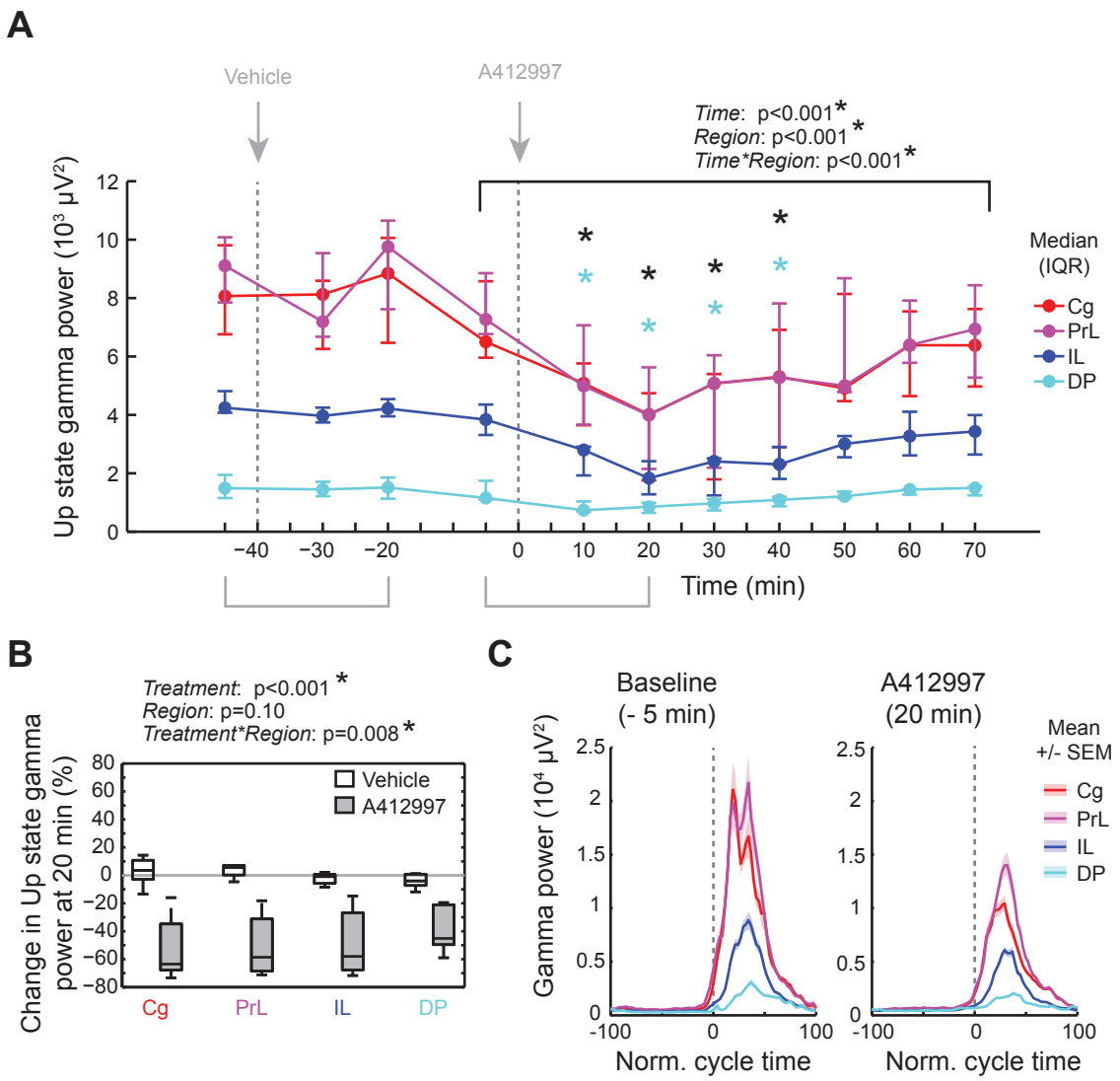

Figure 5.11. The dopamine D_4 receptor agonist A412997 decreased Up state gamma power. *(A)* Line plot showing median Up state gamma power (error bars represent IQRs) over the time course of the experiment, for the four mPFC subregions (n=5); p-values are from a two-way RM ANOVA on aligned ranks, performed on the time points indicated by the black bracket. * indicates time points that were significantly different from baseline, * indicates time points that were significantly different from baseline in DP; grey brackets mark the timepoints used for vehicle comparison. *(B)* Box plot showing percentage change in Up state gamma power 20 minutes after vehicle and A412997 injection for the four mPFC subregions (n=5); p-values are from a two-way RM ANOVA on aligned ranks. *(C)* Example from one experiment showing gamma power aligned to the normalised Down-Up state cycle (mean +/-SEM over all Up states occurring within the 10-minute data segment). *Left:* aligned gamma power at 5 minutes before A412997 injection, *right*: aligned gamma power 20 minutes after A412997 injection.

Example data

Figure 5.11 C shows an example of gamma power from a single experiment, aligned to the normalised Down-Up state cycle, exhibiting a marked decrease in Up state gamma power 20 minutes after D_4R activation with A412997 injection.

5.4.13 *Effects of systemic administration of the dopamine D_4 R agonist A412997 on Up state high gamma power*

Time course

Up state high gamma power over the time course of the experiment is shown in Figure 5.12 A. Analysing over all time points from -5 to 70 minutes, A412997 did have an effect (main effect of *Time* $F_{(7,84)}$=3.90, p<0.01, n=5). However, no single time point was different from the baseline in a post-hoc comparison (Holm-Sidak test). There was a sub-regional difference in Up state high gamma power (main effect of *Region*: $F_{(3,84)}$=22.217, p<0.001), as well as a significant interaction (*Time*Region:* $F_{(21,84)}$=2.62, p<0.001). However, none of the post-hoc comparisons were significant (Holm-Sidak test).

Comparison with vehicle

The percentage change 20 minutes after injection of A412997 was different from the vehicle injection (main effect of *Treatment*: $F_{(1,12)}$=44.10, p<0.01, n=5). Figure 5.12 B shows the percentage change for the four sub-regions. There was no sub-regional difference in Up state high gamma power (main effect of *Region*: $F_{(3,12)}$=3.02, p>0.05). There was no sub-regional difference in the D_4R agonist effect (interaction *Treatment*Region*: $F_{(3,12)}$=0.11, p>0.05). Hence, the D_4R agonist decreased Up state high gamma power equally in all mPFC sub-regions. The median percentage change and IQR values are shown in table Table 5.5.

Example data

Figure 5.12 C shows an example of high gamma power from a single experiment, aligned to the normalised Down-Up state cycle, before and 20 minute after A412997 injection. A decrease in high gamma power is clearly visible in all sub-regions, the timing of the peak at the beginning of the Up state seems retained.

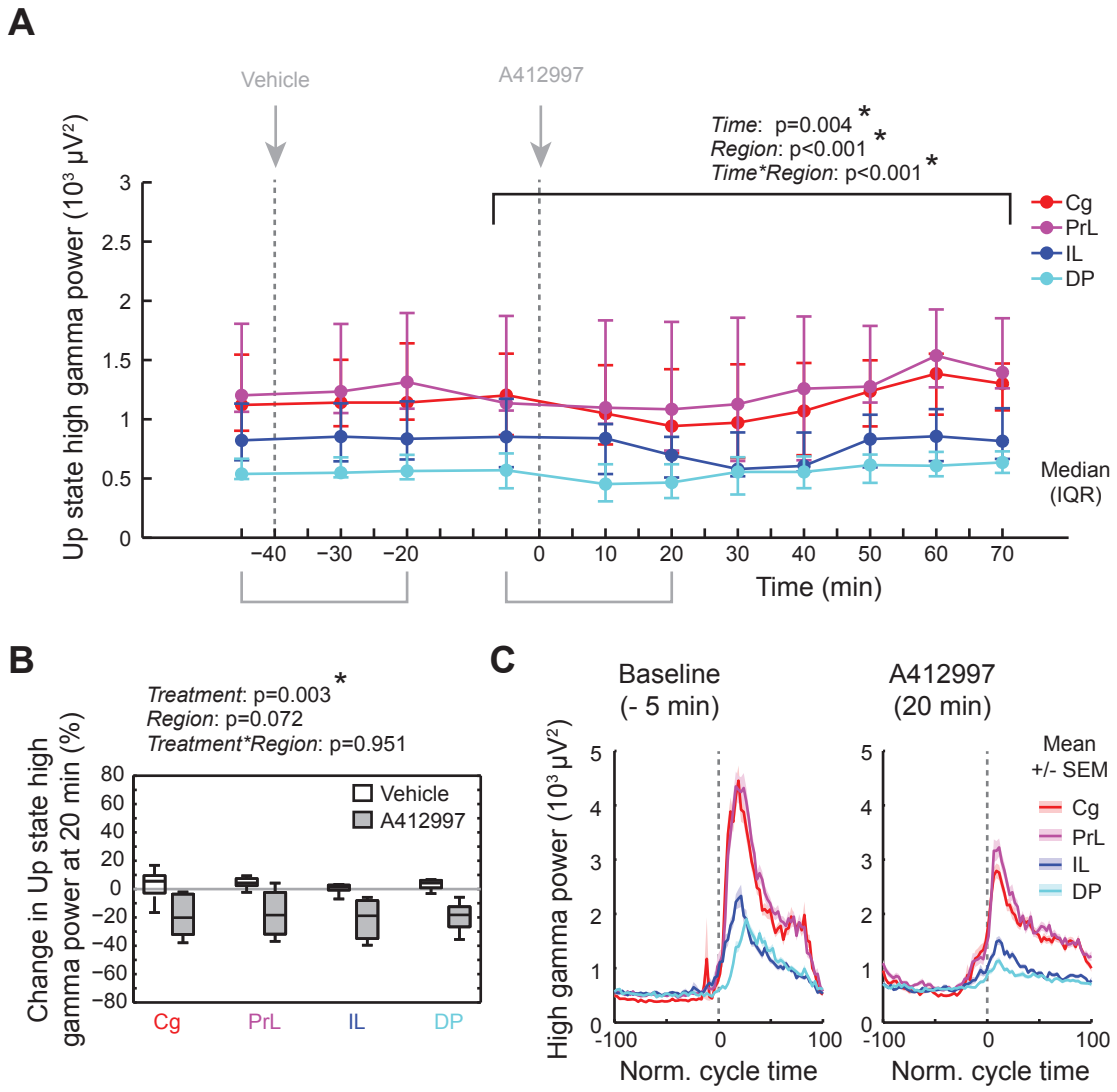

Figure 5.12. The dopamine D_4 receptor agonist A412997 decreased Up state high gamma power. *(A)* Line plot showing median Up state high gamma power (error bars represent IQRs) for the four mPFC subregions (n=5); p-values are from a two-way RM ANOVA on aligned ranks, performed on the time points indicated by the black bracket. Grey brackets mark the timepoints for the vehicle comparison. *(B)* Boxplot showing percentage change in Up state high gamma power 20 minutes after vehicle and A412997 injection for the four mPFC subregions (n=5 animals); p-values are from a two-way RM ANOVA on aligned ranks. *(C)* Example from one animal showing high gamma power aligned to the normalised Down-Up state cycle (mean +/-SEM over all Up states occurring within the 10-minute data segment). *Left:* aligned gamma power at 5 minutes before A412997 injection, *right*: aligned gamma power 20 minutes after A412997 injection (mean +/-SEM).

5.4.14 *Effects of systemic administration of the dopamine D_4 R agonist A412997 on Up state spindle power*

Time course

Up state spindle power over the time course of the experiment is shown in Figure 5.13 A. The analysis of the full A412997-related time course from -5 to 70 minutes revealed a late increase in spindle power (main effect of *Time*: ($F_{(7,84)}$=8.22, p<0.001, n=5), with time points 50, 60 and 70 minutes significantly different from the baseline (Holm-Sidak post-hoc test, Figure 5.13 A). There was no sub-regional difference in Up state spindle power (no main effect of factor *Region*: $F_{(3,84)}$=0.90, p>0.05). The increase in spindle power was not sub-region dependent (interaction *Time*Region:* $F_{(21,84)}$=0.668 p>0.05).

Comparison with vehicle

There was a trend for A412997 to briefly decrease Up state spindle power (Figure 5.13 A). However, the percentage change, 20 min after injection, induced by A412997, did not differ from the effect of the vehicle (main effect of factor *Treatment* $F_{(1,12)}$=0.017, p>0.05, n=5, Figure 5.13 B). There was neither a sub-regional difference in Up state spindle power (main effect of factor *Region* $F_{(3,12)}$=0.07, p>0.05), nor an interaction between sub-region and treatment (*Treatment*Region* $F_{(3,12)}$=1.84, p>0.05). Median and IQR values are shown in Table 5.6.

Example

Figure 5.13 C shows spindle power from one animal (aligned to the normalised Down state-Up state cycle) over the time course of the experiment. As can be seen from this example, the increase in spindle power (50-70 min afer injection) was time-locked to the Up state, and more specifically, showed the typical temporal pattern with time-locking to the start and end of the Up state.

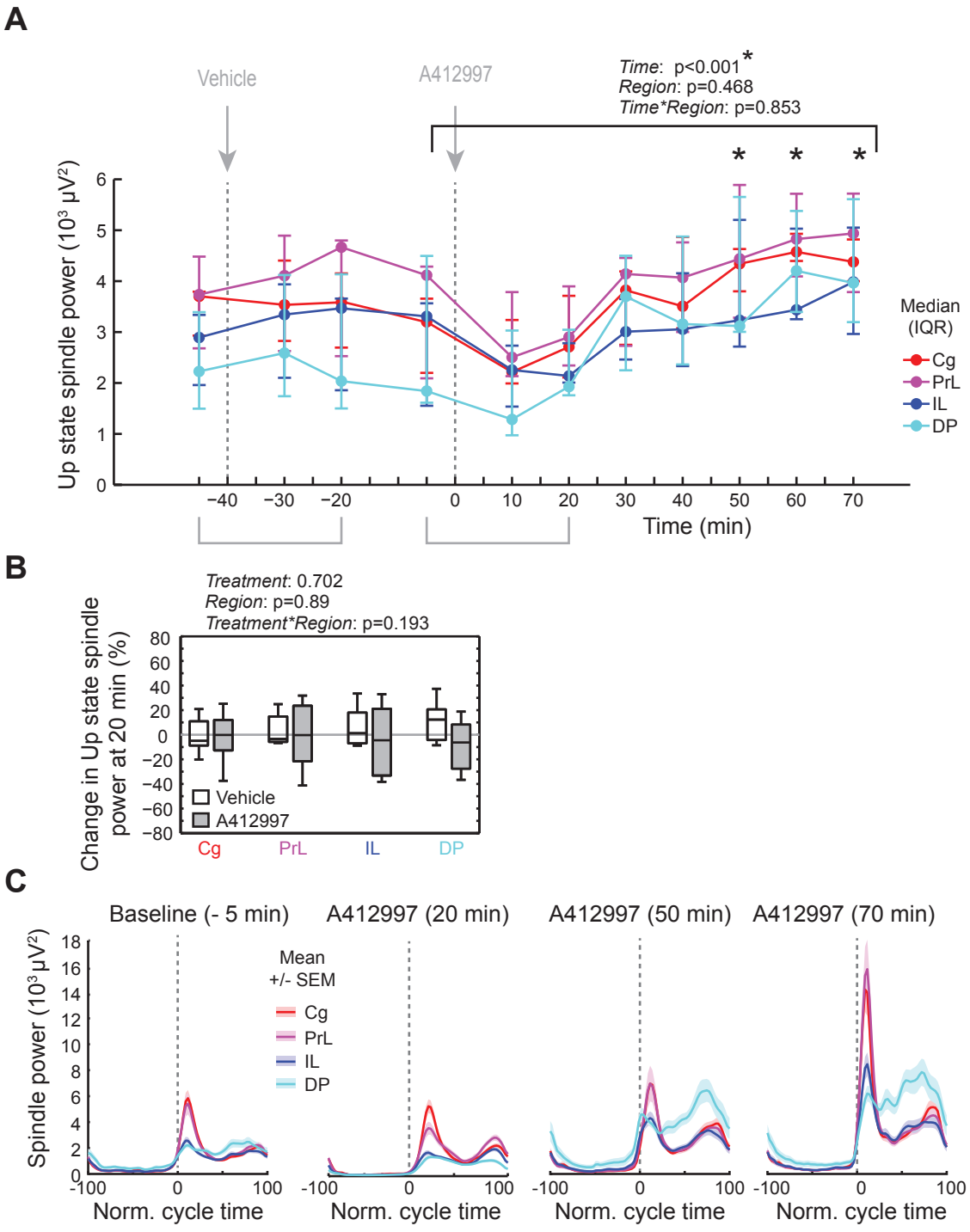

Figure 5.13. The dopamine D_4 receptor agonist A412997 increased Up state spindle power. *(A)* Line graph showing median Up state spindle power (error bars indicate IQR error bars for the four mP FC subregions (n=5); p-values are from a two-way RM ANOVA on aligned ranks; * indicates time points that were significantly different from the baseline (Holm-Sidak post hoc test at overall significance level 0.05). Grey brackets indicate time points used in vehicle comparison in (B). *(B)* Box plot showing percentage change in Up state spindle power 20 minutes after vehicle and A412997 injection for the four mPFC subregions (n=5 animals); p-values are from a two-way RM ANOVA on aligned ranks. *(C)* Example from one animal showing spindle power aligned to the normalised Down-Up state cycle (mean +/-SEM over all Up states occurring within the 10-minute data segment) at baseline, 20, 50 and 70 minutes after A412997 injection showing a late increase in spindle power.

	Gamma % change 20 min post inj.		*High Gamma % change 20 min post inj.*	
	Vehicle	**A412997**	**Vehicle**	**SKF38393**
Cg	3.56	-63.49	5.60	-20.16
	(-2.86 – 10.79)	(-67.82 – 34.81)	(-2.84 – 9.53)	(-31.96 - -3.57)
PrL	5.66	-58.60	4.26	-18.37
	(0.26 – 7.12)	(-68.57 - -31.21)	(2.38 – 7.43)	(-31.76 - -2.36)
IL	-0.89	-57.98	1.47	-18.85
	(-5.81 – 0.73)	(-67.63 - -26.76)	(-0.75 – 2.87)	(-34.91 - -8.13)
DP	-4.00	-45.12	4.35	-18.24
	(-7.26 – 0.85)	(-49.58 - -21.06)	(0.91 – 6.21)	(-26.66 - -12.46)

Table 5.5. Percentage change (median and IQR values in brackets) in Up state gamma and high gamma power 20 minutes after vehicle and A412997 injection.

	Spindle % change 20 min post inj.	
	Vehicle	**A412997**
Cg	-4.98	-0.15
	(-8.80 – 10.94)	(-12.75 – 1.97)
PrL	-3.46	-0.29
	(-5.83 – 14.85)	(-21.51 – 23.56)
IL	1.22	-4.48
	-7.05 – 18.04)	(-33.13 – 21.06)
DP	12.31	-6.29
	(-4.30 – 20.65)	(-27.57 – 8.28)

Table 5.6. Percentage change (median and IQR values) in Up state spindle power 20 minutes after Vehicle and A412997 injection

A412997 decreased Up state gamma and high gamma power (for up to 40 minutes after injection) and increased Up state spindle power from 50-70 minutes after injection. Although these effects were observed in the same data set, it might not mean that they occur to the same extend in one individual animal. It might be that in some animals, the early decrease in the gamma bands was the dominant effect, whereas in others, the late

increase in spindle power was the dominant effect. In addition, the suppression of the VSMP observed after administration of A412997 in two out of five experiments (see also section 4.4.8) could influence the Up state power (Figure 5.14 C). Indeed, Up state power in the gamma and high gamma power seemed reduced during the suppression of the VSMP. Figure 5.14 A shows an LPF segment containing a 'high power state' of the VSMP (under baseline condition). Figure 5.14 B shows the LFP eight minutes after injection of A412997, when the VSMP was supressed. A marked reduction of Up state gamma and high power can be observed in the DP but not in the Cg (Figure 5.14 B). Seventy minutes after A412997 injection, the 'high power states' of the VSMP had re-occurred and, in particular, Up states occurring during or just prior to the 'high power state' of the VSMP were characterised by strong spindle oscillations at ~13 Hz (Figure 5.14 C). Hence, this example indicates that the suppressive effect of A412997 on the VSMP might be related to the early reduction in gamma and spindle power.

To see if the early decrease in gamma and high gamma power and the late increase in spindle power occurred in a single experiment, and if the suppression of the VSMP played a role in the initial decrease in Up state gamma and high gamma power in the DP, data from the DP region from all experiments was plotted (Figure 5.15), indicating experiments with and without suppression of the VSMP. A decrease in Up state gamma power occurred in all experiments (n=5, Figure 5.15 A), whereas the temporary suppression of the VSMP occurred only in two out of five experiments. No obvious difference between experiments with and without the VSMP was apparent for the Up state high gamma power (Figure 5.15 B). The late increase in Up state spindle power also occurred in all experiments (Figure 5.15 C). Hence, the effects of A412997 on the nested fast oscillation power occur independently of its effect on the VSMP.

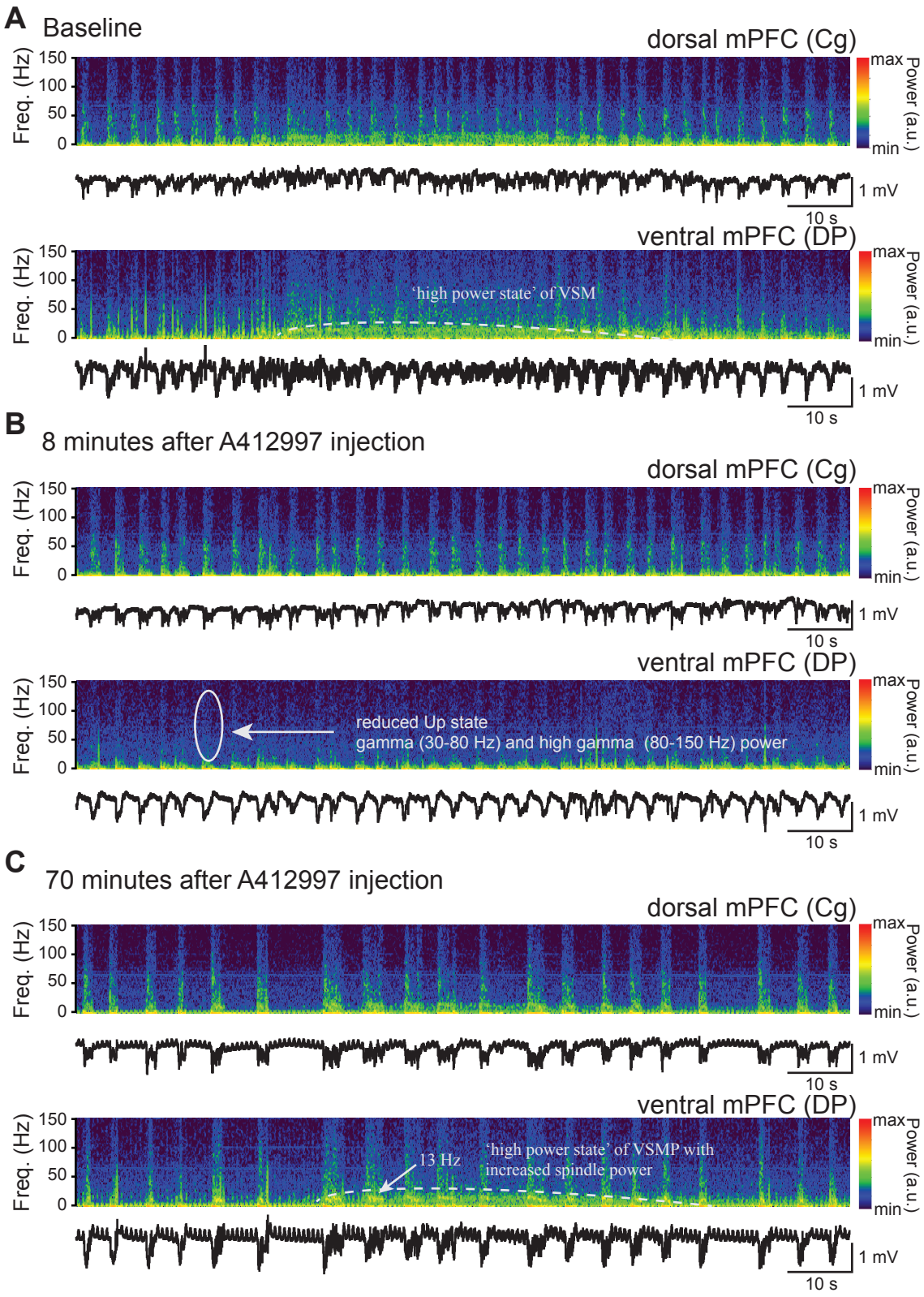

Figure 5.14. Example recordings showing early decrease in Up state gamma and high gamma power and late increase in Up state spindle power. *(A)* LFPs (black) and spectrograms of LFP recorded from Cg and DP during baseline conditions. *(B)* LFPs and spectrograms of LFP recorded from Cg and DP 8 minutes after A412997 injection. In this example, the high power state of the VSMP was abolished and the Up state gamma and high gamma power was reduced. (*C)* LFPs and spectrograms of LFP recorded in Cg and DP during baseline conditions 70 minutes after A412997 injection.The VSMP had returned and was accompanied by strong spindle activity. This biphasic effect was observed in two out of five experiments.

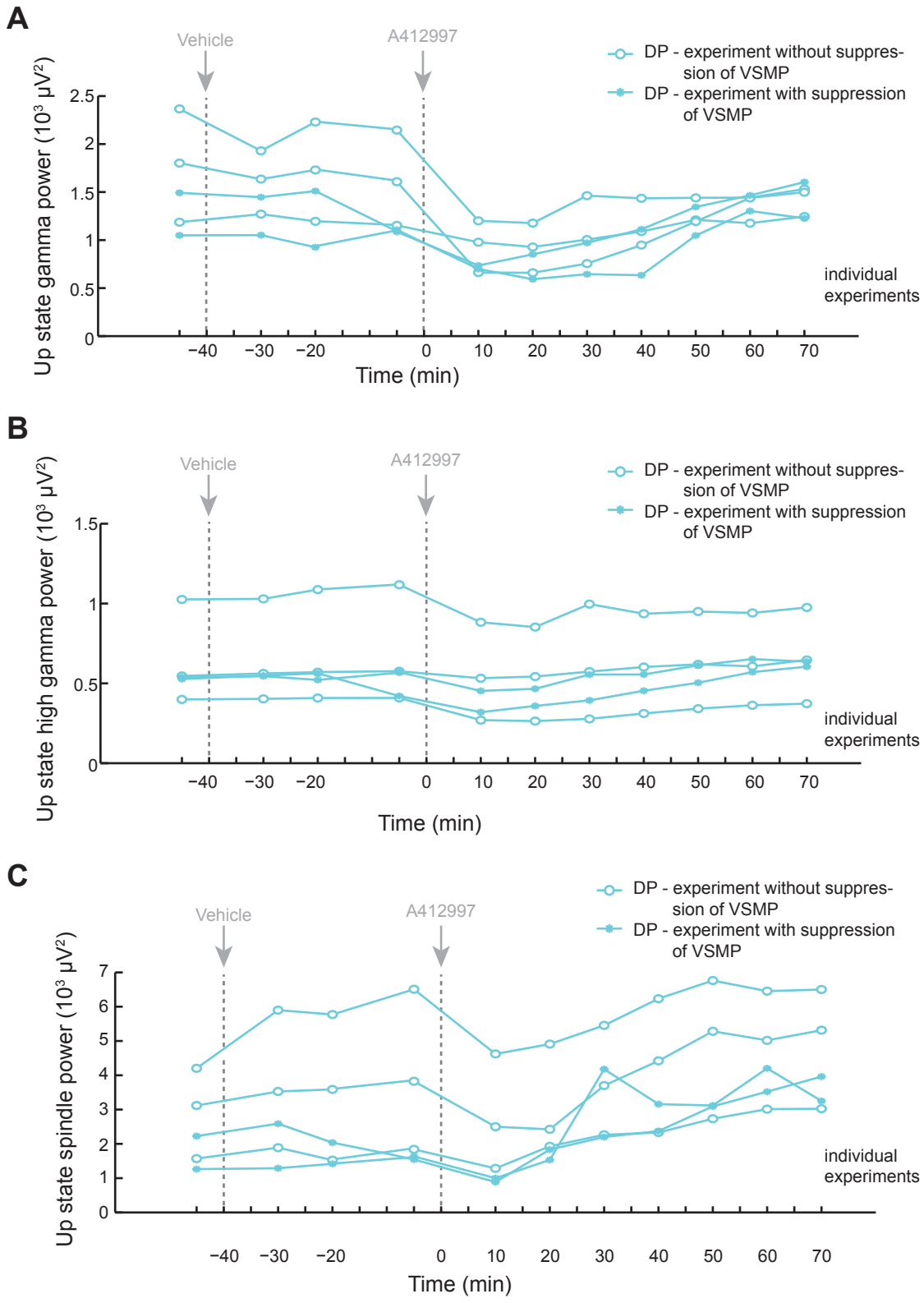

Figure 5.15. Effect of the D_4R agonist A412997 on Up state gamma, high gamma and spindle power in the DP. *(A)* Effect of the D_4R agonist A412997 on Up state gamma power in the DP. *(B)* Effect of the D_4R agonist A412997 on Up state high gamma power in the DP. *(C)* Effect of the D_4R agonist A412997 on Up state spindle power in the DP. Data from all five experiments is shown, indicating experiments with and without suppression of the VSMP.

5.5 Discussion

5.5.1 *Summary of results*

Here I summarise the results of this section. As a quantitative overview, I also show a summary of my results in Figure 5.16 (except the delayed A412997 effect on Up state spindle power).

- The UDS parameters were not stable over time, hence effects of the dopamine-modulating drugs could not be reliably assessed.
- The parameters of the nested fast oscillations were stable over several hours, hence effects of the dopamine-modulating drugs could be assessed.
- Amphetamine markedly decreased Up state gamma power as well as Up state spindle power within 20 minutes, but did not affect high gamma power.
- The $D_{1.5}R$ agonist SKF38393 decreased Up state gamma power as well as Up state high gamma power within 20 minutes, but did not affect spindle power.
- The D_4R agonist A412997 decreased Up state gamma power as well as Up state high gamma power within 20 minutes. A412996 additionally had a delayed effect, in that it increased spindle power after 50 minutes (the increase was significant from 50-70 minutes).

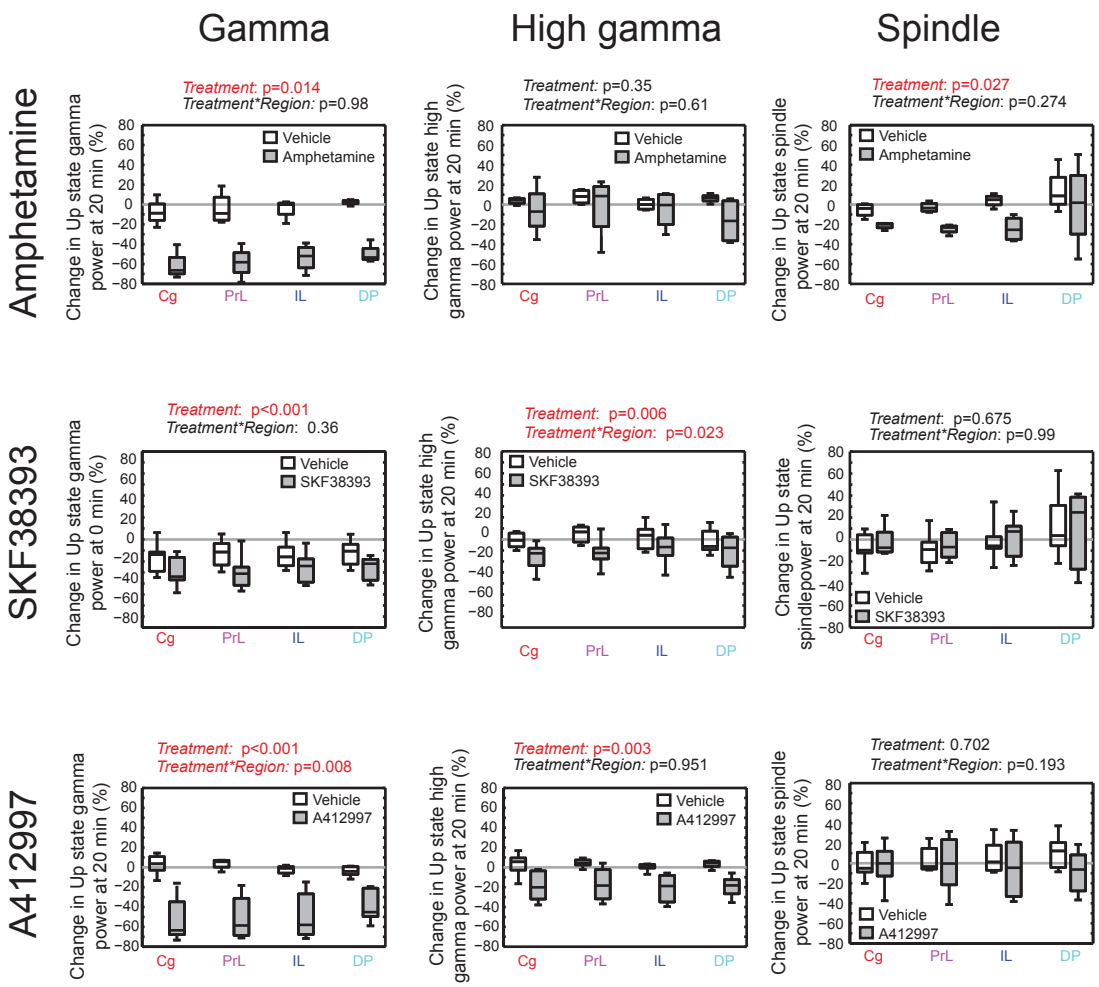

Figure 5.16. Summary of the results regarding application of dopaminergic agents. Boxplots showing percentage change following 20 minutes of vehicle and drug (within-animal control) for amphetamine (n=4), the $D_{1,5}$R agonist SKF38393 (n=7), and the D_4R agonist A412997 (n=5), for the four mPFC subregions.

The results in this chapter were obtained from urethane-anaesthetised rats and drugs were applied systemically. These methodological caveats will be discussed in detail in Chapter 6.

5.5.2 *Long-term stability of UDS parameters during urethane anaesthesia*

When recording mPFC UDS activity for the duration of three hours, the Up state frequency consistently increases from hour 1 to hour 3, whereas the Down state duration consistently decreased from hour 1 to hour 3, making the interpretation of any results difficult. The change observed for both parameters was gradual rather than fluctuating, which matches the constant decline of urethane concentration in the blood (Nomeir et al., 1989; Sotomayor and Collins, 1990). There was a trend for amphetamine to increase UDS frequency and decrease Down state length within 10 minutes after injection, which would be in line with the fact that dopamine-enhancing drugs have can speed up emergence from general anaesthesia (Benveniste and Volkow, 2013). This trend could only be further investigated by testing against a time-control group.

5.5.3 *Effects of dopaminergic agents on Up state gamma oscillations in the mPFC*

My results suggest that amphetamine, the $D_{1,5}$R agonist SKF38393, and the D_4R agonist A412997, all decrease Up state gamma power in urethane anaesthetised rats.

Amphetamine and $D_{1,5}$ receptor activation decreased Up state gamma oscillations

In line with the amphetamine-induced decrease in Up state gamma observed in the mPFC in my experiments, *in vitro* experiments in hippocampal sliced have revealed a reduction of gamma power following dopamine application (Weiss et al., 2003; Wójtowicz et al., 2009). In line with the $D_{1,5}$R agonist-induced decrease in Up state gamma observed in the mPFC in my experiments, a reduction of gamma power after D_1R activation has also been reported in the hippocampus (Weiss et al., 2003). Another study, however, failed to confirm the effect of dopamine or D_1R activation on gamma oscillations (Andersson et al., 2012b).

One could speculate that these differences in dopamine/D_1R-agonist effects are related to the differences in the pharmacological agents used for the induction of oscillations in slice preparations. These agents were either kainate or carbachol, and interestingly kainate alters glutamatergic function and glutamate-dopamine interactions

have been observed (Tseng, 2004). Surprisingly, however, another *in vitro* study found that dopamine did decrease hippocampal oscillations induced by bath application of kainate (Wójtowicz et al., 2009). Both studies investigated effects in CA3 of the hippocampus, and the kainate dose to induce oscillations is comparable between the two studies. (Wójtowicz et al., 2009) found a 20%-70% reduction of gamma power after application of 30 μM-100 μM of dopamine. (Andersson et al., 2012b), however, found no effect at 10μM and 200 μM of dopamine. Hence, it is not clear what causes these differences.

Amphetamine and D_4 receptor activation decreased Up state gamma oscillations – comparison with PFC in vivo study

In contrast to my findings, previous studies have shown that systemic injection of amphetamine or direct D_4R activation, increase gamma oscillations in the prefrontal cortex in *awake* rats (Wood et al., 2012; Kocsis et al., 2013). Kocsis and Colleagues (2013) used the same D_4R agonist, A412997, at the same dose (10 mg/kg) as I have reported in this thesis. Hence, this difference is likely due to the difference between anaesthesia and wakefulness, and indeed it has previously been reported that dopaminergic effects can be the opposite under anaesthesia from those seen during wakefulness (Seamans and Yang, 2004).

Seamans and Yang (2004) have performed a meta-analysis of rat and monkey studies of the effects of dopamine on PFC firing rates and came to the conclusion that background activity determines the dopamine response, with dopamine having inhibitory effects on PFC firing rates under anaesthesia, but excitatory effects on PFC firing rates in awake rats and monkeys (Seamans and Yang, 2004). Seamans and Yang (2004) suggest that these opposing effects occur because dopamine modulates both inhibitory $GABA_A$-mediated responses as well as NMDA receptor-mediated responses. Specifically, they suggest that, in *in vitro* slice preparations, as well as in anaesthetized animals, low-level background NMDA receptor activity leads to inhibitory responses outweighing excitatory responses, whereas in awake animals, high-level background NMDA receptor activity means that dopamine exerts a strong excitatory effect (Seamans and Yang, 2004). It is plausible that such reduced background NMDA receptor activity under urethane anaesthesia (Hara and Harris, 2002) is the cause of the contrast between my findings, and those previously reported in awake rodents. Results obtained under urethane anaesthesia might thus be more comparable to *in vitro* results.

The difference between the effect observed in (Kocsis et al., 2013) and my study could also be due to difference between awake gamma activity and nested gamma activity as it occurs during SWA. Results obtained in anaesthetised animals might be more applicable to natural SWS than to awake state.

D_4 receptor activation decreased Up state gamma oscillations – comparison with hippocampus in vitro study

Again in contrast to my findings of a D_4R agonist induced decrease in mPFC Up state gamma oscillations, a hippocampal slice study (Andersson et al., 2012a) has found that D_4R activation induces an increase in kainate-induced gamma oscillation. There are a number of possible explanations for the differences seen between hippocampal *in vitro* studies and my PFC *in vivo* findings.

Firstly, it is important to note that the kainate-induced hippocampal gamma oscillations are persistent, whereas the periods of gamma activity investigated in this thesis are transient. It is also worth noting that the frequency band definition of the gamma band used by (Andersson et al., 2012b) (20-50 Hz and therefore in the beta/low-gamma range) differs greatly from the definition used by me in this thesis (30-80 Hz, which is a more typical consensus definition in the literature).

Given the opposite effects of D_4R activation seen in the two areas (mPFC and hippocampus), the mechanistic basis of these effects must clearly be different. (Andersson et al., 2012a) found that their D_4R agonist-induced increase in gamma oscillations was due to increased coupling of fast-spiking interneuron activity with the ongoing gamma rhythm, and could be blocked by the selective NMDA receptor antagonist *(2R)*-amino-5-phosphonovaleric acid (AP5). They therefore suggest a role for NMDA receptors on fast-spiking interneurons in this response (although this is not directly proven).

In contrast, in the PFC, D_4R activation has been shown to alter glutamate and GABA signalling: Specifically, D_4R activation can decrease surface clusters of AMPA receptors on inhibitory GABAergic interneurons, leading to a decrease in glutamate transmission (Yuen and Yan, 2009). D_4R activation has also been shown to decrease $GABA_A$ signaling in PFC pyramidal cells (Wang et al., 2002). In addition D_4R activation can lead to internalisation of NMDA receptors (Wang et al., 2003).

As D_1R activation has the opposite effect in that it increases expression of AMPA receptors (Sun, 2005) and NMDA receptors (Gao and Wolf, 2008), the observed decrease in gamma after D_1R activation and D_4R activation are unlikely modulated by these receptors, as opposing effects on gamma would be expected with D_1R and D_4R activation.

Given the above, $GABA_A$ receptors seem to be a likely candidate to be involved in the mechanisms of dopaminergic modulation of Up state gamma described in this chapter. In the PFC, D_4R activation decreases post-synaptic $GABA_A$ receptor-mediated currents in pyramidal neurons. D_1R activation inhibits interneuron-interneuron $GABA_A$ receptor-mediated transmission (Towers and Hestrin, 2008) and pyramidal cell IPSPs (Gonzalez-Islas and Hablitz, 2001). Gamma oscillations are generated by synchronous firing of inhibitory interneurons, which impose well-timed inhibition on large numbers of pyramidal cells. Hence disruption of interneuron-interneuron communication as well as decreased responses of pyramidal cells to interneuron-mediated inhibition could disrupt gamma oscillations and result in a decreased power of these oscillations.

To summarise, the literature suggests that the increase in gamma activity observed after D_4R activation in hippocampal slices seems likely to be NMDAR-mediated, whereas the decrease in Up state gamma observed in this thesis in the PFC may be $GABA_A$ receptor-mediated. Indeed, (Andersson et al., 2012a) show that in the hippocampus, D_4R activation does not affect GABAergic currents in hippocampal pyramidal cells (Andersson et al., 2012b).

It is finally worth noting that there is some controversy regarding D_4R expression. In some studies, D_4R expression is suggested to be similar in PFC and hippocampus (Defagot et al., 2003; Andersson et al., 2012b), although another study finds PFC expression to be higher (Ariano et al., 1997), and in both regions, D_4 receptors are located in pyramidal cells and interneurons (Mrzljak et al., 1996), with stronger expression in interneurons (Mrzljak et al., 1996). (Andersson et al., 2012b) find D_4 receptors to be mainly expressed in hippocampal interneurons, and very low in pyramidal cells. And yet another study finds the D_4 receptor to be expressed in the prefrontal cortex, but not in the hippocampus (Noaín et al., 2006).

To conclude, whereas the $D_{1,5}$R agonist-induced decrease in Up state gamma power observed in the mPFC in this thesis is in agreement with several hippocampal slice studies, the D_4 receptor agonist-induced decrease in Up state gamma power in the mPFC is in contrast with another *in vivo* study in the PFC, as well as an *in vitro* study in the hippocampus. As discussed, these discrepancies are likely due to brain state (anaesthesia versus awake) and regional differences in D_4R modulation (PFC versus hippocampus).

5.5.4 *Effect of dopaminergic agents on Up state high gamma oscillations in the mPFC*

Both the $D_{1,5}$R agonist and the D_4R agonist moderately decreased high gamma power. Amphetamine, however, did not affect high gamma power.

Given that amphetamine leads to dopamine release and thus, a non-specific receptor activation, which will also activate $D_{2,3}$ receptors, the effect of the amphetamine-induced activation of $D_{1,5}$ and D_4 receptors might be counteracted by simultaneous $D_{2,3}$ receptor activation. Indeed, in mPFC cells, $D_{1,5}$R and $D_{2,3}$R activation have been reported to have opposing effects on $GABA_A$-mediated IPSCs (Trantham-Davidson et al., 2004) as well as NMDA currents (Zheng et al., 1999). Hence, a co-activation of $D_{1,5}$ receptors and $D_{2,3}$ receptors could possibly lead to a masking of any receptor-specific effects. Masking of a D_4 receptor-mediated effect due to background of $D_{1,5}$R activity has been observed for hippocampal gamma *in vitro* (Andersson et al., 2012b).

As amphetamine increases not only dopamine, but also noradrenaline levels, noradrenaline could also counter-act the effects of dopamine $D_{1,5}$R and D_4R activation and mask an effect.

Another possible explanation for the lack of an effect with amphetamine involves gap junction coupling. As discussed in section 1.4.7, gap junctions are likely involved in the mechanisms of generation of high gamma oscillations and the results might also be explained by dopaminergic modulation of gap junction coupling. Non-selective stimulation of dopamine receptors by exogenous dopamine seems not to affect gap junction coupling, whereas D_1R and D_4R activation decreases gap junction coupling (Furth et al., 2013). This could explain why SKF38393 and A412997 decrease high gamma oscillations, but amphetamine does not.

5.5.5 *Effect of dopaminergic agents on Up state spindle oscillations in the mPFC*

Of the dopaminergic agents, only amphetamine significantly affected mean Up state spindle power after 20 minutes, exerting an inhibitory effect. The timing of the first spindle peak was retained in Cg and IL. SKF3839, despite not changing the mean Up state spindle power, had some effects on the width of the spindle peak, and on the timing of spindles relative to the normalized UDS cycle.

The D_4R agonist A412997 changed neither the mean Up state spindle power, nor the timing of the two spindle peaks relative to the UDS cycle. Interestingly, the D_4R agonist lead to a late increase in Up state spindle power with a long latency of 50 minutes after injection. This effect lasted at least up to 70 minutes after the injection. This increased spindle power was still well-timed with respect to the UDS cycle, indicating that it does not constitute aberrant activity.

In awake rats, systemic block of D_2-like receptors with raclopride or haloperidol (which also has a high affinity for the D_4R), increases power of high voltage spindles (5-13 Hz) in globus pallidus and motor cortex in freely moving rats (Yang et al., 2013). However, differences between this study and my study might be ascribed to differences between awake behaving and anaesthetized rats. Specifically, spindles observed during SWA under urethane anaesthesia might be very different to high voltage spindles observed in awake rats. In addition, it is likely that D_2R activation might play a part in the spindle increase observed by (Yang et al., 2013). The D_4R agonist we used (A412997) is highly selective for D_4 receptors (binding affinity K_i=12.1 for D_4 receptors), and has negligible affinity for other known receptors (K_i>1000nM). A third difference is the brain area, these spindles were observed in globus pallidus and motor cortex, whereas I recorded in the prefrontal cortex.

In humans, the D_1R *antagonist* NNC-687 has been shown to increase spindle density and spindle burst duration (Eder et al., 2003) during NREM sleep, suggesting a facilitatory role of low-level D_1R activation for spindles. This indicates that either active D_1R activation inhibits spindle activity, or that block of D_1 receptors unmasks the facilitating effect of dopamine on spindles of another dopamine receptor, possibly the D_4R. Unmasking of a D_4 receptor effect by blocking D_1 receptors has been observed previously (Andersson et al., 2012b). However, there is no evidence from the original study that this is the case. Both of these possibilities would be in agreement with my

results, as 1.) SKF38393, while it did not change the mean Up state spindle power, seemed to alter the spindle timing, and 2.) D_4R activation with A412997 increased spindle power (with a long latency).

Possible mechanisms for D_4 receptor mediated late increase in spindle power

The thalamic reticular nucleus (TRN) can generate cortical spindles (Halassa et al., 2011) and expresses dopamine D_4 receptors (Mrzljak et al., 1996). Dopamine D_4R activation suppresses TRN IPSCs induced by globus pallidus stimulation *in vitro* (Govindaiah et al., 2010). This might result in disinhibition of TRN neurons, which, through its effects on thalamocortical neurons, could increase cortical spindle activity. (Govindaiah et al., 2010)

As described previously, D_4R activation elevates hippocampal gamma *in vitro*, possibly via activation of NMDA receptors on inhibitory interneurons (Andersson et al., 2012a). PV^+ interneurons might also play a role in the manifestation of cortical spindles, as a possible coupling of PV^+ basket cell firing to Up state spindles has been observed (Massi et al., 2012). Hence, another possibility is that the late increase in spindle power after D_4R agonist application might be mediated by NMDA receptors on GABAergic interneurons.

In my results, I observed a phenomenon of increased Up state spindle power at 50 minutes after the administration of the D_4R agonist A412997.

Dopamine can have long-lasting effects (up to hours after release), even after it has been washed out. For D_1 receptor activation it has been shown that these long-lasting effects may be mediated by Ca^{2+}-dependent kinases and phosphatases, which are themselves activated by Ca^{2+} influx via NMDA receptors and voltage-dependent Ca^{2+} channels (Seamans and Yang, 2004).

A recent study finds biphasic, long-lasting effects of the D_4R agonist PD168077 on PV^+ interneurons *in vitro* (Zhong and Yan, 2014). From five to eleven minutes after PD168007 application, PV^+ interneuron firing rate was strongly increased, and then significantly decreased, remaining below baseline at least until 30 minutes after drug application. This effect might be related to my results, as D_4Rs are predominantly expressed on PV^+ interneurons in the mPFC (section 1.5.3), fast spiking interneurons are involved in gamma rhythm generation (section 1.4.7).

In summary, long-lasting dopamine effects have previously been observed, but to my knowledge, I am the first to show a 50-minutes delayed increase in Up state spindle power after D_4R activation.

5.5.6 *Susceptibility of spindle temporal pattern to disruption by dopaminergic agents*

In my experiments, gamma and high gamma power seemed to retain their temporal pattern during the Down-Up state cycle, even when the mean power varied. However, spindle activity seemed to be more susceptible to changes in its fine temporal pattern during the Up state. Specifically, it was disrupted in the ventral sub-regions of the mPFC in response to amphetamine, and in all sub-regions of the mPFC in response to SKF38393. So far this is just an observation. Further analysis of the phase locking of the spindle peak to the UDS cycle would shed light on these possible changes.

5.5.7 *Sub-regional differences*

Only very small differences were found in the dopamine-mediated responses between the sub-regions. The effect seen in my experiments had the same direction of effect across the different sub-regions, except in the case of SKF38393 on spindle power, where the median change in Cg and PrL was negative, but the median change in IL and DP was positive.

A statistically significant difference between the sub-regions was found for the decrease in gamma power induced by A412997 application and the decrease in high gamma power induced by SKF38393 application. However, no post-hoc test was significant, so which region was different could not be identified. Comparing the percentage changes in high gamma after SKF38393 application for the four sub-regions, there was only a small difference in median change. However, the percentage change in gamma power induced by the D_4R agonist A412997 seemed to be less strong in the DP region compared to the other three mPFC sub-regions. This seems surprising, given that the ventral mPFC shows stronger dopaminergic innervation, and a recent study showed an increasing density of tyrosine hydroxylase positive fibres from dorsal to ventral mPFC (Cg<PrL<IL) (Zhang et al., 2010). There is also an indication of higher D_4R expression in the ventral mPFC (Wedzony et al., 2000). Hence, the smaller percentage change in gamma power in the DP region compared to the rest of the mPFC after D_4R

agonist application might not be due to lower dopamine innervation, or lower receptor expression, but rather related to the fact that baseline gamma activity was already very low in the DP.

5.6 Conclusions and future research

In this chapter, I have revealed previously unreported dopaminergic modulation of Up state-nested gamma, high gamma and spindle oscillations during mPFC SWA.

The three dopaminergic agents used had distinct effects on spindle activity, either affecting mean spindle power or the timing of spindle oscillations, with different time courses. Both the magnitude of spindle activity as well as the timing are likely to be crucial for memory processes during sleep. Hence, studies in chronically implanted rats, which perform a memory task and then receive dopaminergic stimulation in a subsequent sleep period in the attempt to enhance spindle power or disrupt spindle timing, would shed light on whether dopamine plays a role in sleep-dependent memory consolidation via its action on Up state fast oscillations.

The effect of the dopaminergic agents on spindle timing with respect to the UDS cycle should be further investigated by applying different analysis techniques to the obtained data and investigate phase-locking of spindle activity to the slow oscillation or the Down-Up state cycle comparing phase-locking before and after application of the dopaminergic agents. Interestingly, it seems that spindle activity timing (compared to gamma and high gamma) with respect to the UDS cycle seems to be more susceptible to disruption by dopaminergic agents than gamma and high gamma timing. Possibly this is due to the fact that spindles are generated in the thalamus, whereas gamma and high gamma activity are generated in local networks.

Future work could localise the observed effect, by applying $D_{1,5}R$ agonists directly into the mPFC and D_4R agonists into the mPFC and to the TRN (for example by using iontophoresis) to localise the observed effects.

Chapter 6. General discussion

SWA is observed during SWS and anaesthesia in many species, and consists of a slow (<1 Hz) rhythm, that is characterised by long-range synchrony (Volgushev et al., 2006; Sheroziya and Timofeev, 2014) and is associated with faster (>6 Hz) rhythms on the Up state that are more locally synchronised (Le Van Quyen et al., 2010; Nir et al., 2011). The physiological role of these oscillations is debated, although many human studies have found that aspects of learning and memory are associated with SWA (Huber et al., 2004; Marshall et al., 2006), including spindle (Gais et al., 2002; Mölle et al., 2011) and gamma frequency (Mölle et al., 2004) rhythms.

The mPFC, supported by the hippocampus, is implicated in learning and memory (Euston et al., 2012). The mPFC and hippocampus are synchronously activated during SWA, displaying fast oscillations at different frequencies simultaneously (Siapas and Wilson, 1998; Sirota et al., 2003; Mölle et al., 2006), which have been associated with memory replay (Peyrache et al., 2009; Johnson et al., 2010). Hippocampal fast sleep rhythms have been extensively studied. However, a detailed study of SWA and these nested fast oscillations in the mPFC, along with consideration of its heterogeneous structure, has not been undertaken.

Dopamine is important for PFC function during wakefulness, and dopamine has been shown to modulate fast oscillations that are associated with a variety of cognitive functions. Dopamine is also implicated in sleep. However, if dopamine is involved in sleep stage regulation and whether dopamine modulates slow and nested fast mPFC rhythms during sleep is unknown. I have attempted to address these issues in my experiments.

In this thesis, SWA induced by urethane anaesthesia in rats was used as a model of sleep SWA. The aim of this thesis was to investigate SWA with respect to the mPFC sub-regions (Chapter 3); to investigate if the VTA plays a role in the induction of REM sleep-like fast forebrain activity observed under urethane anaesthesia (Chapter 4); and finally, to investigate whether dopamine modulates mPFC fast rhythms during the slow wave Up state (Chapter 5).

6.1 Sub-regional and laminar characteristics of mPFC SWA (Chapter 3)

The rat mPFC is a brain region consisting of four sub-regions with different laminar structure, connectivity, and function; the strongest regional differences being between dorsal (Cg, PrL) versus ventral sub-regions (IL, DP) (Heidbreder and Groenewegen, 2003). However, many studies do not acknowledge this heterogeneity and do not even identify the mPFC sub-region they investigated. Hence, I first set out to investigate if the mPFC sub-regions differ in the properties of the slow and fast oscillations during SWA.

In Chapter 3, I characterised the mPFC with regard to sub-regional and laminar differences in the SWA observed during urethane anaesthesia. As expected, SWA occurred with high synchrony in the entire mPFC bilaterally. SWA amplitude in layer III was consistent across the entire dorso-ventral axis, however differences along the dorsal-to-ventral axis were observed in layers I/II and III-VI. Interestingly, strong dorsal-to-ventral differences were observed in Up-state associated gamma, high gamma, and spindle power. Laminar differences in oscillation power were also observed for all fast frequency bands.

In addition, a very slow modulation of LFP power (VSMP) with a cycle length of several minutes was observed in the mPFC. This VSMP could be observed under urethane anaesthesia during the REM-like state as well as during SWA and was most evident in the ventral mPFC.

6.1.1 *Dorsal-to-ventral versus sub-regional division of mPFC?*

I have already discussed the regional differences in gamma, high gamma and spindle oscillations with respect to the existing literature on differences in laminar structure, cell types and connectivity. My results add to the body of evidence on the heterogeneity of the mPFC, supporting both the sub-regional division as well as the dorsal-to-ventral division. The gradual change in gamma power, with gamma power decreasing in the dorsal-to-ventral direction, indicates differences between the four sub-regions. In addition, an abrupt change in high gamma power at the border between dorsal and ventral mPFC supports the hypothesis that the main mPFC distinction is between the dorsal and the ventral mPFC.

6.1.2 *Do nested fast oscillations support communication with the hippocampus?*

As discussed before, fast oscillations during the SWA Up state are thought to be important for memory consolidation, as they might support communication between distant brain regions. Many studies have reported that coordinated activity has been observed between mPFC and hippocampus.

My findings show that the oscillatory power for all investigated frequency bands was higher in dorsal mPFC compared to ventral mPFC, with the strongest differences for gamma and high gamma activity. This seems surprising, as the ventral mPFC is highly connected with the hippocampus, whereas the dorsal mPFC has connections to the dorsal striatum and sensory-motor areas. Possibly, gamma and high gamma oscillations in mPFC are not related to communication with the hippocampus, but related to communication with other cortical areas the mPFC is connected to.

6.1.3 *How applicable are these results obtained in rats under urethane anaesthesia to SWA in humans during natural sleep?*

Although the basic cell types and neurotransmitters are similar between rat and human, one might question the comparability between these two species. Obvious differences are the larger size of the human brain, and the cortical folding, which is absent in rats. Although rats can perform some PFC-dependent tasks in similar ways to humans, human cognitive performance far surpasses the cognitive abilities of rats. In addition, a direct comparison between rat and human is made difficult because of the difficulty establishing homologies between regions. The mPFC is considered the equivalent of the human dorsolateral PFC, but also shares function with the medial PFC in humans. Another difference is that in contrast to human PFC areas, the rat mPFC lacks layer IV, which is the layer receiving thalamic inputs. Hence, whereas in human PFC thalamic inputs arrive in layer IV, in rat mPFC, thalamic inputs arrive mostly in layer III. As the thalamus is crucially involved in the generation of SWA, this difference could hinder the applicability of data obtained in rat mPFC to human PFC. However, there are several key similarities that make the use of rodent models useful to understand human SWA.

In rodents and cats, SWA under urethane anaesthesia occurs at frequencies of 0.3-0.4 Hz, which is slower than that seen under ketamine anaesthesia, where SWA occurs

at 0.6-1 Hz (see (Steriade et al., 1993d) for a direct comparison in cats). In naturally sleeping humans, SWA has been shown to occur at a mean frequency of 0.3 Hz and a range 0.2-0.3 Hz (Csercsa et al., 2010). Hence, the frequency of SWA during SWS in humans is the same as the frequency of SWA observed in anaesthetised cats (Steriade et al., 1993d) and the frequency seen in urethane-anaesthetised rats in this thesis, suggesting similarity between urethane-generated SWA in animals with human SWA during natural sleep.

In addition, both human SWA during natural sleep, and rat SWA during urethane anaesthesia are characterised by fast oscillatory activity that occurs nested within the SWA Up state. Many studies recording EEG and LFP in human cortex have now reported that high-frequency activity in the spindle band (Fell et al., 2002) as well as in the gamma and high gamma bands (Csercsa et al., 2010; Le Van Quyen et al., 2010; Valderrama et al., 2012) occurs on the slow wave Up state (surface-positive, depth-negative state). Csercsa and colleagues (2010) find an Up state-associated broadband increase in activity, which is consistent with the animal literature, whereas Valderrama and colleagues (2012) as well as Le Van Quyen and colleagues (2010) find events with distinct peaks either in the low gamma (defined as 30-50 Hz or 40-80 Hz) or high gamma (defined as 60-120 Hz or 80-120 Hz) bands. Interestingly, although occurring simultaneously most of the times, low and high gamma peaks can occur independently (Le Van Quyen et al., 2010), on different Up states, suggesting that different mechanisms might be involved in the generation of gamma and high gamma oscillations. The sub-regional comparison of fast oscillations, performed in Chapter 3, indicates that gamma power decreased gradually in the dorsal to ventral direction in the mPFC, whereas high gamma power was greater in the dorsal mPFC and lower in the ventral mPFC, with an abrupt transition at the border. The different spatial patterns of gamma and high gamma power in the mPFC support the hypothesis that different mechanisms underlie the generation of gamma and high gamma frequency activity.

As already discussed in 3.4.3 two kinds of spindles, differing in frequency and location in the cortex, occur in sequence in humans. Fast parietal spindles occur at the beginning of the Up state and slow frontal spindles occur at the end of the Up state (Mölle et al., 2011). It has been suggested that the early spindles might be related to cortico-hippocampal information transfer, whereas the late spindles might be related to cortico-cortical information transfer (Mölle et al., 2011). Within mPFC, I have

discovered a dorsal-to-ventral distinction in the timing of spindles relative to the slow wave Up state. In the dorsal mPFC, spindles occur at the beginning of the Up state, whereas in the ventral mPFC, spindles occur at then end of the Up state. The fact that the early spindles occur in the dorsal mPFC, which is connected to the striatum and sensorimotor areas, whereas the late spindles occur in the ventral mPFC, which is strongly connected to hippocampus and amygdala, suggests a possible role for early mPFC spindles in cortico-cortical processing, and a role for late mPFC spindles in cortico-hippocampal processing. This would, however, be the opposite association to the one that has been suggested for human parietal and frontal spindles. Again, this highlights the differences between dorsal and ventral mPFC.

With respect to laminar differences, I found that the amplitude of the slow oscillation, as well as the power of nested fast oscillations, were higher in deep layers (V-VI) compared to superficial layers (I-II). Hence, my results also further support the finding that in anaesthetised animals SWA is generated in the deep cortical layers. However, SWA and nested fast activity during human SWS is likely generated in superficial layers (Csercsa et al., 2010). It is not clear if these differences are due to species-differences, possibly related to the lack of layer IV, or if they are due to differences between anaesthesia and natural sleep.

To conclude, despite obvious differences between rat and human brain, sleep is highly conserved across mammals, and the similarity between rodent and human SWA might indicate that similar processes occur during sleep. Sleep-dependent memory consolidation might also be based on similar mechanisms in rats and humans, supporting the case for further study of SWA in rats.

6.2 Effects of VTA stimulation on mPFC SWA (Chapter 4)

VTA dopamine neuron activity (Dahan et al., 2006) as well as PFC dopamine levels (Léna et al., 2005) increase during REM sleep compared to SWS. However, whether dopamine or the VTA play a causal role in generation of the REM-associated fast forebrain activity is unclear. In Chapter 4, I addressed the question of whether VTA stimulation could induce a transition to a REM-like forebrain activity state. I examined this question by investigating the effect of electrical stimulation of the VTA on mPFC SWA. I found that electrical stimulation of the VTA can indeed induce a transition to a

LAF rhythm in the mPFC. This rhythm was similar to the spontaneous REM-like state under urethane anaesthesia, in that it contained delta-and theta-frequency activity. The transition to the LAF rhythm occurred with a latency of several seconds, which is similar to the time interval between increased VTA dopamine neuron burst firing and the onset of REM sleep in naturally sleeping rats (Dahan et al., 2006). My results indicate a possible $D_{1,5}$ receptor involvement in this transition to the LAF rhyhm, but not a D_2 receptor involvement.

As presumed VTA dopamine neurons (identified by their electrophysiological properties) fire time-locked to the cortical Down state (Gao et al., 2007), they might play a role in SWA. Note, that the VTA LFP, however, is in phase with the PFC Up state (Gao et al., 2007), indicating that the VTA LFP may be reflecting mainly activity of non-dopaminergic neurons. Using a burst pattern stimulation, with bursts occurring at a frequency near the SWA band (1 Hz), electrical stimulation of the VTA could entrain Down states. Again, this effect occurred with a latency of several seconds after stimulation onset.

The results obtained in Chapter 4 suggest firstly, a possible role for the VTA in the generation of fast forebrain activity as observed during REM sleep, and secondly, a possible involvement of the VTA in Down state generation. These two points are discussed in more detail in the following sections.

6.2.1 *Does the VTA have a role in REM sleep?*

In rats, increased bursting of VTA neurons during REM sleep (Dahan et al., 2006) and increased dopamine levels in mPFC and nucleus accumbens during REM sleep (Léna et al., 2005) suggest a role of the VTA in REM sleep. I have shown that electrical stimulation of the VTA can indeed induce a REM-like activation pattern in the mPFC under urethane anaesthesia.

However, the VTA is not thought to be an *originator* of REM sleep transitions or the associated rhythms in hippocampus and cortex. Several mesopontine nuclei that are active during REM sleep project to the VTA and thus might trigger activation of neurons in the VTA. Likely candidates for the initiation of VTA neuronal burst firing during REM sleep are the PPN and laterodorsal tegmental nuclei (LDT). Neurons in these areas increase their activity one minute before the REM sleep-associated EEG

synchronisation in cats (Steriade et al., 1990; Boucetta and Jones, 2009). Dahan and colleagues (2006) suggested the PPN as the likely initiator of VTA neuron bursting during REM sleep and suggested a role of the PPN-VTA-septum-hippocampus pathway in modulating hippocampal theta. This is likely to be mediated by $D_{1,5}$ receptors in the septum, as activation of these receptors in the septum increases theta in the hippocampus (Miura et al., 1987; Fitch, 2006). Note, however, that there are also direct projections from the VTA to the hippocampus (Scatton et al., 1980).

My results indicate that during REM sleep, the PPN–VTA pathway might not only modulate hippocampal theta via the mesolimbic dopamine system, but also induce a LAF rhythm in the mPFC via the mesocortical system, and this might also be mediated by $D_{1,5}$ receptors.

The PPN-induced activation of the VTA might be mediated by glutamate or acetylcholine, as glutamate-immunoreactive (Parent et al., 1999), as well as choline acetyl transferase (ChAT)-immunoreactive fibres (Kasa, 1986) innervate VTA and substantia nigra. Iontophoretic application of NMDA (Chergui et al., 1993), or a muscarinic agonist (Gronier and Rasmussen, 1998) into the VTA induces burst firing in midbrain dopamine neurons. Iontophoretic application of a nicotinic agonist increases VTA dopamine neuron firing rate, also through an interaction with muscarinic receptors (Gronier and Rasmussen, 1998). Hence, cholinergic and non-cholinergic PPN neurons could induce VTA burst firing. Indeed, an increase in firing during the spontaneous REM-like state under anaesthesia, as well as during the activated state induced by sensory stimulation has been shown to occur in immunohistochemically identified cholinergic PPN neurons in rats (Mena-Segovia et al., 2008). However, non-cholinergic neurons can also increase their firing at transitions from SWA to an induced activated state under anaesthesia (Roš et al., 2010).

The pathways via which PPN-induced VTA bursting could induce hippocampal theta and PFC activation are shown in Figure 6.1. Note that the projections to PFC and septum originate from different neurons in the VTA (Deniau et al., 1980; Fallon, 1981).

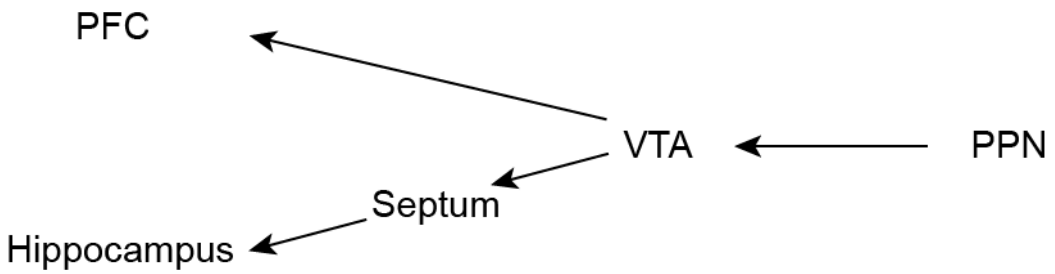

Figure 6.1. Pathways for hippocampal theta induction and mPFC LAF rhythm induction during REM sleep.

Two models for REM sleep generation are the 'reciprocal interaction model' and the 'flip-flop model' of REM generation.

According to the 'reciprocal interaction model', REM sleep is generated by interactions between the LDT/PPN and the reticular formation (Brown et al., 2012), and hippocampal theta and cortical activation are induced through acetylcholine release from the septum and basal forebrain.

However, according to the 'flip-flop model' of REM generation, although the PPN is established as a REM 'modulator', neither VTA nor PPN are part of the 'flip-flop switch' of REM generation (Lu et al., 2006; Fuller et al., 2007). According to this model, REM-NREM switching is thought to rely on mutual inhibitory interactions of "REM-on" areas (namely sublaterodorsal nucleus [SLD], precoeruleus [PC] and parabrachial nucleus [PB]) and "REM-off" areas (namely venterolateral periaqueductal grey [vlPAG] and lateral pontine tegmentum [LPT]) and an inhibitory influence from the extended part of the VLPO. According to this model, hippocampal theta and cortical activation are induced through excitatory connections from the PC/PB to the septum and the basal forebrain (Fuller et al., 2007).

My results indicate that in addition to acetylcholine released from septum and basal forebrain, dopamine and $D_{1,5}$ receptors might, in addition to playing a role in hippocampal theta induction, also play a role in the cortical LAF rhythms associated with REM.

6.2.2 *Possible role for the VTA in Down state synchrony*

It is widely accepted that the cortical Up state is terminated by the inability of the network to sustain activity, rather than an external influence. However, this does not explain the high degree of synchrony of the Down state onset. Down state onset amongst cortical cells is even more synchronized than the Up state onset (Volgushev et

al., 2006; Sheroziya and Timofeev, 2014). It has been suggested that cortical recruitment of the thalamus might play a role in this tight synchrony of the Down state (Volgushev et al., 2006). In the light of my findings, I will discuss a possible role for the VTA in synchronizing Down state onset.

In Chapter 4 I have shown that VTA stimulation using a burst pattern, with an inter-burst-interval of 1 s can entrain Down states in the mPFC. In these experiments, I did not attempt to block the Down state transition driven by VTA burst-stimulation, so I can only speculate which neurons and receptors might be involved. It has to be noted, however, that the Down state entrainment was not a stable response, in that it was observed in each animal (n=3), but not every time this stimulation pattern was applied, so repeatability would need to be ensured before investigating the receptor involvement. Glutamate released from VTA glutamatergic neurons is likely to induce Up states, as it has been suggested by Lewis and O'Donnell (2000). Hence, either VTA GABAergic neurons or VTA dopamine neurons might mediate the Down state entrainment.

It has been shown that there are GABA neurons in the VTA that project to the mPFC (Carr and Sesack, 2000), hence GABA release from their terminals could lead to synchronous inhibition of pyramidal cell firing, thus initiating synchronous Down states in pyramidal cells. However, it is not known when, during the mPFC slow oscillation cycle, VTA GABAergic neurons fire.

The Down states induced by VTA-stimulation with bursts occurring at low frequency, could also be dopamine neuron-mediated, as it has been shown that VTA dopamine neurons fire during PFC Down states, indicating an inhibitory relationship between dopamine neuron firing and PFC neuron firing (Gao et al., 2007). However, this action is likely *not* mediated by D_1-like receptors, as two lines of evidence suggest that $D_{1,5}R$ activation supports the Up state. Firstly, I have shown that the VTA-stimulation induced LAF rhythms, can be blocked by a $D_{1,5}R$ antagonist. Hence, when dopamine levels are high (due to high-frequency tonic stimulation), and $D_{1,5}$ receptors activated, no Down state can be generated. However, when dopamine levels are high and $D_{1,5}$ receptors blocked, Down states can occur again. Secondly, Lewis and O'Donnel (2000) have shown that $D_{1,5}R$ block decreases the duration of an Up state induced by VTA-stimulation and suggest an involvement of $D_{1,5}$ receptors in Up state maintenance. However, because of the 'inverted U' response function of D_1R action, it

is possible, that both effects might be $D_{1,5}R$ mediated. Alternatively, other dopamine receptors might be involved, or co-release of other neurotransmitters from dopamine neuron terminals.

In summary, synchronous cortical pyramidal cell Down states could be achieved through VTA activation, either by GABA release from terminals of VTA GABAergic neurons or by inhibition imposed on pyramidal cells by activation of mPFC inhibitory interneurons via D_4 receptors. Either way, the effect might be mediated by $GABA_B$ receptors, as cortical $GABA_B$ receptors have been suggested to play a role in initiation of cortical Down states (Mann et al., 2009). It is also possible that both VTA GABAergic as well as VTA dopamine neurons are involved in inhibiting PFC activity during the Down state as both a GABAergic component as well as a dopaminergic component are implicated in inhibitory PFC responses to VTA stimulation (Pirot et al., 1992).

6.2.3 *PPN neuron firing and VTA neuron firing during the slow oscillation*

As previously mentioned, the PPN is likely to induce VTA burst firing, which in turn might initiate REM-associated forebrain activation. The connectivity between PPN and VTA during SWA might also be of relevance as indicated by the timing of firing of VTA and PPN neurons. As already mentioned, VTA dopamine neurons fire during the PFC Down state, whereas VTA non-dopaminergic neurons fire during the PFC Up state (Gao et al., 2007). Interestingly, PPN cholinergic neurons fire during the cortical Up state, whereas PPN non-cholinergic neurons fire during the cortical Down state (Mena-Segovia et al., 2008). This means that PPN cholinergic neurons and VTA non-dopaminergic neurons fire during the same phase of the UDS cycle, as do PPN non-cholinergic neurons and VTA dopaminergic neurons.

Activation of NMDA receptors increases firing of midbrain dopamine neurons (Chergui et al., 1993). Hence, PPN glutamatergic neurons, firing during the cortical Down state, might induce Down state firing of VTA dopamine neurons.

Muscarinic receptor activation, however, can depolarise or hyperpolarise VTA dopamine neurons, depending on the amount and duration of release (Fiorillo and Williams, 2000). Hence, PPN cholinergic neurons, firing during the cortical Up state, might inhibit dopamine neuron firing during the Up state.

6.3 Dopaminergic modulation of nested fast oscillations during the Up state (Chapter 5)

Dopamine modulates PFC function during wakefulness. Many PFC functions have been associated with oscillations in specific frequency bands. Dopamine has been shown to modulate fast (>15 Hz) PFC oscillations *in vitro* and *in vivo* in awake animals, however, it is not known if dopamine also modulates fast sleep oscillations that occur during SWA on the Up state.

In Chapter 5, I investigated the effect of systemic application of dopaminergic agents on SWA, focusing on nested fast oscillations. I found that amphetamine, as well as $D_{1,5}R$ activation, and D_4R activation, modulated Up state nested fast oscillations. Most effects occurred within 10-20 minutes after injection. Amphetamine decreased Up state gamma and spindle oscillation power. The $D_{1,5}R$ agonist SKF3839 as well as the D_4R agonist A412997 decreased the power of Up state gamma and high gamma oscillations. Interestingly, the D_4R agonist A412997 had an additional effect with a very long latency (50 minutes after injection), namely that A412997 increased Up state spindle power, whilst seemingly retaining the time-locking of the spindle activity to the start and end of the Up state.

6.3.1 *Relevance of dopaminergic modulation of Up state fast oscillations*

The results presented in Chapter 5 show that tonic $D_{1,5}R$ activation as well as tonic D_4R activation with agonists can modulate Up state-associated fast oscillations. However, as stated before, it has been shown that VTA dopamine neurons fire during the cortical Down state (Gao et al., 2007). Can the dopaminergic modulation of nested fast Up state oscillations observed in my experiments still be relevant?

It is possible that the amount of dopamine released during a Down state (which might, for example, be dependent on the length of the Down state), sets the dopaminergic tone for the following Up state. A lower dopaminergic tone might allow for higher oscillatory power in the following Up state, whereas a higher dopaminergic tone might lead to lower oscillatory power in the following Up state. This hypothesis could be tested by correlating Down state length with Up state oscillation power for each cycle.

Another possibility is that the reduction of dopamine release during the Up state is what allows the Up state oscillations to occur at all. It might even be that the PFC, via inhibitory relay neurons, inhibits VTA dopamine neurons during the Up state (Gao et al., 2007), so that the Up state-associated oscillations can be generated.

6.3.2 *Implications of dopaminergic modulation of fast oscillations for memory function in health and disease*

My results indicate that dopamine seems to mainly have inhibitory effects on Up state associated oscillations.

In the case that dopamine release during the Down state sets the tone for the following Up state, thereby regulating the strength of Up state oscillations, then dopamine could have an impact on the strength of memory reactivation during these oscillations. However, even if this is not the case, a disruption of precise VTA dopamine neuron firing could have negative impact on SWA. If VTA dopamine neuron activity is disrupted (for example if the timing of these neurons in relation to the slow oscillation were less precise, which could lead to abnormal dopamine neuron firing during the Up state) this could have a detrimental effect on the Up state associated fast oscillations. Assuming dopamine's inhibitory effect on the mPFC is important for the generation of synchronous Down state onset in the mPFC, then a deficit in VTA dopamine neuron firing during the Down state could alter synchrony of SWA in the mPFC.

I have found a previously unreported enhancing effect of D_4R activation on mPFC spindle oscillations. Spindles are strongly implicated in memory consolidation. Hence, if the facilitatory effect of tonic D_4R activation could be confirmed in naturally sleeping humans, this effect could possibly be exploited to enhance spindle activity in diseases with spindle deficits, such as schizophrenia, to improve sleep-dependent memory consolidation.

6.4 Summary

Taken together, my results show, firstly, that the heterogeneity of the rat mPFC is reflected in sub-regional and laminar differences in SWA-associated oscillations. Secondly, my findings also indicate a role for dopamine and $D_{1,5}$ receptors in the generation of fast activity during REM sleep, and possibly a role for the VTA in the strong synchrony of the onset of cortical Down states. Finally, I have shown a role for dopamine in the modulation of fast oscillatory activity in the spindle, gamma and high gamma bands during SWA, with $D_{1,5}$R and D_4R involvement.

However, these results need to be considered in the context of a number of methodological caveats. In the following I will discuss the advantages and disadvantages of the approach chosen for the investigation in this thesis.

6.5 Methodological considerations

6.5.1 *Animal model*

This study was performed in rats, which are a well-established animal model in neuroscience research. Rat brain anatomy, as well as receptor profiles, are well studied and documented. The rat medial prefrontal cortex is characterised by similar function and connectivity to the human dorsolateral prefrontal cortex, but also shares function with the human medial prefrontal cortex.

Male rats were used as they do not undergo the hormonal changes associated with ovulation. Experiments were performed when rats weighed ~ 290 g, which is the weight that most brain atlases use. At this time, the rats were ~ 9 weeks old, which corresponds to young adulthood, so had been through the hormonal changes associated with puberty. Experiments were always performed at the same time of day, which was during the light-phase, and thus the time the rats would normally spent sleeping.

Rats are mammals, and as such express the two main sleep stages observed in humans - REM sleep and SWS - although sleep state alternations occur with different frequencies.

It was noted during the course of my experiments that the oxygen saturation in the animals deeply anaesthetized was sometimes very low (< 70%), hence in the majority of the experiments performed, oxygen was provided to achieve higher saturations (>90%).

6.5.2 *Local field potential recordings (LFP) in the study of sleep*

Sleep studies in healthy humans have to be non-invasive, and thus mostly investigate oscillations that can be observed in the EEG. SWS is characterised the EEG by brain oscillations in various frequency bands, with the slow oscillation (<1 Hz) grouping faster rhythms. These activity patterns are very similar to the activity observed in cats, rats and mice during natural sleep and anaesthesia. By using LFP recordings, the recorded activity can be compared to human brain activity during sleep.

The LFP recording is an extracellular recording, usually low-pass filtered at around 300 Hz. The LFP is thought to represent mainly the summation of excitatory and inhibitory post-synaptic potentials, but also synchronous spiking activity, as well as intrinsic membrane oscillations and synchronous after-hyperpolarisations.

SWA is characterised by very synchronous fluctuations of the cellular membrane potential, and maintained by strong excitatory and inhibitory synaptic barrages during the Up state, and their absence during the Down state. Hence, LFP recordings seem suitable to investigate SWA.

6.5.3 *Anaesthesia*

Care has to be taken, however, when interpreting the results presented in this thesis in relation to sleep, as the VTA stimulation experiments were performed under anaesthesia. Urethane in this study was chosen for a number of reasons. Firstly, because it has been used in many studies to investigate SWA (Steriade et al., 1993a; 1993d; Sharma et al., 2010; Bragin et al., 2012; Pagliardini et al., 2012; 2013). Secondly, it produces only minor effects on the respiration and cardiovascular function (Hara and Harris, 2002). Finally, in contrast to other anaesthetics commonly used in animal studies (e.g. isoflurane, ketamine, barbiturates), urethane has only moderate effects on excitatory and inhibitory neural transmission (Hara and Harris, 2002). Urethane anaesthesia is commonly used for electrophysiological studies as it only minimally affects sensory evoked responses and signal transmission in EEG recordings (Maggi and Meli, 1986; Albrecht and Davidowa, 1989; Dringenberg and Vanderwolf, 1995).

The mechanisms by which urethane induces general anaesthesia are still unknown. Its main effect is that it decreases intrinsic pyramidal cell excitability through a K^+ leak conductance (Sceniak and Maciver, 2006).

Urethane anaesthesia in the study of sleep state transitions

Spontaneous brain state alternations, with properties similar to those transitions seen in natural sleep, can be observed under urethane anaesthesia in rats (Clement et al., 2008) and mice (Pagliardini et al., 2013). This suggests that the mechanisms generating sleep state transitions are still active in animals during general anaesthesia induced by urethane injection, making it possible to study SWS-REM transitions under urethane anaesthesia.

Urethane anaesthesia in the study of sleep rhythms

Urethane anaesthesia is commonly used to study SWA and it has been shown that both sleep states -the REM-like state and SWA - have a similar frequency profile to that observed during natural REM sleep and SWS in rats (Clement et al., 2008).

Study of memory-related systems under urethane anaesthesia

In section 1.4.8 and section 1.4.9 I have highlighted the possible role of UDS and associated nested oscillations in sleep-dependent memory consolidation. The association of SWA features with memory has been established by investigating SWA during natural SWS. However, how far memory-related processing occurs during SWA under urethane anaesthesia is not known. Promising results come from a recent study by (Xu et al., 2012). The authors exposed awake, head-fixed as well as urethane-anaesthetised rats repeatedly to a moving spot, which evoked sequential firing in an ensemble of primary visual cortex neurons. Briefly flashing the starting point of the moving spot induced replay of the previously conditioned ensemble firing, during quiet wakefulness as well as during urethane anaesthesia (Xu et al., 2012). It has also been shown that exposure to odours during anaesthesia improves pirifom cortex cell's ability to discriminate between odours, suggesting that odour memory on the cellular level can be induced under urethane anaesthesia (Wilson, 2003).

Study of dopaminergic systems under urethane anaesthesia

In contrast to other anaesthetics, such as chloral hydrate and ketamine, urethane seems to have little effect on dopamine function. Urethane does not alter amphetamine's electrophysiological effects on striatal neurons (Warenycia and McKenzie, 1988), and, at anaesthetic doses, does not affect dopamine clearance by DAT (Sabeti et al., 2003).

It has to be noted, however, that results regarding effects of dopamine obtained under anaesthesia are often the opposite from studies in awake subjects, which is thought to be because of differences in the excitation-inhibition balance between wakefulness and anaesthesia. Hence, results obtained during anaesthesia are not necessarily applicable to awake conditions. However, they might still be relevant to natural sleep conditions.

6.5.4 *Route of application and specificity of pharmacological agents*

Drugs used in Chapters 4 and 5 were administered systemically, via i.p. injection. Hence, it is difficult to draw conclusions regarding the exact site of action of the agent in question.

It has also be noted, that most of the drugs were not very specific, as it is difficult to produce drugs that selectively target a certain dopamine receptor. Sulpiride has got similar selectivity for D_2 and D_3 receptors. SCH23390 and SKF have got similar selectivity for D_1 and D_5 receptors. SCH23390 also affects serotonin (5-hydroxytryptamine) 5-HT_{2C} receptors. Only the D_4R agonist used, A412997, is highly selective.

6.6 Conclusions and impact

Taking into account these limitations and caveats, I am able to present the following final conclusions to this thesis.

I found strong regional differences in Up state-associated mPFC oscillations under urethane anaesthesia (Chapter 3). Future studies on mPFC oscillations should always report the sub-region that was investigated, and take care when averaging data across different mPFC recording sites. I also reported a very slow spontaneous modulation of LFP power (VSMP) that seemed to originate near the ventral mPFC, possibly from the dTT.

In Chapter 4, I have shown show that VTA stimulation can induce a low amplitude fast (LAF) rhythm in the mPFC of anaesthetised rodents, similar to the LAF activity observed in the forebrain during REM sleep, which is $D_{1,5}$R-dependent.

In addition, I have shown a possible role for the VTA in synchronising Down state onset. Assuming dopamine's inhibitory effect on the mPFC is important for the generation of synchronous Down state onset in the mPFC, then a deficit in VTA

dopamine neuron firing during the Down state could alter synchrony of SWA in the mPFC.

In Chapter 5, I have shown that dopamine receptor activation seems to have mainly inhibitory effects on Up state associated oscillations. If dopamine release during the Down state sets the tone for the following Up state, thereby regulating the strength of Up state oscillations, then dopamine could have an impact on the strength of memory reactivation during these oscillations.

In addition, I have found an enhancing effect of D_4 receptor activation on mPFC spindle oscillations (Chapter 5). Spindles are highly implicated in memory consolidation. Hence, if the facilitatory effect of tonic D_4R activation could be confirmed in naturally sleeping humans, this could be exploited to enhance spindle activity in diseases with spindle deficits, such as SCZ, to improve sleep-dependent memory consolidation.

The results obtained in this thesis shed light on dopamine function during sleep, which is relevant for a number of neuro-psychiatric disorders. Disorders in which a major part of the pathology is dopamine dysfunction, such as SCZ, PD and ADHD, are often accompanied by sleep disruptions and abnormalities in slow and fast sleep rhythms, which might be related to some of the cognitive deficits that are also observed in these disorders. The experiments presented in this thesis suggest that dopamine can modulate fast sleep rhythms during REM and SWA, and hence might contribute to the sleep abnormalities in these disorders.

For example, it is thought that in schizophrenia, prefrontal hypo-dopaminergia leads to a compensatory increased D_1R expression (Abi-Dargham et al., 2002). Assuming that dopamine release *during sleep* in schizophrenia were normal, dopamine would be released onto a PFC with a pathological increase of D_1 receptors. My results, and other studies indicate that that would be likely to reduce SWA, as it has been observed in schizophrenia (Wulff et al., 2010).

My results also show that $D_{1,5}R$ activation might disrupt spindle timing and amphetamine decreased spindle power. On the other hand, I have shown that D_4R activation increased spindle power, while retaining the strong time-locking to SWA. Hence, the increase in D_4 receptors observed in schizophrenia (Seeman et al., 1993)

might also be compensatory to counter-act the negative impact (decrease in power/disruption of timing) of activation of other dopamine receptors (e.g. $D_{1,5}R$ or $D_{2,3}R$) on spindles.

6.7 Outlook and future work

I have discovered that early and late spindles in the mPFC have a different profile along the D-V axis. The occurrence of early and late spindles is consistent with the human literature. In humans, these two kinds of spindles occur at different frequencies (Mölle et al., 2011), which still needs to confirmed for rats. It has been suggested that the two spindle types are involved in different stages of memory consolidation, possibly supported by cortico-cortical versus cortico-hippocampal communication.

Parallel recordings from mPFC and projection areas could show if early spindles in dorsal mPFC occur in synchrony with spindles in sensory-motor areas, and if late spindles, in ventral mPFC, occur in synchrony with spindles in the amygdala, or hippocampal ripples. This would give further evidence for the theory that the mPFC can communicate with different brain regions through coordinated oscillatory activity during SWA.

I have shown that VTA stimulation can induce a REM-like LAF rhythm in the mPFC. Although VTA stimulation can also induce hippocampal theta activity, another hallmark of REM sleep, the literature suggests that the VTA is not the originator of this activity, but likely the PPN. The 'reciprocal interaction model', however, suggests that the PPN-basal forebrain pathway induces hippocampal theta and forebrain activation. Hence, the role of the VTA in the generation of hippocampal theta and LAF activity in the PFC could be further investigated, by stimulating the PPN to induce cortical activation, while blocking VTA activity, to see if VTA activation is necessary, or if the PPN-basal forebrain pathway is sufficient to generate hippocampal and cortical REM-like states.

However, the fact that cortical arousal can be induced by stimulation of a brain area during anaesthesia does not prove its involvement in REM sleep. Electrical stimulation of the LC in anaesthetised rats for example induces a REM-like LAF rhythm (Marzo et al., 2014). However, the noradrenaline levels are low during REM sleep (Hobson and Pace-Schott, 2002), and optogenetic stimulation of LC neurons during natural sleep

always induces sleep-to-wake transitions (Carter et al., 2010), indicating a role for LC in wakefulness, but not REM sleep.

Hence, I suggest to investigate if stimulation of the VTA during natural SWS can induce REM transitions, as is the case for the basal forebrain: optogenetic stimulation of cholinergic basal forebrain neurons can induce transitions from sleep to wake as well as SWS to REM (Han et al., 2014). Using optogenetic techniques, selective stimulation of either VTA dopamine neurons or VTA glutamatergic neurons would show if dopamine neurons or glutamate neurons are involved in the induction of the LAF rhythm. Assuming that VTA dopamine neurons would be involved, local application of dopamine antagonists and glutamate antagonists in the PFC could then answer the question whether glutamate co-release from dopaminergic terminals is involved.

I have shown that $D_{1,5}R$ and D_4R activation can modulate Up state associated oscillations under urethane anaesthesia. However, it remains to be seen if the observed effects of $D_{1,5}R$ and D_4R activation on gamma, high gamma and spindle power during the Up state can also be observed during natural sleep, and if dopaminergic modulation of these rhythms might have implications for memory consolidation.

I have found a very slow modulation of LFP power (VSMP) that has not previously been reported. There are similarities to very slow phenomena reported in both human and rat literature, which I have discussed in detail in section 3.5.4. Briefly, very slow oscillations (< 0.1 Hz) have been observed in the EEG and BOLD signal in awake humans, and recently they have been shown to be correlated with each other (Hiltunen et al., 2014). Very slow fluctuations between activated and non-activated states have also been observed during NREM sleep in humans (cyclic alternating pattern [CAP]), however not during REM sleep. However, the comparison between different recording methods and different species and brain states is complex. Hence, it remains to be investigated whether the VSMP is related to very slow phenomena observed in human EEG or BOLD signal, and if the VSMP is present during wake, and SWS and REM.

It also remains to be investigated what implications these slow modulations have, for example whether they affect other oscillatory parameters. Studies in humans and animals could investigate if the very slow background activity is retained during all brain states and what implications this might have for behaviour (e.g CAP and abnormal breathing and movements during sleep). Thereby, activity should be recorded with the same method during SWS, REM sleep and wakefulness.

The observed enhancing effect on cortical arousal levels of D_4R activation has, to the best of my knowledge, not been reported before. It would be crucial to locate the receptors mediating this effect. D_4 receptors are expressed in the PFC as well as in the thalamus, which is where spindle activity originates. Iontophoretic administration of a D_4R agonist to these areas would give further insights. This might be of relevance for schizophrenia, as in this disorder, PFC as well as the thalamus are implicated, D_4R expression is altered, and reduced spindle activity and coordination have been reported in schizophrenia patients (Ferrarelli et al., 2010; Keshavan et al., 2011; Wamsley et al., 2012) as well as in animal models (Phillips et al., 2012) of this disease.

Bibliography

Aarts E, Verhage M, Veenvliet JV, Dolan CV, van der Sluis S (2014) A solution to dependency: using multilevel analysis to accommodate nested data. Nat Neurosci 17:491–496.

Abi-Dargham A, Mawlawi O, Lombardo I, Gil R, Martinez D, Huang Y, Hwang D-R, Keilp J, Kochan L, Van Heertum R, Gorman JM, Laruelle M (2002) Prefrontal dopamine D1 receptors and working memory in schizophrenia. J Neurosci 22:3708–3719.

Ackermann S, Rasch B (2014) Differential Effects of Non-REM and REM Sleep on Memory Consolidation? Curr Neurol Neurosci Rep 14:430.

Adler CH (2005) Nonmotor complications in Parkinson's disease. Mov Disord 20:S23–S29.

Ahveninen J, Kähkönen S, Tiitinen H, Pekkonen E, Huttunen J, Kaakkola S, Ilmoniemi RJ, Jääskeläinen IP (2000) Suppression of transient 40-Hz auditory response by haloperidol suggests modulation of human selective attention by dopamine D 2 receptors. Neurosci Lett 292:29–32.

Ainsworth M, Lee S, Cunningham MO, Roopun AK, Traub RD, Kopell NJ, Whittington MA (2011) Dual Gamma Rhythm Generators Control Interlaminar Synchrony in Auditory Cortex. J Neurosci 31:17040–17051.

Akhter F, Haque T, Sato F, Kato T, Ohara H, Fujio T, Tsutsumi K, Uchino K, Sessle BJ, Yoshida A (2014) Projections from the dorsal peduncular cortex to the trigeminal subnucleus caudalis (medullary dorsal horn) and other lower brainstem areas in rats. Neuroscience 266:23–37.

Aladjalova NA (1957) Infra-slow rhythmic oscillations of the steady potential of the cerebral cortex. Nature 179:957–959.

Albrecht D, Davidowa H (1989) Action of urethane on dorsal lateral geniculate neurons. Brain Research Bulletin 22:923–927.

Amzica F, Steriade M (1997) The K-complex: Its slow (<1-Hz) rhythmicity and relation to delta waves. Neurology 49:952–959.

Anderer P, Klösch G, Gruber G, Trenker E (2001) Low-resolution brain electromagnetic tomography revealed simultaneously active frontal and parietal sleep spindle sources in the human cortex. Neuroscience.

Andersson R, Johnston A, Fisahn A (2012a) Dopamine D4 Receptor Activation Increases Hippocampal Gamma Oscillations by Enhancing Synchronization of Fast-Spiking Interneurons. PLoS ONE 7:e40906.

Andersson RH, Johnston A, Herman PA, Winzer-Serhan UH, Karavanova I, Vullhorst D, Fisahn A, Buonanno A (2012b) Neuregulin and dopamine modulation of hippocampal gamma oscillations is dependent on dopamine D4 receptors. PNAS 109:13118–13123.

Andrillon T, Nir Y, Staba RJ, Ferrarelli F, Cirelli C, Tononi G, Fried I (2011) Sleep Spindles in Humans: Insights from Intracranial EEG and Unit Recordings. J Neurosci 31:17821–17834.

Ariano MA, Wang J, Noblett KL, Larson ER, Sibley DR (1997) Cellular distribution of the rat D4 dopamine receptor protein in the CNS using anti-receptor antisera. Brain Research 752:26–34.

Astori S, Lüthi A (2013) Synaptic Plasticity at Intrathalamic Connections via CaV3.3 T-type Ca2+ Channels and GluN2B-Containing NMDA Receptors. J Neurosci 33:624–630.

Baldwin HA, Frenk S, Lettvin JY (1965) Glass-Coated Tungsten Microelectrodes. Science 148:1462–1464.

Barthó P, Slézia A, Mátyás F, Faradzs-Zade L, Ulbert I, Harris KD, Acsády L (2014) Ongoing Network State Controls the Length of Sleep Spindles via Inhibitory Activity. Neuron 82:1367–1379.

Bauer M, Oostenveld R, Peeters M, Fries P (2006) Tactile spatial attention enhances gamma-band activity in somatosensory cortex and reduces low-frequency activity in parieto-occipital areas. J Neurosci 26:490–501.

Bechara A, Damasio H, Tranel D, Anderson SW (1998) Dissociation Of working memory from decision making within the human prefrontal cortex. J Neurosci 18:428–437.

Belluscio MA, Mizuseki K, Schmidt R, Kempter R, Buzsaki G (2012) Cross-Frequency Phase-Phase Coupling between Theta and Gamma Oscillations in the Hippocampus. J Neurosci 32:423–435.

Beltramo R, D'Urso G, Dal Maschio M, Farisello P, Bovetti S, Clovis Y, Lassi G, Tucci V, De Pietri Tonelli D, Fellin T (2013) Layer-specific excitatory circuits differentially control recurrent network dynamics in the neocortex. Nat Neurosci 16:227–234.

Belujon P, Grace AA (2008) Critical Role of the Prefrontal Cortex in the Regulation of Hippocampus-Accumbens Information Flow. J Neurosci 28:9797–9805.

Benchenane K, Tiesinga PH, Battaglia FP (2011) Oscillations in the prefrontal cortex: a gateway to memory and attention. Curr Opin Neurobiol:1–11.

Benveniste H, Volkow ND (2013) Dopamine-enhancing medications to accelerate emergence from general anesthesia. Anesthesiology 118:5–6.

Berendse HW, Groenewegen HJ (1991) Restricted cortical termination fields of the midline and intralaminar thalamic nuclei in the rat. Neuroscience 42:73–102.

Bergmann BM, Winter JB, Rosenberg RS, Rechtschaffen A (1987) NREM Sleep with Low-Voltage EEG in the Rat. Sleep 10(1):1-11.

Bieri KW, Bobbitt KN, Colgin LL (2014) Slow and Fast Gamma Rhythms Coordinate Different Spatial Coding Modes in Hippocampal Place Cells. Neuron 82:670–681.

Björklund A, Dunnett SB (2007) Dopamine neuron systems in the brain: an update. Trends in Neurosciences 30:194–202.

Blethyn KL, Hughes SW, Tóth TI, Cope DW, Crunelli V (2006) Neuronal Basis of the Slow (<1 Hz) Oscillation in Neurons of the Nucleus Reticularis Thalami *In Vitro*. J Neurosci 26:2474–2486.

Boucetta S, Jones BE (2009) Activity Profiles of Cholinergic and Intermingled GABAergic and Putative Glutamatergic Neurons in the Pontomesencephalic Tegmentum of Urethane-Anesthetized Rats. J Neurosci 29:4664–4674.

Bragin A, Benassi SK, Engel J (2012) Patterns of the UP-Down state in normal and epileptic mice. Neuroscience 225:76–87.

Brown RE, Basheer R, McKenna JT, Strecker RE, McCarley RW (2012) Control of Sleep and Wakefulness. Physiol Rev 92:1087–1187.

Bunney BS, Walters JR, Roth RH, Aghajanian GK (1973) Dopaminergic neurons: effect of antipsychotic drugs and amphetamine on single cell activity. J Pharmacol Exp Ther 185:560–571.

Buzsáki G, Anastassiou CA, Koch C (2012) The origin of extracellular fields and currents--EEG, ECoG, LFP and spikes. Nat Rev Neurosci 13:407–420.

Calipari ES, Ferris MJ (2013) Amphetamine Mechanisms and Actions at the Dopamine Terminal Revisited. J Neurosci 33:8923–8925.

Cardin JA (2005) Stimulus-Dependent (30-50 Hz) Oscillations in Simple and Complex Fast Rhythmic Bursting Cells in Primary Visual Cortex. J Neurosci 25:5339–5350.

Cardin JA, Carlén M, Meletis K, Knoblich U, Zhang F, Deisseroth K, Tsai L-H, Moore CI (2009) Driving fast-spiking cells induces gamma rhythm and controls sensory responses. Nature 459:663–667.

Carlen M, Meletis K, Siegle JH, Cardin JA, Futai K, Vierling-Claassen D, Rühlmann C, Jones SR, Deisseroth K, Sheng M, Moore CI, Tsai L-H (2012) A critical role for NMDA receptors in parvalbumin interneurons for gamma rhythm induction and behavior. Mol Psychiatry 17:537–548.

Carr DB, Sesack SR (2000) GABA-containing neurons in the rat ventral tegmental area project to the prefrontal cortex. Synapse 38:114–123.

Carr MF, Karlsson MP, Frank LM (2012) Transient Slow Gamma Synchrony Underlies Hippocampal Memory Replay. Neuron 75:700–713.

Carracedo LM, Kjeldsen H, Cunnington L, Jenkins A, Schofield I, Cunningham MO, Davies CH, Traub RD, Whittington MA (2013) A Neocortical Delta Rhythm Facilitates Reciprocal Interlaminar Interactions via Nested Theta Rhythms. J Neurosci 33:10750–10761.

Carter ME, Yizhar O, Chikahisa S, Nguyen H, Adamantidis A, Nishino S, Deisseroth K, de Lecea L (2010) Tuning arousal with optogenetic modulation of locus coeruleus neurons. Nat Neurosci 13:1526–1533.

Cavas M, Navarro JF (2006) Effects of selective dopamine D4 receptor antagonist, L-741,741, on sleep and wakefulness in the rat. Prog Neuropsychopharmacol Biol Psychiatry 30:668–678.

Chauvette S, Crochet S, Volgushev M, Timofeev I (2011) Properties of slow oscillation during slow-wave sleep and anesthesia in cats. J Neurosci 31:14998–15008.

Chauvette S, Seigneur J, Timofeev I (2012) Sleep oscillations in the thalamocortical system induce long-term neuronal plasticity. Neuron 75:1105–1113.

Chauvette S, Volgushev M, Timofeev I (2010) Origin of Active States in Local Neocortical Networks during Slow Sleep Oscillation. Cereb Cortex 20:2660–2674.

Chen L, Yang CR (2002) Dopamine D1 receptor modulation of NMDA EPSC exhibits an inverted "U" dose-response profile in rat prefrontal cortex (PFC) *in vitro*. Society for Neuroscience Abstracts.

Chergui K, Charléty PJ, Akaoka H, Saunier CF, Brunet JL, Buda M, Svensson TH, Chouvet G (1993) Tonic activation of NMDA receptors causes spontaneous burst discharge of rat midbrain dopamine neurons in vivo. Eur J Neurosci 5:137–144.

Chiovini B, Turi GF, Katona G, Kaszás A, Pálfi D, Maák P, Szalay G, Szabó MF, Szabó G, Szadai Z, Káli S, Rózsa B (2014) Dendritic Spikes Induce Ripples in Parvalbumin Interneurons during Hippocampal Sharp Waves. Neuron 82:908–924.

Clement EA, Richard A, Thwaites M, Ailon J, Peters S, Dickson CT (2008) Cyclic and sleep-like spontaneous alternations of brain state under urethane anaesthesia. PLoS ONE 3:e2004.

Compte A, Reig R, Descalzo VF, Harvey MA, Puccini GD, Sanchez-Vives MV (2008) Spontaneous High-Frequency (10-80 Hz) Oscillations during Up States in the Cerebral Cortex In Vitro. J Neurosci 28:13828–13844.

Contreras D, Destexhe A, Steriade M (1997) Spindle oscillations during cortical spreading depression in naturally sleeping cats. Neuroscience 77:933–936.

Contreras DD, Steriade MM (1995) Cellular basis of EEG slow rhythms: a study of dynamic corticothalamic relationships. J Neurosci 15:604–622.

Crunelli V, Hughes SW (2010) The slow (<1 Hz) rhythm of non-REM sleep: a dialogue between three cardinal oscillators. Nat Neurosci 13:9–17.

Csercsa R et al. (2010) Laminar analysis of slow wave activity in humans. Brain 133:2814–2829.

Cunningham MO, Pervouchine DD, Racca C, Kopell NJ, Davies CH, Jones RSG, Traub RD, Whittington MA (2006) Neuronal metabolism governs cortical network response state. Proc Natl Acad Sci USA 103:5597–5601.

Cunningham MO, Whittington MA, Bibbig A, Roopun A, LeBeau FEN, Vogt A, Monyer H, Buhl EH, Traub RD (2004) A role for fast rhythmic bursting neurons in cortical gamma oscillations in vitro. Proc Natl Acad Sci USA 101:7152–7157.

Dahan L, Astier B, Vautrelle N, Urbain N, Kocsis B, Chouvet G (2006) Prominent

Burst Firing of Dopaminergic Neurons in the Ventral Tegmental Area during Paradoxical Sleep. Neuropsychopharmacology 32:1232–1241.

Dang-Vu TT, Bonjean M, Schabus M, Boly M, Darsaud A, Desseilles M, Degueldre C, Balteau E, Phillips C, Luxen A, Sejnowski TJ, Maquet P (2011) Interplay between spontaneous and induced brain activity during human non-rapid eye movement sleep. PNAS 108:15438–15443.

David F, Schmiedt JT (2014) Thalamus and cortex: inseparable partners in shaping sleep slow waves? J Neurosci 34:11517–11518.

David F, Schmiedt JT, Taylor HL, Orban G, Di Giovanni G, Uebele VN, Renger JJ, Lambert RC, Leresche N, Crunelli V (2013) Essential Thalamic Contribution to Slow Waves of Natural Sleep. J Neurosci 33:19599–19610.

de Almeida J, Mengod G (2010) D2 and D4 dopamine receptor mRNA distribution in pyramidal neurons and GABAergic subpopulations in monkey prefrontal cortex: implications for schizophrenia treatment. Neuroscience 170:1133–1139.

De Cock VC, Vidailhet M, Arnulf I (2008) Sleep disturbances in patients with parkinsonism. Nat Clin Pract Neurol 4:254–266.

De Cock VC, Vidailhet M, Leu S, Texeira A, Apartis E, Elbaz A, Roze E, Willer JC, Derenne JP, Agid Y, Arnulf I (2007) Restoration of normal motor control in Parkinson's disease during REM sleep. Brain 130:450–456.

de Lima MNM, Presti-Torres J, Dornelles A, Scalco FS, Roesler R, Garcia VA, Schröder N (2011) Modulatory influence of dopamine receptors on consolidation of object recognition memory. Neurobiol Learn & Mem 95:305–310.

Debener S, Herrmann CS, Kranczioch C, Gembris D, Engel AK (2003) Top-down attentional processing enhances auditory evoked gamma band activity. NeuroReport 14:683–686.

Defagot MC, Malchiodi EL, Villar MJ, Antonelli MC (2003) Distribution of D4 dopamine receptor in rat brain with sequence-specific antibodies. Brain Res Mol Brain Res 45:1–12.

Demiralp T, Herrmann CS, Erdal ME, Ergenoglu T, Keskin YH, Ergen M, Beydagi H (2007) DRD4 and DAT1 polymorphisms modulate human gamma band responses. Cereb Cortex 17:1007–1019.

Deniau JM, Thierry AM, Feger J (1980) Electrophysiological identification of mesencephalic ventromedial tegmental (VMT) neurons projecting to the frontal cortex, septum and nucleus accumbens. Brain Research 189:315–326.

Descarries L, Lemay B, Doucet G, Berger B (1987) Regional and laminar density of the dopamine innervation in adult rat cerebral cortex. Neuroscience 21:807–824.

Destexhe A, Contreras D, Steriade M (1999) Spatiotemporal analysis of local field potentials and unit discharges in cat cerebral cortex during natural wake and sleep states. J Neurosci 19:4595–4608.

Destexhe A, Hughes SW, Rudolph M, Crunelli V (2007) Are corticothalamic “up”

states fragments of wakefulness? Trends in Neurosciences 30:334–342.

Deutch AY (1993) Prefrontal cortical dopamine systems and the elaboration of functional corticostriatal circuits: implications for schizophrenia and Parkinson's disease. J Neural Transm Gen Sect 91:197–221.

Diekelmann S, Born J (2010) The memory function of sleep. Nat Rev Neurosci 11:114–126.

Dringenberg HC, Vanderwolf CH (1995) Some general anesthetics reduce serotonergic neocortical activation and enhance the action of serotonergic antagonists. Brain Research Bulletin 36:285–292.

Dzirasa K, Ribeiro S, Costa R, Santos LM, Lin SC, Grosmark A, Sotnikova TD, Gainetdinov RR, Caron MG, Nicolelis MAL (2006) Dopaminergic Control of Sleep-Wake States. J Neurosci 26:10577–10589.

Eder DN, Zdravkovic M, Wildschiødtz G (2003) Selective alterations of the first NREM sleep cycle in humans by a dopamine D1 receptor antagonist (NNC-687). Journal of Psychiatric Research 37:305–312.

Euston DR, Gruber AJ, McNaughton BL (2012) The Role of Medial Prefrontal Cortex in Memory and Decision Making. Neuron 76:1057–1070.

Euston DR, Tatsuno M, McNaughton BL (2007) Fast-forward playback of recent memory sequences in prefrontal cortex during sleep. Science 318:1147–1150.

Fallon JH (1981) Collateralization of monoamine neurons: mesotelencephalic dopamine projections to caudate, septum, and frontal cortex. J Neurosci 1:1361–1368.

Fell J, Elfadil H, Röschke J, Burr W, Klaver P, Elger CE, Fernández G (2002) Human scalp recorded sigma activity is modulated by slow EEG oscillations during deep sleep. Int J Neurosci 112:893–900.

Fell J, Klaver P, Elfadil H, Schaller C, Elger CE, Fernández G (2003) Rhinal-hippocampal theta coherence during declarative memory formation: interaction with gamma synchronization? Eur J Neurosci 17:1082–1088.

Ferrarelli F, Huber R, Peterson MJ, Massimini M, Murphy M, Riedner BA, Watson A, Bria P, Tononi G (2007) Reduced sleep spindle activity in schizophrenia patients. Am J Psychiatry 164:483–492.

Ferrarelli F, Peterson MJ, Sarasso S, Riedner BA, Murphy MJ, Benca RM, Bria P, Kalin NH, Tononi G (2010) Thalamic dysfunction in schizophrenia suggested by whole-night deficits in slow and fast spindles. Am J Psychiatry 167:1339–1348.

Filippov IV (2005) Very slow brain potential fluctuations (<0.5 Hz) in visual thalamus and striate cortex after their successive electrical stimulation in lightly anesthetized rats. Brain Research 1066:179–186.

Filippov IV, Williams WC, Krebs AA, Pugachev KS (2008) Dynamics of infraslow potentials in the primary auditory cortex: component analysis and contribution of specific thalamic-cortical and non-specific brainstem-cortical influences. Brain Research 1219:66–77.

Fiorillo CD, Williams JT (2000) Cholinergic inhibition of ventral midbrain dopamine neurons. J Neurosci 20:7855–7860.

Fitch TE (2006) Dopamine D1/5 Receptor Modulation of Firing Rate and Bidirectional Theta Burst Firing in Medial Septal/Vertical Limb of Diagonal Band Neurons In Vivo. J Neurophysiol 95:2808–2820.

Floresco SB, Blaha CD, Yang CR, Phillips AG (2001) Modulation of hippocampal and amygdalar-evoked activity of nucleus accumbens neurons by dopamine: cellular mechanisms of input selection. J Neurosci 21:2851–2860.

Floresco SB, Magyar O (2006) Mesocortical dopamine modulation of executive functions: beyond working memory. Psychopharm 188:567–585.

Floresco SB, Magyar O, Ghods-Sharifi S, Vexelman C, Tse MTL (2006) Multiple dopamine receptor subtypes in the medial prefrontal cortex of the rat regulate set-shifting. Neuropsychopharmacology 31:297–309.

Floresco SB, West AR, Ash B, Moore H, Grace AA (2003) Afferent modulation of dopamine neuron firing differentially regulates tonic and phasic dopamine transmission. Nat Neurosci 6:968–973.

Fogel SM, Smith CT, Cote KA (2007) Dissociable learning-dependent changes in REM and non-REM sleep in declarative and procedural memory systems. Beh Brain Res 180:48–61.

Fox MD, Raichle ME (2007) Spontaneous fluctuations in brain activity observed with functional magnetic resonance imaging. Nat Rev Neurosci 8:700–711.

Fries P (2005) A mechanism for cognitive dynamics: neuronal communication through neuronal coherence. Trends in Cognitive Sciences 9:474–480.

Fuchs EC, Zivkovic AR, Cunningham MO, Middleton S, LeBeau FEN, Bannerman DM, Rozov A, Whittington MA, Traub RD, Rawlins JNP, Monyer H (2007) Recruitment of parvalbumin-positive interneurons determines hippocampal function and associated behavior. Neuron 53:591–604.

Fujisawa S, Buzsáki G (2011) A 4 Hz Oscillation Adaptively Synchronizes Prefrontal, VTA, and Hippocampal Activities. Neuron 72:153–165.

Fuller PM, Saper CB, Lu J (2007) The pontine REM switch: past and present. J Physiol (Lond) 584:735–741.

Furth KE, Mastwal S, Wang KH, Buonanno A, Vullhorst D (2013) Dopamine, cognitive function, and gamma oscillations: role of D4 receptors. Front Cell Neurosci 7:102.

Gabbott PLA, Dickie BGM, Vaid RR, Headlam AJN, Bacon SJ (1997) Local-circuit neurones in the medial prefrontal cortex (areas 25, 32 and 24b) in the rat: Morphology and quantitative distribution. J Comp Neurol 377:465–499.

Gais S, Mölle M, Helms K, Born J (2002) Learning-dependent increases in sleep spindle density. J Neurosci 22:6830–6834.

Ganelin-Cohen E, Ashkenasi A (2013) Disordered sleep in pediatric patients with attention deficit hyperactivity disorder: an overview. Isr Med Assoc J 15:705–709.

Gao C, Wolf ME (2008) Dopamine receptors regulate NMDA receptor surface expression in prefrontal cortex neurons. J Neurochem 106:2489–2501.

Gao M, Liu CL, Yang S, Jin GZ, Bunney BS, Shi WX (2007) Functional Coupling between the Prefrontal Cortex and Dopamine Neurons in the Ventral Tegmental Area. J Neurosci 27:5414–5421.

Genzel L, Kroes MCW, Dresler M, Battaglia FP (2014) Light sleep versus slow wave sleep in memory consolidation: a question of global versus local processes? Trends in Neurosciences 37:10–19.

Ghosh D, Rajan PV, Das D, Datta P, Rothner AD, Erenberg G (2014) Sleep disorders in children with Tourette syndrome. Pediatr Neurol 51:31–35.

Gilbert SJ, Burgess PW (2008) Executive function. Current Biology 18:R110–R114.

Giros B, Jaber M, Jones SR, Wightman RM, Caron MG (1996) Hyperlocomotion and indifference to cocaine and amphetamine in mice lacking the dopamine transporter. Nature 379:15.

Gisquet-Verrier P, Winocur G, Delatour B (2000) Functional dissociation between dorsal and ventral regions of the medial prefrontal cortex in rats. Psychobiology 28:248–260.

Glykos V (2013) Generation and modulation of network oscillations in the rodent prefrontal cortex in vitro LeBeau FEN, ed. Available at: http://hdl.handle.net/10443/2187.

Goldman-Rakic PS, Muly EC, Williams GV (2000) D1 receptors in prefrontal cells and circuits. Brain Res Brain Res Rev 31:295–301.

Gonzalez-Islas C, Hablitz JJ (2001) Dopamine inhibition of evoked IPSCs in rat prefrontal cortex. J Neurophysiol 86:2911–2918.

Gorelova N, Mulholland PJ, Chandler LJ, Seamans JK (2012) The Glutamatergic Component of the Mesocortical Pathway Emanating from Different Subregions of the Ventral Midbrain. Cerebral Cortex 22:327–336.

Gorelova N, Seamans JK, Yang CR (2002) Mechanisms of dopamine activation of fast-spiking interneurons that exert inhibition in rat prefrontal cortex. J Neurophysiol 88:3150–3166.

Gottesmann, C (1992) Detection of Seven Sleep-Waking Stages in the Rat. Neurosci Biobehav Rev 16(1): 31-38.

Govindaiah G, Wang T, Gillette MU, Crandall SR, Cox CL (2010) Regulation of Inhibitory Synapses by Presynaptic D4 Dopamine Receptors in Thalamus. J Neurophysiol 104:2757–2765.

Gray CM, McCormick DA (1996) Chattering Cells: Superficial Pyramidal Neurons Contributing to the Generation of Synchronous Oscillations in the Visual Cortex.

Science 274:109–113.

Grenier F, Timofeev I, Steriade M (2001) Focal synchronization of ripples (80-200 Hz) in neocortex and their neuronal correlates. J Neurophysiol 86:1884–1898.

Gronier B, Rasmussen K (1998) Activation of midbrain presumed dopaminergic neurones by muscarinic cholinergic receptors: an in vivo electrophysiological study in the rat. British Journal of Pharmacology 124:455–464.

Gu XL (2010) Deciphering the Corelease of Glutamate from Dopaminergic Terminals Derived from the Ventral Tegmental Area. J Neurosci 30:13549–13551.

Haenschel C, Bittner RA, Waltz J, Haertling F, Wibral M, Singer W, Linden DEJ, Rodriguez E (2009) Cortical Oscillatory Activity Is Critical for Working Memory as Revealed by Deficits in Early-Onset Schizophrenia. J Neurosci 29:9481–9489.

Haider B (2006) Neocortical Network Activity In Vivo Is Generated through a Dynamic Balance of Excitation and Inhibition. J Neurosci 26:4535–4545.

Halassa MM, Siegle JH, Ritt JT, Ting JT, Feng G, Moore CI (2011) Selective optical drive of thalamic reticular nucleus generates thalamic bursts and cortical spindles. Nat Neurosci 14:1118–1120.

Han Y, Shi Y-F, Xi W, Zhou R, Tan Z-B, Wang H, Li X-M, Chen Z, Feng G, Luo M, Huang Z-L, Duan S, Yu Y-Q (2014) Selective Activation of Cholinergic Basal Forebrain Neurons Induces Immediate Sleep-wake Transitions. Current Biology 24:693–698.

Hara K, Harris RA (2002) The anesthetic mechanism of urethane: the effects on neurotransmitter-gated ion channels. Anesth Analg 94:313–318.

Hasenstaub A, Sachdev RNS, McCormick DA (2007) State changes rapidly modulate cortical neuronal responsiveness. J Neurosci 27:9607–9622.

Hasenstaub A, Shu Y, Haider B, Kraushaar U, Duque A, McCormick DA (2005) Inhibitory postsynaptic potentials carry synchronized frequency information in active cortical networks. Neuron 47:423–435.

Heib DPJ, Hoedlmoser K, Anderer P, Zeitlhofer J, Gruber G, Klimesch W, Schabus M (2013) Slow Oscillation Amplitudes and Up-State Lengths Relate to Memory Improvement. PLoS ONE 8:e82049.

Heidbreder CA, Groenewegen HJ (2003) The medial prefrontal cortex in the rat: evidence for a dorso-ventral distinction based upon functional and anatomical characteristics. Neuroscience & Biobehavioral Reviews 27:555–579.

Henry CE, Scoville WB (1952) Suppression-burst activity from isolated cerebral cortex in man. EEG & Clin Neurophys 4:1–22.

Hiltunen T, Kantola J, Abou Elseoud A, Lepola P, Suominen K, Starck T, Nikkinen J, Remes J, Tervonen O, Palva S, Kiviniemi V, Palva JM (2014) Infra-Slow EEG Fluctuations Are Correlated with Resting-State Network Dynamics in fMRI. J Neurosci 34:356–362.

Hobson JA, Pace-Schott EF (2002) The cognitive neuroscience of sleep: neuronal systems, consciousness and learning. Nat Rev Neurosci 3:679–693.

Hoffman KL, McNaughton BL (2002) Coordinated reactivation of distributed memory traces in primate neocortex. Science 297:2070–2073.

Hollnagel JO, Maslarova A, Haq RU, Heinemann U (2014) GABAB receptor dependent modulation of sharp wave-ripple complexes in the rat hippocampus in vitro. Neurosci Lett 574:15–20.

Holz J, Piosczyk H, Feige B, Spiegelhalder K, Baglioni C, Riemann D, Nissen C (2012) EEG Σ and slow-wave activity during NREM sleep correlate with overnight declarative and procedural memory consolidation. J Sleep Res 21:612–619.

Hosp JA, Pekanovic A, Rioult-Pedotti MS, Luft AR (2011) Dopaminergic projections from midbrain to primary motor cortex mediate motor skill learning. J Neurosci 31:2481–2487.

Howard MW (2003) Gamma Oscillations Correlate with Working Memory Load in Humans. Cerebral Cortex 13:1369–1374.

Huber R, Ghilardi MF, Massimini M, Ferrarelli F, Riedner BA, Peterson MJ, Tononi G (2006) Arm immobilization causes cortical plastic changes and locally decreases sleep slow wave activity. Nat Neurosci 9:1169–1176.

Huber R, Ghilardi MF, Massimini M, Tononi G (2004) Local sleep and learning. Nature 430:78–81.

Hughes SW, Cope DW, Blethyn KL, Crunelli V (2002) Cellular Mechanisms of the Slow (<1 Hz) Oscillation in Thalamocortical Neurons *In Vitro*. Neuron 33:947–958.

Isomura Y, Sirota A, Ozen S, Montgomery S, Mizuseki K, Henze DA, Buzsáki G (2006) Integration and segregation of activity in entorhinal-hippocampal subregions by neocortical slow oscillations. Neuron 52:871–882.

Javitch JA, D'Amato RJ, Strittmatter SM, Snyder SH (1985) Parkinsonism-inducing neurotoxin, N-methyl-4-phenyl-1, 2, 3, 6-tetrahydropyridine: uptake of the metabolite N-methyl-4-phenylpyridine by dopamine neurons explains selective toxicity. Proc Natl Acad Sci USA 82:2173–2177.

Jellinger KA (1999) Post mortem studies in Parkinson's disease--is it possible to detect brain areas for specific symptoms? J Neural Transm Suppl 56:1–29.

Ji D, Wilson MA (2007) Coordinated memory replay in the visual cortex and hippocampus during sleep. Nat Neurosci 10:100–107.

Johnson LA, Euston DR, Tatsuno M, McNaughton BL (2010) Stored-Trace Reactivation in Rat Prefrontal Cortex Is Correlated with Down-to-Up State Fluctuation Density. J Neurosci 30:2650–2661.

Jones BF, Groenewegen HJ, Witter MP (2005) Intrinsic connections of the cingulate cortex in the rat suggest the existence of multiple functionally segregated networks. Neuroscience 133:193–207.

Jutras MJ, Fries P, Buffalo EA (2009) Gamma-band synchronization in the macaque hippocampus and memory formation. J Neurosci 29:12521–12531.

Kajikawa Y, Schroeder CE (2011) How Local Is the Local Field Potential? Neuron 72:847–858.

Kasa P (1986) The cholinergic systems in brain and spinal cord. Progress in Neurobiology 26:211–272.

Keita MS, Frankel-Kohn L, Bertrand N, Lecanu L, Monmaur P (2000) Acetylcholine release in the hippocampus of the urethane anaesthetised rat positively correlates with both peak theta frequency and relative power in the theta band. Brain Research 887:323–334.

Kennerley SW, Wallis JD (2009) Reward-Dependent Modulation of Working Memory in Lateral Prefrontal Cortex. J Neurosci 29:3259–3270.

Keshavan MS, Montrose DM, Miewald JM, Jindal RD (2011) Sleep correlates of cognition in early course psychotic disorders. Schizophr Res 131:231–234.

Kesner RP (2000) Subregional analysis of mnemonic functions of the prefrontal cortex in the rat. Psychobiology 28:219–228.

Klausberger T, Magill PJ, Márton LF, Roberts JDB, Cobden PM, Buzsáki G, Somogyi P (2003) Brain-state- and cell-type-specific firing of hippocampal interneurons in vivo. Nature 421:844–848.

Kocsis B, Lee P, Deth R (2013) Enhancement of gamma activity after selective activation of dopamine D4 receptors in freely moving rats and in a neurodevelopmental model of schizophrenia. Brain Struct Funct Available at: http://link.springer.com/article/10.1007%2Fs00429-013-0607-6.

Krettek JE, Price JL (1977) The cortical projections of the mediodorsal nucleus and adjacent thalamic nuclei in the rat. Journal of Comparative Neurology 171:157–191.

Krystal AD (2012) Psychiatric Disorders and Sleep. Neurologic Clinics 30:1389–1413.

Kucewicz MT, Cimbalnik J, Matsumoto JY, Brinkmann BH, Bower MR, Vasoli V, Sulc V, Meyer F, Marsh WR, Stead SM, Worrell GA (2014) High frequency oscillations are associated with cognitive processing in human recognition memory. Brain 137:2231–2244.

Kunori N, Kajiwara R, Takashima I (2014) Voltage-sensitive dye imaging of primary motor cortex activity produced by ventral tegmental area stimulation. J Neurosci 34:8894–8903.

Lai YY, Shalita T, Hajnik T, Wu JP, Kuo JS, Chia LG, Siegel JM (1999) Neurotoxic N-methyl-D-aspartate lesion of the ventral midbrain and mesopontine junction alters sleep-wake organization. Neuroscience 90:469–483.

Land BB, Narayanan NS, Liu R-J, Gianessi CA, Brayton CE, Grimaldi DM, Sarhan M, Guarnieri DJ, Deisseroth K, Aghajanian GK, DiLeone RJ (2014) Medial prefrontal D1 dopamine neurons control food intake. Nat Neurosci 17:248–253.

Lauzon NM, Bishop SF, Laviolette SR (2009) Dopamine D1 versus D4 Receptors Differentially Modulate the Encoding of Salient versus Nonsalient Emotional Information in the Medial Prefrontal Cortex. J Neurosci 29:4836–4845.

Laviolette SR (2005) A Subpopulation of Neurons in the Medial Prefrontal Cortex Encodes Emotional Learning with Burst and Frequency Codes through a Dopamine D4 Receptor-Dependent Basolateral Amygdala Input. J Neurosci 25:6066–6075.

Le Bon-Jego M, Yuste R (2007) Persistently active, pacemaker-like neurons in neocortex. Front Neurosci 1:123–129.

Le Van Quyen M, Staba R, Bragin A, Dickson C, Valderrama M, Fried I, Engel J (2010) Large-scale microelectrode recordings of high-frequency gamma oscillations in human cortex during sleep. J Neurosci 30:7770–7782.

Lejeune S, Dourmap N, Martres M-P, Giros B, Daugé V, Naudon L (2013) The dopamine D1 receptor agonist SKF 38393 improves temporal order memory performance in maternally deprived rats. Neurobiol Learn & Mem 106:268–273.

Lemieux M, Chen JY, Lonjers P, Bazhenov M, Timofeev I (2014) The Impact of Cortical Deafferentation on the Neocortical Slow Oscillation. J Neurosci 34:5689–5703.

Lewis BL, O'Donnell P (2000) Ventral tegmental area afferents to the prefrontal cortex maintain membrane potential "up" states in pyramidal neurons via D(1) dopamine receptors. Cereb Cortex 10:1168–1175.

Léna I, Parrot S, Deschaux O, Muffat-Joly S, Sauvinet V, Renaud B, Suaud-Chagny MF, Gottesmann C (2005) Variations in extracellular levels of dopamine, noradrenaline, glutamate, and aspartate across the sleep-wake cycle in the medial prefrontal cortex and nucleus accumbens of freely moving rats. J Neurosci Res 81:891–899.

Li CYT, Poo MM, Dan Y (2009) Burst Spiking of a Single Cortical Neuron Modifies Global Brain State. Science 324:643–646.

Lima MMS (2013) Sleep disturbances in Parkinson. Sleep Med Rev 17:367–375.

Liu Y, San Liang X, Weisberg RH (2007) Rectification of the Bias in the Wavelet Power Spectrum. J Atmos Oceanic Technol 24:2093–2102.

Loureiro M, Cholvin T, Lopez J, Merienne N, Latreche A, Cosquer B, Geiger K, Kelche C, Cassel JC, Pereira de Vasconcelos A (2012) The Ventral Midline Thalamus (Reuniens and Rhomboid Nuclei) Contributes to the Persistence of Spatial Memory in Rats. J Neurosci 32:9947–9959.

Lu J (2006) Identification of Wake-Active Dopaminergic Neurons in the Ventral Periaqueductal Gray Matter. J Neurosci 26:193–202.

Lu J, Sherman D, Devor M, Saper CB (2006) A putative flip–flop switch for control of REM sleep. Nature 441:589–594.

Luo AH, Aston-Jones G (2009) Circuit projection from suprachiasmatic nucleus to ventral tegmental area: a novel circadian output pathway. Eur J Neurosci 29:748–

760.

Luo AH, Georges FE, Aston-Jones GS (2008) Novel neurons in ventral tegmental area fire selectively during the active phase of the diurnal cycle. Eur J Neurosci 27:408–422.

Lüthi A (2014) Sleep Spindles: Where They Come From, What They Do. The Neuroscientist 20:243–256.

Maggi CA, Meli A (1986) Suitability of urethane anesthesia for physiopharmacological investigations in various systems. Part 1: General considerations. Experientia 42:109–114.

Mann EO, Kohl MM, Paulsen O (2009) Distinct Roles of GABAA and GABAB Receptors in Balancing and Terminating Persistent Cortical Activity. J Neurosci 29:7513–7518.

Marshall L, Helgadóttir H, Mölle M, Born J (2006) Boosting slow oscillations during sleep potentiates memory. Nature 444:610–613.

Martinovic J, Gruber T, Hantsch A, Müller MM (2008) Induced gamma-band activity is related to the time point of object identification. Brain Research 1198:93–106.

Martinovic J, Gruber T, Müller MM (2007) Induced gamma band responses predict recognition delays during object identification. J Cogn Neurosci 19:921–934.

Marzo A, Totah NK, Neves RM, Logothetis NK, Eschenko O (2014) Unilateral electrical stimulation of rat locus coeruleus elicits bilateral response of norepinephrine neurons and sustained activation of medial prefrontal cortex. J Neurophysiol 111:2570–2588.

Massi L, Lagler M, Hartwich K, Borhegyi Z, Somogyi P, Klausberger T (2012) Temporal Dynamics of Parvalbumin-Expressing Axo-axonic and Basket Cells in the Rat Medial Prefrontal Cortex In Vivo. J Neurosci 32:16496–16502.

Massimini M (2004) The Sleep Slow Oscillation as a Traveling Wave. J Neurosci 24:6862–6870.

Matheson JK, Saper CB (2003) REM sleep behavior disorder: a dopaminergic deficiency disorder? Neurology 61:1328–1329.

Mayhew JE, Askew S, Zheng Y, Porrill J, Westby GW, Redgrave P, Rector DM, Harper RM (1996) Cerebral vasomotion: a 0.1-Hz oscillation in reflected light imaging of neural activity. NeuroImage 4:183–193.

Mayne EW, Craig MT, McBain CJ, Paulsen O (2013) Dopamine suppresses persistent network activity via D(1) -like dopamine receptors in rat medial entorhinal cortex. Eur J Neurosci 37:1242–1247.

McNamara F, Lijowska AS, Thach BT (2002) Spontaneous arousal activity in infants during NREM and REM sleep. J Physiol (Lond) 538:263–269.

Mena-Segovia J, Sims HM, Magill PJ, Bolam JP (2008) Cholinergic brainstem neurons modulate cortical gamma activity during slow oscillations. J Physiol (Lond)

586:2947–2960.

Merrill EG, Ainsworth A (1972) Glass-coated platinum-plated tungsten microelectrodes. Medical and Biological Engineering 10:662–672.

Middleton S, Jalics J, Kispersky T, LeBeau FEN, Roopun AK, Kopell NJ, Whittington MA, Cunningham MO (2008) NMDA receptor-dependent switching between different gamma rhythm-generating microcircuits in entorhinal cortex. PNAS 105:18572–18577.

Miller JD, Farber J, Gatz P, Roffwarg H, German DC (1983) Activity of mesencephalic dopamine and non-dopamine neurons across stages of sleep and walking in the rat. Brain Research 273:133–141.

Minlebaev M, Colonnese M, Tsintsadze T, Sirota A, Khazipov R (2011) Early Gamma Oscillations Synchronize Developing Thalamus and Cortex. Science 334:226–229.

Missale C, Nash SR, Robinson SW, Jaber M, Caron MG (1998) Dopamine receptors: from structure to function. Physiol Rev 78:189–225.

Miura Y, Ito T, Kadokawa T (1987) Effects of intraseptally injected dopamine and noradrenaline on hippocampal synchronized theta wave activity in rats. Jpn J Pharmacol 44:471–479.

Mohajerani MH, McVea DA, Fingas M, Murphy TH (2010) Mirrored bilateral slow-wave cortical activity within local circuits revealed by fast bihemispheric voltage-sensitive dye imaging in anesthetized and awake mice. J Neurosci 30:3745–3751.

Montgomery SM, Buzsáki G (2007) Gamma oscillations dynamically couple hippocampal CA3 and CA1 regions during memory task performance. Proc Natl Acad Sci USA 104:14495–14500.

Monti JM, Monti D (2007) The involvement of dopamine in the modulation of sleep and waking. Sleep Med Rev 11:113–133.

Mora F, Sweeney KF, Rolls ET, Sanguinetti AM (1976) Spontaneous firing rate of neurones in the prefrontal cortex of the rat: evidence for a dopaminergic inhibition. Brain Research 116:516–522.

Morin A, Doyon J, Dostie V, Barakat M, Hadj Tahar A, Korman M, Benali H, Karni A, Ungerleider LG, Carrier J (2008) Motor sequence learning increases sleep spindles and fast frequencies in post-training sleep. Sleep 31:1149–1156.

Moruzzi G, Magoun HW (1949) Brain stem reticular formation and activation of the EEG. EEG & Clin Neurophys 1:455–473.

Mölle M, Bergmann TO, Marshall L, Born J (2011) Fast and slow spindles during the sleep slow oscillation: disparate coalescence and engagement in memory processing. Sleep 34:1411–1421.

Mölle M, Marshall L, Gais S, Born J (2002) Grouping of spindle activity during slow oscillations in human non-rapid eye movement sleep. J Neurosci 22:10941–10947.

Mölle M, Marshall L, Gais S, Born J (2004) Learning increases human

electroencephalographic coherence during subsequent slow sleep oscillations. Proc Natl Acad Sci USA 101:13963–13968.

Mölle M, Yeshenko O, Marshall L, Sara SJ, Born J (2006) Hippocampal Sharp Wave-Ripples Linked to Slow Oscillations in Rat Slow-Wave Sleep. J Neurophysiol 96:62–70.

Mrzljak L, Bergson C, Pappy M, Huff R, Levenson R, Goldman-Rakic PS (1996) Localization of dopamine D4 receptors in GABAergic neurons of the primate brain. Nature 381:245–248.

Nádasdy Z, Hirase H, Czurkó A, Csicsvari J, Buzsaki G (1999) Replay and time compression of recurring spike sequences in the hippocampus. J Neurosci 19:9497–9507.

Nir Y, Staba RJ, Andrillon T, Vyazovskiy VV, Cirelli C, Fried I, Tononi G (2011) Regional Slow Waves and Spindles in Human Sleep. Neuron 70:153–169.

Noaín D, Avale ME, Wedemeyer C, Calvo D, Peper M, Rubinstein M (2006) Identification of brain neurons expressing the dopamine D4 receptor gene using BAC transgenic mice. European Journal of Neuroscience 24:2429–2438.

Nomeir AA, Ioannou YM, Sanders JM, Matthews HB (1989) Comparative metabolism and disposition of ethyl carbamate (urethane) in male Fischer 344 rats and male B6C3F1 mice. Toxicol Appl Pharmacol 97:203–215.

Oades RD, Halliday GM (1987) Ventral tegmental (A10) system: neurobiology. 1. Anatomy and connectivity. Brain Research 434:117–165.

Orzeł-Gryglewska J, Kuśmierczak M, Jurkowlaniec E (2010) Involvement of GABAergic transmission in the midbrain ventral tegmental area in the regulation of hippocampal theta rhythm. Brain Research Bulletin 83:310–320.

Orzeł-Gryglewska J, Kuśmierczak M, Majkutewicz I, Jurkowlaniec E (2012) Induction of hippocampal theta rhythm by electrical stimulation of the ventral tegmental area and its loss after septum inactivation. Brain Research 1436:51–67.

Osipova D (2006) Theta and Gamma Oscillations Predict Encoding and Retrieval of Declarative Memory. J Neurosci 26:7523–7531.

O'Neill J, Senior TJ, Allen K, Huxter JR, Csicsvari J (2008) Reactivation of experience-dependent cell assembly patterns in the hippocampus. Nat Neurosci 11:209–215.

Pace-Schott EF, Hobson JA (2002) The neurobiology of sleep: genetics, cellular physiology and subcortical networks. Nat Rev Neurosci 3:591–605.

Pagliardini S, Gosgnach S, Dickson CT (2013) Spontaneous Sleep-Like Brain State Alternations and Breathing Characteristics in Urethane Anesthetized Mice. PLoS ONE 8:e70411.

Pagliardini S, Greer JJ, Funk GD, Dickson CT (2012) State-dependent modulation of breathing in urethane-anesthetized rats. J Neurosci 32:11259–11270.

Parent A, Parent M, Charara A (1999) Glutamatergic inputs to midbrain dopaminergic neurons in primates. Parkinsonism and Related Disorders 5:193–201.

Park J, Lee H, Kim T, Park GY, Lee EM, Baek S, Ku J, Kim IY, Kim SI, Jang DP, Kang JK (2014) Role of low- and high-frequency oscillations in the human hippocampus for encoding environmental novelty during a spatial navigation task. Hippocampus 00:1–12.

Parrino L, Halász P, Tassinari CA, Terzano MG (2006) CAP, epilepsy and motor events during sleep: the unifying role of arousal. Sleep Med Rev 10:267–285.

Paxinos G, Kus L, Ashwell KWS, Watson C (1999) Chemoarchitectonic Atlas of the Rat Forebrain, 1st ed. Academic Press.

Pedroarena C, Llinás R (1997) Dendritic calcium conductances generate high-frequency oscillation in thalamocortical neurons. Proc Natl Acad Sci USA 94:724–728.

Penttonen M, Nurminen N, Miettinen R, Sirviö J, Henze DA, Csicsvari J, Buzsaki G (1999) Ultra-slow oscillation (0.025 Hz) triggers hippocampal afterdischarges in Wistar rats. Neuroscience 94:735–743.

Peters Y, Barnhardt NE, O'Donnell P (2004) Prefrontal cortical up states are synchronized with ventral tegmental area activity. Synapse 52:143–152.

Petersen CC, Hahn TT, Mehta M, Grinvald A, Sakmann B (2003) Interaction of sensory responses with spontaneous depolarization in layer 2/3 barrel cortex. Proc Natl Acad Sci USA 100:13638–13643.

Peyrache A, Battaglia FP, Destexhe A (2011) Inhibition recruitment in prefrontal cortex during sleep spindles and gating of hippocampal inputs. PNAS 108:17207–17212.

Peyrache A, Khamassi M, Benchenane K, Wiener SI, Battaglia FP (2009) Replay of rule-learning related neural patterns in the prefrontal cortex during sleep. Nat Neurosci 12:919–926.

Phillips KG, Bartsch U, McCarthy AP, Edgar DM, Tricklebank MD, Wafford KA, Jones MW (2012) Decoupling of Sleep-Dependent Cortical and Hippocampal Interactions in a Neurodevelopmental Model of Schizophrenia. Neuron 76:526–533.

Pirot S, Godbout R, Mantz J, Tassin JP, Glowinski J, Thierry AM (1992) Inhibitory effects of ventral tegmental area stimulation on the activity of prefrontal cortical neurons: evidence for the involvement of both dopaminergic and GABAergic components. Neuroscience 49:857–865.

Preuss TM (1995) Do Rats Have Prefrontal Cortex? The Rose-Woolsey-Akert Program Reconsidered. J Cogn Neurosci 7:1–24.

Puig MV, Miller EK (2012) The Role of Prefrontal Dopamine D1 Receptorsin the Neural Mechanisms of Associative Learning. Neuron 74:874–886.

Puig MV, Miller EK (2014) Neural Substrates of Dopamine D2 Receptor Modulated Executive Functions in the Monkey Prefrontal Cortex. Cerebral Cortex.

Puig MV, Ushimaru M, Kawaguchi Y (2008) Two distinct activity patterns of fast-spiking interneurons during neocortical UP states. PNAS 105:8428–8433.

Pungor K, Papp M, Kékesi K, Juhász G (1990) A novel effect of MPTP: the selective suppression of paradoxical sleep in cats. Brain Research.

Qu WM, Xu XH, Yan MM, Wang YQ, Urade Y, Huang ZL (2010) Essential Role of Dopamine D2 Receptor in the Maintenance of Wakefulness, But Not in Homeostatic Regulation of Sleep, in Mice. J Neurosci 30:4382–4389.

Ray S, Maunsell JHR (2011) Different Origins of Gamma Rhythm and High-Gamma Activity in Macaque Visual Cortex. Plos Biol 9:e1000610.

Ray S, Niebur E, Hsiao SS, Sinai A, Crone NE (2008) High-frequency gamma activity (80–150Hz) is increased in human cortex during selective attention. Clinical Neurophysiology.

Richter SJ (1999) Nearly exact tests in factorial experiments using the aligned rank transform. Journal of Applied Statistics 26:203–217.

Riedner BA, Vyazovskiy VV, Huber R, Massimini M, Esser S, Murphy M, Tononi G (2007) Sleep homeostasis and cortical synchronization: III. A high-density EEG study of sleep slow waves in humans. Sleep 30:1643–1657.

Rigas P, Castro-Alamancos MA (2007) Thalamocortical Up States: Differential Effects of Intrinsic and Extrinsic Cortical Inputs on Persistent Activity. J Neurosci 27:4261–4272.

Roopun AK, Kramer MA, Carracedo LM, Kaiser M, Davies CH, Traub RD, Kopell NJ, Whittington MA (2008) Temporal Interactions between Cortical Rhythms. Front Neurosci 2:145–154.

Rosanova M, Ulrich D (2005) Pattern-specific associative long-term potentiation induced by a sleep spindle-related spike train. J Neurosci 25:9398–9405.

Rose JE, Woolsey CN (1948) The orbitofrontal cortex and its connections with the mediodorsal nucleus in rabbit, sheep and cat. Res Publ Assoc Res Nerv Ment Dis 27 (1 vol.):210–232.

Roš H, Magill PJ, Moss J, Bolam JP, Mena-Segovia J (2010) Distinct types of non-cholinergic pedunculopontine neurons are differentially modulated during global brain states. Neuroscience 170:78–91.

Roth BL, Tandra S, Burgess LH, Sibley DR, Meltzer HY (1995) D4 dopamine receptor binding affinity does not distinguish between typical and atypical antipsychotic drugs. Psychopharm 120:365–368.

Ruiz-Mejias M, Ciria-Suarez L, Mattia M, Sanchez-Vives MV (2011) Slow and fast rhythms generated in the cerebral cortex of the anesthetized mouse. J Neurophysiol 106:2910–2921.

Rye DB (2004) The two faces of eve dopamine's modulation of wakefulness and sleep. Neurology 63:S2–S7.

Sabeti J, Gerhardt GA, Zahniser NR (2003) Chloral hydrate and ethanol, but not urethane, alter the clearance of exogenous dopamine recorded by chronoamperometry in striatum of unrestrained rats. Neurosci Lett 343:9–12.

Salter KC, Fawcett RF (1993) The art test of interaction: a robust and powerful rank test of interaction in factorial models. Communications in Statistics - Simulation and Computation 22:137–153.

Sanchez-Vives MV, McCormick DA (2000) Cellular and network mechanisms of rhythmic recurrent activity in neocortex. Nat Neurosci 3:1027–1034.

Sawaguchi T, Goldman-Rakic PS (1991) D1 dopamine receptors in prefrontal cortex: involvement in working memory. Science 251:947–950.

Sawaguchi T, Goldman-Rakic PS (1994) The role of D1-dopamine receptor in working memory: local injections of dopamine antagonists into the prefrontal cortex of rhesus monkeys performing an oculomotor delayed-response task. J Neurophysiol 71:515–528.

Scatton B, Simon H, Le Moal M, Bischoff S (1980) Origin of dopaminergic innervation of the rat hippocampal formation. Neurosci Lett 18(2):125-131.

Sceniak MP, Maciver MB (2006) Cellular actions of urethane on rat visual cortical neurons in vitro. J Neurophysiol 95:3865–3874.

Schabus M, Dang-Vu TT, Heib DPJ, Boly M, Desseilles M, Vandewalle G, Schmidt C, Albouy G, Darsaud A, Gais S, Degueldre C, Balteau E, Phillips C, Luxen A, Maquet P (2012) The Fate of Incoming Stimuli during NREM Sleep is Determined by Spindles and the Phase of the Slow Oscillation. Front Neurol 3:40.

Schabus M, Gruber G, Parapatics S, Sauter C, Klösch G, Anderer P, Klimesch W, Saletu B, Zeitlhofer J (2004) Sleep spindles and their significance for declarative memory consolidation. Sleep 27:1479–1485.

Schultz W (2007) Multiple dopamine functions at different time courses. Annu Rev Neurosci 30:259–288.

Schulz SB, Heidmann KE, Mike A, Klaft Z-J, Heinemann U, Gerevich Z (2012) First and second generation antipsychotics influence hippocampal gamma oscillations by interactions with 5-HT 3and D 3receptors. British Journal of Pharmacology 167:1480–1491.

Seamans JK, Yang CR (2004) The principal features and mechanisms of dopamine modulation in the prefrontal cortex. Progress in Neurobiology 74:1–58.

Seeman P, Guan H-C, Van Tol HHM (1993) Dopamine D4 receptors elevated in schizophrenia. Nature 365:441–445.

Sharma AV, Wolansky T, Dickson CT (2010) A Comparison of Sleeplike Slow Oscillations in the Hippocampus Under Ketamine and Urethane Anesthesia. J Neurophysiol 104:932–939.

Shen J, Kudrimoti HS, McNaughton BL, Barnes CA (1998) Reactivation of neuronal ensembles in hippocampal dentate gyrus during sleep after spatial experience. J

Sleep Res 7 Suppl 1:6–16.

Sheroziya M, Timofeev I (2014) Global Intracellular Slow-Wave Dynamics of the Thalamocortical System. J Neurosci 34:8875–8893.

Shi CJ, Cassell MD (1998) Cortical, thalamic, and amygdaloid connections of the anterior and posterior insular cortices. J Comp Neurol 399:440–468.

Shu Y, Hasenstaub A, McCormick DA (2003) Turning on and off recurrent balanced cortical activity. Nature 423:288–293.

Siapas AG, Wilson MA (1998) Coordinated interactions between hippocampal ripples and cortical spindles during slow-wave sleep. Neuron 21:1123–1128.

Simon A, Traub RD, Vladimirov N, Jenkins A, Nicholson C, Whittaker RG, Schofield I, Clowry GJ, Cunningham MO, Whittington MA (2013) Gap junction networks can generate both ripple-like and fast ripple-like oscillations. Eur J Neurosci 39:46–60.

Sirota A, Csicsvari J, Buhl D, Buzsáki G (2003) Communication between neocortex and hippocampus during sleep in rodents. Proc Natl Acad Sci USA 100:2065–2069.

Skaggs WE, McNaughton BL (1996) Replay of Neuronal Firing Sequences in Rat Hippocampus During Sleep Following Spatial Experience. Science 271:1870–1873.

Sohal VS, Zhang F, Yizhar O, Deisseroth K (2009) Parvalbumin neurons and gamma rhythms enhance cortical circuit performance. Nature 459:698–702.

Sokolov A, Pavlova M, Lutzenberger W, Birbaumer N (2004) Reciprocal modulation of neuromagnetic induced gamma activity by attention in the human visual and auditory cortex. NeuroImage 22:521–529.

Sotomayor RE, Collins TF (1990) Mutagenicity, metabolism, and DNA interactions of urethane. Toxicol Ind Health 6:71–108.

Steriade M (2006) Grouping of brain rhythms in corticothalamic systems. Neuroscience 137:1087–1106.

Steriade M, Amzica F, Nuñez A (1993a) Cholinergic and noradrenergic modulation of the slow (approximately 0.3 Hz) oscillation in neocortical cells. J Neurophysiol 70:1385–1400.

Steriade M, Contreras D, Curró Dossi R, Nuñez A (1993b) The Slow (<1 Hz) Oscillation in Reticular Thalamic and Thalamocortical Neurons: Scenario of Sleep Rhythm Generation in Interacting Thalamic and Neocortical Networks. J Neurosci 13:3284–3299.

Steriade M, Datta S, Paré D, Oakson G, Curró Dossi RC (1990) Neuronal activities in brain-stem cholinergic nuclei related to tonic activation processes in thalamocortical systems. J Neurosci 10:2541–2559.

Steriade M, Dossi RC, Nuñez A (1991) Network modulation of a slow intrinsic oscillation of cat thalamocortical neurons implicated in sleep delta waves: cortically induced synchronization and brainstem cholinergic suppression. J Neurosci

11:3200–3217.

Steriade M, Nuñez A, Amzica F (1993c) Intracellular Analysis of Relations between the Slow (<1 Hz) Neocortical Oscillation and Other Sleep Rhythms of the Electroencephalogram. J Neurosci 13:3266–3283.

Steriade M, Nuñez A, Amzica F (1993d) A Novel Slow (<1 Hz) Oscillation of Neocortical Neurons *in vivo*: Depolarizing and Hyperpolarizing Components. J Neurosci 13:3252–3265.

Steriade MM, Amzica FF, Contreras DD (1996) Synchronization of fast (30-40 Hz) spontaneous cortical rhythms during brain activation. J Neurosci 16:392–417.

Steullet P, Cabungcal J-H, Cuénod M, Do KQ (2014) Fast oscillatory activity in the anterior cingulate cortex: dopaminergic modulation and effect of perineuronal net loss. Front Cell Neurosci 8:244.

Stuber GD, Hnasko TS, Britt JP, Edwards RH, Bonci A (2010) Dopaminergic Terminals in the Nucleus Accumbens But Not the Dorsal Striatum Corelease Glutamate. J Neurosci 30:8229–8233.

Sullivan D, Csicsvari J, Mizuseki K, Montgomery S, Diba K, Buzsaki G (2011) Relationships between Hippocampal Sharp Waves, Ripples, and Fast Gamma Oscillation: Influence of Dentate and Entorhinal Cortical Activity. J Neurosci 31:8605–8616.

Sun X (2005) Dopamine Receptor Stimulation Modulates AMPA Receptor Synaptic Insertion in Prefrontal Cortex Neurons. J Neurosci 25:7342–7351.

Suzuki K, Miyamoto M, Miyamoto T, Iwanami M, Hirata K (2011) Sleep Disturbances Associated with Parkinson's Disease. Parkinson's Disease 2011:1–10.

Swanson LW (1982) The projections of the ventral tegmental area and adjacent regions: a combined fluorescent retrograde tracer and immunofluorescence study in the rat. Brain Research Bulletin 9:321–353.

Tamaki M, Huang TR, Yotsumoto Y, Hamalainen M, Lin FH, Nanez JE, Watanabe T, Sasaki Y (2013) Enhanced Spontaneous Oscillations in the Supplementary Motor Area Are Associated with Sleep-Dependent Offline Learning of Finger-Tapping Motor-Sequence Task. J Neurosci 33:13894–13902.

Tamaki M, Matsuoka T, Nittono H, Hori T (2008) Fast sleep spindle (13-15 hz) activity correlates with sleep-dependent improvement in visuomotor performance. Sleep 31:204–211.

Terzano MG, Mancia D, Salati MR, Costani G, Decembrino A, Parrino L (1985) The cyclic alternating pattern as a physiologic component of normal NREM sleep. Sleep 8:137–145.

Terzano MG, Parrino L (1993) Clinical applications of cyclic alternating pattern. Physiology & Behavior 54:807–813.

Terzano MG, Parrino L (2000) Origin and Significance of the Cyclic Alternating Pattern (CAP). REVIEW ARTICLE. Sleep Med Rev 4:101–123.

Terzano MG, Parrino L, Smerieri A, Chervin R, Chokroverty S, Guilleminault C, Hirshkowitz M, Mahowald M, Moldofsky H, Rosa A, Thomas R, Walters A (2002) Atlas, rules, and recording techniques for the scoring of cyclic alternating pattern (CAP) in human sleep. Sleep Med 3:187–199.

Tiitinen H, Sinkkonen J, Reinikainen K, Alho K, Lavikainen J, Näätänen R (1993) Selective attention enhances the auditory 40-Hz transient response in humans. Nature 364:59–60.

Timofeev I, Bazhenov M (2005) Mechanisms and biological role of thalamocortical oscillations. Trends in chronobiology research.

Timofeev I, Grenier F, Bazhenov M, Sejnowski TJ, Steriade M (2000) Origin of slow cortical oscillations in deafferented cortical slabs. Cereb Cortex 10:1185–1199.

Timofeev I, Steriade M (1996) Low-frequency rhythms in the thalamus of intact-cortex and decorticated cats. J Neurophysiol 76:4152–4168.

Tort ABL, Komorowski RW, Manns JR, Kopell NJ, Eichenbaum H (2009) Theta-gamma coupling increases during the learning of item-context associations. PNAS 106:20942–20947.

Towers SK, Hestrin, S (2008) D1-like dopamine receptor activation modulates GABAergic inhibition but not electrical coupling between neocortical fast-spiking interneurons. J Neurosci 28(10): 2663-2641.

Trampus M, Ferri N, Adami M, Ongini E (1993) The dopamine D1 receptor agonists, A68930 and SKF 38393, induce arousal and suppress REM sleep in the rat. Eur J Pharmacol 235:83–87.

Trampus M, Ferri N, Monopoli A, Ongini E (1991) The dopamine D1 receptor is involved in the regulation of REM sleep in the rat. Eur J Pharmacol 194:189–194.

Trampus M, Ongini E (1990) The D1 dopamine receptor antagonist SCH 23390 enhances REM sleep in the rat. Neuropharmacology 29:889–893.

Trantham-Davidson H, Neely LC, Lavin A, Seamans JK (2004) Mechanisms underlying differential D1 versus D2 dopamine receptor regulation of inhibition in prefrontal cortex. J Neurosci 24:10652–10659.

Traub RD, Duncan R, Russell AJC, Baldeweg T, Tu Y, Cunningham MO, Whittington MA (2010) Spatiotemporal patterns of electrocorticographic very fast oscillations (> 80 Hz) consistent with a network model based on electrical coupling between principal neurons. Epilepsia 51:1587–1597.

Traub RD, Whittington MA, Colling SB, Buzsaki G, Jefferys JG (1996) Analysis of gamma rhythms in the rat hippocampus in vitro and in vivo. J Physiol (Lond) 493:471–484.

Tritsch NX, Sabatini BL (2012) Dopaminergic Modulation of Synaptic Transmission in Cortex and Striatum. Neuron 76:33–50.

Trulson ME, Preussler DW (1984) Dopamine-containing ventral tegmental area neurons in freely moving cats: activity during the sleep-waking cycle and effects of stress.

Exp Neurol 83:367–377.

Tseng KY (2004) Dopamine-Glutamate Interactions Controlling Prefrontal Cortical Pyramidal Cell Excitability Involve Multiple Signaling Mechanisms. J Neurosci 24:5131–5139.

Ushimaru M, Ueta Y, Kawaguchi Y (2012) Differentiated participation of thalamocortical subnetworks in slow/spindle waves and desynchronization. J Neurosci 32:1730–1746.

Uylings HBM, Groenewegen HJ, Kolb B (2003) Do rats have a prefrontal cortex? Beh Brain Res 146:3–17.

Valderrama M, Crépon B, Botella-Soler V, Martinerie J, Hasboun D, Alvarado-Rojas C, Baulac M, Adam C, Navarro V, Le Van Quyen M (2012) Human gamma oscillations during slow wave sleep. PLoS ONE 7:e33477.

Valencia M, Artieda J, Bolam JP, Mena-Segovia J (2013) Dynamic interaction of spindles and gamma activity during cortical slow oscillations and its modulation by subcortical afferents. PLoS ONE 8:e67540.

van Aerde KI, Heistek TS, Mansvelder HD (2008) Prelimbic and infralimbic prefrontal cortex interact during fast network oscillations. PLoS ONE 3:e2725.

van Aerde KI, Mann EO, Canto CB, Heistek TS, Linkenkaer-Hansen K, Mulder AB, van der Roest M, Paulsen O, Brussaard AB, Mansvelder HD (2009) Flexible spike timing of layer 5 neurons during dynamic beta oscillation shifts in rat prefrontal cortex. J Physiol (Lond) 587:5177–5196.

Van Eden CG, Hoorneman EM, Buijs RM, Matthijssen MA, Geffard M, Uylings HB (1987) Immunocytochemical localization of dopamine in the prefrontal cortex of the rat at the light and electron microscopical level. Neuroscience 22:849–862.

Vertes RP (2006) Interactions among the medial prefrontal cortex, hippocampus and midline thalamus in emotional and cognitive processing in the rat. Neuroscience 142:1–20.

Vertes RP, Hoover WB, Rodriguez JJ (2012) Projections of the central medial nucleus of the thalamus in the rat: node in cortical, striatal and limbic forebrain circuitry. Neuroscience 219:120–136.

Vertes RP, Hoover WB, Szigeti-Buck K, Leranth C (2007) Nucleus reuniens of the midline thalamus: Link between the medial prefrontal cortex and the hippocampus. Brain Research Bulletin 71:601–609.

Volgushev M, Chauvette S, Mukovski M, Timofeev I (2006) Precise long-range synchronization of activity and silence in neocortical neurons during slow-wave oscillations [corrected]. J Neurosci 26:5665–5672.

Wamsley EJ, Tucker MA, Shinn AK, Ono KE, McKinley SK, Ely AV, Goff DC, Stickgold R, Manoach DS (2012) Reduced Sleep Spindles and Spindle Coherence in Schizophrenia: Mechanisms of Impaired Memory Consolidation? Biol Psychiatry 71:154–161.

Wang X, Zhong P, Gu Z, Yan Z (2003) Regulation of NMDA receptors by dopamine D4 signaling in prefrontal cortex. J Neurosci 23:9852–9861.

Wang X, Zhong P, Yan Z (2002) Dopamine D4 receptors modulate GABAergic signaling in pyramidal neurons of prefrontal cortex. J Neurosci 22:9185–9193.

Warenycia MW, McKenzie GM (1988) Excitation of striatal neurons by dexamphetamine is not abolished by either chloral hydrate or urethane anaesthesia. Neuropharmacology 27:1309–1312.

Watanabe S, Fusa K, Takada K, Aono Y, Saigusa T, Koshikawa N, Cools AR (2005) Effects of alpha-methyl-p-tyrosine on extracellular dopamine levels in the nucleus accumbens and the dorsal striatum of freely moving rats. J Oral Sci 47:185–190.

Watson BO, MacLean JN, Yuste R (2008) UP states protect ongoing cortical activity from thalamic inputs. PLoS ONE 3:e3971.

Wedzony K, Chocyk A, Mackowiak M, Fijał K, Czyrak A (2000) Cortical localization of dopamine D4 receptors in the rat brain--immunocytochemical study. J Physiol Pharmacol 51:205–221.

Weiss T, Veh RW, Heinemann U (2003) Dopamine depresses cholinergic oscillatory network activity in rat hippocampus. Eur J Neurosci 18:2573–2580.

West AR, Grace AA (2001) Opposite influences of endogenous dopamine D1 and D2 receptor activation on activity states and electrophysiological properties of striatal neurons: studies combining in vivo intracellular recordings and reverse microdialysis. J Neurosci 22:294–304.

Whittington MA, Cunningham MO, LeBeau FEN, Racca C, Traub RD (2011) Multiple origins of the cortical gamma rhythm. Dev Neurobiol 71:92–106.

Whittington MA, Traub RD (2003) Interneuron diversity series: inhibitory interneurons and network oscillations in vitro. Trends in Neurosciences 26:676–682.

Whittington MA, Traub RD, Jefferys JG (1995) Synchronized oscillations in interneuron networks driven by metabotropic glutamate receptor activation. Nature 373:612–615.

Wierzynski CM, Lubenov EV, Gu M, Siapas AG (2009) State-Dependent Spike-Timing Relationships between Hippocampal and Prefrontal Circuits during Sleep. Neuron 61:587–596.

Wilson CJ, Kawaguchi Y (1996) The origins of two-state spontaneous membrane potential fluctuations of neostriatal spiny neurons. J Neurosci 16:2397–2410.

Wilson DA (2003) Rapid, experience-induced enhancement in odorant discrimination by anterior piriform cortex neurons. J Neurophysiol 90:65–72.

Wilson MA, McNaughton BL (1994) Reactivation of hippocampal ensemble memories during sleep. Science 265:676–679.

Wisor JP, Nishino S, Sora I, Uhl GH, Mignot E, Edgar DM (2001) Dopaminergic role in stimulant-induced wakefulness. J Neurosci 21:1787–1794.

Wobbrock JO, Findlater L, Gergle D, Higgins JJ (2011) The Aligned Rank Transform for Nonparametric Factorial Analyses Using Only ANOVA Procedures. In, pp 143–146. Vancouver: ACM.

Wolansky T (2006) Hippocampal Slow Oscillation: A Novel EEG State and Its Coordination with Ongoing Neocortical Activity. J Neurosci 26:6213–6229.

Womelsdorf T, Schoffelen JM, Oostenveld R, Singer W, Desimone R, Engel, AK, Fries, P (2007) Modulation of neuronal interactions through neuronal synchronization. Science 316: 1609–1612.

Wood J, Kim Y, Moghaddam B (2012) Disruption of Prefrontal Cortex Large Scale Neuronal Activity by Different Classes of Psychotomimetic Drugs. J Neurosci 32:3022–3031.

Wójtowicz AM, van den Boom L, Chakrabarty A, Maggio N, Haq RU, Behrens CJ, Heinemann U (2009) Monoamines block kainate- and carbachol-induced gamma-oscillations but augment stimulus-induced gamma-oscillations in rat hippocampus in vitro. Hippocampus 19:273–288.

Wulff K, Gatti S, Wettstein JG, Foster RG (2010) Sleep and circadian rhythm disruption in psychiatric and neurodegenerative disease. Nat Rev Neurosci 11:589–599.

Xu S, Jiang W, Poo M-M, Dan Y (2012) Activity recall in a visual cortical ensemble. Nat Neurosci 15:449–455.

Yamaguchi T, Sheen W, Morales M (2007) Glutamatergic neurons are present in the rat ventral tegmental area. European Journal of Neuroscience 25:106–118.

Yamamoto J, Suh J, Takeuchi D, Tonegawa S (2014) Successful execution of working memory linked to synchronized high-frequency gamma oscillations. Cell 157:845–857.

Yang C, Ge S-N, Zhang J-R, Chen L, Yan Z-Q, Heng L-J, Zhao T-Z, Li W-X, Jia D, Zhu J-L, Gao G-D (2013) Systemic blockade of dopamine D2-like receptors increases high-voltage spindles in the globus pallidus and motor cortex of freely moving rats. PLoS ONE 8:e64637.

Yuen EY, Yan Z (2009) Dopamine D4 Receptors Regulate AMPA Receptor Trafficking and Glutamatergic Transmission in GABAergic Interneurons of Prefrontal Cortex. J Neurosci 29:550–562.

Zhang Z-W, Burke MW, Calakos N, Beaulieu J-M, Vaucher E (2010) Confocal Analysis of Cholinergic and Dopaminergic Inputs onto Pyramidal Cells in the Prefrontal Cortex of Rodents. Front Neuroanat 4:21.

Zheng P, Zhang XX, Bunney BS, Shi WX (1999) Opposite modulation of cortical N-methyl-D-aspartate receptor-mediated responses by low and high concentrations of dopamine. Neuroscience 91:527–535.

Zhong P, Yan Z (2014) Distinct Physiological Effects of Dopamine D4 Receptors on Prefrontal Cortical Pyramidal Neurons and Fast-Spiking Interneurons. Cerebral Cortex.

Zingg B, Hintiryan H, Gou L, Song MY, Bay M, Bienkowski MS, Foster NN, Yamashita S, Bowman I, Toga AW, Dong H-W (2014) Neural Networks of the Mouse Neocortex. Cell 156:1096–1111.